Preparation and Characterization of Some Perovskite Oxides

Wankassama Haron

A Thesis Submitted in Fulfillment of the Requirements for the
Degree of Doctor of Philosophy in Chemistry
Prince of Songkla University
2016

Preparation and Characterization of Some Perovskite Oxides

Wankassama Haron

A Thesis Submitted in Fulfillment of the Requirements for the
Degree of Doctor of Philosophy in Chemistry
Prince of Songkla University
2016

Thesis Title Preparation and Characterization of Some Perovskite Oxide

Author Mrs. Wankassama Haron

Major Program Chemistry

Major Advisor

.....

(Assoc. Prof. Dr. Sumpun Wongnawa)

Co-advisor

.....

(Dr. Anurat Wisitsoraat)

Examining Committee :

.....Chairperson

(Assoc. Prof. Dr. Apisit Songsasen)

.....Committee

(Assoc. Prof. Dr. Sumpun Wongnawa)

.....Committee

(Assoc. Prof. Dr. Pongsaton Amornpitoksuk)

.....Committee

(Assoc. Prof. Dr. Sumetha Suwanboon)

.....Committee

(Asst. Prof. Dr. Orawan Sirichote)

The Graduate School, Prince of Songkla University, has approved this thesis as fulfillment of the requirements for Doctor of Philosophy Degree in Chemistry

.....

(Assoc. Prof. Dr. Teerapol Srichana)

Dean of Graduate School

This is to certify that the work here submitted is the result of the candidate's own investigations. Due acknowledgement has been made of any assistance received.

.....Signature
(Assoc. Prof. Dr. Sumpun Wongnawa)
Major Advisor

.....Signature
(Mrs. Wankassama Haron)
Candidate

I hereby certify that this work has not been accepted in substance for any degree, and is not being currently submitted in candidature for any degree.

.....Signature
(Mrs. Wankassama Haron)
Candidate

ชื่อวิทยานิพนธ์ การเตรียมและวิเคราะห์สมบัติทางกายภาพของสารประกอบออกไซด์เพอรอพสไกต์บางชนิด
ผู้เขียน นางวรรณกัษมา ฮารน
สาขาวิชา เคมี
ปีการศึกษา 2559

บทคัดย่อ

ผลึกขนาดนาโนเมตรของสารประกอบเพอรอพสไกต์ $LaMO_3$ (M = Al, Fe, Co, Gd) สามารถเตรียมได้ด้วยวิธีการตกตะกอนร่วมทางเคมีโดยใช้สารตั้งต้นของโลหะไนเตรตและเกลือคาร์บอเนต เทคนิคที่ใช้ในการวิเคราะห์สมบัติกายภาพของผลิตภัณฑ์ทั้งหมด มีดังนี้ : X-ray diffractometer (XRD), energy dispersive X-ray spectrometer (EDX), scanning electron microscope (SEM), พื้นที่ผิวแบบ Brunauer– Emmett–Teller (BET) และ UV-vis diffused reflectance spectroscopy (DRS) จากการศึกษาพบว่าข้อมูลสเปกตรัม XRD ของสารประกอบที่เตรียมได้เป็นเพอรอพสไกต์ ภาพถ่าย SEM ระบุได้ว่าสารประกอบเพอรอพสไกต์ที่เตรียมได้ด้วยวิธีนี้มีขนาดอนุภาคระดับนาโนเมตรและมีพื้นผิวประกอบไปด้วยรูพรุน การวัด pH_{pzc} ของ $LaAlO_3$, $LaCoO_3$, $LaFeO_3$, และ $LaGdO_3$ ของงานวิจัยนี้ พบว่า pH_{pzc} ที่วัดได้มีค่าเท่ากับ 8.6, 9.2, 9.0 และ 8.1, ตามลำดับ ค่าพลังงาน band gap ที่คำนวณได้จากสเปกตรัม DRS ของ $LaAlO_3$, $LaCoO_3$, $LaFeO_3$, และ $LaGdO_3$ มีค่าเท่ากับ 2.50, 1.50, 2.00, และ 2.90 eV, ตามลำดับ

การศึกษาการนำไปประยุกต์ใช้เป็นตัวตรวจวัดแก๊ส พบว่า $LaAlO_3$ ที่สังเคราะห์ด้วยการเผาที่ 900°C ให้ผลดีที่สุดกับแก๊สเอทานอลเมื่อเปรียบเทียบกับ $LaMO_3$ (M = Co, Fe) เนื่องจากมีพื้นที่ผิวสูงที่สุดเมื่อเปรียบเทียบกับสารประกอบทั้งหมดที่เตรียมที่อุณหภูมิ 900°C และต่ำกว่า 900°C

การนำไปประยุกต์ใช้เป็นตัวดูดซับไอออนโลหะหนักแคดเมียม และตะกั่ว พบว่า ให้ผลดี รูปแบบการดูดซับโลหะหนักได้ศึกษาจากรูปแบบของไอโซเทอมแบบแลงเมียร์ และไอโซเทอมแบบฟรอยด์ลิค สารประกอบ เพอรอพสไกต์ของ $LaMO_3$ (M = Al, Fe, Co, Gd) ที่เตรียมได้จากงานวิจัยนี้ สามารถดูดซับแคดเมียมและตะกั่วได้ แต่ $LaAlO_3$ เป็นตัวที่มีประสิทธิภาพสูงที่สุดจากที่สังเคราะห์ทั้งหมดสี่ชนิด และน่าจะได้รับความสนใจนำไปประยุกต์ใช้เป็นตัวดูดซับโลหะหนักในการบำบัดน้ำเสีย

Thesis Title Preparation and Characterization of Some Perovskite Oxides
Author Mrs. Wankassama Haron
Major Program Chemistry
Academic Year 2016

ABSTRACT

Nanocrystalline $LaMO_3$ (M = Al, Fe, Co, Gd) perovskites were synthesized by the co-precipitation method using metal nitrate and carbonate salts as starting materials. The products were characterized with X-ray diffractometer (XRD), energy dispersive X-ray spectrometer (EDX), scanning electron microscope (SEM), Brunauer – Emmett – Teller (BET) specific surface area measurement, and UV-vis diffused reflection spectroscopy (DRS). The XRD patterns confirmed the formation of perovskite phase. The SEM micrographs indicated that perovskite samples were nanosized particles with morphology containing porosity due to inter-particle voids. The measured pH_{pzc} of $LaAlO_3$, $LaCoO_3$, $LaFeO_3$, and $LaGdO_3$ in this work were 8.6, 9.2, 9.0 and 8.1, respectively. From the DRS spectra, the band gap energies of $LaAlO_3$, $LaCoO_3$, $LaFeO_3$, and $LaGdO_3$ were calculated as 2.50, 1.50, 2.00, and 2.90 eV, respectively.

Application as gas sensor was investigated and found positive with ethanol gas. The $LaAlO_3$ obtained from calcination at 900 °C showed better performance as ethanol sensor than the other $LaMO_3$ (M = Co, Fe) because of the higher surface area than other compounds calcined at 900 °C and lower 900 °C.

Application as heavy metal ions adsorption was investigated and found positive with cadmium and lead. Langmuir and Freundlich isotherms were used to describe the adsorption behavior of heavy metal ions. The $LaMO_3$ (M = Al, Fe, Co, Gd)-perovskite obtained from this work could adsorb heavy metal ions but $LaAlO_3$ was the best among all four perovskites under studied which should be of interest in application such as wastewater treatment.

ACKNOWLEDGEMENTS

I would like to express my sincere thanks to my advisor, Associate Professor Dr. Sumpun Wongnawa, who suggested this research problem, for his numerous suggestions, encouragement, and criticism without which I would have been unable to complete this work.

I am very grateful to thank my co-advisor, Dr. Anurat Wisitsoraat for the valuable comments on my thesis, and re-calculation of the gas sensor part. Thanks are also extended to the examination committee members of this thesis for their valuable time and comments.

I am deeply indebted to the Office of the Higher Education Commission for the scholarship and the Graduate School, Prince of Songkla University, for the partial supports of the research fund.

I would like to thank Department of Chemistry, Faculty of Science, Prince of Songkla University, National Electronics and Computer Technology Center (NECTEC), and School of Chemical Science, Universiti Sains Malaysia, Malaysia, for all necessary laboratory facilities used throughout this research.

I would like to thank my family, my friends, and all of my collaborators who helped creating an enjoyable atmosphere to for working and for their helpful in many countless ways throughout the years.

Wankassama Haron

CONTENTS

Page

CONTENTS (CONTINUED)

LISTS OF FIGURES

LISTS OF FIGURES (CONTINUED)

LISTS OF FIGURES (CONTINUED)

LISTS OF FIGURES (CONTINUED)

LISTS OF FIGURES (CONTINUED)

LISTS OF TABLES

CHAPTER 1

INTRODUCTION

1.1 Introduction

Geologist Gustav Rose, the first person who discovered first perovskite of $CaTiO_3$ in the Ural Mountains in 1839 and it was named perovskite in recognition beholden to Count Lev Alexevich von Perovski, an eminent Russian mineralogist. The name perovskite represented any compound that has ABO_3 formula where an octahedron of O ions surrounded the B ion (F. Nada, et al., 2016).

Perovskite oxide with formula ABO_3 or A_2BO_4 are very important class of functional materials that exhibit a range of stoichiometries and crystal structure. Because of the structure features, they could accommodate around 90% of the metallic natural elements of the periodic table that stand solely or partially at the A and/or B positions without destroying the matrix structure, offering a way of correlating solid state chemistry to catalytic properties. Moreover, their high thermal and hydrothermal stability enable them suitable catalytic materials either for gas or solid reactions carried out at high temperatures, or liquid reaction carried out at low temperatures (J. Zhu, et al., 2014).

Perovskite oxides exhibit an array of electrical properties and a variety of solid-state phenomena from insulating, semiconducting, metallic, and superconducting characters; therefore, they are very fascinating to be studied and applied in a large scale (F. Nada, et al., 2016). Perovskites can find applications to many fields of solid oxide fuel cells (as electrode materials), chemical sensors, oxygen-permeating membranes, thermoelectric devices, and as catalyst for combustion of CO, hydrocarbons, and NOx decomposition. For these applications, it is important to prepare high-quality and homogeneous powders with controlled stoichiometry and microstructure. In most cases, the presence of secondary phases may reduce the functional properties, so the single phase materials are preferred (O. Haas, et al., 2004, H.F. Yu, et al., 2009, M.M. Rao, et al., 2006).

La-base oxide of $LaMO_3$ has interesting electrical and electrocatalytic properties, such as very high electronic conductivity and good ionic conductivity. The properties of this material are strongly dependent on the preparation method and, hence, in real applications the performance may be varied depending on preparation (S. Farhadi, et al., 2010, X. Chu, et al., 2009, Z. Tian, et al., 2009). Many methods to

prepare nanostructured materials have been reported: reverse microemulsion nanoreactor method (X. Wang, et al., 2013, Z. Tian, et al., 2009, R. Abazari, et al., 2013), solid state reaction or thermal decomposition (S. Farhadi, et al., 2010, X. Chu, et al., 2009, W. Kaituo, et al., 2014, M.C. Carotta, et al., 1997, Z. Kaiwen, et al., 2013, S. Zhao, et al., 2000, Y.M. Zhang, et al., 2014, X. Liu, et al., 2008), sol-gel method (S. Zhao, et al., 2000, Y.M. Zhang, et al., 2014, X. Liu, et al., 2008, K. Rusevova, et al., 2014, K. Fan, et al., 2012), combustion process (R. Ianos, et al., 2014, Z.Q. Tian, et al., 2007), electrospinning method (W.Y. Lee, et al., 2014, S. E. Moon, et al., 2012), biotemplate method (P. Song, et al., 2014, P. Song, et al., 2012), glycine nitrate method (K. Kleveland, et al., 2000), nanocasting method (J. Zhao, et al., 2013), citrate method (K. Li, et al., 2000), polymerizable complex method (M. Popa, et al., 2012), and co-precipitation method (S. Tao, et al., 2000, Z. Junwu, et al., 2007). These techniques, however, have some disadvantages for the preparation of high specific surface area perovskites. The temperature required to induce the perovskite structure in the conventional ceramic methods is usually high. The high temperature can be lowered slightly in the above mentioned methods due to the finely dispersed oxides in the precursors. Nevertheless, this “low” temperature is still high enough (> 600 °C) to enhance grain growth and, hence, to reduce the specific surface area (M. Ghasdi, et al., 2010).

1.2 Review of Literature

1.2.1 Perovskite and structure

The perovskite oxides have the general formula ABO_3 (A cation of larger size than B). Although the most numerous and most interesting compounds with the perovskite structure are oxide, some carbides, nitrides, halides, and hydrides also crystallize in this structure. The broad diversity of properties that these compounds exhibit is derived from the fact that around 90% of the metallic natural elements of the Periodic Table are known to be stable in a perovskite type oxide structure and also from the possibility of synthesizing multicomponent perovskite by partial substitution of cation in positions A and B, giving rise to substituted compounds with formula of $A_{1-x}A'_xB_{1-x}B'_xO_3$. These characteristics account for the large variety of reaction in which they are used as catalysts.

The ideal perovskite-type structure is cubic. In the unit formular of perovskite-type oxides ABO_3, A is the large cation and B is the smaller cation. In this

structure, the B cation is 6- fold coordinated and the A cation is 12-fold coordinated with the oxygen anions. In the ideal structure, where the atoms are touching one another, the B-O distance is equal to a/2 (a is the cubic unit cell parameter) while the A-O distance is (a/√2) and the following relationship between the ionic radii holds: $r_A + r_O = \sqrt{2}\,(r_B + r_O)$. However, it was found that the cubic structure was still retained in ABO_3 compounds, even though this equation is not exactly obeyed. As a measure of the deviation from the ideal situation, Goldschmidt introduced a tolerance factor (t), defined by the equation:

$$t = (r_A + r_O) / \sqrt{2}\,(r_B + r_O)$$

which is applicable at room temperature to empirical ionic radii. Although for an ideal perovskite t is unity, this structure is also found for lower t- value ($0.75 < t < 1.0$). The ideal cubic perovskite structure appears in a few cases for t- values very close to 1 and at hight temperatures. In most cases, difference distortions of the perovskite structure appear. The naturally occurring compound $CaTiO_3$ was originally thought to be cubic, but its true symmetry was later shown to be orthorhombic.

The simple perovskites structure may be appropriately modified by incorporating two types of B ions with suitable difference size and charge. The most frequent substitutions are the equiatomic proportions of the two ions at the B-site, for which the general formula of the perovskite is $A_2BB'O_6$ (or $AB_{0.5}B'_{0.5}O_3$). The resulting unit cell may be viewed as doubled along the three axes, regarding the primitive cell of ABO_3. If the charge of B and B' is difference, in the orderd the more charge cation although the octahedral symmetry of B and B' cations is preserved.

Deviations from the ideal structure with orthorhombic, rhombohedral, tetragonal, monoclinic, and triclinic symmetry are known, although the latter three are scarce and poorly characterized. The distorted structure may exist at room temperature, but it transforms to the cubic structure at high temperature. This transition may occur in several steps through intermediate distorted phases. These deviations from the cubic perovskite structure may proceed from a simple distortion of the cubic unit cell, or an enlargement of the cubic unit cell, or a combination of both (M.A. Pena, et al., 2001).

1.2.2 The method for synthesized perovskite compound

There have been many researches having studied the syntheses of $LaMO_3$ (M = Al, Co, Fe, Gd) perovskite compounds such as :

R. Ianosn, *et al* (2014) prepared single-phase $LaAlO_3$ by a simple combustion synthesis procedure, which relied on using urea and β-alanine fuel mixture, instead of a single fuel. The aqueous solution of $La(NO_3)_3$, $Al(NO_3)_3$, urea, and β-alanine underwent a strong exothermic reaction at 281 ℃, thus enabling the formation of single-phase $LaAlO_3$ directly from the combustion reaction without the need of supplementary annealing. The combustion synthesized $LaAlO_3$ had an average crystallite size of 46 nm and a BET surface area of 3.0 m^2/g. The addition of NaCl to the reaction mixture decreased the combustion temperature, promoting an increase of the BET surface area (8.5 m^2/g). At the same time the $LaAlO_3$ crystallite size decreased to 36 nm. After sintering at 1500 ℃ for 5h, $LaAlO_3$ pellets developed a fine microstructure, reaching 94% of the theoretical density.

H. H. Sonsteby, *et al* (2014) synthesized highly epitaxial thin films of lanthanum aluminate ($LaAlO_3$) from strontium titanate ($SrTiO_3$) substrates by means of atomic layer deposition using $La(thd)_3$ (Hthd = 2,2,6,6-tetramethylhepta-3,5-dione), $Al(CH_3)_3$, and ozone as precursors. The system showed a near linear relationship between pulsed and deposited composition. Thin films with stoichiometric composition was annealed at 650 ℃ under oxygen atmosphere, thereby achieving epitaxial films on Ti-O-terminated substrates of $SrTiO_3$. The thin film was characterized as $LaAlO_3$(100) and $SrTiO_3$(100) using of synchrotron radiation. Selected films were also deposited on $LaAlO_3$(100) to achieve homoepitaxy. This resulted in the observation of split peaks for high q-reflections, pointing towards slight differences in stoichiometry. For ultrathin films, Bragg satellites were observed around the specular reflections, coming from either surface or interface reconstruction.

W. Kaitou, *et al* (2014) synthesized $LaCoO_3$ by solid-state reaction at low temperatures using $La(NO_3)_3.6H_2O$, $CoSO_4.7H_2O$, and $Na_2C_2O_4$ as raw materials. $LaCoO_3$ was obtained by calcining a precursor,0.97/2 $La_2(C_2O_4)_3$–$CoC_2O_{4x}5.3H_2O$, at 1123 K in air. The precursor and its calcined products were characterized by thermogravimetry and differential scanning calorimetry, Fourier-transformed infrared spectroscopy, X-ray powder diffraction, and scanning electronmicroscopy. A high-crystallized $LaCoO_3$

with a rhombohedral structure was obtained when the precursor was calcined at 1123 K in air for 2 h. The values of the activation energies associated with the thermal transformation of 0.97/2 $La_2(C_2O_4)_3$–CoC_2O_4x $5.3H_2O$ were determined based on the Starink equation. In conclusion, the authors successfully synthesized a rhombohedral $LaCoO_3$ by calcining $0.97/2La_2(C_2O_4)_3$–$CoC_2O_{4.5}.3H_2O$ in air. The XRD analysis suggested a rhombohedral $LaCoO_3$ with a crystallite size of 52 nm was obtained by calcining $0.97/2La_2(C_2O_4)_3$–$CoC_2O_{4.5}.3H_2O$ at 1123 K in air for 2 h. The thermal transformation of $0.97/2La_2(C_2O_4)_3$–CoC_2O_4·$5.3H_2O$ from ambient temperature to 1150 K experienced six steps, namely, the dehydration of 0.3 adsorption water, the dehydration of 2.5 crystal waters, the dehydration of 2.5 crystal waters, the reaction of CoC_2O_4 with $2/3O_2$ into $1/3Co_3O_4$, the reaction of $0.97/2La_2(C_2O_4)_3$ with $0.7275O_2$ into $0.97/2La_2O_2CO_3$, and the reaction of $0.97/2La_2O_2CO_3$ and $1/3Co_3O_4$ with $0.5/6O_2$ into the rhombohedral $LaCoO_3$. The thermal transformation of $0.97/2La_2(C_2O_4)_3$– $CoC_2O_{4.5}.3H_2O$ for steps 1, 2, 5, and 6 was multi-step reaction mechanisms, whereas those for steps 3 and 4 were simple reaction mechanisms.

Y.M. Zhang, *et al* (2014) investigated the $LaFeO_3$ modified with silver (Ag–$LaFeO_3$) and further modified by single-walled carbon nanotubes(SWCNTs–Ag–$LaFeO_3$) with different weight ratio using a sol–gel method combined with the microwave chemical synthesis. The phase structures and micro-morphology of SWCNTs–Ag–$LaFeO_3$ were characterized by X-ray diffraction (XRD) and transmission electron microscope (TEM), respectively. Indirect-heating sensors using SWCNTs–Ag–$LaFeO_3$ sensitive materials were fabricated on an alumina tube with Au electrodes and platinum wires. Gas-sensing characteristic of SWCNTs–Ag–$LaFeO_3$ to formaldehyde was investigated. It was found that the structure of SWCNTs–Ag–$LaFeO_3$ was of orthogonal perovskite. The gas-sensing properties of the Ag–$LaFeO_3$ sample modified by SWCNTs with 0.75% weight ratio (0.75% SWCNTs–Ag–$LaFeO_3$) was the best. The response of 0.75% SWCNTs–Ag–$LaFeO_3$ powder to 0.5 ppm formaldehyde was 23 at 86 ˚C. The detection limit to formaldehyde was 0.2 ppm. The response and recovery times were 6 s and 20 s, respectively. Those good properties made them the promising candidates for practical detectors to formaldehyde.

P. Song, *et al* (2014) studied biomorphic porous $LaFeO_3$ which had been successfully fabricated using sorghum straw as biotemplate. This simple synthesis route could be expected to be extended for the preparation of biomorphic porous

metal oxide gas-sensing materials. The structure and morphology of the products were characterized by X-ray diffraction (XRD), scanning electron microscope (SEM), transmission electron microscope (TEM), and N_2 adsorption–desorption analyses. Testing results revealed that the as-prepared $LaFeO_3$ showed the porous and network frameworks was replicated the structure of sorghum straw. Moreover, the framework was assembled by a large amount of interconnected nanocrystallites with the sizes of about 20–30 nm, and there were plenty of voids between the nanocrystallites in the framework. Gas sensing investigation showed that the sensor based on biomorphic porous $LaFeO_3$ exhibited higher response to acetone gas compared with that of bulk $LaFeO_3$ particles. The enhancement in gas sensing properties was attributed to their porous structure, large surface areas, numerous surface active sites and more oxygen vacancies.

S.P. Pavunny, *et al* (2014) studied the room temperature crystal structure of potential high-k dielectric $LaGdO_3$ had been analyzed by X-ray diffraction techniques and its structural evolution with temperature had been probed by Raman spectroscopy. Rietveld refinement of the ambient XRD data established the perfectly layered B-type monoclinic crystal structure with a = 14.43 Å , b = 3.68 Å, c = 8.99 Å and β = 100.578 which was further validated by the 21 (14 A_g and 7 B_g) Raman-active vibrational modes with centro-symmetric space group C^3_{2h} or C2/m. Atomic positions, coordination numbers, inter-ionic lengths, etc. were derived using Rietveld analysis. All prominent Bragg peaks were successfully indexed. Temperature dependent Raman spectra of $LaGdO_3$ from 80 to 1400 K were analyzed using the damped harmonic oscillator model. The softening and hardening of vibrational modes were reported. Above 900 K, disappearance of all high frequency modes (>600 cm^{-1}) and merger of several mid frequency modes (between 200 and 500 cm^{-1}) into two distinct modes was observed, a direct evidence of a possible structural phase transition from monoclinic to tetragonal/ pseudocubic.

W.C. Lo, *et al* (2013) studied tuning transport properties of two-dimensional electron gas (2DEG) at the $LaAlO_3/SrTiO_3$ interface by surface modification which was of great interest due to its rich physics and potential application in gas sensors. From first-principle calculations, they found that the adsorption of a thin layer of polar water molecules on the surface of $LaAlO_3$ could remarkably enhance the carrier density of the interfacial 2DEG by over at least 50% which was qualitatively consistent with reported experimental result. This result sheded light on the charge

coupling between surface polar molecules and interfacial 2DEG and suggested that sensor devices might be built using the hetero-oxide interfacial 2DEG.

X. Wang, *et al* (2013) studied the preparation of $LaFeO_3$ nanocrystalline powders by sol-gel method with annealing at 800°C for 2 h. The sensor based on $LaFeO_3$ powder showed considerable sensing response to carbon dioxide. With increasing concentration of carbon dioxide, the resistance of the $LaFeO_3$ sensor increased. At 300 °C, the responses of $LaFeO_3$ sensor to 1000, 2000, and 4000 ppm CO_2 gas were 1.74, 2.19, and 2.74. respectively. The response and recovery times at 300 °C for the sensor to 2000 ppm CO_2 were about 4 and 8 min, respectively. Their first-principle calculations demonstrated that CO_2 could release electrons to the surface of $LaFeO_3$ (010) pre-adsorbed with high concentration of oxygen (M5 mode) which was consistent with the experimental results.

S. Fu, *et al* (2013) synthesized perovskite-type $LaCoO_3$ hollow nanospheres by a simple method in relatively low calcinations temperature at 550 °C by utilizing the carbonaceous colloids as template and internal heat source. The influence of calcinations temperature and time on the morphology and crystallinity of the product was investigated. The UV-vis analysis showed that the product had a broad and strong absorption at 220-550 nm region with narrow band gap of 2.07 eV. The $LaCoO_3$ hollow nanospheres exhibited excellent photocatalytic activity for degradation of methylene blue, methyl orange, and neutral red, making it a promising candidate for other environmentally friendly applications.

R. Abazari, *et al* (2013) synthesized spherical $LaFeO_3$ NPs using in reverse microemulsion route. The obtained NPs were characterized by various techniques (such as FE-SEM, TEM, EDAX, XRD, UV-Vis, PL. and FT-IR analyses). The surface morphological studies confirmed the formation of highly monodispersed $LaFeO_3$ NPs with size of about 4 – 32 nm. Through this method, highly crystalline and well-dispersed perovskite $LaFeO_3$ NPs with a pure phase were successfully synthesized. The calcinated particles of $LaFeO_3$ NPs exhibited orthorhombic structure as determined through XRD analysis. In addition, optical properties of the obtained NPs were tested and discussed. UV-Vis spectrum results showed that the prepared $LaFeO_3$ NPs had strong UV-light absorption at about 322 nm. The chemical structure information of the particles was also studied by FT-IR spectroscopy. In general, the important advantage offered by this method was performing the process in one step

and at room temperature. Moreover, the surfactants surrounding the particles in the solution could easily be removed. Thus, the method was an economic procedure from both energy and time perspectives.

L. Predoana, *et al* (2013) presented the correlation between the structure and properties of the $LaCoO_3$ powders obtained by aqueous sol–gel method with citric acid and their sintering behavior in order to obtain fully densified ceramics with perovskite structure. Two types of cobalt and lanthanum reagents were used in synthesis, namely nitrates and acetates. The sintering was realized at temperatures ranging between 800 and 1200 °C for 2 h. The sintered samples were investigated by classical ceramic methods (shrinkage, density, porosity) and by structural and morphological investigations: XRD, SEM, AFM and XPS. The electrical properties of the samples were determined by impedance spectroscopy. The ceramics obtained from acetates showed a lower sintering ability compared to the samples obtained from nitrates. $LaCoO_3$ ceramics with best properties was obtained from powders starting with nitrates sintered at 1100 °C. Sintering studies of $LaCoO_3$ powders prepared by sol–gel method using two types of precursors, nitrates or acetates and citric acid as chelating agent were done. Pure $LaCoO_3$ perovskite nano-powder was obtained at 600 °C for both precursors, a low temperature as compared to the data mentioned in the literature. Dense ceramics could be obtained from both synthesized powders in the 1000–1200 °C temperature range. The sintered samples were characterized by SEM, XRD, AFM and XPS. The best results were obtained $LaCoO_3$ powders obtained from nitrates and sintered at 1100 °C. The electrical properties of the samples were investigated by impedance spectroscopy. The higher electronic conductivity of ceramics obtained from powder based on acetates at low temperature could be explained by the presence of Co_3O_4 on its surface.

J. Zhao, *et al* (2013) prepared mesoporous $LaFeO_3$ with high surface area and pore volume through a nanocasting route by using mesoporous silica SBA-15 as a hard template. The structure and chemical composition of the sample were characterized by X-ray diffraction (XRD), nitrogen adsorption–desorption, transmission electron microscopy (TEM), and inductively coupled plasma mass spectrometry (ICP-MS). The humidity sensing properties of the mesoporous $LaFeO_3$ were investigated. Impedance greatly changes by more than five orders magnitude (1.7×10^6 to 4.5 kΩ) when the relative humidity varied from 11% to 98% at 10 Hz, and it also exhibited the satisfactory response time, hysteresis and stability. The sensor utilizing

mesoporous $LaFeO_3$ via nanocasting method displayed superior humidity performance compared to that using bulk $LaFeO_3$ via sol–gel technique. Such sensing behavior of the mesoporous $LaFeO_3$ could be attributed to the high surface area (83.2 m^2/g) and porosity, which led to highly effective interaction between the water molecules and the surface active sites. A possible mechanism was discussed to explain the excellent performance of the humidity sensing device using the mesoporous $LaFeO_3$.

M.C.A Consuelo, *et al* (2011) prepared $LaCoO_3$ perovskite by simultaneous precipitation of cobalt and lanthanum from a solution of nitrate salts of cobalt and lanthanum after using K_2CO_3 precipitating agent.

The following conclusions were derived from the results of their work : CO and CO_2-TPD along with XPS studies conducted over pre-reduced (10%H_2/N_2 gas mixture at 50^{o}C for 2 h) $LaCoO_3$ and Ru /$LaCoO_3$ solids led to the conclusion that cannot be completely reduced to Co^{2+} species was obtained for the solid derived from $LaCoO_3$ after pre-reduction than cobalt cannot be completely reduced to Co^{o}. A greater fraction of unreduced Co^{2+}spcies was obtained for the solid derived from $LaCoO_3$ after per-reduction at 750^{o}C for 2h in 10% H_2/N_2 gas mixture. This had a detrimental effect in the propane since unreduced cobalt is not active towards the latter process. In addition, the presence of an increased surface concentration of Co^{2+}favours re-adsorption of the main reaction products, CO and CO_2 which could eventually reduce catalyst activity by blocking active catalytic sites dissociation at least. TPSR of propane indicated then surface lattice oxygen present in pre-oxidized $LaCoO_3$ and Ru/ $LaCoO_3$ solids participate in the oxidation of propane which resulted in the catalysts in the formation of CO,CO_2 , H_2 and CH_4 and “carbonaceous” deposits on the catalyst surface. It was found that the presence of Ru in the Ru/ $LaCoO_3$ solid composition largely reduced the rate of formation of “carbonaceous” deposits. Also, the kinetics of H_2 formation was found to be largely influenced by the catalyst pre-treatment performed (oxidation versus reduction) and largely promoted by the presence of Ru and of reduction cobalt phase. Enhanced reactivity of Ru propane over the Ru / $LaCoO_3$ than $LaCoO_3$ surface for either oxidative or reductive pre-treatments was observed during TPSR. It appeared that the presence of Ru retards “carbonaceous” deposits and premoted syngas (CO/H_2) formation.

C. Feng, *et al* (2011) prepared $LaCo_xFe_{1-x}O_3$ nanoparticles (x = 0, 0.1, 0.2, and 0.3) by a sol–gel method, and the effects of calcination temperature, Co-doping,

and carbon nanotube (CNT)-treatment on their ethanol sensing properties were investigated. The highest response was found based on the $LaCo_{0.1}Fe_{0.9}O_3$ nanoparticles calcined at 600 °C, and the sensing properties of this sample could be further improved by adding CNT in the precursor. The responses of un-treated and CNT-treated $LaCo_{0.1}Fe_{0.9}O_3$ nanoparticles were about 120.1 and 137.3 – 500 ppm ethanol at 140 °C, respectively. Simultaneously, by CNT-treatment, the response time decreased from 56 to 10 s, and the recovery time decreased from 95 to 35 s. The results not only made $LaCo_{0.1}Fe_{0.9}O_3$ nanoparticles good candidates for fabricating practical gas sensors, but also provided a possible route for employing CNTs as a pore-forming agent.

J.A. Villoria, *et al* (2011) studied oxidative reforming of diesel fuel over Co/La_2O_3 catalysts derived from $LaCoO_3$ perovskite precursors synthesized by co-precipitation (COP), sol–gel (PEC), and combustion (SCS) methods. Physical–chemical characterization of perovskite precursors by N2-adsorption isotherms, Hg-intrusion porosimetry, XRD, XPS, TPR and SEM showed that the method of preparation produced changes in the porosity and homogeneity both at bulk and surface levels of the $LaCoO_3$ perovskite precursors. The perovskite prepared by the SCS method achieved a higher development of the porous network as well as higher homogeneity in bulk and surface compared to COP and PEC counterparts. By contrast, the PEC and COP methods produced perovskites with lower porosity and with the presence of some secondary phases such as Co_3O_4 and $La(OH)_3$. The modifications of the characteristics of $LaCoO_3$ perovskites directly affected the structure and morphology of the catalytic materials derived from the thermal pre-treatment of perovskites before the activity tests. The differences in catalyst characteristics resulted from a different reduction and interaction between the gaseous reducing stream and the initial $LaCoO_3$ perovskites which occurred during the thermal pre-treatment. The activity of the samples at the beginning of the reaction test followed the order: PEC > SCS > COP. The latter could be related to the different interaction of the catalysts with the reactants as well as with the larger presence of the La_2CoO_4 phase produced during the thermal pre-treatment. The evolution of the catalysts for long times on stream resulted in the activity order: SCS > PEC > COP. Characterization of used samples disclosed the key role of the Co^0 exposure on the catalyst surface as concerns the achieved catalytic activities and the extent of the $La_2O_2CO_3$ phase on catalysts as regards the inhibition of coke deposition.

M. Ghasdi, *et al* (2011) prepared a series of nanostructred $La_{1-x}Ce_xCoO_3$ perovskite-type (x ranging from 0 to 0.2), with a crystallite size of around 10 nm and a specific surface area of up to 55 m^2/g using the activated reactive grinding method. XRD results showed that Ce segregates as CeO_2 when the addition level exceeds 10 at%. CO was chosen as a typical reducing gas and its interaction with surface oxygen was investigated. TPD - O_2 was used to investigate the effect of Ce-doping on total surface oxygen. The experimental results confirmed a positive effect of Ce-doping of up to 10 at% on total surface oxygen. TPD-CO and XPS analyses were performed to find the total carbon adsorption (i.e. related to the adsorption of CO) on the surface of the synthesized samples. Both methods confirmed that more carbon adsorbs on the surface of doped formulations compared to the pure $LaCoO_3$. Ce-doping increases the surface oxygen, thereby facilitating the adsorption and oxidation processes. CO gas sensing properties of thick $La_{1-x}Ce_xCoO_3$ films were performed. $La_{0.9}Ce_{0.1}CoO_3$ showing the highest conductivity and the lowest activation energy. The optimum CO sensing temperature for doped formulation was found to be 100 °C compared to 130 °C for pure perovskite. Ce-doped samples showed a maximum response ratio of 240% with respect to 100ppm CO in air compared to 60% obtained with pure $LaCoO_3$.

J. Feng, *et al* (2011) studied the effect of PVA base by sol-gel method to synthesize $LaFeO_3$. The effects of the molar ratios of positively charged valences to hydroxyl groups of PVA (M^{n+}/-OH) on the formation of $LaFeO_3$ were studied. Single-phase and well-crystallized $LaFeO_3$ was obtained from the M^{n+}/-OH = 4:1 precursor at 700 °C and the $La_2O_2CO_2$ phase was observed as reaction intermediates. For the precursor with M^{n+}/-OH = 2:1, nano-crystalline $LaFeO_3$with an average particle size of ~50 nm can be directly obtained from the charring procedure, without any other undesired phases. With increase of PVA content to M^{n+}/-OH= 1:1, phase pure $LaFeO_3$ was achieved at 500 °C.

H.T. Ginang, *et al* (2011) synthesized nano-crystalline oxides $LnFeO_3$ (Ln= La, Nd, and Sm) with orthorhombic structure by sol-gel citrate technique. The $LnFeO_3$-based sensors were investigated for the gas sensing characteristics in air containing methane, propane, and n-hexane gas. It was found that rare earth elements play the important roles to gas sensitivities of nano-crystalline oxides $LnFeO_3$. The oxygen adsorption characteristics governed by the magnitude of the relative structural distortions of the $LnFeO_3$ lattices as well as the strength of carbon

hydrogen bonds in n-hexane compound might be the parameters to explain the extreme sensitivities to n-hexane of the $NdFeO_3$ and $SmFeO_3$ sensors. The decrease of response and recovery times in sequence of $LaFeO_3$, $NdFeO_3$, and $SmFeO_3$ sensors could be accounted over the distortion of perovskite structure

S.P. Pavunny, *et al* (2011) studied the electrical properties of $LaGdO_3$ (LGO) where high-k dielectric thin films prepared by pulsed laser deposition (PLD) on SiO_x/p-Si substrate were studied. The equivalent oxide thickness (EOT) and gate leakage current density (J_g) were determined on metal-oxide-semiconductor (MOS) structures. Capacitance-Voltage characteristics showed negligible hysteresis, ~8 mV. The extracted dielectric constant (k) of LGO layer from the EOT-physical thickness plot was ~21.6 ± 1.7. LGO layers with EOT of 3nm had a Jg ~ 3 x 10^{-8} A/cm^2 at accumulation (Vg = V_{FB}-1). The estimated interfacial trap density at the flat band voltage as determined by Lehovec method was in the range 10^{12} $eV^{-1}cm^{-2}$. N-channel LGO metal-oxide-semiconductor field effect transistors (MOSFET) were fabricated and electrically characterized. The threshold voltage (V_t) was ~0.3 V.

M. Ghasdi, *et al* (2010) prepared $LaCoO_3$ perovskite samples in powder form using solid-sate reaction, sol-gel and high energy ball milling (HEBM) methods. X-ray diffraction patterns, SEM images, and TPD-O_2 profiles revealed the significant differences in physical properties. Dip-coating process was used to prepare continuous thick sensing films on alumina substrate. Compared to the other methods, HEBM resulted in the lowest crystallite size of 11 nm, the highest amount of grain boundaries, and the best CO gas sensing properties while the specific surface area of all samples remained similar. Mean crystallite size and grain boundary volume were found to affect the gas sensing properties. The maximum response ratio was increased from 7% for the SSR samples to 17% and 26% for the sol-gel and BM samples, respectively. The maximum response ratio temperature was also decreased from 175 °C for the sol-gel samples (20 nm) to 125 °C for the BM samples (11 nm). Specific surface area of the BM sample was successfully increased from 4m^2/g to an optimum value of 66 m^2/g by an additional milling step. The oxygen mobility was also drastically increased by increasing the second milling time and surface area. Maximum response ratio of all samples with respect to CO showed a good correlation with the total amount of desorbed oxygen measured by TPD-O_2. The results showed that the response ratio could be increased by up to 75% at 125 °C. which is four and ten times better than those obtained by sol-gel and solid-state

reaction methods, respectively. HEBM technique could therefore be considered as a low cost and waste free technique to synthesize nanocrystalline perovskite materials with improved response ratio and low operation temperature.

J. Yang, *et al* (2010) synthesized $LaFeO_3$ nanocrystals in molten $NaNO_2$ at 450-750 °C. molten $NaNO_3$-KNO_3 at 650 - 800 °C and molten $NaNO_3$-KNO_3 with Na_2O_2 at 800-850 °C for 2h, respectively. $LaCoO_3$ nanocrystals were successfully synthesized in molten $NaNO_2$ at 550 - 750 °C, molten $NaNO_3$-KNO_3 at 650-850 °C and molten $NaNO_3$-KNO_3 with Na_2O_2 at 550-750 °C for 2h. respectively. $LaNiO_3$ nanocrystals were successfully synthesized in molten $NaNO_2$ at 750 °C, and molten $NaNO_3$-KNO_3 with Na_2O_2 at 550-750 °C for 2 h. respectively. The oxidising properties and basicity of the melt play an important role in the synthesis of $LaMO_3$. The addition of Na_2O_2 increased the basicity and the ability to stabilise high oxidation states. With the addition of Na_2O_2, the morphology of $LaCoO_3$ synthesized at 750 °C changed from agglomerates of spherical particles (system B2) to cubic particles (system C2) and the particle size increased sharply from about 0.63 μm to 4.0 μm. The $LaNiO_3$ prepared in $NaNO_3$-KNO_3 eutectic with Na_2O_2 had a much larger particle size than that synthesized in molten $NaNO_2$.

J. Yang, *et al* (2010) prepared biomorphic $LaFeO_3$ hollow fibers with porous walls using cotton fibers as biotemplates. XRD patterns showed that all the samples were perovskite phase with orthorhombic structure as the only detectable phase. As shown in SEM images, all samples were very long and hollow, with inner diameters ranging from 4 to 10 μm, and with porous walls, which could increase the active surface area and gas diffusion. The maximum response (64%) was found in the case of sample calcined at 800 °C, which was lager than that of pure $LaFeO_3$ powders, due to its well-defined structure with hollow and porous wall.

S. Farhadi, *et al* (2010) investigated synthesis of $LaCoO_3$ by rapid decomposition of the $La[Co(CN)_6]\cdot 5H_2O$ under microwave irradiation with the assistance of CuO as the secondary heater. The obtained $LaCoO_3$ nanoparticles had narrow size distribution (10–30 nm) with high specific surface area (27 $m^2\ g^{-1}$). The smaller particles of the $LaCoO_3$ with high purity and short reaction time were other significant advantages of this method compared with most reported methods. This method was used for synthesizing other $LnCoO_3$ such as $SmCoO_3$, $NdCoO_3$ and $GdCoO_3$ and they expected that the $LaCoO_3$ nanoparticles would be more attractive

in electrical and catalytic applications. This method should be promising for preparation of other mixed oxide and related compounds.

Z. Tian, *et al* (2009) prepared spherical $LaAlO_3$ nanoparticles in a reverse microemulsion consisting of solution (water phase), Tween-80 and Span-80 (surfactant), n-butanol (cosurfactant, and cyclohexane (oil phase). A pure perovskite $LaAlO_3$ formed when the precursor hydroxides calcined at 800 °C for 2 h. The particle size was about 50 nm and the shape of the monodisperse particles was spherical. The reverse microemulsion process could dramatically lower the crystallization temperature of $LaAlO_3$ about 700 °C than the classical solid-state reaction method.

S. Farhadi, *et al* (2009) synthesized $LaFeO_3$ by rapid decomposition of the $La[Fe(CN)_6]$-$5H_2O$ under microwave irradiation in the presence of SiC as the secondary heater. The obtained $LaFeO_3$ with nanometer size showed a relatively high value in specific surface area of about 36.5 $m^2 g^{-1}$. The smaller particles of the $LaFeO_3$ with high purity and short reaction time were the significant advantages of this method as compared with the well-known thermal decomposition of La $[Fe(CN)_6]$ and other reported methods. This method could also be applicable to the synthesis of other mixed oxides such as $SmFeO_3$, $NdFeO_3$, and $GdFeO_3$ and the obtained $LaFeO_3$ nanoparticles might be more attractive in the catalytic application.

S. Haiyun, *et al* (2009) prepared perovskite-type oxide nanocrystalline $LaCoO_{3-}$ using the citrate method. The mechanism of the citrate method was suggested as follows: initially the metal complex was formed by a combination of citric molecules, and was than decomposed into the aconitic acid complex. Finally, the aconitic acid complex decomposed into an oxycarbonate and then into the pervoskite-type oxide. The mechanism was proved by the IR spectra. The structure and morphology of the samples were characterized by powder X- ray diffraction (XRD) and transmission microscopy (TEM). The intermediate products were analyzed by thermal gravimetric and differential thermal analysis (TG-DTA) techniques. The results that nanocrystalling $LaCoO_{3-}$ with a granula of 30-50 nm had a cubic perovskite structure.

L.J. Berchmans, *et al* (2008) prepared lanthanum aluminate ($LaAlO_3$) by combustion synthesis process using nitrate salts of lanthanum and aluminium as cation precursors and urea as the fuel. The powder density and the compacted

pellet density were determined. Sintering process reduced the porosity of the pellets by the agglomeration process. The conductivity of $LaAlO_3$ increased with sintering temperature and the value was found to be 1.75 Scm^{-1} at 1000 °C. The dielectric constant and loss tangent values are found to decrease with the applied frequency. This might be due to the change in orientation and ionic effects resulted from the inertia of ions and molecular levels. The XRD studies revealed that the material was assigned to be a pseudocubic structure. The FTIR spectra showed higher frequency and lower frequency bands which were assigned to AlO_6 octahedra in $LaAlO_3$. SEM micrographs revealed the presence of platelet aggregated into globular mass with larger surface area. The electrochemical polarization was performed in 0.5–2.0 M KOH. In general, the corrosion kinetic parameters showed that the green samples were found to be prone to corrosion than the sintered materials.

A. Worayingyong, *et al* (2008) investigated a novel Schiff base complex sol–gel method has been used to prepare $LaCoO_3$ producing high ratios of adsorbed (or surface) oxygen to lattice oxygen. The as-prepared gels, characterized by Fourier-transformed infrared spectroscopy (FTIR), showed that both lanthanum and cobalt ions were complexed before calcinations. IR spectra revealed that CO_3^{2-} and NO_3^- presented on the sample surfaces during heat treatment. High-resolution transmission electron microscopic (HRTEM) images of all samples showed resolved lattice fringes with the inter-planar spacing 0.37–0.39 nm of the (0 1 2) plane in hexagonal perovskite. BET surface areas of $LaCoO_3$ nano-crystals were 11.7–18.6 m^2/g. Ratios of adsorbed (or surface) oxygen to lattice oxygen quantified by X-ray photoemission spectroscopy showed that $LaCoO_3$ prepared by the Schiff base complex method produced higher ratios when bases had higher nitrogen content in molecules. Carbonate and nitrate resulting from the oxidation of functional groups in the Schiff base complex produced gaseous compounds and left vacant sites for oxygen in the gas phase to adsorb.

Z.Q. Tian, *et al* (2007) prepared pure $LaAlO_3$ powder by a combustion synthesis processing using a concentrated solution of nitrates of lanthanum and aluminate as oxidiser, and glycine acid as fuel, with the aim of obtaining nanosized crystallites of this material with high specific area at relatively low temperature. Precursor powders and calcined powders were characterized by differential thermal analysis (DTA), thermogravimetry analysis (TG), X-ray powder diffraction (XRD), and transmission electron microscopy (TEM). The results demonstrated that pure

perovskite $LaAlO_3$ powder formed at 700 °C for 2 h and the particle size ranges 78–100 nm. The specimen sintered at 1500 °C for 12 h showed the maximum bulk density and gave the best microwave dielectric properties: ε_r = 23 and Q_f = 38,000 GHz.

L. Predoana, *et al* (2007) prepared $LaCoO_3$ by sol-gel method using citric acid as chelating agent and different metal precursors. In all cases the dried gels obtained were amorphous and presented the characteristic IR vibration bands assigned to the reagents used in the reaction. The thermal decomposition of the dried gels occured stepwise upon heating 400 °C for acetate-based precursors, respectively, with a major exothermal effect at about 340 °C. Different crystalline phases were obtained by thermal treatment, depending on the starting composition of the sol-gel solutions. Pure perovskite $LaCoO_3$ phase is formed after heating at 600 °C for samples prepared starting with nitrates (N1,N2) and for A1 (prepared with acetates), while sample A2 was a mixture of La_2O_3, $La(OH)_3$, Co_3O_4 and $LaCoO_3$ in low amount. This behaviour was under further investigation. Some preliminary electrical and catalytic investigations performed on the N1 powder indicated that up to 400 °C the sample behaves as a n-type semiconductor. Propylene deep oxidation occured by Mars van Krevelen (redox) mechanism. Based on conductivity data, the lattice oxygen mobility was relatively low up to 400 °C

Z. Li, *et al* (2007) synthesised rhombohedral $LaAlO_3$ powder by reacting equimolar La_2O_3 and Al_2O_3 in a molten KF–KCl eutectic salt for 3 h between 630 and 800 °C. The lowest synthesis temperature (630 °C) was about 1000 °C lower than that of conventional mixed oxide synthesis, and close to or lower than those used by most wet chemical methods. The $LaAlO_3$ particle size increased from <3 to 3–7 μm with increasing temperature from 630 to 700 °C, but changed little on further increasing temperature to 800 °C. On the other hand, it decreased with increasing salt/oxide weight ratio from 1:1 to 6:1. The “dissolution–precipitation” mechanism played a dominant role in the molten salt synthesis of $LaAlO_3$.

Z. Junwu, *et al* (2007) developed a facile co-precipitation route for the synthesis of well-dispersed $LaCoO_3$ nanocrystals. The as prepared products were characterized by X-ray diffraction (XRD), transmission electron microscopy (TEM), energy dispersive X-ray spectrometer (EDX), and laser Raman spectroscopy (LRS). The results showed that modulating the growth parameters, such as the addition of

surfactants as well as the adding manner of the precipitator, had a significant effect on the overall shape and size of the obtained nanocrystals. The nanorods with the diameter of 20 nm and spherical $LaCoO_3$ nanocrystals with the size of about 25 nm could be obtained at a relatively low calcining temperature of 600 ℃.

Y. Wang, *et al* (2006) studied the synthesis of $LaFeO_3$ nanocrystals via the glycine combustion method and obtained $LaFeO_3$ crystals with fine grains of nanometer size give a relatively high value in specific surface area of about 7.9 m^2/g. This method could be also applicable to the synthesis of other complex oxides such as $LaCoO_3$, $LaNiO_3$, $NdFeO_3$.

S. Ajami, *et al* (2006) used $LaCoO_3$ perovskite as an active filter for elimination of the sensor sensitivity to CO and ethanol. Both CO and ethanol were completely removed by the filter at temperatures as low as 190 ℃. At 250 ˚C, the sensor sensitivity to ethanol dramatically decreased from 158 to 0.44 and that to CO declined from 2.2 to 0.9, when active filter was used. Only methane reached the Pt/SnO_2 sensor at temperatures higher than 190 ℃, for which the sensor showed high sensitivity to methane. As a result, $LaCoO_3$ perovskite filter eliminated the sensor sensitivity to CO and ethanol, making the sensor highly selective to methane in presence of CO and ethanol in air.

Y. Wang, *et al* (2004) synthesized nano $LaAlO_3$ powders with a size of about 50 nm through a simple co-precipitation method by using $La(NO_3)_3$ and $Al(NO_3)_3$ as raw materials and keeping the pH $\approx$ 9. A pure perovskite $LaAlO_3$ formed by heat treatment of the powder precursor at 700 ℃ for 32 h or at 800 ℃ for 2 h. The nano-$LaAlO_3$ powders had excellent sintering ability, a high relative density of about 97% could be reached after sintering at 1550 ℃ for 4 h.

D. Zhou, *et al* (2004) synthesized $LaAlO_3$ ceramic powders using a polymeric precursor derived from a mixed-metal ethylenediaminetetraacetic acid (EDTA)/ ethylene glycol solution. The precursors and derived oxide powders were characterized by differential thermal analysis, thermogravimetric analysis, infrared spectroscopy, X-ray diffraction and transmission electron microscopy. $LaAlO_3$ was found to crystallize directly from an amorphous precursor at 750 ℃ for 2 h in air, without intermediate phase formation.

W. Li, *et al* (2004) synthesized nano $LaAlO_3$ by co-preparation method powders. By using $La(NO_3)_3$ and $Al(NO_3)_3$ as raw materials and keeping the pH = 9, the co-preparation process could be obtained at room temperature. Pure $LaAlO_3$ nano powders with a size of about 50 nm could be obtained after calcining at 700–800 °C. These nano $LaAlO_3$ powders could be sintered at 1550 °C for 4 h, a high relative density of about 97% could be reached. Nano $LaAlO_3$ powders with a size of about 50 nm were successfully synthesized through this simple coprecipitation method. A pure perovskite $LaAlO_3$ formed by heat treatment of the powder precursor at 700 °C for 32 h or at 800 °C for 2 h.

M. Popa, *et al* (2004) prepared $LaMO_3$ (M = Mn, Fe, Co) perovskites by polymerizable complex method at 900 °C for 6 h with grain size of 80 nm. The products were examined by X-ray diffraction (XRD), scanning electron microscopy (SEM) and Raman spectroscopy. The Raman active phonons in perovskites crystallized in rhombohedral symmetry—($LaMnO_{3.15}$ and $LaCoO_3$) and orthorhombic symmetry—($LaFeO_3$) were reported. Raman spectra obtained for the studied systems are related to many factors as the laser irradiation and the structure of $LaMnO_{3.15}$, $LaFeO_3$, and $LaCoO_3$ which greatly depends on the method of preparation, particle size, oxygen content, symmetry, temperature or the oxygen partial pressure.

J. Shi, *et al* (2003) investigated combination of a novel NH_3 converter based on nanosized materials with chemiluminescence (CL) detector for the determination of NH_3 gas. NH_3 gas is oxidized on different nanosized catalysts to produce NO_x which reacted with luminol to generate CL emission. Eight nanosized materials were investigated as catalyst, and CL was detected from seven of them. The nanosized $LaCoO_3$ was chosen as the catalyst for preparing the converter because of its higher activity than others. Under the optimized conditions, the linear range of CL intensity versus concentration of NH_3 gas was 0.04 -10 ppm (r =/0.9951, n =/14) with the detection limit of 0.014 ppm. The method offered advantages of long lifetime of the converter, fast response and high selectivity to NH_3. There was no response while the foreign substances, such as hydrogen, oxygen, nitrogen, formaldehyde, acetone and gasoline passing through the CL detection system, and the interference of CCl_4, ethanol, ethylene and toluene was insignificant.

Y. Wang, *et al* (2002) prepared pure single-phase nanopowders of $LaMO_3$ (M = Mn, Co, Fe) with homogenous microstructure at low crystallization temperature by

polymerizable complex method. The Raman spectra of $LaMnO_{3.15}$, $LaFeO_3$, and $LaCoO_3$ with deviations from the ideal cubic perovskite structure were studied. The Raman spectra of $LaMnO_{3.15}$ and $LaCoO_3$ were strongly dependent on the laser beam power. Less than 24 modes allowed for the orthorhombic symmetry of $LaFeO_3$ and less than five modes allowed for the rhombohedral $LaMO_{3.15}$and $LaCoO_3$ were detected. The Raman intensity from the $LaFeO_3$ powders was the highest among the three studied compounds.

V.V. Kharton, *et al* (2001) prepared dense $LaCoO_3$ ceramics with different microstructures using the standard ceramic synthesis route (Method 1), the cellulose-precursor technique (Method 2) and a commercial powder obtained via combustion synthesis. The powders with submicron particle size, formed in Method 2 and via combustion synthesis, exhibited much higher reactivity and sinterability but worse compactability with respect to the powder obtained by the standard ceramic technique. Lanthanum cobaltite repared by the standard ceramic technique showed significantly higher oxygen permeation fluxes than those prepared using organic precursors. This was believed to be caused by a low grain-boundary resistance to oxygen ionic transport.

S. Zhao, *et al* (2000) studied the $LaFeO_3$ nano-crystalline thin-film of perovskite-type composite-oxides obtained by using a sol–gel coating technique, and the photo-etching technique was employed to etch and pattern the film. Combining this thin-film technology with the NMO_S integrated circuit technology, they developed an ethanol-sensitive field-effect transistor by using a $LaFeO_3$ nano-crystalline thin-film as a gate electrode of an ordinary n-channel MOSFET. The sensor has excellent selectivity, good sensitivity to ethanol, and a good stability.

E. L. Brosha, *et al* (2000) developed a new type of mixed potential sensor that utilizing a dense, thin film LCO electrode vs. a gold counter electrode. Mixed potential responses to CO and HCs at 600 °C and 700 °C were measured in air and this response increased as *P* levels were decreased. Some O_2 hysteresis was detected with varying oxygen partial pressure. The signal level exhibited by the sensors studied in this work was dependent on the annealing temperatures and extent of recrystallization of the Au counter electrode.

K. Kleveland, *et al* (2000) studied the densification, microstructure and phase evolution of near stoichiometric, co-excess and co-deficient perovskite $La_{1-x}M_xCoO_3$ (M = Ca, Sr; x = 0, 0.2) powders by electron microscopy and powder X-ray diffraction. Sub-micron powders were prepared from nitrate precursors using the glycin-nitrate and the EDTA methods. The sintering temperature was observed to decrease with Ca or Sr substitution. Dense materials with grain size in the order of 3±5 mm have been obtained at 1200 ℃ for near stoichiometric powders. Considerable grain growth was observed at higher sintering temperatures. The presence of other crystalline phases in addition to the perovskite due to co-excess/-deficiency considerably affected the microstructure and acted as grain growth inhibitors by grain boundary pinning. The volume fraction of secondary phases was particularly large in the case of co-deficient $LaCoO_3$ due to the formation of $La_4Co_3O_{10}$. In non-stoichiometric $La_{0.8}Ca_{0.2}CoO_3$, a liquid phase consisting mainly of CaO and CoO was observed at 1400 ℃ causing exaggerated grain growth. Considerable pore coarsening was observed in co-excess $La_{0.8}Ca_{0.2}CoO_3$ at 1350 ℃. This study demonstrated the importance of controlling the stoichiometry of $LaCoO_3$ based ceramics in order to obtain dense materials with well defined microstructure.

G.A. Tompsett, *et al* (1998) prepared $LaGdO_3$ via a reverse-strike coprecipitation method and sintered at temperatures of 1350-1450 ℃ for 6 h. Raman spectroscopy of the sintered materials revealed profiles similar to that observed for pure B-type Gd_2O_3. Low temperature (-196 ℃) Raman spectra showed a total of 18 bands of a possible 21 allowed modes predicted for the monoclinic B-type mixed rare earth oxide with C2/m space group. These bands were assigned to modes in comparison to the band assignments for Gd_2O_3 as follows; 71 (B_g), 82 (A_g), 98 (B_g), 109 (A_g), 124 (A_g 158 (A_g),182 (A_g)219 (A_g) 242 (A_g), 279 (A_g) 315 (B_g), 366 (A_g),390 (B_g), 419[B_g + (A_g)], 436 (A_g) 458 (A_g), 560 (A_g) and 575 (A_g) cm^{-1}. Powder X-ray diffraction patterns revealed a monoclinic pattern for materials sintered at all three temperatures; 1350, 1400 and 1450 ℃.

1.2.3 Gas sensor using perovskite materials

There have been many researches studying the gas sensing properties of perovskite such as :

Y.M. Zhang, *et al* (2014) modified $LaFeO_3$ with silver (Ag–$LaFeO_3$) and further modified by single-walled carbon nanotubes (SWCNTs–Ag–$LaFeO_3$) with different weight ratio using a sol–gel method combined with the microwave chemical synthesis. The phase structures and micro-morphology of SWCNTs–Ag–$LaFeO_3$ were characterized by X-ray diffraction (XRD) and transmission electron microscope (TEM), respectively. Indirect-heating sensors using SWCNTs–Ag–$LaFeO_3$ sensitive materials were fabricated on an alumina tube with Au electrodes and platinum wires. Gas-sensing characteristic of SWCNTs–Ag–$LaFeO_3$ to formaldehyde was investigated. The structure of SWCNTs–Ag–$LaFeO_3$ was orthogonal perovskite. The gas-sensing properties of the Ag–$LaFeO_3$ sample modified by SWCNTs with 0.75% weight ratio (0.75%SWCNTs–Ag–$LaFeO_3$) were the best. The response of 0.75%SWCNTs–Ag–$LaFeO_3$ powder to 0.5 ppm formaldehyde was 23 at 86 °C. The detecting limit to formaldehyde was 0.2 ppm. The response and recovery times were 6 s and 20 s, respectively. Those good properties made them the promising candidates for practical detectors to formaldehyde. The gas-sensing response of 1/99Ag–$LaFeO_3$ could be improved by incorporating with SWCNTs. That 1/99Ag–$LaFeO_3$ powder was uniform in size and dispersed homogeneously on the surface of SWCNTs to yield SWCNTs–Ag–$LaFeO_3$ composite powder which exhibited orthogonal perovskite crystal structure. The optimal amount of SWCNTs was x = 0.75%, the average grain size of the 0.75%SWCNTs–Ag–$LaFeO_3$ powder was about 28 nm. 0.75%SWCNTs–Ag–$LaFeO_3$ powder had high response and good selectivity for low concentration formaldehyde. As 1/99Ag–$LaFeO_3$ sample could detect formaldehyde concentrations higher than 1 ppm reasonably well, SWCNTs–Ag–$LaFeO_3$ composite powders having 0.75%SWCNTs could detect formaldehyde at concentrations even lower than 1 ppm with a reasonable response. The sensor response based on 0.75%SWCNTs–Ag–$LaFeO_3$ was 23 to 0.5 ppm formaldehyde at an operating temperature of 86 °C and the sensor also yielded a distinctive response to 0.2 ppm formaldehyde with very short response (6 s) and recovery (20 s) times. These findings indicated that the incorporation of SWCNTs with modified $LaFeO_3$ powder was a feasible way for exploring the capabilities of $LaFeO_3$-based sensing materials.

P. Song, *et al* (2014) presented the fabrication of biomorphic porous $LaFeO_3$ using sorghum straw as biotemplate. This simple synthesis route could be expected to be extended for the preparation of biomorphic porous metal oxide gas-sensing materials. The structure and morphology of the products were characterized by X-ray diffraction (XRD), scanning electron microscope (SEM), transmission electron microscope (TEM), and N_2 adsorption–desorption analyses. Testing results revealed that the as-prepared $LaFeO_3$ showed the porous and network frameworks replicating the structure characterizations of sorghum straw. Moreover, the framework was assembled by a large amount of interconnected nanocrystallites with the sizes of about 20–30 nm and there were plenty of voids between the nanocrystallites in the framework. Gas sensing investigation showed that the sensor based on biomorphic porous $LaFeO_3$ exhibited higher response to acetone gas compared with that of bulk $LaFeO_3$ particles. The enhancement in gas sensing properties was attributed to their porous structure, large surface areas, numerous surface active sites and more oxygen vacancies. In summary, a simple synthesis route was developed for the fabrication of biomorphic porous $LaFeO_3$ with the help of sorghum straw biotemplate. Morphologies, microstructures, and compositions of the samples were characterized by a series of techniques. The gas sensing tests exhibited that the biomorphic porous $LaFeO_3$ showed superior gas sensing performance toward acetone, in comparison to the bulk $LaFeO_3$ particles, which was mainly attributed to their porous structure, large surface areas, numerous surface active sites and more oxygen vacancies. Furthermore, the result suggested that the as-prepared porous structure, large surface areas and more surface active sites was promising candidates for good performance acetone sensor.

K.K. Bhargav, *et al* (2014) reported the highly sensitive, low temperature butane sensing for nano-crystalline lanthanum iron oxide sensor. The improved butane sensing characteristics of these sensors were explained to be due to their efficient catalytic nature toward butane oxidation. Through infrared spectroscopy in conjunction with X-ray photoelectron spectroscopy analysis they demonstrated that the sensor catalytic activity was due to the presence of surface adsorbed oxygen species and hydroxyl ions. The desorbed water and oxygen molecules (originate from the surface adsorbed oxygen and hydroxyl group), initiated the catalytic oxidative dehydrogenation of butane at an operating temperature as low as 250 °C. They also investigated the hydrogen, carbon monoxide, and methane sensing performance of lanthanum ferrite sensors. The sensor found to be cross-sensitive to these gases. The

selectivity coefficients for lanthanum ferrite butane sensors were estimated to be 1.67 and 4.67 for 50 ppm hydrogen and carbon monoxide sensing, respectively. The authors investigated butane sensing characteristic of nano-crystalline lanthanum ferrite sensing elements at various test gas concentration (10–1660 ppm) in the operating temperature ranging 200–350 °C. For this sensor, excellent response (%) = 93% was achieved (at 1660 ppm butane sensing) at operating temperature as low as 250 °C. The butane and methane sensing characteristics were compared with a wide variety of sensor materials reported in the literature. The superior butane (and methane) sensing characteristics of nano-crystalline lanthanum ferrite sensor were explained to be due to its catalytic activity toward efficient alkane oxidation at lower operating temperature.

X. Wang, *et al* (2013) prepared $LaFeO_3$ nanocrystalline powder by sol–gel method with annealing at 800 °C for 2 h which exhibited considerable sensing response for CO_2 gas. The resistance of the $LaFeO_3$ sensor increased with increasing concentration of CO_2. At 300 °C, the response of the sensor to 2000 ppm CO_2 was 2.19, and its response and recovery times were about 4 and 8 min, respectively. The possible CO_2 sensing mechanisms for $LaFeO_3$ sensor are investigated with first principles calculations. Calculated results demonstrated that CO_2 could release electrons to the surface of $LaFeO_3$ (0 1 0) pre-adsorbed with high concentration of oxygen, which was consistent with the experimental observation. The sensor based on the $LaFeO_3$ powders showed considerable sensing response to carbon dioxide. With increasing concentration of carbon dioxide, the resistance of the $LaFeO_3$ sensor increased. At 300 °C, the responses of $LaFeO_3$ sensor to 1000, 2000, and 4000 ppm CO_2 gas were 1.74, 2.19, and 2.74, respectively. The response and recovery times at 300 °C for the sensor to 2000 ppm CO_2 were about 4 and 8 min,respectively. Our first-principle calculations demonstrated that CO_2 could release electrons to the surface of $LaFeO_3$ (0 1 0) pre-adsorbed with high concentration of oxygen (M5 mode), which was consistent with the experimental results.

J. Zhao, *et al* (2013) prepared mesoporous $LaFeO_3$ with high surface area and pore volume through a nanocasting route by using mesoporous silica SBA-15 as a hard template. The structure and chemical composition of the sample were characterized by X-ray diffraction (XRD), nitrogen adsorption–desorption, transmission electron microscopy (TEM) and inductively coupled plasma mass spectrometry (ICP-MS). The humidity sensing properties of the mesoporous $LaFeO_3$ were investigated.

Impedance greatly changed by more than five orders magnitude (1.7 × 106 to 4.5 kv) when the relative humidity varied from 11% to 98% at 10 Hz, and it also exhibited the satisfactory response time, hysteresis and stability. The sensor utilizing mesoporous $LaFeO_3$ via nanocasting method displayed superior humidity performance compared to that using bulk $LaFeO_3$ via sol–gel technique. Such sensing behavior of the mesoporous $LaFeO_3$ could be attributed to the high surface area (83.2 m^2/g) and porosity, which led to highly effective interaction between the water molecules and the surface active sites. A possible mechanism was discussed to explain the excellent performance of the humidity sensing device using the mesoporous $LaFeO_3$. Mesoporous $LaFeO_3$ was successfully synthesized via the nanocasting method by using SBA-15 as a replica matrix. A ceramic humidity sensor based on the mesoporous $LaFeO_3$ was fabricated and evaluated. Humidity sensing measurements revealed that impedance greatly changed by more than five orders magnitude when the relative humidity varied from 11% to 98% at 10 Hz, and it also displayed high response, fast response time, low hysteresis and long-time stability in the entire humidity region. The sensing mechanism of humidity sensors was interpreted by the complex impedance spectra (Nyquist plot). Furthermore, the sensor based on the mesoporous $LaFeO_3$ displayed the higher response compared with that of bulk $LaFeO_3$ prepared by the sol–gel method. It could be concluded that the obtained mesoporous $LaFeO_3$ was an excellent material for application as humidity sensor because of its high surface area and pore volume with mesoporous structure.

R. Abazaria, *et al* (2013) synthesized the orthorhombic structure of lanthanum ferrite nanoparticles ($LaFeO_3$ NPs) with perovskite type phase with water-in-oil (W/O) microemulsion consisted of water/dioctyl sulfosuccinate sodium (aerosol-OT)/isooctane at room temperature. That aerosol-OT reverse microemulsion solution was appropriate for synthesizing perovskite $LaFeO_3$ NPs in the absence of any co-surfactants. Field emission scanning electron microscope (FE-SEM), transmission electron microscopy (TEM), energy dispersive analysis of X-ray (EDAX), X-ray diffraction (XRD), ultraviolet–visible absorption spectroscopy (UV–Vis), and Fourier-transformed infrared spectroscopy (FT-IR) were used for characterization of surface morphology, size, phase composition, structure, and optical properties of the considered NPs. Furthermore, the optical properties of $LaFeO_3$ NPs were further analyzed via photoluminescence (PL) spectroscopy. Single phase lanthanum ferrite were obtained at 500 °C. The surface morphological studies confirm the formation of

highly monodispersed LaFeO3 NPs with size of about 4 – 32 nm. The calcinated particles of $LaFeO_3$ NPs exhibited orthorhombic structure as determined through XRD analysis. UV–Vis spectrum showed that the prepared $LaFeO_3$ NPs had strong UV-light absorption at about of 322 nm. The important advantage offered by this method was that the process was done in one step and at room temperature. Moreover, the surfactants surrounding the particles in the solution could easily be removed. Thus, it was an economic procedure from both energy and time perspectives.

Z. Kaiwen, *et al* (2013) synthesized nanocrystalline $LaFeO_3$ by calcining precursor $La_2(CO_3)_2(OH)_2$–Fe_2O_3·$1.5H_2O$ in air. XRD analysis showed that precursor dried at 80 °C was a mixture containing orthorhombic $La_2(CO_3)_2(OH)_2$ and amorphous $Fe_2O_3.1.5H_2O$. Orthorhombic $LaFeO_3$ with highly crystallization was obtained when $La_2(CO_3)_2(OH)_2$–Fe_2O_3·$1.5H_2O$ was calcined at 900 °C in air for 2 h. Magnetic characterization indicated that the calcined product at 900 °C showed weak magnetic behavior at room temperature. The thermal process of $La_2(CO_3)_2(OH)_2$–Fe_2O_3·$1.5H_2O$ showed five steps involving, at first, dehydration of 0.8 absorption water, then dehydration of 0.7 crystal water, decomposition of orthorhombic $La_2(CO_3)_2(OH)_2$ into orthorhombic $LaCO_3OH$, reaction of two $LaCO_3OH$ into hexagonal $La_2O_2CO_3$ and crystallization of tetragonal Fe_2O_3, at last, reaction of hexagonal $La_2O_2CO_3$ with tetragonal Fe_2O_3 into orthorhombic $LaFeO_3$. In the DTG curve, four DTG peaks indicated the precursor experienced mass loss of four steps.

S.E. Moon, *et al* (2013) fabricated micro C_2H_5OH gas sensor based on micro-heater and tin oxide thick film by using complementary metal-oxide semiconductor (CMOS) compatible micro electro mechanical systems (MEMS) process, which showed low power consumption and high response. Semiconducting SnO_2 nanopowders were synthesized via co-precipitation method, and rare metal dopants were added to increase the sensitivity for alcohol gas. Bridge type micro-heater based on Si substrate was fabricated by surface micromachining technique and in the structure of micro-heater, the resistances of two semi-circled Pt heaters were connected to the spreader for thermal uniformity. The response of the micro gas sensor was 0.78 for 2 ppm alcohol with lower power consumption (35 mW) than that of the commercial alcohol gas sensor. The mechanical stability of the sensor was tested under the higher direct current (DC) power than that of the normal operation power and the variation rate of the micro-heater resistance was below 2% after 105 times repetitive 35 mW pulse operations.

X. Chen, *et al* (2013) demonstrated the fabrication and gas sensing properties of room temperature surface acoustic wave (SAW) NH_3 gas sensors based on polypyrrole (PPy) film of different layers and Pt doped 2 layer PPy film. The PPy film was deposited on the photolithography patterned sensitive area by layer-by layer (LBL) self-assembly method. The doping of Pt was conducted by immersing substrates with PPy film in the solution of H_2PtCl_6 and then reduced by $NaBH_4$. Gas sensing properties of SAW devices with different layer of PPy films and Pt doped 2 layer PPy film were investigated and compared. They found that device with 2 layer PPy film showed best performance among devices with different layers of PPy films. Response and stability of device with 2 layer PPy could be further improved by the doping of Pt. Gas sensing properties of the device in different carrier gases (air and N_2) were also investigated.

T. Sathitwitayakul, *et al* (2012) studied the gas-sensing properties of spinel and orthorhombic ferrites ($NiFe_2O_4$, $CoFe_2O_4$, and $LaFeO_3$) as well as cubic nickel–zinc stannates $Zn_{2-x}Ni_xSnO_4$ (with x = 0, 0.8) prepared by selfpropagating high-temperature synthesis (SHS). This was the first report of using an SHS derived powder for gas sensing applications. The gas response of the materials was investigated against a range of gases (ethanol, ammonia, propane, CO, ethane, ethene) at a variety of operating temperatures. Good gas response behavior was found in the case of the cubic nickel–zinc stannates with excellent selectivity toward ethanol. A novel self-propagating high-temperature synthesis of these materials was performed and their application as gas sensors for environmental monitoring was demonstrated. SHS gave good control over phenomena such as particle size and morphology that allowed gas sensor performance and gas selectivity to be greatly improved.

K. Fan, *et al* (2012) fabricated $La_{0.75}Ba_{0.25}FeO_3$ thick films by printing the paste (a mixture of $La_{0.75}Ba_{0.25}FeO_3$ powders and binder) on an alumina substrate pre-deposited with Ag electrodes. After the printing process, the thick films were annealed at various temperatures. When the $La_{0.75}Ba_{0.25}FeO_3$ powders were prepared through annealing at 800 °C for 3 h, the optimal final annealing temperature was about 700 °C for the $La_{0.75}Ba_{0.25}FeO_3$ thick film to obtain a large sensing response. The gas sensing properties of $La_{0.75}Ba_{0.25}FeO_3$ thick-film sensors depended on the film thickness. The film with thickness of D = 50 μm exhibited the largest response among the four thick films (D = 30, 50, 70, and 100 μm). $La_{0.75}Ba_{0.25}FeO_3$ thick-film sensors could detect acetone and ethanol with very low concentrations (e.g. 5 ppm).

H. Fan, *et al* (2011) prepared Fe_2O_3 nanobelts and P-type $LaFeO_3$ nanobelts by electrospinning. The structure and micro-morphology of the materials were characterized by X-ray diffraction (XRD) and scanning of electron microscopy (SEM). The gas sensing properties of the materials were investigated. The results showed that the optimum operating temperature of the gas sensors fabricated from Fe_2O_3 nanobelts was 285 °C, whereas that from $LaFeO_3$ nanobelts was 170 °C. Under optimum operating temperatures at 500 ppm ethanol, the responses of the gas sensors based on these two materials were 4.9 and 8.9, respectively. The response of $LaFeO_3$-based gas sensors behaved linearly with the ethanol concentration at 10–200 ppm. Sensitivities to different gases were examined, and the results showed that $LaFeO_3$ nanobelts exhibited good selectivity to ethanol making them promising candidates as practical detectors of ethanol.

C. Feng, *et al* (2011) prepared $LaCo_xFe_{1-x}O_3$ nanoparticles (x = 0, 0.1, 0.2, and 0.3) by a sol–gel method, and the effects of calcination temperature, Co-doping, and carbon nanotube (CNT)-treatment on their ethanol sensing properties were investigated. The highest response was found based on the $LaCo_{0.1}Fe_{0.9}O_3$ nanoparticles calcined at 600 °C, and the sensing properties of the sample could be further improved by adding CNT in the precursor. The responses of un-treated and CNT-treated $LaCo_{0.1}Fe_{0.9}O_3$ nanoparticles were about 120.1 and 137.3–500 ppm ethanol at 140 °C, respectively. Simultaneously, by CNT-treatment, the response time was decreased from 56 to 10 s, and the recovery time was decreased from 95 to 35 s. The results not only made $LaCo_{0.1}Fe_{0.9}O_3$ nanoparticles good candidates for fabricating practical gas sensors, but also provided a possible route for employing CNTs as a pore-forming agent.

M. Ghasdi, *et al* (2010) prepared $LaCoO_3$ perovskite samples in powder form using solid-sate reaction, sol–gel, and high energy ball milling (HEBM) methods. X-ray diffraction patterns, SEM images, and TPD-O_2 profiles revealed the significant differences in physical properties and sensing performance of the samples. Dip-coating process was used to prepare continuous thick sensing films on alumina substrate. Compared to the other methods, HEBM resulted in the lowest crystallite size of 11 nm, the highest amount of grain boundaries and the best CO gas sensing properties while the specific surface area of all samples remained similar. Mean crystallite size and grain boundary volume were found to affect the gas sensing properties. The maximum response ratio was increased from 7% for the SSR samples

to 17% and 26% for the sol–gel and BM samples, respectively. The maximum response ratio temperature was also decreased from 175 °C for the sol–gel samples (20 nm) to 125 °C for the BM samples (11 nm). Specific surface area of the BM sample was successfully increased from 4 m^2/g to an optimum value of 66 m_2/g by an additional milling step. The oxygen mobility was also drastically increased by increasing the second milling time and surface area. Maximum response ratio of all samples with respect to CO showed a good correlation with the total amount of desorbed oxygen measured by TPD-O_2. The results showed that the response ratio could be increased by up to 75% at 125 °C, which was four and ten times better than those obtained by sol–gel and solid-state reaction methods, respectively. HEBM technique could therefore be considered as a low cost and waste free technique to synthesize nanocrystalline perovskite materials with improved response ratio and low operation temperature.

P. Song, *et al* (2010) fabricated biomorphic $LaFeO_3$ hollow fibers with porous walls using cotton as biotemplates. Cotton fibers were infiltrated with lanthanum nitrate and ferric nitrate solution and subsequently sintered in air at high temperatures to produce the final $LaFeO_3$ hollow fibers. The samples had further distinctions in structure, morphology and crystallite size of the nanocrystallites, BET surface area, and the pore size distribution. Growth mechanism of $LaFeO_3$ hollow fibers was proposed. Furthermore, gas sensors were fabricated and an investigation of CO sensing property was conducted. Compared with $LaFeO_3$ particles, the hollow fibers displayed much better CO sensing properties, which was mainly due to the increasing of active surface area and gas diffusion. The maximum response (64%) was found in the case of sample calcined at 800 °C, which was higher than that of pure $LaFeO_3$ powders, due to its well-defined structure with hollow and porous wall.

X. Chu, *et al* (2009) prepared $LaFeO_3$ precursors using solid-state reaction in the presence of PEG400, and then $LaFeO_3$ nano-powders were obtained through heating these precursors under different conditions. Eventually, $LaFeO_3$ thick film sensors were fabricated by using $LaFeO_3$ nano-materials as sensing materials. The phase composition and morphology of particles in these materials were characterized through X-ray diffraction (XRD) and transmission electron microscopy (TEM), respectively. The XRD analysis results revealed that $LaFeO_3$ could be obtained by heating at 400–900 °C. TEM images manifested that the average particle sizes increase with heating temperature increasing, the particle sizes were in the range of

50–80 nm when heating temperature was increased to 800 °C. Furthermore, the influence of the heating duration and the heating temperature on the gas-sensing properties of the sensors based on $LaFeO_3$ nano-materials was also investigated. The sensitivities to several organic gases, such as $(CH_3)_3N$ and $(CH_3)_2CO$ were studied. It was found that the sensor based on $LaFeO_3$ nano-material (800 °C, 2 h) exhibited best performance in all sensors investigated in this work. In details, the sensitivities of the sensor based on $LaFeO_3$ nanomaterial (800 °C, 2 h) to 1000 and 0.001 ppm $(CH_3)_3N$ at 208 °C were as high as 2553 and 1.6, respectively; and the response time and recovery time for 10 ppm trimethylamine were 8 and 50 s, respectively.

X. Liu, *et al* (2008) prepared the $LaMg_xFe_{1-x}O_3$ powder by a sol–gel method using citric acid. The compounds crystallized as a perovskite phase with orthorhombic structure. The Mg-doping restrained the growth of the grain size. The resistance and gas sensing of the $LaMg_xFe_{1-x}O_3$ based sensors were investigated. The Mg-doping decreased the resistance of $LaFeO_3$. The conductivity of $LaMg_xFe_{1-x}O_3$ depended on both electrovalence compensation and oxygen vacancy compensation. It was found that the $LaMg_{0.1}Fe_{0.9}O_3$ based sensor had the best response and selectivity to ethanol gas. Great differences on the conductance temperature curves of the $LaMg_{0.1}Fe_{0.9}O_3$ based sensor in ethanol gas and air or other gases were also found. The conductance in ethanol gas decreased with an increase in temperature from 130 to 200 °C. But in air and other gases the conductance increased all the time. It indicated that at about 200 °C the conductance difference between in air and ethanol was the highest and the response reached the maximum. The $LaMg_{0.1}Fe_{0.9}O_3$-based sensor showed higher response and better selectivity to C_2H_5OH.

J. W. Fergus, *et al* (2007) studied the oxygen partial pressure dependence of the point defect concentration, and thus conductivity, in oxide semiconductors allowing for their use in high-temperature gas sensors. In addition to responding to oxygen partial pressure, the resistance of oxide semiconductors could be affected by other gases, such as carbon monoxide, hydrocarbons and ethanol, which created opportunities for developing new sensors, but also led to interference problems. The most common oxide used in such sensors was tin oxide, although other simple oxides, and some mixed oxides, were also used. The focus of this paper was on the use of perovskite oxides in semiconductor-based gas sensors. The perovskite structure, with two differently-sized cations, was amenable to a variety of dopant

additions. This flexibility allowed for control of the transport and catalytic properties, which were important for improving sensor performance. Semiconducting perovskites could be used in a variety of resistance-based gas sensors. Strontium titanate was the perovskite oxide most commonly used for oxygen sensing, while ferrites and cobaltites were more commonly used for sensing other gases.

X.H. Wu, *et al* (2002) reported the $MSnO_3$ semiconducting oxide that could be used as a gas sensitive material for detecting ethanol gas. $MSnO_3$ powders were prepared by a chemical coprecipitation synthesis method. The preparation conditions were carefully controlled. After calcinations at appropriate temperature, the n type semiconductor gas-sensing materials were obtained. The phases and microstructures of the obtained powders were characterized by X-ray diffraction (XRD). The products corresponded to a small particle size range of 0.1–0.4 μm and high surface area of 60–65 m^2/g. The electrical properties, sensitivity, synthetic conditions, operating temperatures, and selectivity of $MSnO_3$-based sensors were investigated. It was found that sensors had good sensitivity to vapor of C_2H_5OH. Gas-sensing mechanism was studied with x-ray photoelectron energy spectra (XPS). The gas-sensing mechanism analysis revealed that operating temperatures of the sensor influenced the conductive change of the $MSnO_3$ sensor in reducing C_2H_5OH. The gas sensors based on $MnSnO_3$ had good sensitivity and selectivity to C_2H_5OH.

S. Tao, *et al* (2000) prepared perovskite-type oxide $BaSnO_3$ at reduced temperature. The cubic $BaSnO_3$ phase formed at 400 °C when a precipitation method was applied. Thermal analysis indicated that the decomposition temperature of $BaSn(OH)_6$ was below 600 °C. The trace amounts of $BaCO_3$ in the precipitate were due to the reaction of barium ions with the atmospheric CO_2 in a strong basic solution. Conductance measurement between 200 and 550 °C indirectly demonstrated the gas-sensing mechanism of $BaSnO_3$ might be a surface-controlled process. The sensor made of the $BaSnO_3$ prepared by a precipitation method exhibited low responses to LPG, petrol, H_2 and CO but high response and good selectivity to ethanol. The as-prepared $BaSnO_3$ was a promising ethanol-sensing material.

K. Li, *et al* (2000) studied the electron transport types and photovoltage gas-sensitive characters of nano-$LaFeO_3$ surface after adsorption of active gas. Surface photovoltage spectroscopy under different environment could be used to probe

information on photovoltage gas-sensitive characters and electronic behavior of nanomaterial surface adsorbed by the active gas. The results showed that photovoltage characters and electronic transport types of nano-$LaFeO_3$ sample exposed to the sensor gas (such as ethanol vapor) are different from that exposed to air. The effects of surface and quantum confinement of the nanomaterial were obviously shown under exposure of the sample to ethanol vapor (Pethanol = 2.52 kPa) and a negative induced field (-1.0 V). These effects enabled nano-$LaFeO_3$ compared with the conventional crystal to form a new surface state band ca. 0.61 eV above the valence band, to produce the photogenic exciton pair in the relevant transition, and to increase quantum-optical efficiency. In addition, it was interesting to note that in terms of nano-$LaFeO_3$ samples with different size d the optimum phase of surface photovoltage response depended directly on ln d when d was smaller than 100 nm. This relation, however, would no longer exist for the conventional crystalline $LaFeO_3$.

W. Yude, *et al* (2000) found that perovskite-type $NiSnO_3$ semiconducting oxide could be used as a new type of gas sensitive material for detecting ethanol gas. $NiSnO_3$ powder was prepared by a chemical co-precipitation synthesis method. The preparation conditions were carefully controlled. After calcination at 500°C for 6 h, the n-type semiconductor gas-sensing material was obtained. The phase and microstructure of the powders obtained were characterized by X-ray diffraction. The product showed perovskite-type $NiSnO_3$, with a cubic habit over a small particle size range of 1–3 μm. The conductance, sensitivity, operating temperature, calcination temperature, sensitivity, gas concentration properties of $NiSnO_3$-based sensors were investigated. It was found that sensors had good sensitivity to vapor of C_2H_5OH and good selectivity to petrol. Gas-sensing mechanism was studied with infrared and XPS spectra. The preparation of $NiSnO_3$ was shown to be feasible. By chemical coprecipitation synthesis method, $NiSnO_3$ material of cubic perovskite-type and good gas-sensing properties could be obtained with low reactant concentration at low synthetical temperature and 500 °C of calcination temperature. The gas sensing mechanism analysis revealed that the calcining and operating temperatures of the sensor influenced the conductive change of the $NiSnO_3$ sensor in reducing C_2H_5OH. At 500 °C calcining temperature and 250 °C operating temperature, the gas sensors based on $NiSnO_3$ had good sensitivity to C_2H_5OH and good selectivity to petrol.

S. Zhao, *et al* (2000) prepared $LaFeO_3$ nano-crystalline thin-film of perovskite-type composite-oxides by using a sol–gel coating technique, and the photo-etching technique was employed to etch and patterned the film. Combining this thin-film technology with the NMOS integrated circuit technology, they developed an ethanol sensitive field-effect transistor by using a $LaFeO_3$ nano-crystalline thin-film as a gate electrode of an ordinary n-channel MOSFET. The sensor had excellent selectivity, good sensitivity to ethanol, and a good stability. In order to improve the recovery transient of the sensor, the $LaFeO_3$ doped with strontium ions was investigated. The perovskite-type nano-crystalline thin-film of $LaFeO_3$ was obtained by a solid phase reaction at about 600 °C for 1 h. The film was uniform in thickness, and its crystal sizes were about 40 nm characterized by XRD and SEM. The OSFET substrate was fabricated by the ordinary NMOS technology by integrating the gas sensor, heater, thermo-sensor, and electrical parameter checker. The NCTF-OSFET ethanol sensor could be used as a detector for a wide range of C_2H_5OH concentration of 100–1000 ppm. It had good anti-disturbance property to gasoline, isobutane, carbonyl and sulphuretted hydrogen. The recovery transient of the sensor was obviously improved by strontium doping. The recovery time of the sensor with $La_{0.7}Sr_{0.3}FeO_3$ thin-film decreased 38% compared to that without strontium doping. The sensor showed excellent stability.

M.C. Carotta, *et al* (1997) prepared nanosized, single-phase perovskite-type $LaFeO_3$ powders by the thermal decomposition at 600°C of a hexacyanocomplex, $La[Fe(CN)_6].5H_2O$. The formation of $LaFeO_3$ and its microstructural evolution with the temperature were studied by simultaneous thermogravimetric and differential thermal analysis (TG/DTA), X-ray diffraction (XRD), scanning electron microscopy (SEM), and transmission electron microscopy (TEM). $LaFeO_3$ was formed by the decomposition of the complex with a peculiar morphology, consisting of nanosized particles in soft agglomerates with the same size and shape of the complex grains. The nanosized particles were free of pores, making the powders suitable for application in thick film fabrication, after disruption of the agglomerates, for their use as active elements for gas sensors. Preliminary experiences were encouraging the use of this sensor for NO_2 detection in the real environment. The thermal decomposition of the $La[Fe(CN)_6].5H_2O$ heteronuclear complex was a rather simple preparation method, which leads to the formation of pure, nanosized $LaFeO_3$ powders at low temperatures. The powders microstructure, consisting of nanosized particles free of pores, was particularly suitable for the application in thick film fabrication, after

disruption of the soft agglomerates. The characteristics of the products were promising for their use as active elements for chemical sensors; some preliminary measurements of the response to NO_2 showed that the range of applicability was proper for ambient monitoring.

1.2.4 Perovskite and heavy metal adsorption

The adsorption is a process where molecules from the gas phase or from solution bind in a condensed layer on a solid or liquid surface. The molecule that bind to the surface are called the adsorbate while the substance that holds the adsorbate is called the adsorbent. The process when the molecules bind is called adsorption. Removal of the molecule from the surface is called desorption. There are two different types of adsorption : 1. chemisorptions (or chemical adsorption), where there is a direct chemical bond between the adsorbate and the surface, and 2. physisorption (or physical adsorption), where the adsorbates were held by physical (i.e. Van der Waals) forces.

Chemisorption and physical adsorption are usually distinguishable from each other without any great difficulty. Table 1 summarizes the main criteria.

Table 1. Criteria for distinguishing between chemisorption and physical adsorption (Bond, 1987: 13)

Criteria	Chemisorption	Physisorption
Enthalpy of adsorption, $-\Delta H_{ads}$	40 - 800 kJ /mol	8 - 20 kJ /mol
Activation energy, E_a	Usually small	Zero
Temperature of occurrence	Depends on E_a but usually low	Depends on boiling point, but usually low
Number of layers adsorbed	Not more than 1	More than one possible

The adsorption characteristics between the adsorbent and adsorbate are explained by the adsorption isotherm in general. The Langmuir and Freundlich models are widely used since they are simple and can describe experimental results over a wide range of concentration. They can easily be transformed into linear form to obtain adjustable parameters by graphical means or linear regression analysis (Kim and Chung, 2001).

The Langmuir isotherm is commonly used on the assumption that the adsorbed surface state is homogeneous and the adsorption layer is a monolayer (Kim and Chung, 2001). The Langmuir isotherm is given by :

$$q = \frac{q_{max} K_L C}{1 + K_L C} \qquad \text{..... (1)}$$

where K_L is the equilibrium constant (L/mg),
q_{max} is the maximum adsorption capacity (mg/g) of adsorbent,
C is the equilibrium concentrations (mg/L), and
q is the amount of metals adsorbed at equilibrium (mg/g).

Equation (1) is usually linearlized by inversion to obtain the following form.

$$\frac{C}{q} = \frac{1}{K_l q_{max}} + \frac{C}{q_{max}} \qquad \text{.....(2)}$$

Equation (2) is usually used to analyse batch equilibrium data by plotting $1/q_e$ versus $1/C_e$, which yields a linear if data conform to the Langmuir isotherm.

The Freundlich isotherm is the most widely used non-linear sorption model. It is given by the general form :

$$q_e = K_F C_e^{1/n} \qquad \text{..... (3)}$$

where K_F is related to sorption capacity and n to sorption intensity. The logarithmic form of equation (3) given below is usually used to fit data from batch equilibrium studies :

$$\log q_e = \log K_F + 1/n \log C_e \qquad \text{..... (4)}$$

Equation (2) and (4) are usually used for the analysis of equilibrium batch experimental data assuming Langmiur and Freudlich isotherm, respectively (Gharaibeh, et al., 1998)

There were many investigations dealing with the adsorption of metal ions on oxide surface. This interest is due both to the importance of the process in, for example, analytical chemistry, colloid chemistry and water chemistry, and also to

the possibilities of the syntheses of the new ion exchange type catalysts (Hadjiivanov, et al., 1991).

J. Huang, *et al* (2012) synthesized titanate nanoflowers through a facile hydrothermal treatment of anatase nanopowders in concentrated NaOH solution. The as-obtained nanoflowers had large specific surface area and showed availability for the removal of heavy metal ions from water system. Comparative studies showed that titanate nanoflowers possess larger adsorption capacity and more rapid kinetics than titanate nanotubes/ nanowires. Furthermore, they also showed high selectivity in the removal of highly toxic heavy metal ion (Cd(II)) than less toxic ions (Zn(II) and Ni(II)). Titanate nanoflowers from this study were potential adsorbents for efficient removal of toxic metal ions. The adsorption mechanism was also discussed. It was found that the equilibrium data fitted well with the Langmuir model, while the adsorption kinetics followed the preudo-second-order model.

D. Zhang, *et al* (2011) prepared porous nano-calcium titanate microspheres (PCTOM) using D311 resin as a template by a citric acid complex sol–gel method and characterized by X-ray diffraction (XRD), SEM, and FTIR. The adsorption capabilities for heavy metal ions such as lead, cadmium, and zinc were studied. The adsorption and elution conditions were investigated. Moreover, taking the cadmium ion as an example, the thermodynamics and kinetics of the adsorption were studied. The results showed that the microspheres were porous and were made of perovskite nano-calcium titanate ($CaTiO_3$). The adsorption capacities of PCTOM for lead, cadmium, and zinc were found to be 141.8 $mg.g^{-1}$, 18.0 $mg.g^{-1}$, and 24.4 $mg.g^{-1}$, respectively. The adsorption behavior followed Langmuir adsorption isotherm and pseudo-second-order kinetic model, where adsorption was an endothermic and spontaneous physical process. The adsorbed metal ions could be completely eluated using 2 mol /L HNO_3 with preconcentration factors over 100 for all studied heavy metal ions. The method was also applied to the preconcentration and FAAS determination of trace lead, cadmium, and zinc ion in water samples with satisfactory results.

C. Gargori, *et al* (2012) studied solid solutions $Ca(D_xM_{1-x})O_3$ (M = Ti, Zr and D = Fe, Cr), as ceramic pigment in conventional ceramic glazes using 0.5 mol/ mol of NH_4Cl as flux agent by solid state reaction and by ammonia coprecipitation route. $Ca(Cr_xTi_{1-x})O_3$ compositions obtained without addition of NH_4Cl as mineralizer

produced pink color in glazes at low x but $CaCrO_4$ crystallized when x increased, producing undesired green colors. The crystallization of chromates was avoided using NH_4Cl as mineralizer, giving a complete solid solution, that produced pink color in glazes at low x and dark blue shades at high x. Coprecipitated sample produced blue colors at low x and at low temperature than ceramic sample (1000 °C instead 1200 °C for CE sample). Cr^{4+} ion acted as red chromophore, but at higher x values (blue samples) Cr^{3+} ion affected the color. $Ca(Fe_xTi_{1-x})O_3$ system crystallized perovskite $CaTiO_3$ and pseudobrookite Fe_2TiO_5 together with rutile as residual crystalline phase, glazed samples changed from a yellow to a pink color associated to the increase of pseudo brookite with firing temperature. $Ca(Fe_xTi_{1-x})O_3$ and $Ca(Fe_xZr_{1-x})O_3$ systems crystallized perovskite $CaZrO_3$ and zirconia (ZrO_2) in both monoclinic and cubic polymorphs, but iron or chromium oxides were not detected in the powders. Coprecipitated sample stabilised cubic form. The solid solution was not reached completely in these samples and was not stable in glazes.

E. Eren, *et al* (2011) investigated adsorption of Pb(II) by sepiolite (ICS) sample as a function of the initial Pb(II) concentration, solution pH, ionic strength, temperature and inorganic ligand (Cl^-). Changes in the surfaces and structure of sepiolite samples were characterized by means of IR and thermal analysis (TGDTA). The perturbation observed on the zeolitic and bound water vibrations of ICS indicated that some of iron oxide particles entered the interior channels and replaced zeolitic water molecules. The exothermal peak at 834 °C for RS and at 774 °C for ICS in the thermal analysis curves was assigned to the phase transformation of sepiolite to enstatite ($MgSiO_3$). The Langmuir monolayer adsorption capacities of RS and ICS in 0.1 M $NaNO_3$ solution at 298 K were estimated as 5.36 and 75.79 mg/g, respectively. Thermodynamic parameters such as change in free energy (ΔG), enthalpy (ΔH) and entropy (ΔS) were evaluated for RS and ICS to be -15.46 kJ/ mol (at 298 K), 47.78 kJ/mol and 212 J/mol K, and -16.03 kJ/mol (at 298 K), 47.48 kJ/mol and 213 J/mol K, respectively.

S.M. Lee, *et al* (2012) obtained iron-oxide nano-particles-immobilized sand (INS) by simple impregnation process using locally available sand with prior acid activation. The INS sample was characterized by XRD and SEM / EDX analytical methods. The solid was studied for its possible use in the removal of several toxic heavy metal ions viz., Cu(II), Cd(II) and Pb(II) from aqueous solutions under the static and dynamic experimental conditions. Batch experiments were carried out analyzing

various physico-chemical parametric studies viz., effect of solution pH, ionic strength and sorptive concentration. The equilibrium state data obtained by concentration dependence study was utilized to obtain the Langmuir and Freundlich adsorption modeling. INS sample was also employed to assess the suitability of material in the removal of these heavy metal toxic ions under the dynamic conditions i.e., in column studies. The breakthrough data obtained by column studies were then utilized to model it with Thomas equation and hence, estimated the loading capacity of Cu(II)/or Cd(II)/or Pb(II) under the specified column conditions. Results obtained showed that INS could to be one of promising and effective solid material and could be used in several wastewater treatment strategies in particular, the treatment wastewaters contaminated with these heavy metal toxic ions.

K. Y. Kumar, *et al* (2013) synthesized metal oxide nanoparticles, such as ZnO and SnO_2 with specific surface areas of 15.75 and 24.48 m^2/g, respectively, successfully by precipitation method and then employed as adsorbents for removal of malachite green oxalate (MGO) and hexavalent chromium (Cr) from aqueous solution. The nanoparticles were characterized by XRD, SEM, TEM, SAED, FT-IR, and BET surface area analysis. The adsorption of MGO and Cr was achieved under different adsorbate concentration, contact time, adsorbent dosage, pH and temperature conditions. Adsorption equilibrium was studied with Langmuir and Freundlich isotherm models. Equilibrium data were best fitted with the Langmuir and Freundlich isotherm models. Kinetic studies indicated that the adsorption process followed second order kinetics and particle diffusion mechanisms were operative. Thermodynamic parameters were studied in detail to know the nature and mechanism of adsorption. The spent adsorbents were regenerated with CH_3COOH or NaOH solutions and regenerated adsorbents showed very good adsorption efficiencies. All the above results demonstrated that metal oxide nanoparticles could be used as a possible alternative low-cost adsorbent for the efficient removal of dyes and heavy metals from aqueous solution.

M. Hua, *et al* (2012) reviewed nanosized metal oxides (NMOs) (including nanosized ferric oxides, manganese oxides, aluminum oxides, titanium oxides, magnesium oxides and cerium oxides) having high surface area and specific affinity for heavy metal adsorption from aqueous systems. The review mainly focused on NMOs' preparation, their physicochemical properties, adsorption characteristics and mechanism, as well as their application in heavy metal removal. In addition, porous

host supported NMOs were particularly concerned because of their great advantages for practical application as compared to the original NMOs. Also, some magnetic NMOs were included due to their unique separation performance.

V. Venkatesham, *et al* (2013) prepared nanosized large surface area zinc oxide (ZnO) by gel combustion method and used as an adsorbent to remove lead (II) (Pb^{2+}) from aqueous solution. The nano ZnO was characterized by X-ray diffraction (XRD), scanning electron microscopy (SEM), energy dispersive X-ray analysis (EDAX) and surface area analysis. Effect of lead concentration, adsorbent dosage and pH on adsorption were studied. Increase in the initial concentration of Pb decreased the percentage of adsorption, whereas increase in the adsorbent dosage and pH of the solution increased the adsorption of Pb^{2+} on ZnO. Synthesized nano ZnO showed almost complete Pb adsorption at lower initial concentration. The equilibrium adsorption capacity of Pb on nano ZnO adsorbent were measured and extrapolated using Langmuir and Freundlich adsorption isotherm models and the experimental data perfectly fitted both adsorption isotherms.

M.B. Jazi, *et al* (2014) reported the preparation of three new Schiff base ligands modified SiO_2 - Al_2O_3 mixed oxide adsorbents, and their use for removal of Pb(II) and Cd(II) from aqueous solutions. Equilibrium and kinetic models for Pb(II) and Cd(II) sorption were applied by considering the effect of the contact time, initial Pb(II) and Cd(II) concentrations, effect of temperature, and initial pH. The contact time to attain equilibrium for maximum adsorption was 120 min. These heterogeneous Schiff base ligands were found to be effective adsorbents for the removal of heavy metal ions from solution, with Si/Al-pr-NH-et-N-pyridine-2-carbaldehyde having a high adsorption capacity for Pb(II) and Cd(II) ions from aqueous solution. The adsorption of heavy metal ions was studied in terms of pseudo-first- and second-order kinetics, and the Freundlich, Langmuir and Langmuir–Freundlich isotherms models were also used to analyze the equilibrium adsorption data. The adsorption kinetics followed the mechanism of the pseudo-second order equation for all systems studied, confirming chemical sorption as the rate-limiting step of adsorption mechanisms and not involving mass transfer in solution, which were confirmed by DS UV–vis and FT-IR techniques. The thermodynamic parameters (DG, DH and DS) indicated that the adsorption of Pb(II) and Cd(II) ions were feasible, spontaneous and endothermic between 25 and 80 °C.

A. Rahmani, *et al* (2010) synthesized nano structured γ-Al_2O_3 by ammonium acetate fuel and an effective adsorbent for the adsorption of Pb^{2+}, Ni^{2+}, and Zn^{2+} from aqueous solutions. The maximum percentage of metal adsorption by nano structured γ-Al_2O_3 was at pH 4. All kinetic results suggested that the sorption of lead (II), nickel (II), and zinc (II) by nano structured γ-Al_2O_3 followed the second-order kinetics model, which relied on the assumption that sorption might be the rate-limiting step involving valence forces through sharing or exchange of electrons between adsorbent and sorbate. The adsorption isotherms could be well fitted by the Langmuir adsorption isotherm equation. The maximum capacity of adsorbent for Pb^{2+}, Ni^{2+} and Zn^{2+} were 125, 83.33, and 58.82, respectively. The results obtained in this study showed that the nano structured γ-alumina was a good and reusable adsorbent for removal of heavy metals and could be used in water and wastewater treatment.

J. N. Bhakta, *et al* (2011) investigated the adsorption capacity (265±8.5 μg/g) of MgO impregnated a volcanic ash soil ceramic (MA-ceramic) and found that it was significantly higher (~12 times) than that of the only akadama volcanic ash soil-ceramic (A-ceramic) probably due to the presence of additional mineral of MgO periclase developed by the impregnation of MgO and chemical modification by heating process. The BET and mineralogical characteristics supported the adsorption mechanism of Hg(II) onto MA-ceramic was highly influenced by the chemical interaction between additional functional group of MA-ceramic, periclase and Hg(II) resulting in the chemisorptions process rather than only surface adsorption. Results of the contact time also revealed the adsorption equilibrium time of MA ceramic was 20 h period. Hg(II) adsorption was largely pH dependent and neutral pH (7.0) greatly increases the adsorption capacity of the ceramics. The results also demonstrated that ceramic dosage and initial concentration of the Hg(II) significantly influenced the adsorption capacity of the ceramics. The Freundlich isotherm was well fitted. Adsorption, desorption, and resorption characteristics signified that MA-ceramic would be an environmentally sound adsorbent which could safely be used in treating the Hg contaminated effluents. Furthermore, this finding would be helpful to develop the improved Hg removing filter for producing the safe Hg free drinking water and treating the Hg contaminated effluents of the industrial sectors especially in the underdeveloped countries with low-cost.

1.3 Objectives

The aim of this work is to study the preparation, characterization and application of La-bases oxide of nano-$LaMO_3$ perovskites. In this study, 4 type of M are Al (metal in group 3A), Co (transition metal that possible to be mix valence cation of Co^{2+} and Co^{3+}), Fe (transition metal with oxidation state +3) and Gd (metal in lanthanide series). nano-$LaMO_3$ (M = Al, Co, Fe, Gd) are very interesting compound with different in typical metal of B-site cation, size, EN energy, etc. The different of M metal in $LaMO_3$ may have effect to physical properties and electrical properties due to the efficiency to be ethanol sensor and heavy metal adsorbent are also different.

In the first stage, to find a simple route to prepare nano-$LaMO_3$ (M = Al, Co, Fe, Gd) perovskites through low calcination temperature that yield high purity perovskite phase. The precursor for $LaMO_3$ will be synthesized by co-precipitation from metal nitrate and carbonate salts. The precursor then will be calcined at high temperature (conventional method) and at varied lower temperatures to obtain the desired perovskites $LaMO_3$. The resulting perovskites obtained from the lower temperature treatment will be studied as ethanol sensor and heavy metal ions adsorber in comparison with the ones from high temperature. This route should have several advantages such as simplicity, low cost, no waste, and no environmental pollution compared with other routes.

The applications presented in this thesis are :

1. The possible use as ethanol gas sensing material of $LaMO_3$ (M = Al, Co, Gd, Fe) perovskite oxide.
2. The possible use as Cd^{2+} and Pb^{2+} remover from aqueous solutions.The adsorption of contact time, temperature, and pH effect shall be investigated. The adsorption capacity the Langmuir and Freundlich isotherms, and the possibility of recyclable use shall be studied and discussed.

CHAPTER 2

EXPERIMENTAL

2.1 Chemicals

1. Lanthanum(III) nitrate hexahydrate, $La(NO_3)_3 \cdot 6H_2O$, A.R., code no 10277-43-7, LOBA Chemie, India.
2. Aluminium(III) nitrate nonahydrate, $Al(NO_3)_3 \cdot 9H_2O$, code no 1104142, UNILAB, New Zealand.
3. Cobalt(II) nitrate hexahydrate, $Co(NO_3)_2 \cdot 6H_2O$, code no 10026-22-9, ALPHA, India.
4. Galdolinium(III) nitrate hexahydrate, $Gd(NO_3)_3 \cdot 6H_2O$, code no 19598-90-4, SIGMA-ALDRICH, U.S.A.
5. Iron(III) nitrate nonahydrate, $Fe(NO_3)_3 \cdot 9H_2O$, code no 7782-61-8, LOBA Chemie, India.
6. Potassium carbonate, $K_2CO_3 \cdot 1.5H_2O$, UNIVAR, Australia.
7. Lead(II) chloride, $PbCl_2$, Merck, Germany.
8. Cadmium(II) chloride, $CdCl_2 \cdot 2.5H_2O$, Merck, Germany.
9. Hydrochloric acid, HCl, A.R., code no. 9535-03, J.T. Baker, U.S.A.
10. Sodium hydroxide, NaOH, A.R., BDH, England.
11. Ethyl cellulose, code no 9004-57-3, ALDRICH, U.S.A.
12. Alpha terpineol, $C_{10}H_{18}O$, Merck, Germany.
13. 2-(2-Butoxyethoxy) ethyl acetate, $C_{10}H_{20}O_4$, SIGMA-ALDRICH, U.S.A.

2.2 Instrument

1. X-ray diffractometer, XRD, PHILIPS X' Pert MPD, the Netherlands.
2. Scanning electron microscope, SEM, JEOL JSM -5800 LV, Japan, attached with energy dispersive X-ray spectroscopy, EDS, Oxford ISIS, England.
3. Transmission electron microscopy, TEM, JEOL 100S microscope, Japan.
4. Energy dispersive X-ray spectrometer, EDX, ISIS 300, Oxford, England.
5. Oven, National, Heinicke Company.
6. pH meter, model 8519, HANNA Instruments, U.S.A.
7. Magnetic stirrer, Jenway 1000, JENWAY, UK.
8. Centrifuge, EBA 20, Hettich, Germany.

9. Brunauer- Emmett – Teller, BET, Autosorb-1-C, Quantachrome, U.S.A. measured at National Metal and Materials Technology Center, National Science and Technology Development Agency and King Mongkut ‘s University of Technology Thonburi.
10. Gas testing system, Nanoelectronics and MEMS Laboratory, National. Electronics and Computer Technology Center (NECTEC) ,Thailand.
11. UV-vis diffused reflectance spectrophotometer (DRS).

2.3 Methods

2.3.1 Preparations of $LaMO_3$ powders (M = Al, Fe, Co, Gd) by conventional methods

$LaMO_3$ (M = Al, Fe, Co, Gd) perovskites were prepared based on the co-precipitation method reported previously (J.A. Villoria, et al.,2011) with some modifications. For $LaAlO_3$, $La(NO_3)_3{\cdot}6H_2O$ and $Al(NO_3)_3{\cdot}6H_2O$ were used as starting materials. A specific amount of each was dissolved in distilled water to make 1 M solutions. All solutions (equal volume) were mixed together with vigorous stirring. Then aqueous solution of $K_2CO_3{\cdot}1.5H_2O$ (2 M) – same volume as one of nitrate solution was rapidly added. Small amount of NaOH solution (1M) was introduced to initiate precipitation. After the precipitation was complete, the precipitate was filtered and washed with distilled water several times until the washed water became neutral (pH =7). The product was then dried at 100 ℃ for 6 h to yield the “precursor” after which it was calcined at 900 ℃ for 2 h to obtain the $LaAlO_3$ perovskite (except Gd calcined at 1200 ℃).

For $LaCoO_3$, $LaFeO_3$, and $LaGdO_3$ perovskites, the same procedure as above was applied but with $Co(NO_3)_2.6H_2O$, $Fe(NO_3)_3.9H_2O$, and $Gd(NO_3)_3.9H_2O$ as starting materials, respectively.

2.3.2 Preparations of precursors for lower calcination temperatures

The same procedure as above was used to prepare the four precursors then calcined at other temperatures lower than 900 ℃: for $LaFeO_3$ at 600, 700, and 800 ℃; for $LaCoO_3$ at 200, 400, and 600 ℃. (For $LaAlO_3$, the lowest calcination temperature still was 900 ℃ since no perovskite phase was formed at temperature lower than 900 ℃. For $LaGdO_3$, the precursor formed perovskite phase at 1200 ℃

after heating for 2 h. These two perovskites, therefore, were not included in the set of low temperature.

2.3.3 Characterization of products

The structural characterization was carried out by powder X-ray diffraction (XRD) using CuK_{α} (α = 0.154 nm) radiation source in a X'Pert MPD, PHILIPS X-ray diffractometer. The diffraction angle (2α) ranged between 20 ° and 80 °. The Debye-Scherrer equation was used to calculate the average crystallite size (D),

$$D = \frac{K.\lambda}{B.\cos\theta} \qquad \text{..... (5)}$$

where D is the average crystallite size, K is a dimensionless shape factor with a value close to unity. The shape factor has a typical value of about 0.89, but varies with the actual shape of the crystallite. λ is the X-ray wavelength, B is the line broadening at half the maximum intensity (FWHM) after subtracting the instrumental line broadening in radians, θ is the Bragg angle. Magnetic moment was measured with the home-made Gouy balance at room temperature (I. Ghiloufi, et al., 2016)

The surface morphology of all sheet samples were studied on a SEM: JEOL JSM – 5800 LV, scanning electron microscopy (SEM) using high vacuum mode with secondary electron image conditions and electron micrograph technique. All data were acquired by the Scientific Equipment Center, Prince of Songkla University, Hat Yai, Songkhla, Thailand. In the sample preparation, $LaMO_3$ (M= Al, Co, Fe, Gd) sheets were cut to 1 cm x 1 cm size to fit in the specimen chamber and mounted rigidly on a specimen holder (called a specimen stub). For conventional imaging in the SEM, all samples must be made electrically conductive by sputtering-coated with gold prior to acquiring image under an SEM apparatus to study the surface morphology of $LaMO_3$ sheet.

The metal constituents of $LaMO_3$ perovskites were investigated by using dispersive X-ray spectrometer (EDAX), ISIS 300, Oxford, England. The specific surface area and pore size distribution of $LaMO_3$ were determined by nitrogen sorption isotherm using the BET method (Coulter, model SA 3100, USA).

2.3.4 Determination of pH at point of zero charge (pH_{pzc})

A sodium chloride solution of 0.1 mol /L was prepared by dissolving an appropriate amount (5.85 g) of NaCl salt in a 1 L volumetric flask followed by dilution. Several portions of 50 mL of this solution were pipetted each time and poured into several 250 mL Erlenmeyer flasks. The pH of these solutions were adjusted to 1-13 using diluted solutions of HCl or NaOH and recorded as initial pH, pH_i (H.K. Liao, et al., 1999)

About 0.05 g of $LaMO_3$ was added into each flask and sealed for 24 h with constant agitation using a magnetic stirrer. The stirring rate was controlled at a rate of 300 rpm. At the end of experiment, the equilibrated solution was decanted and the pH was measured as final pH, pH_f. A graph was constructed by plotting pH_i against pH_f and the pH_{pzc} was determined from the crossover point of pH_i and pH_f in the graph.

2.3.5 The UV-vis diffused reflectance spectroscopy (DRS)

The UV-vis diffused reflectance spectra (DRS) were recorded from 200 nm to 800 nm, the band gap energy was calculated using the Kubelka – Munk equation:

$$(Rh\nu)^2 = A\,(h\nu - Eg) \qquad \text{..... (6)}$$

where R is the absorbance, $h\nu$ is the absorption energy (unit), A is the parameter related to the effective masses associated with the valence and conduction bands, n is refraction index, and Eg is the band gap energy (unit) (Yan, et al., 2013).

2.3.6 Application Studies

2.3.6.1 Sensors fabrication and gas sensing measurement

The powdered $LaMO_3$ was mixed with organic binder (mixture of **α**-terpineal and ethyl cellulose) to make a paste and was dropped onto the alumina substrate (3×2 mm) with gold interdigitated electrodes to form films. The $LaMO_3$ film was then annealed at 450 °C for 2 h to remove organic content.

The gas-sensing properties of $LaMO_3$ sensors were measured towards ethanol over the concentration range of 50-1000 ppm under atmospheric conditions in a sealed stainless steel chamber by the standard flow through technique. In the gas chamber, the electrodes of $LaMO_3$ sensors were connected to stainless steel probes on a heating stage utilizing Ni-Cr coils, which were heated to different operating

temperatures in the range of 200-350 °C by a DC power supply while the temperature was continuously monitored by a thermocouple. The working temperature was limited to 350 °C because working temperature higher than 350 °C would consume excessive power consumption and be impractical for general ethanol-sensing applications. A flux of synthetic dry air as gas carrier was flowed to mix at a standard T-junction with the desired concentration of target gas dispersed in synthetic air with a constant total flow rate (2 L/min). The gas flow rates were precisely manipulated usingcomputer-controlled multichannel mass flow controllers (Brook Instruments model 5850E) while the sensor resistance was continuously by a voltage-amperometric with a DC potential of 10 V. The sensors were exposed to a gas sample for 10 min at each gas concentration and the air flux was then restored for 25 min. The gas selectivity was also measured towards NO_2, SO_2, H_2 and CO. The performances of gas sensors were analyzed in terms of sensor response, response time and recovery time. For *n*-type conductivity, the sensor response (*S*) is defined as the resistance ratio R_a/R_g, where R_a is a stable resistance in dry air and R_g is the stabilized change in resistance in the reducing gas including C_2H_5OH, H_2, SO_2, and CO The response definition is reversed to R_g/R_a for oxidizing gas such as NO_2. For p-type conductivity, the response is inversed for both reducing and oxidizing gases (T. Samerjai, et al., 2012). The response time was defined as the time required for the variation in resistance to reach 90 % of the equilibrium value after a test gas was injected and the recovery time as the time necessary for the sensor to return to 10 % above the original resistance in air after releasing the tested gas. The sensitivity of the $LaMO_3$- based sensor to ethanol gas was expressed in term of response (R) defined as (Y. Chen, et al., 2016).

$$R = \frac{R_E}{R_A} \qquad \text{..... (7)}$$

2.3.6.2 Heavy metal ions adsorption

To study the effect of parameters such as initial concentration, contact time, and pH for the removal of cadmium and lead, 0.20 g of fixed initial concentration of adsorbent was placed in a 100 mL Erlenmeyer flask and stirred at 300 rpm until reaching equilibrium.

The resulting solutions were centrifuged and the supernatant liquids were analyzed with inductively couple plasma – optical emission spectrometer (ICP-OES).

The amount of adsorbed metal ion at equilibrium condition, q_e (mg/g), was calculated by Eq.(8) :

$$q_e = \frac{(C_0 - C_e)\,V}{W} \qquad \text{..... (8)}$$

where C_0 and C_e are the initial and equilibrium contrations (mg/L), respectively. V is the volume of solution (L) and W is the mass of adsorbent used (g).

The removal percentage of these metal ions was calculated by the following equation,

$$\%\ \text{Removal} = \frac{(C_0 - C_f)}{C_0} \times 100 \qquad \text{..... (9)}$$

where C_0 and C_f are the initial and final concentration of metal ions (mg/L).

2.3.6.2.1 Effect of contact time

The effect of contact time was investigated with 1 mmol /L for Cd(II) and Pb(II) solutions. The 100 mL of metal ions solution was pipetted into the beaker containing 0.20 g of $LaMO_3$ at room temperature and was stirred for a specified period (in minutes). The reaction mixture was then filtered and the supernatant was collected. The metal ion concentration in the supernatant was determined by ICP to obtain the endogenous metal ions.

2.3.6.2.2 Effect of metal ion concentration

In order to study the effect of initial concentration of adsorbate on adsorption uptake, solution of cadmium and lead with initial concentrations of 1, 5, 9, 13, 17, 21, and 25 mmol/L were used. The amount of adsorbent was fixed at 0.20 g per 100 mL of metal ion solution.

2.3.6.2.3 Effect of pH

To study the effect of pH on adsorption, 100 mL of initial concentration at different pH values (1 – 6 for cadmium and 1 – 4 for lead) was agitated with 0.20 g

of adsorbent. The pH was adjusted with HCl or NaOH solution. Removal of cadmium and lead were not studied at higher pH due to precipitation at high pH.

2.3.6.2.4 Recyclability of $LaMO_3$ adsorbents

Part 1 Reuse of adsorbents without EDTA treatment

The powder of $LaMO_3$ was separated from the mixture and tested for reuse by allowing it to adsorb heavy metal ion again from a new fresh solution.

Part 2 Reuse of adsorbents with EDTA treatment

The used adsorbent was regenerated by treating with 0.1 M EDTA solution for about 1 h. The powder was separated and dried at 100 °C for 5 h in an oven and reused for adsorption again.

The amounts of heavy metal adsorbed before and after reuse of both untreated and treated (with EDTA) adsorbent were determined by dispersive X-ray spectrometer (EDAX), ISIS 300, Oxford, England.

CHAPTER 3

RESULTS

3.1 Preparations and characterizations of $LaMO_3$ perovskites

3.1.1 Preparations of $LaMO_3$ by the conventional method (M = Al, Co, Fe, Gd)

For M = Al, Co, Fe, Gd : the colors of precursors obtained from the first stage were white, violet, brown, and white, respectively. After calcination at 900 °C for 2 h, the precursors turned to the corresponding perovskites. The colors of perovskites were white, black, dark brown, and white, respectively. The photographs showing color of precursors and perovskites are displayed in Fig. 1.

Fig.1. The precursors prepared by the co -precipitation method and perovskite oxides after being calcined at 900 °C for 2 h : A1) $LaAlO_3$ precursor, A2) $LaAlO_3$ perovskite, B1) $LaCoO_3$ precursor, B2) $LaCoO_3$ perovskite, C1) $LaFeO_3$ precursor, C2) $LaFeO_3$ perovskite, D1) $LaGdO_3$ precursor, D2) $LaGdO_3$ perovskite at 1200 °C.

3.1.2 Characterizations of $LaMO_3$ perovskites (M = Al, Co, Fe, Gd)

3.1.2.1 X-ray powder diffraction patterns (XRD)

The precursor first obtained was a mixture of $La_2(CO_3)_3$ and $M_2(CO_3)_3$ which later was subjected to calcination. The formation of oxides prior to formation of perovskite phase was evidenced from the XRD patterns displayed in Fig. 2 when the heating temperatures were still lower than the threshold perovskite formation temperature. Phase analyses of all samples were studied by powder X-ray diffraction. The XRD pattern of $LaAlO_3$ matched with the JCPDS file number 85-0848 of $LaAlO_3$ perovskite phase having hexagonal structure. For $LaCoO_3$, the pattern was matched with the rhombohedral $LaCoO_3$ perovskite phase of JCPDS file number 48-0123. The XRD pattern of $LaFeO_3$ and $LaGdO_3$ matched with the JCPDS file number 37-1493 and 42-1465 having orthorhombic and monoclinic structure, respectively.

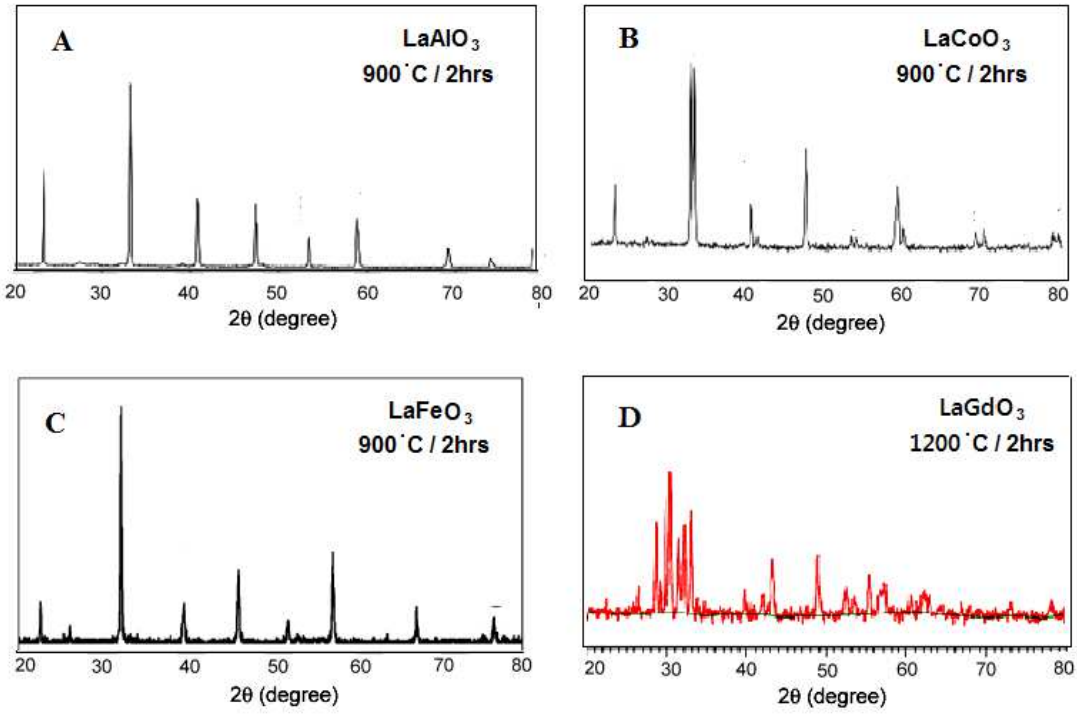

Fig.2. XRD patterns of: (A) $LaAlO_3$, (B) $LaCoO_3$, (C) $LaFeO_3$, and (D) $LaGdO_3$ perovskites

3.1.2.2 Energy dispersive X-ray fluorescence (EDX)

The purity of all samples were also checked with EDX spectrometer (Fig. 3). All the elements detected were those that were expected to be present in the samples. The exception was K and C found in $LaAlO_3$ which could be ascribed to contamination from the glue used to mount the sample.

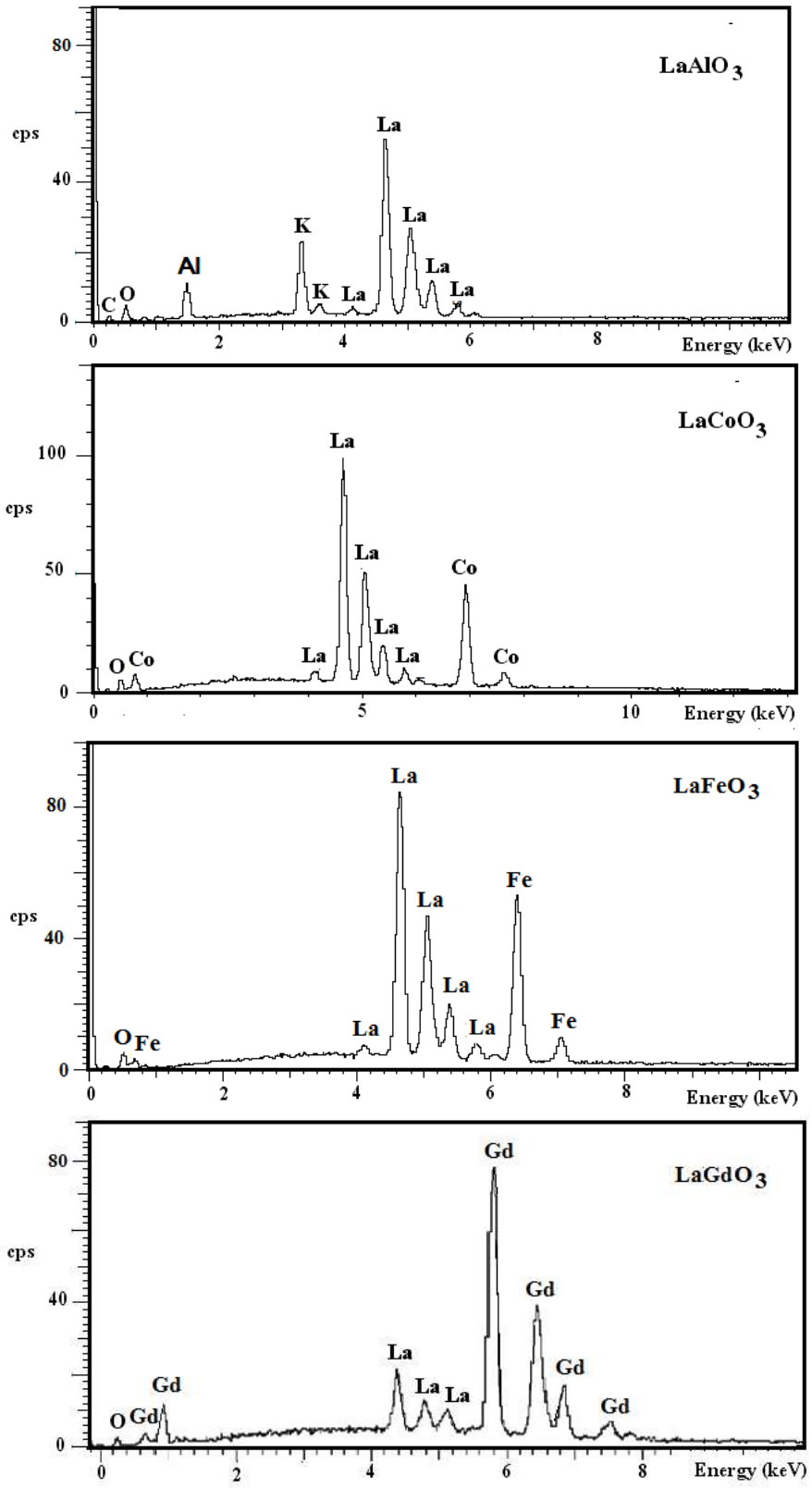

Fig. 3. EDX spectra of $LaMO_3$ perovskites (M = Al, Fe , Co, Gd)

3.1.2.3 Morphologies of products

Fig. 4. shows the scanning electron micrographs of samples, it can be clearly seen that the morphologies of all samples are different. Among the four samples, $LaAlO_3$ has extended cubic shape, the smallest particles size compared with the other three. This should give an advantage in term of bulk surface and high concentration of inter-particle porosity. In contrast, $LaCoO_3$ product contained large aggregates of round-edge particles with different shapes and sizes ranging from few tens of nanometer to several microns. Moreover, merging boundaries can be observed on large particle surfaces, signifying grain growth after high-temperature calcination. In the case of $LaFeO_3$, the structures were mostly micron-sized spheroidal/ellipsoidal aggregated particles and occasionally nanoparticles with much smaller diameter of around ~80-120 nm. Additionally, the larger particles displayed fine surface textures and some cracked boundaries, similar to cracked eggs while the surface of $LaGdO_3$ existed as long grains shape. All samples were also inspected with TEM of which the micrographs are shown in Fig. 6.

$LaAlO_3$

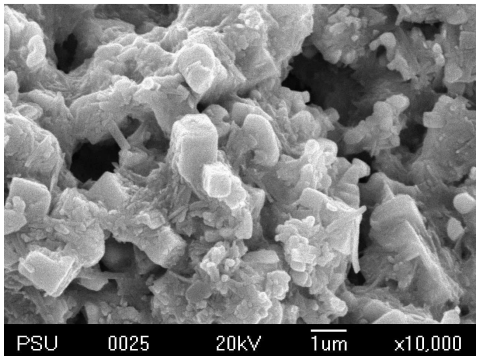

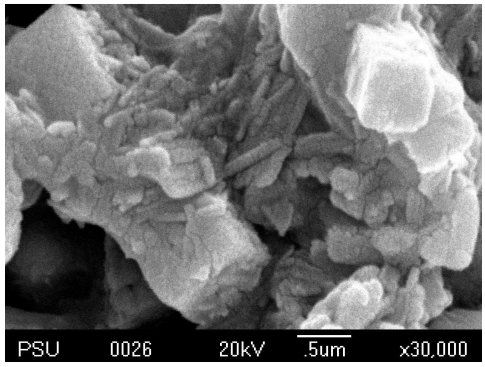

$LaCoO_3$

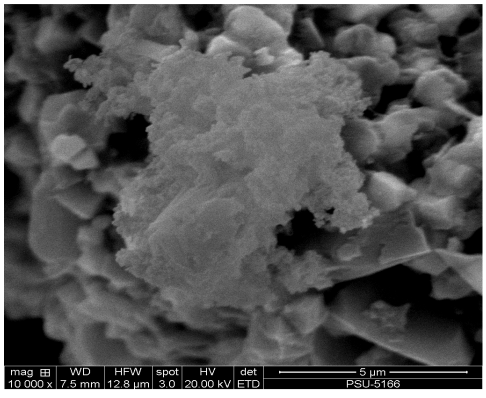

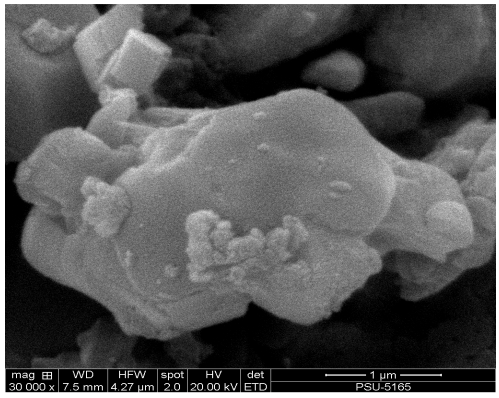

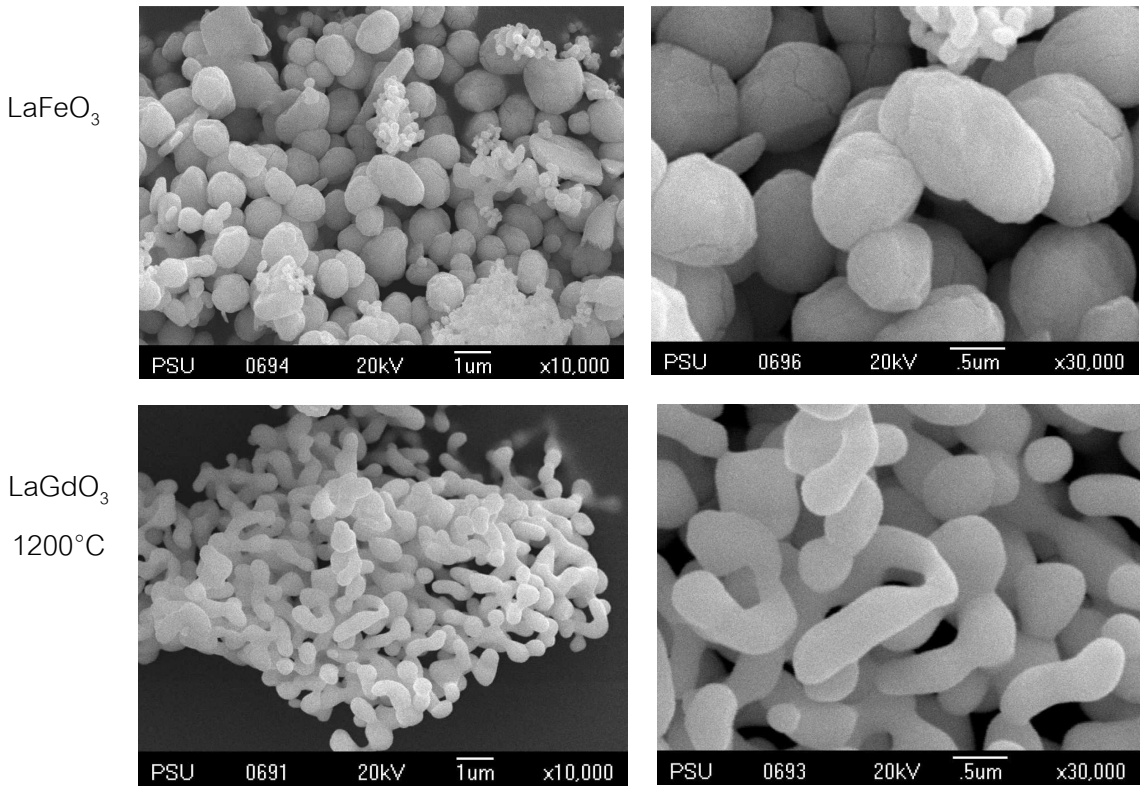

Fig. 4. SEM images of $LaAlO_3$, $LaCoO_3$, $LaFeO_3$, and $LaGdO_3$ powders obtained from 2h of calcination at 900 ℃ and 1200 ℃ for $LaGdO_3$.

The surface morphologies of $LaMO_3$ (M = Al, Co, Fe) perovskite found in this work were similar to those previously by reported by other groups. Z. Li, et al., 2007 studied the SEM of $LaAlO_3$ synthesized by molten salt route at 800 ℃ for 3 hrs. The surface of their sample had extended cubic shape particles similar to the surface of as-synthesized $LaAlO_3$ in this work but stick shape was not observed in their work. The surface revealed many sub-micron particles on some of the large cuboidal particles (Fig. 5(a)). The morphology of the $LaCoO_3$ synthesized by thermal decomposition of oxalates calcined at 850 ℃ for 2 h is shown in Fig. 5(b). It shows that the surface of sample composed of approximately spherical grains and became platelet grains, with a particle size between 600 nm and 1250 nm (W. Kaituo, et al., 2014). The morphology of nanocrystalline $LaFeO_3$ prepared by thermal process of precursor at 900 ℃ for 2 h was studied by Z. Kaiwena, et al., 2013. From Fig. 5(c), it can be seen that the calcined sample obtained at 900 ℃ became platelets grains with particle size about 300 nm in outer diameter.

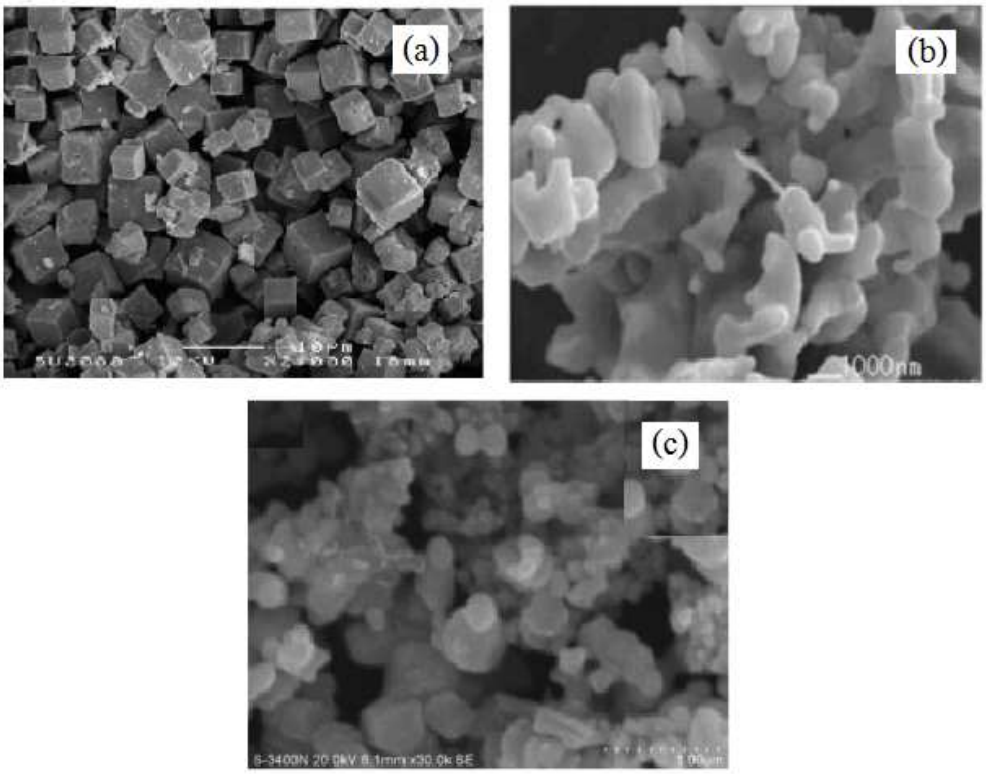

Fig. 5. SEM images of $LaAlO_3$, $LaCoO_3$,and $LaFeO_3$ powders obtained from different routes: (a) $LaAlO_3$ synthesized by molten salt route at 800 °C for 3 h (Z. Li, et al., 2007), (b) $LaCoO_3$ synthesize by thermal decomposition of oxalates at 850 °C for 2 h (W. Kaituo, et al., 2014), and (c) $LaFeO_3$ synthesized by thermal process of precursor at 900 °C for 2 h (Z. Kaiwena, et al., 2013).

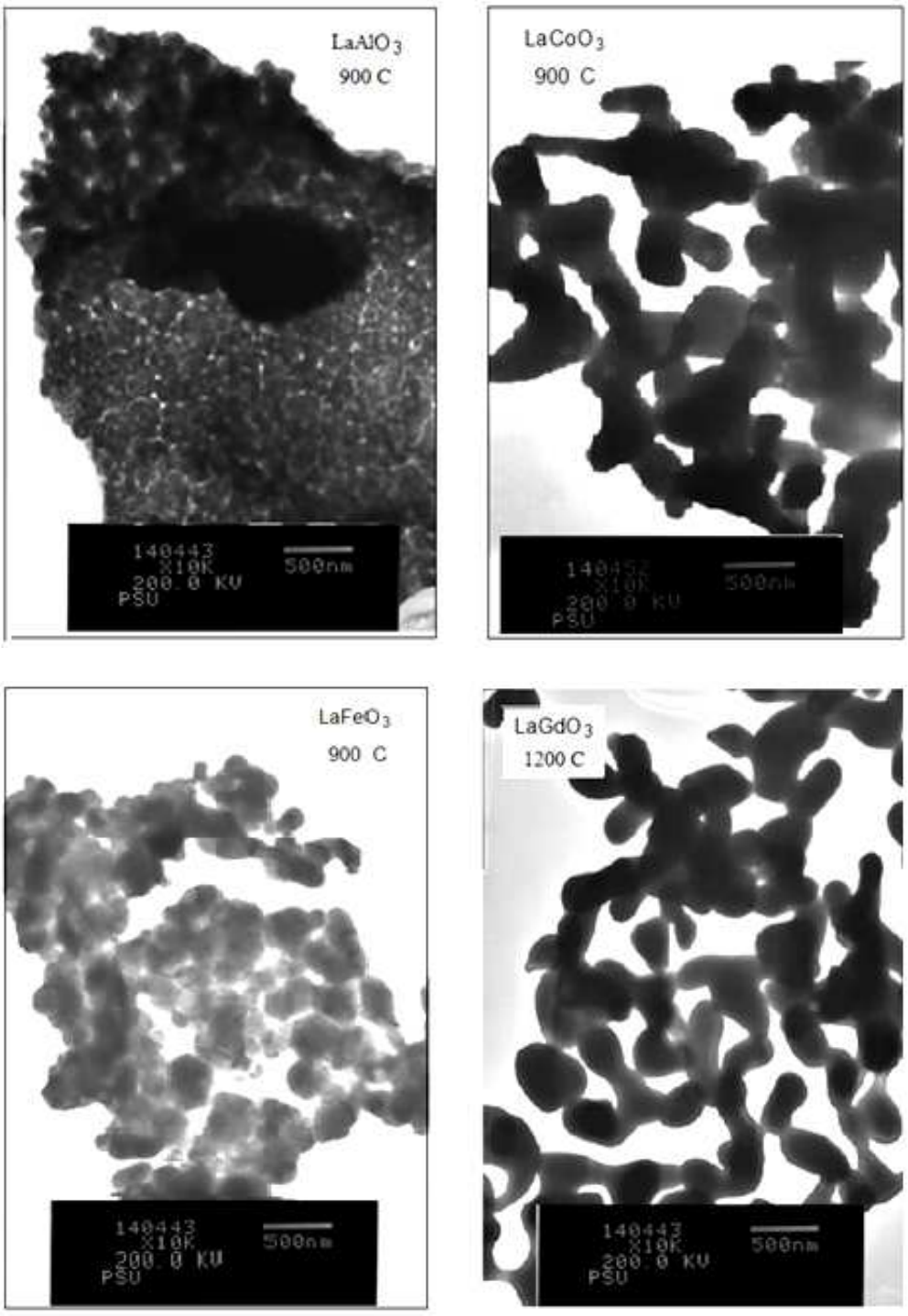

Fig. 6. TEM micrograph of $LaAlO_3$, $LaCoO_3$, $LaFeO_3$, and $LaGdO_3$ powders obtained from 2h of calcination at 900 °C and 1200 °C for $LaGdO_3$.

3.1.2.4 Surface area

The Langmuir surface area and pore volume of $LaMO_3$ at high calcination temperature based on the N_2 adsorption isotherms are given in Table 2. It can be seen that the nano $LaAlO_3$ had the highest Langmuir surface area of 61.670 m^2/g while the $LaCoO_3$, $LaFeO_3$, and $LaGdO_3$ had the surface area of 1.219, 8.925, and 5.431 m^2/g.

The Langmuir surface area can calculated same as the BET surface area but the Langmuir surface area is only monolayer surface area while the BET is multilayers. The surface area of $LaAlO_3$, $LaCoO_3$, and $LaFeO_3$ could not be calculated with the BET method because of the limit of pore size. The three samples had very small size of pores. The $LaGdO_3$ had a larger pore size than the other samples that enabling its surface area can be calculated with the BET method.

Table 2. Langmuir surface area and total pore volume of $LaMO_3$ calcined at high temperature

$LaMO_3$	Calcine temp. (°C)	Total pore volume (cc/g)	Surface area (m^2/g)	Surface area reported by others** (m^2/g)
$LaAlO_3$	900	1.295×10^{-2}	61.670	43.0 (Z. Negahdari, et al., 2009)
$LaCoO_3$	900	3.723×10^{-4}	1.219	18.6 (A. Worayingyong, et al.,2008)
$LaFeO_3$	900	1.036×10^{-3}	8.925	7.9 (Y. Wang, et al., 2006)
$LaGdO_3$*	1200	0.0281	5.431	----------No data----------

* presented as the BET surface area

** no data of the Langmuir surface area or the BET surface area were given

3.1.3 Products from lower calcination temperatures

3.1.3.1 Products characterization

The desired properties of perovskites believed to exhibit good performance as gas sensors and heavy metal adsorbent should have high surface area and smaller crystallite sizes compared with those prepared from the reported conventional method. This is why the lower calcination temperature comes into

focus. The high temperature tends to give good crystallinity with larger crystallite sizes but lower surface area.

The color of precursors were violet and brown which after calcinations at 600 ℃ for $LaCoO_3$ and 800 ℃ for $LaFeO_3$, the precursors turned to perovskite with black and dark brown color. The photographs of each precursor and each perovskite are shown in Fig. 7 – 8.

Fig. 7. The powders of precursor and perovskite oxide of $LaCoO_3$: P) precursor, A) calcined at 200 ℃, B) calcined at 400 ℃, and C) calcined at 600 ℃.

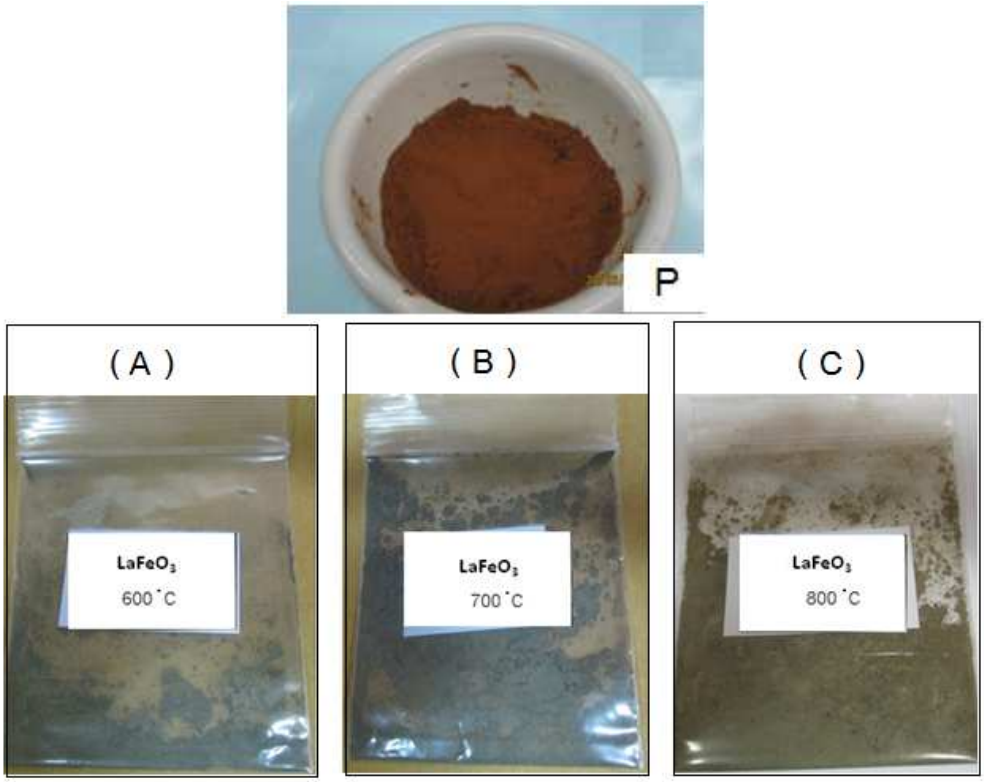

Fig. 8. The powders of precursor and perovskite oxide of $LaFeO_3$: P) precursor, A) calcined at 600 ℃, B) calcined at 700 ℃, and C) calcined at 800 ℃.

The XRD patterns of $LaFeO_3$ and $LaCoO_3$ at various temperatures are shown in Fig. 9. For $LaFeO_3$, the product obtained from calcination at 800 ℃ was $LaFeO_3$ perovskite (matched with JCPDS file no. 37-1493) having orthorhombic structure with particle size of 68 nm. If the calcination temperature was lower than 800 ℃, sample powder existed only as mixture of La_2O_3 and Fe_2O_3. For $LaCoO_3$, the rhombohedral $LaCoO_3$ perovskite formed at 600 ℃ (matched with JCPDS file no. 48-0123), otherwise, the mixture of La_2O_3 and Co_2O_3 was obtained if the calcination temperature was lower than 600 ℃. The particle size of $LaCoO_3$ at 600 ℃ was 69 nm. Both crystallite sizes were smaller than that obtained at 900 ℃.

For $LaAlO_3$, no perovskite phase was detected below 900 ℃ as shown in Fig. 10, hence, no further study was undertaken.

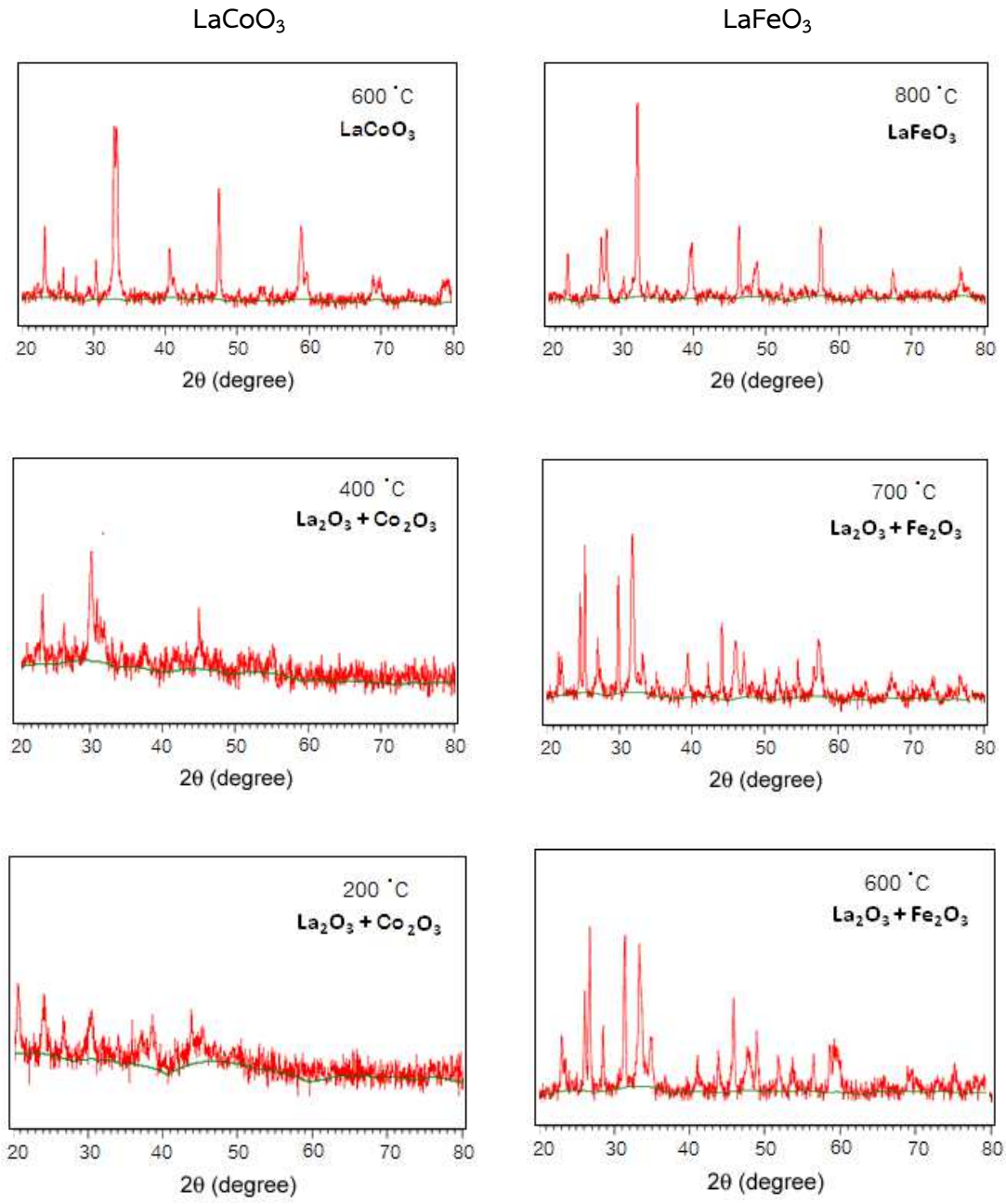

Fig. 9. XRD patterns of $LaFeO_3$ and $LaCoO_3$ perovskites obtained from various temperatures.

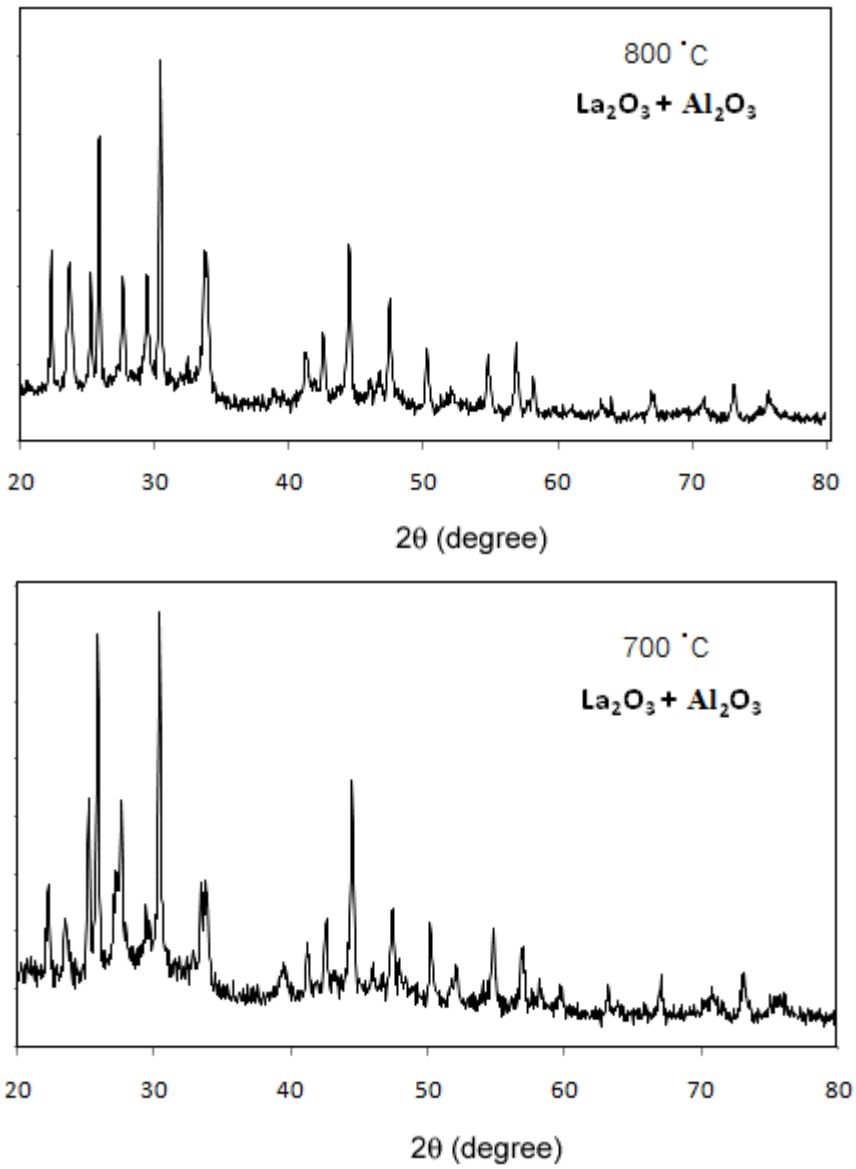

Fig. 10. XRD patterns of $LaAlO_3$ precursor calcined at 700 and 800 °C.

Fig.11. illustrates the clean and impurity free EDX spectra of $LaFeO_3$ and $LaCoO_3$ obtained at lower calcinations attesting the same high purity products could still be obtained eventhough the calcination temperature was lower.

The SEM images of the two low temperature perovskites (Fig.12.) revealed markedly different surface morphologies from those obtained at higher temperature (900 °C). At higher temperature, small particles developed into larger particles accompanied by smoother surfaces. On the other hand, the low temperature

samples exhibited rougher and more irregular surface morphologies which should give them distinct advantage for gas sensor and heavy metal adsorption.

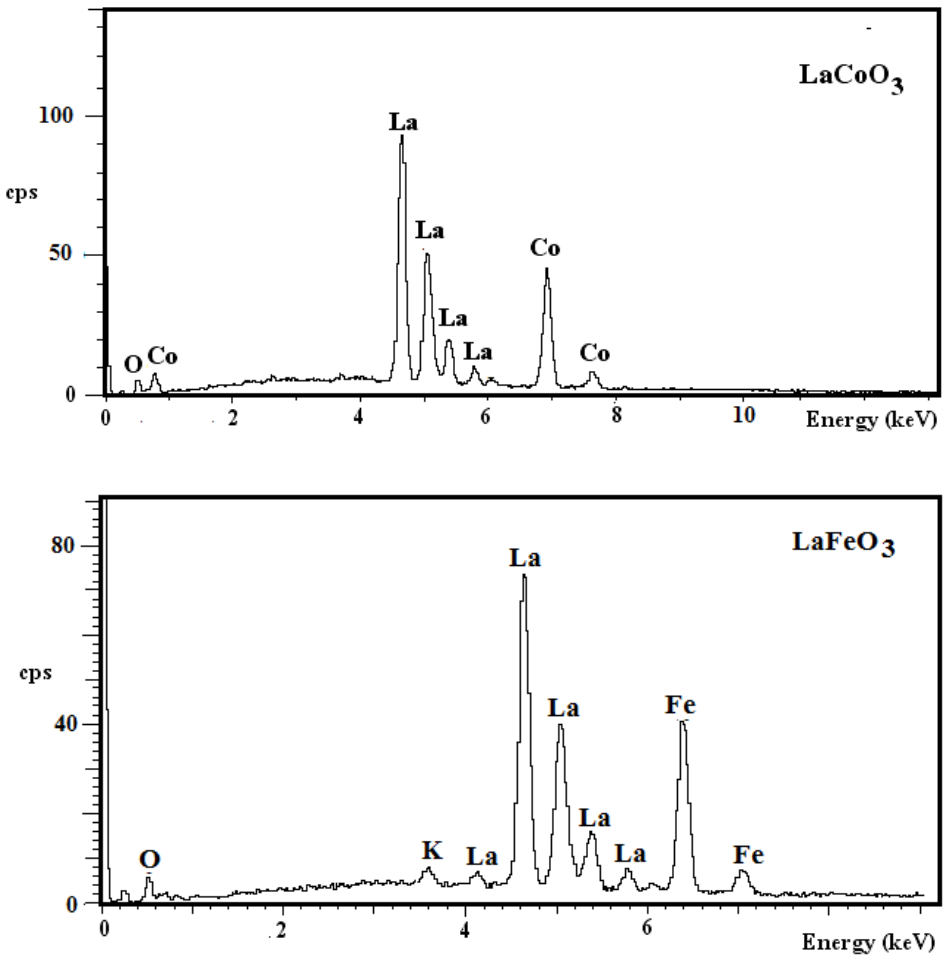

Fig. 11. EDX spectra of $LaCoO_3$ (600 °C) and $LaFeO_3$ (800 °C).

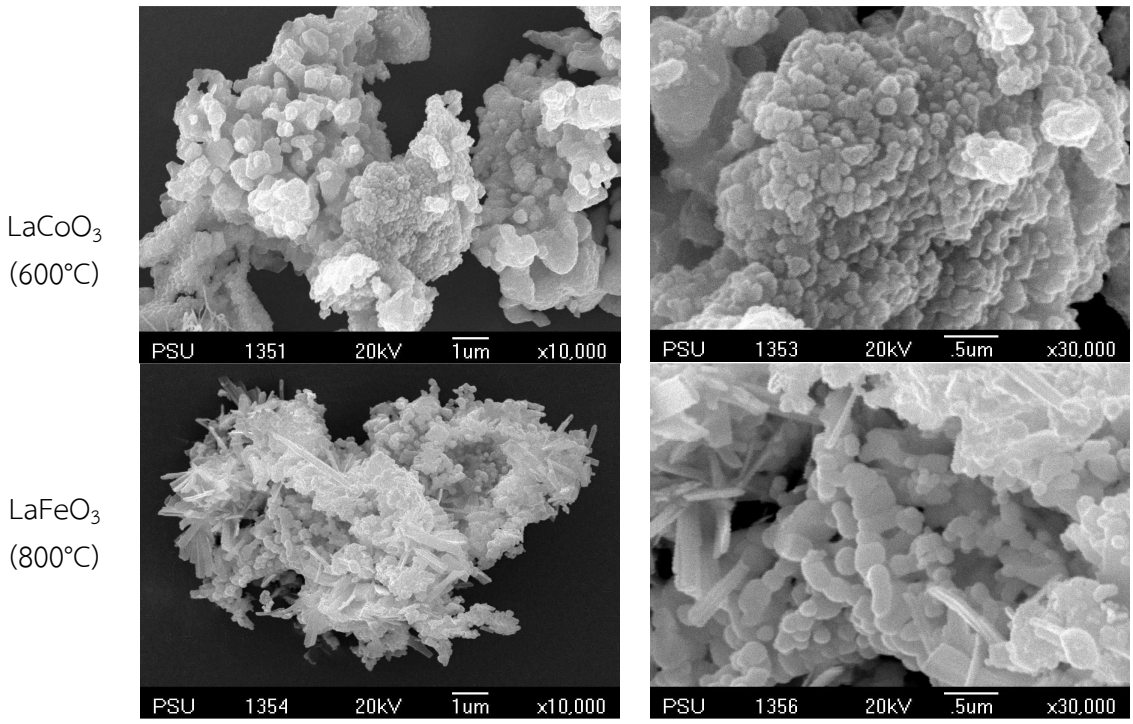

Fig. 12. SEM images of $LaCoO_3$ and $LaFeO_3$ powders calcined at each corresponding temperature.

Fig. 13 shows the SEM micrographs of $LaCoO_3$ and $LaFeO_3$ prepared by other methods and reported in the literatures. The $LaCoO_3$ synthesized with high energy ball milling methods at 600 ℃ for 2 h is shown in Fig. 13(a). It can be seen that the particle morphologies of $LaCoO_3$ are micron size particles with high degree of agglomeration, each agglomerate being composed of nanocrystallites with an average size of 11 nm (M. Ghasdi,et al., 2010). X. Wang, et al., 2013 studied the microstructure of $LaFeO_3$ powders prepared by sol gel method calcined at 800 ℃ for 2 h, the SEM of which is shown in Fig. 13(b). The surface of sample contained grains with large particles accompanied by smoother surfaces.

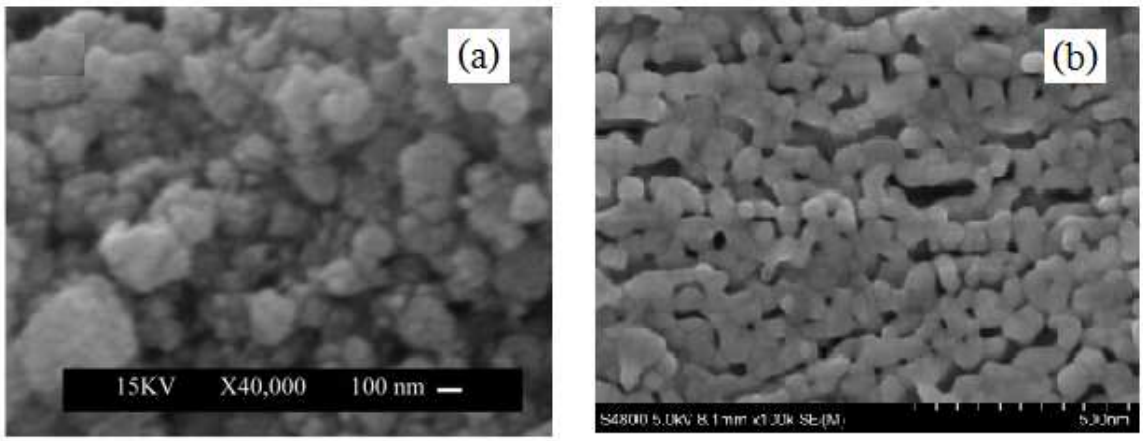

Fig. 13. SEM images of $LaCoO_3$ and $LaFeO_3$ powders reported in other researchs : (a) $LaCoO_3$ synthesized with high energy ball milling methods at 600 ℃ for 2 h (M. Ghasdi,et al., 2010) and (b) $LaFeO_3$ synthesized with sol gel method at 800 ℃ for 2 h (X. Wang, et al., 2013).

The TEM micrographs of $LaCoO_3$ powder calcined at 600 ℃ and $LaFeO_3$ powder calcined at 800 ℃ are shown in Fig. 14 showing slight interparticles void spaces. For comparison, the TEM micrographs of $LaFeO_3$ synthesized with solid state reaction at 900 ℃ for 2 h is shown in Fig. 15. The average crystal sizes of the samples was 60 nm consisting of agglomeration of small particle (X. Chu, et al., 2009).

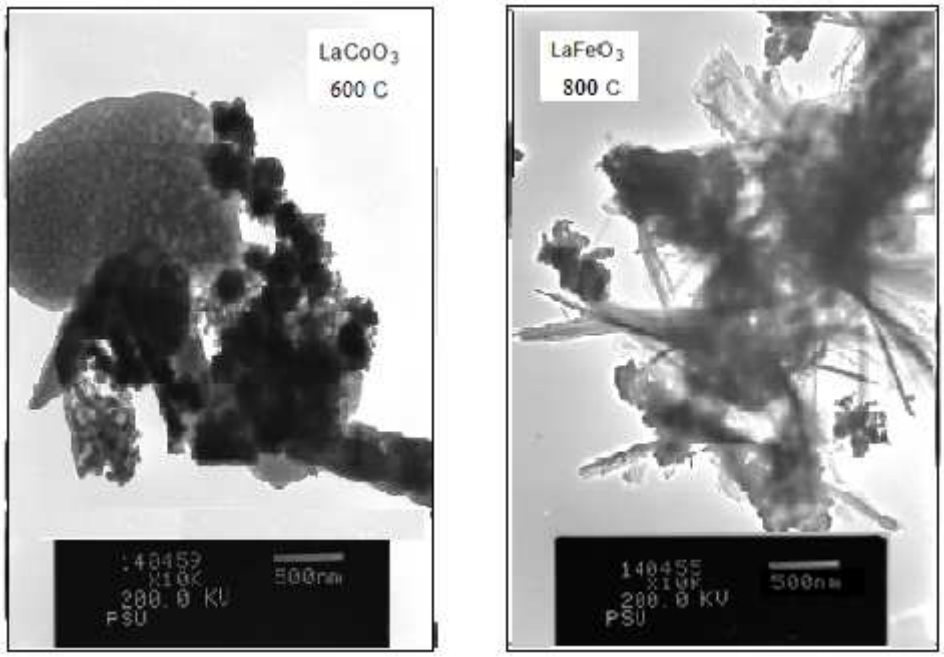

Fig. 14. TEM micrographs of $LaCoO_3$ and $LaFeO_3$ powders obtained from 2h of calcination at 600 ℃ and 800 ℃.

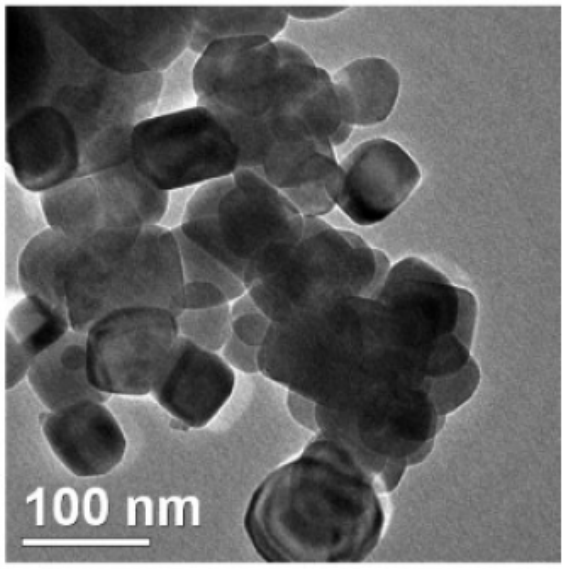

Fig. 15. TEM micrographs of $LaFeO_3$ powders obtained from solid state reaction at 900 ℃ for 2 h (X. Chu, et al., 2009)

3.1.3.2 Surface area of $LaMO_3$ calcined at lower than 900 °C

The BET surface area and pore volume of $LaMO_3$ at lower temperatures based on the N_2 adsorption isotherms are given in Table 3. It can be seen that both nano-$LaCoO_3$ and $LaFeO_3$ have almost identical surface area ~ 23 m^2/g and are similar to those reported in the literatures.

Table 3. BET surface area and total pore volume of $LaCoO_3$ and $LaFeO_3$ prepared by co-precipitation method and calcined at lower than 900 °C

$LaMO_3$	Calcine temp. (°C)	Total pore volume (cc/g)	Surface area (m^2/g)	Surface area reported by others (m^2/g)
$LaCoO_3$	600	0.06	23.07	27.00 (S. Farhadi, et al., 2010)
$LaFeO_3$	800	0.07	23.03	36.50 (S. Farhadi, et al., 2009)

3.1.3.3 pH at point of zero charge (pH_{pzc})

Experimental results of pH_{pzc} determination were carried out using the pH drift method (H.K. Liao et al 1999). The equilibrated pH (pH_f) of the as-prepared $LaMO_3$ (M = Al, Co, Fe, Gd) were plotted against initial pH (pH_i) of the solution having constant ionic strength (0.1 mol/L NaCl). The pH at a point where the initial pH of the solution crossover the equilibrated pH is the pH_{pzc} of the sample (Figs. 16 – 19).

The measured pH_{pzc} of $LaAlO_3$, $LaCoO_3$, $LaFeO_3$, and $LaGdO_3$ in this work were 8.6, 9.2, 9.0, and 8.1, respectively. The pH_{pzc} of $LaAlO_3$, $LaCoO_3$ in this work were not much different from those reported at 9.9 (Z. Negahdari, et al., 2009) and 12.8 (D. Mezaini, et al., 2014), respectively, while there were no data for $LaFeO_3$ and $LaGdO_3$.

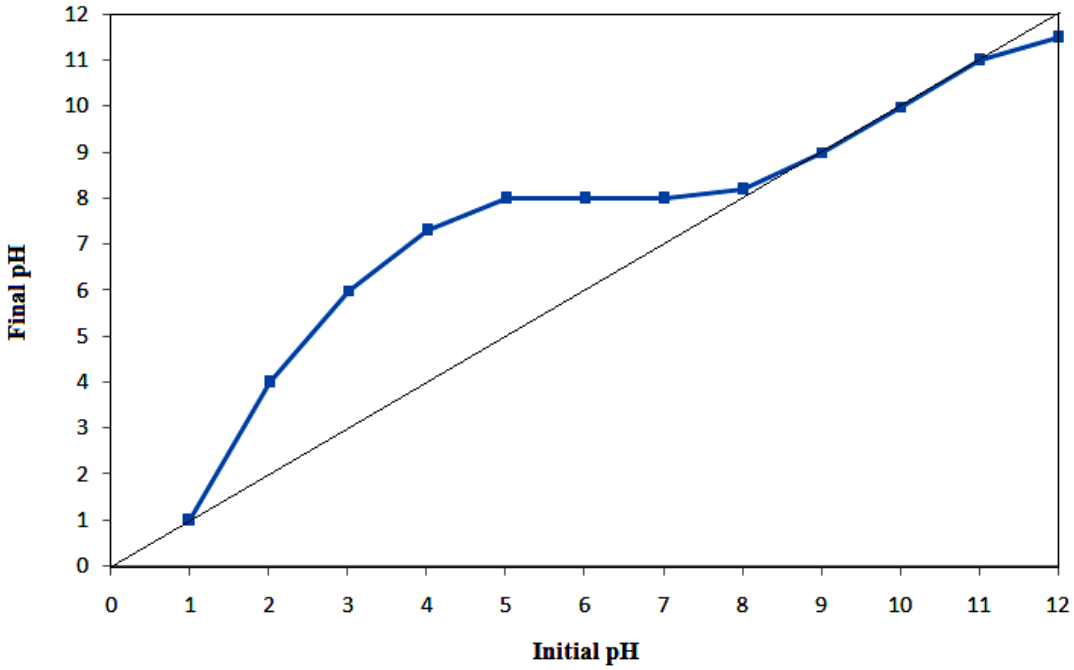

Fig. 16. The plot of final pH (pH_f) versus initial pH (pH_i) of the $LaAlO_3$ sample to determine the pH_{pzc}.

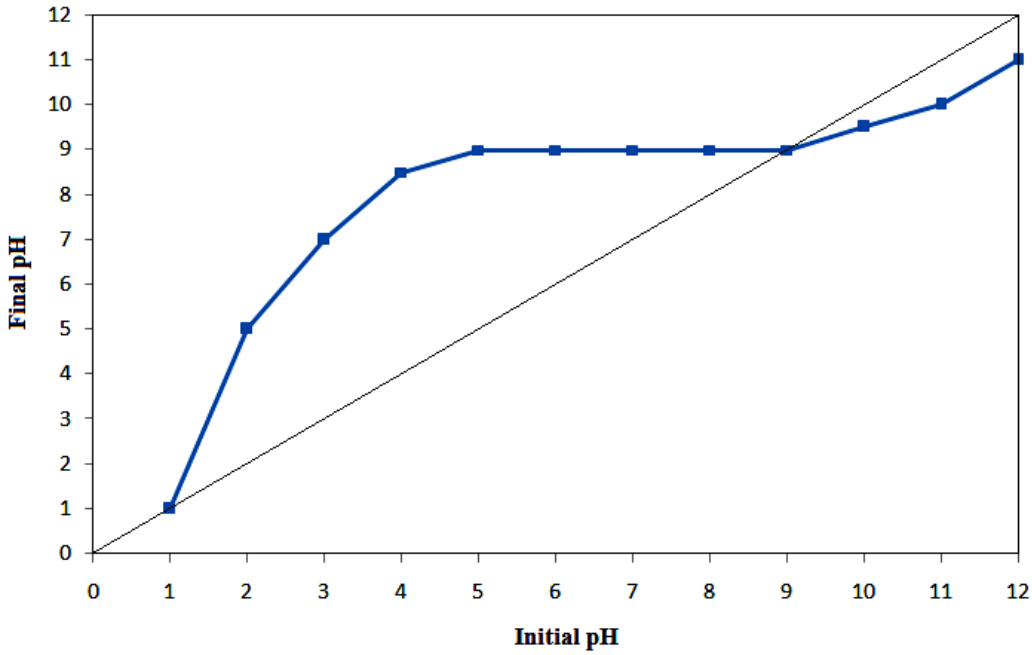

Fig. 17. The plot of final pH (pH_f) versus initial pH (pH_i) of the $LaCoO_3$ sample to determine the pH_{pzc}.

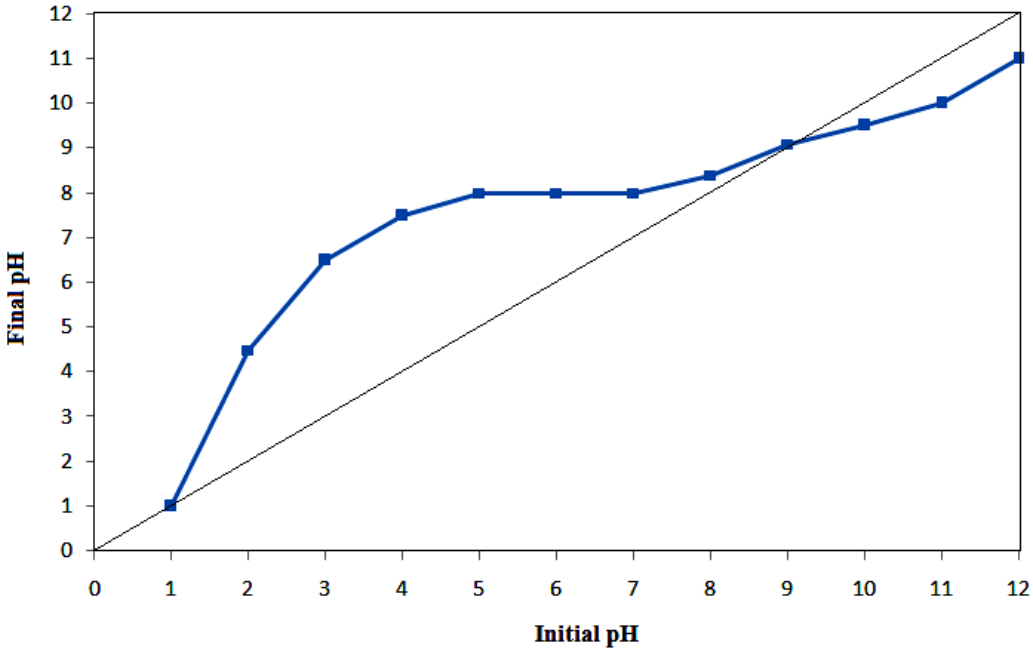

Fig. 18. The plot of final pH (pH_f) versus initial pH (pH_i) of the $LaFeO_3$ sample to determinine the pH_{pzc}.

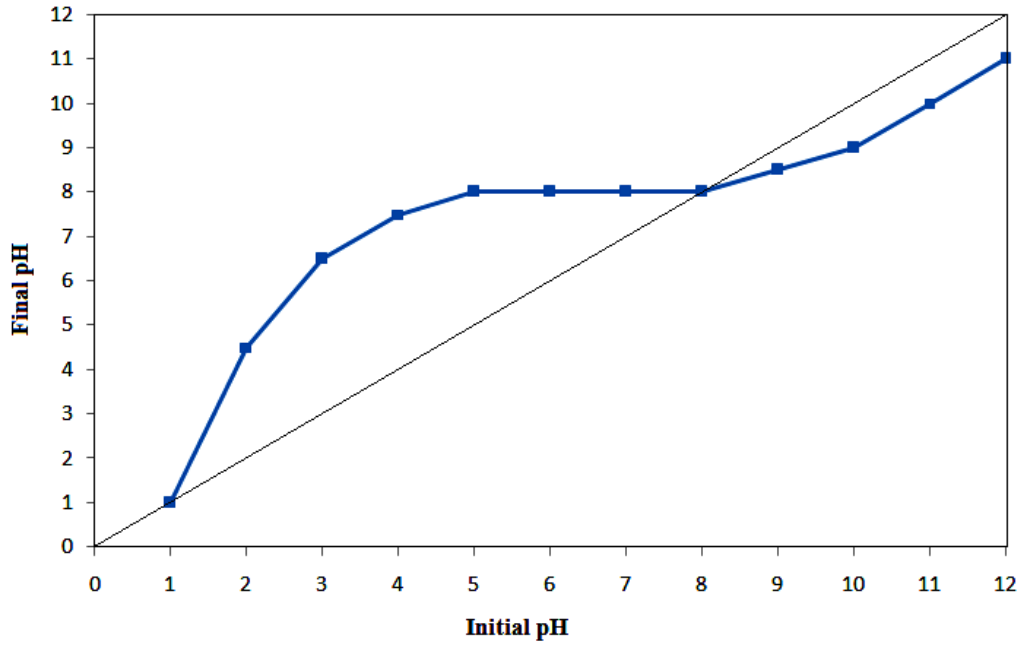

Fig. 19. The plot of final pH (pH_f) versus initial pH (pH_i) of the $LaGdO_3$ sample to determine the pH_{pzc}.

3.1.3.4 The UV-vis diffused reflectance spectroscopy (DRS)

The UV-vis diffused reflectance spectra (DRS) of $LaMO_3$ (M = Al, Co, Fe, Gd) at about 200 – 800 nm are shown in Figs. 20 – 23. The details of spectra were observable only in range 200 – 400 nm for all samples. The band gap energy was calculated using the Kubelka – Munk equation are shown in Figs. 24 – 27 and the obtained band gap energies of $LaAlO_3$, $LaCoO_3$, $LaFeO_3$, and $LaGdO_3$ were 2.60, 1.50, 2.00, and 2.90 eV, respectively.

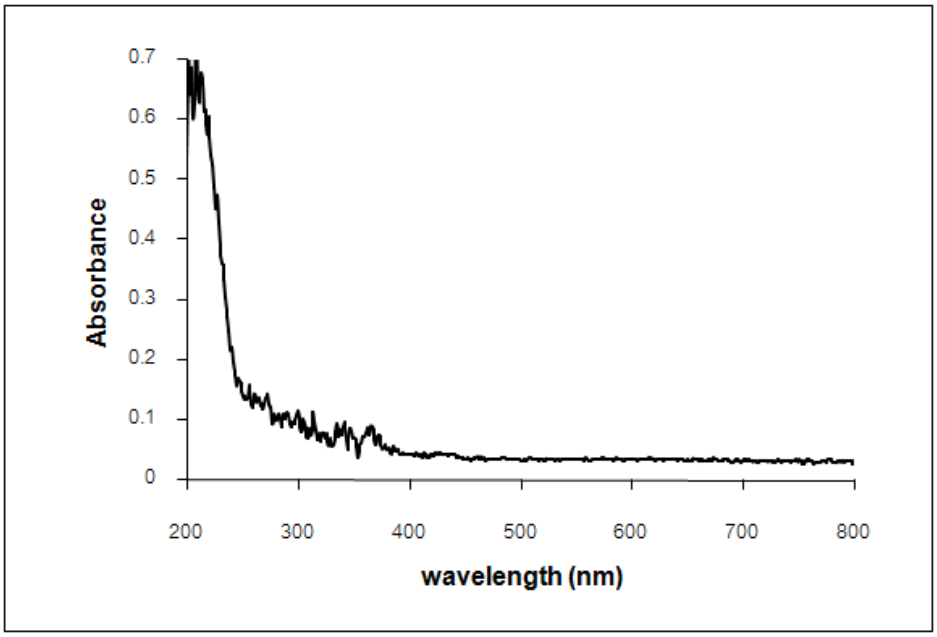

Fig. 20. UV-Vis DRS spectrum of $LaAlO_3$-perovskite.

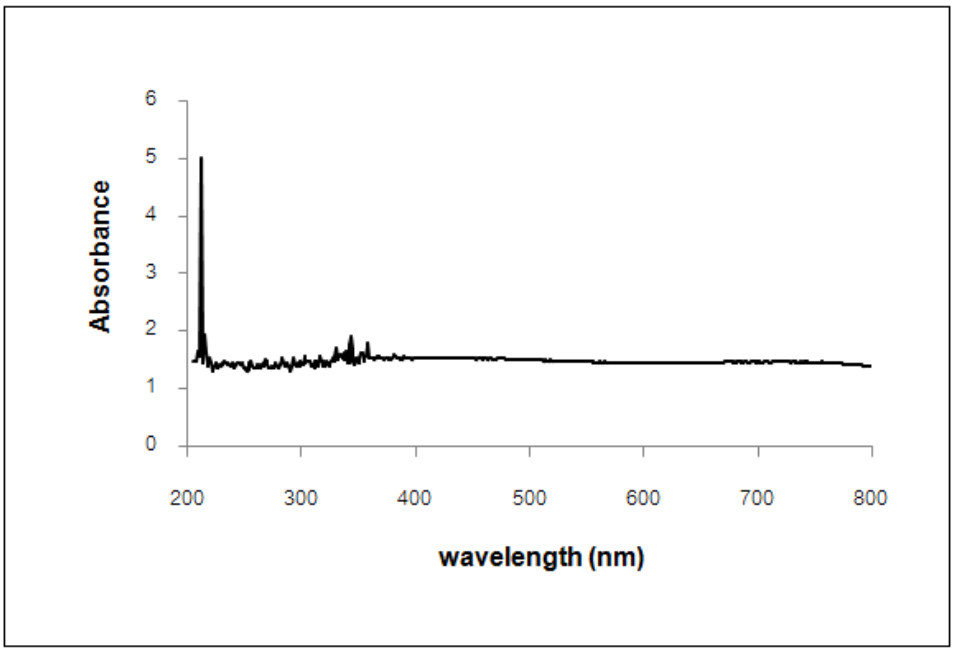

Fig. 21. UV-Vis DRS spectrum of $LaCoO_3$-perovskite.

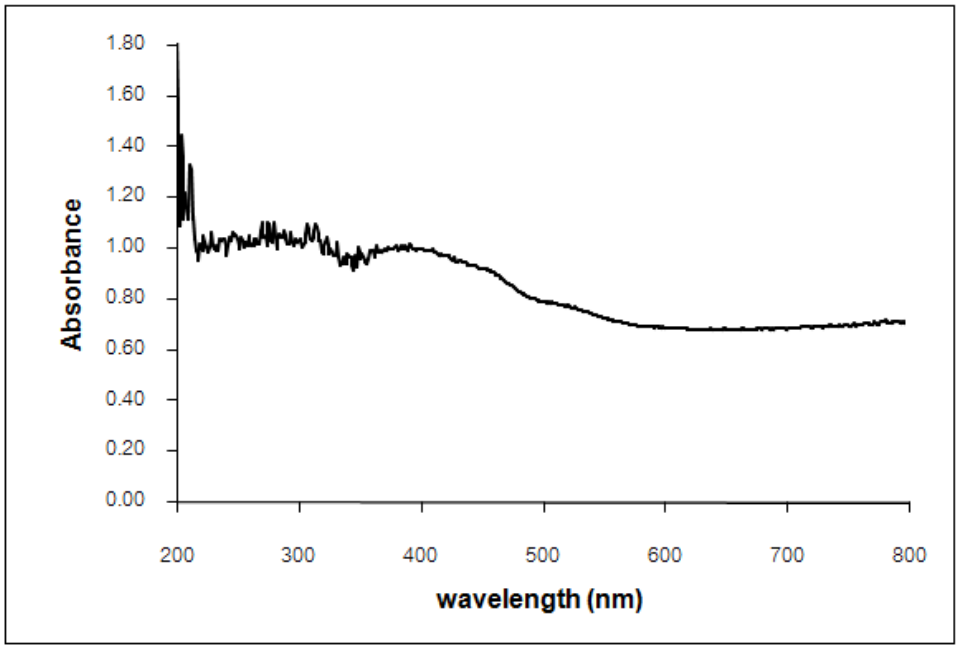

Fig. 22. UV-Vis DRS spectrum of $LaFeO_3$-perovskite.

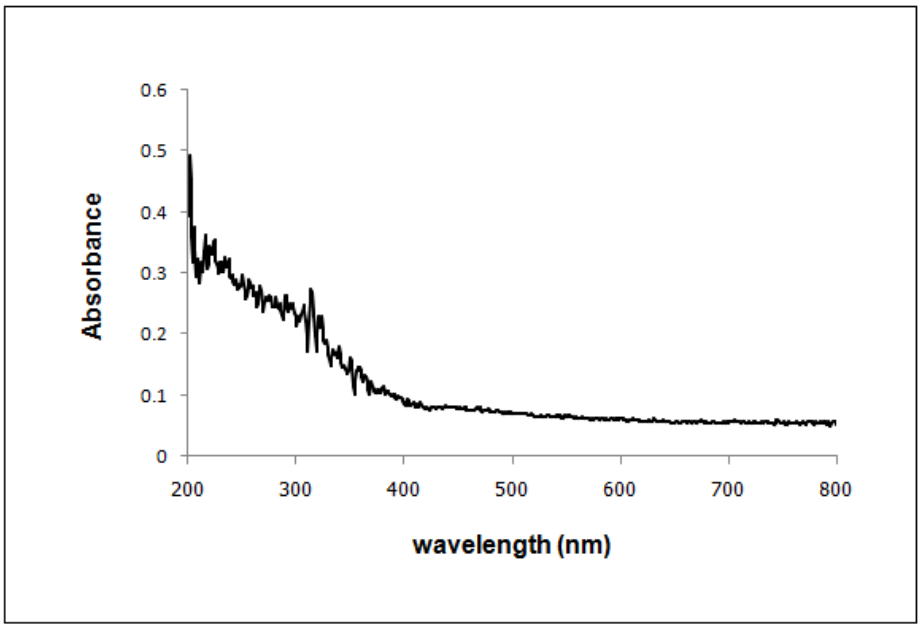

Fig. 23. UV-Vis DRS spectrum of $LaGdO_3$-perovskite.

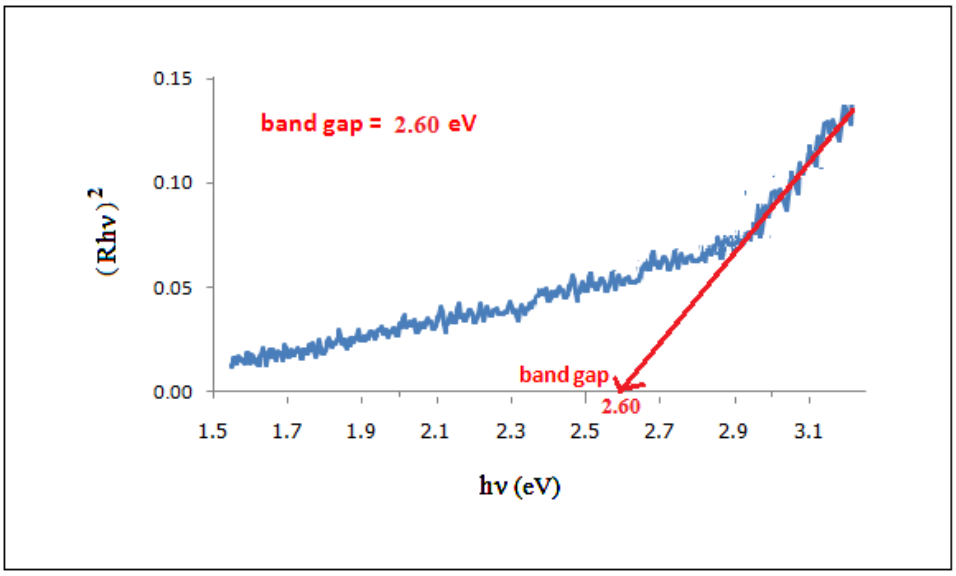

Fig. 24. Band-gap energy calculation for $LaAlO_3$-perovskite.

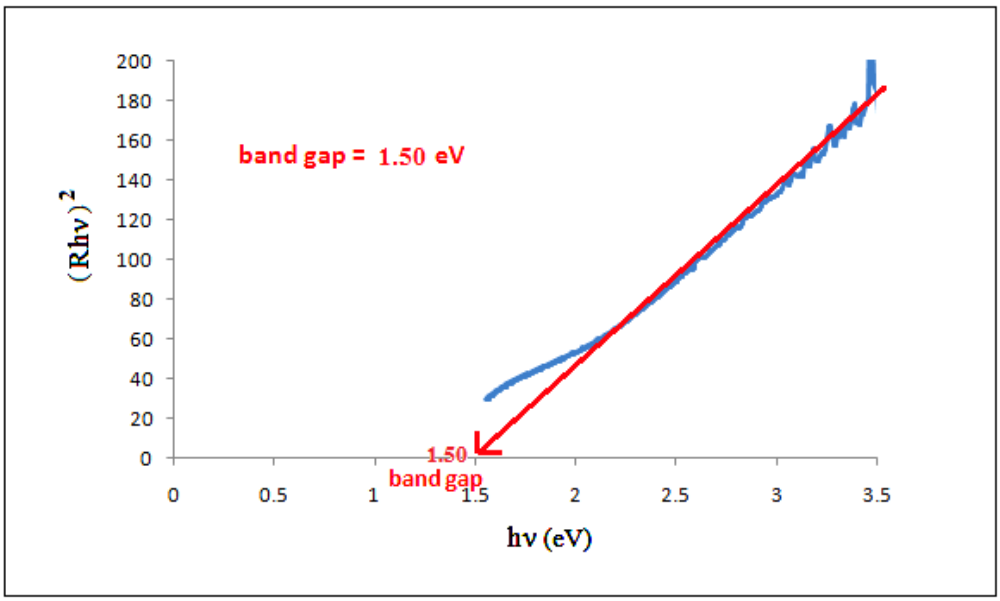

Fig. 25. Band-gap energy calculation for $LaCoO_3$-perovskite.

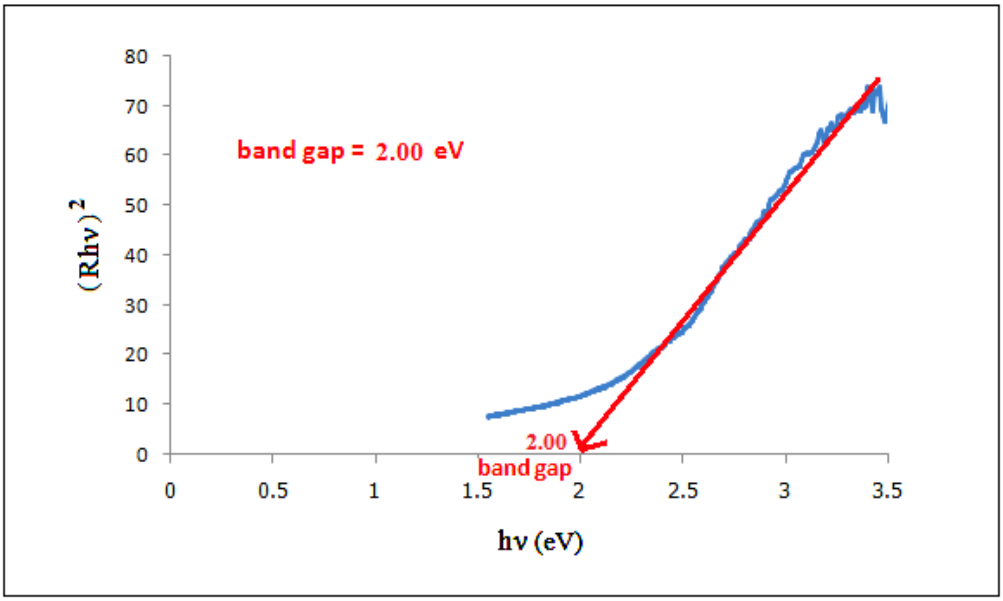

Fig. 26. Band-gap energy calculation for $LaFeO_3$-perovskite.

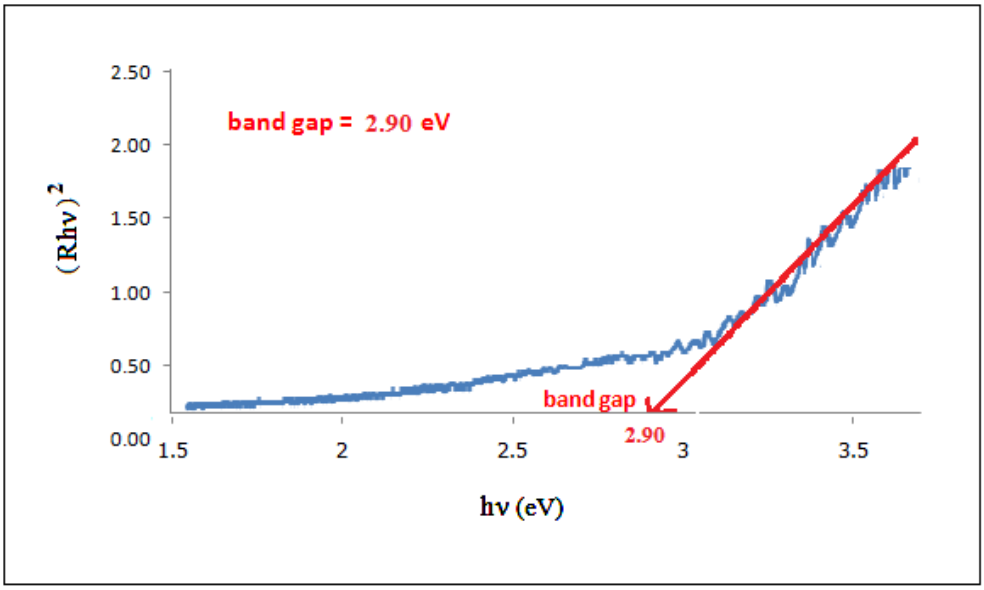

Fig. 27. Band-gap energy calculation for $LaGdO_3$-perovskite.

3.2 Applications of $LaMO_3$- perovskite oxides

3.2.1 As ethanol sensor

The response-recovery behavior is another important characteristic that determines the performance of gas sensors. The response time was defined as the time required for the variation in resistance to reach 90% of the equilibrium value after a test gas was injected and the recovery time as the time necessary for the sensor to return to 10% above the original resistance in air after releasing the test gas (P. Song, et al., 2014). Figs. 28 – 33 show the resistance transient of the sensor based on $LaMO_3$ (M = Al, Co, Fe, Gd) to 50–1000 ppm ethanol at the optimal operating temperature of 350°C which is in good agreement with typical p-type semiconductor materials (P. Song, et al., 2014). It can be seen that the resistance of the sensor increased abruptly on the injection of ethanol, and then decreased rapidly and recovered to its initial value after the test gas was released.

The output resistance signal depicts the drop from the resistance R_{air} to the equilibrium value $R_{ethanol}$ that occurs with the entry of ethanol vapors into the test chamber and after purging brings back to the background value indicating the absence of ethanol vapors. The resistant increased with increasing concentration of ethanol gas. The resistance value of $LaAlO_3$ calcined at 900 °C was very high (Fig. 28) and higher than $LaFeO_3$ (Fig. 30) due to the highest response to ethanol gas. The $LaCoO_3$ calcined at 900 °C had very small surface area due to the resistance

unstability at the end of period (Fig. 30). The $LaGdO_3$ did not possess ethanol sensor property because the resistance signal was unstable throughout the period (Fig. 33).

The responses to ethanol gas of $LaMO_3$ (M = Al, Co, Fe, Gd) calcined at 900 °C are shown in Table 4. It can be seen that the nano-$LaAlO_3$ showed the highest value of response to ethanol while $LaGdO_3$ showed no response to ethanol (Table 4). $LaCoO_3$ (Fig. 31) and $LaFeO_3$ (Fig. 32) calcined at 600 °C and 800 °C showed very high response compared with when calcined 900 °C (Table 5). ($LaAlO_3$ and $LaGdO_3$ are not included in Table 5 because they turned to perovskite phase at high temperature (900 °C or higher) which was out of our scope for lower temperature than 900 °C). In addition, we already showed $LaGdO_3$ in Table 4 that it did not behave as the ethanol gas sensor.

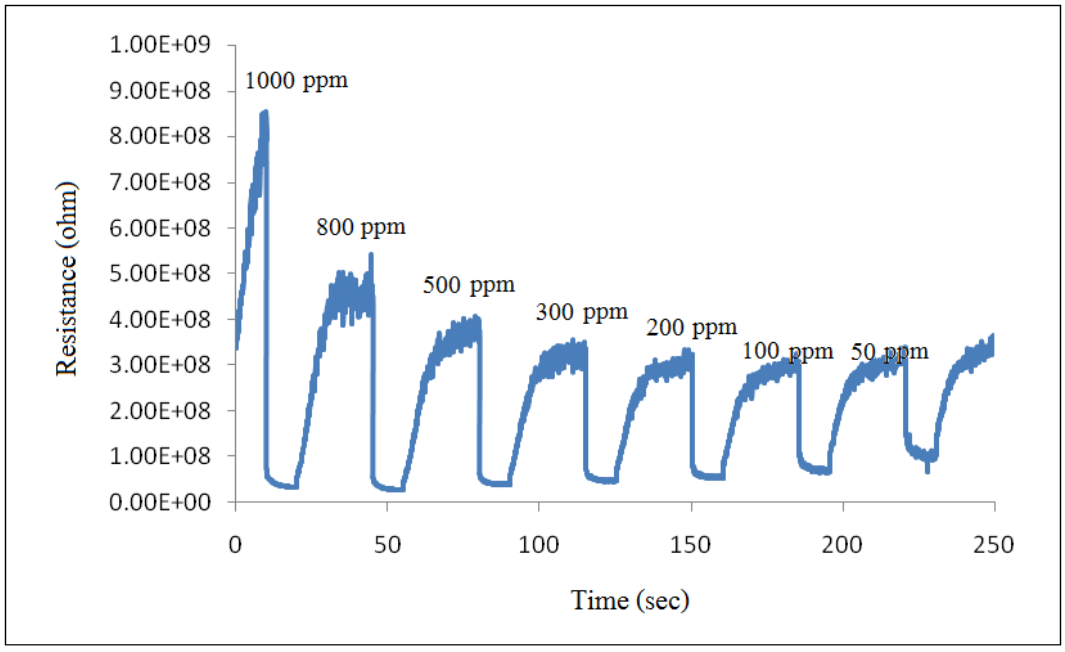

Fig. 28. Response curve of $LaAlO_3$ calcined 900 °C to 50 – 1000 ppm ethanol gas.

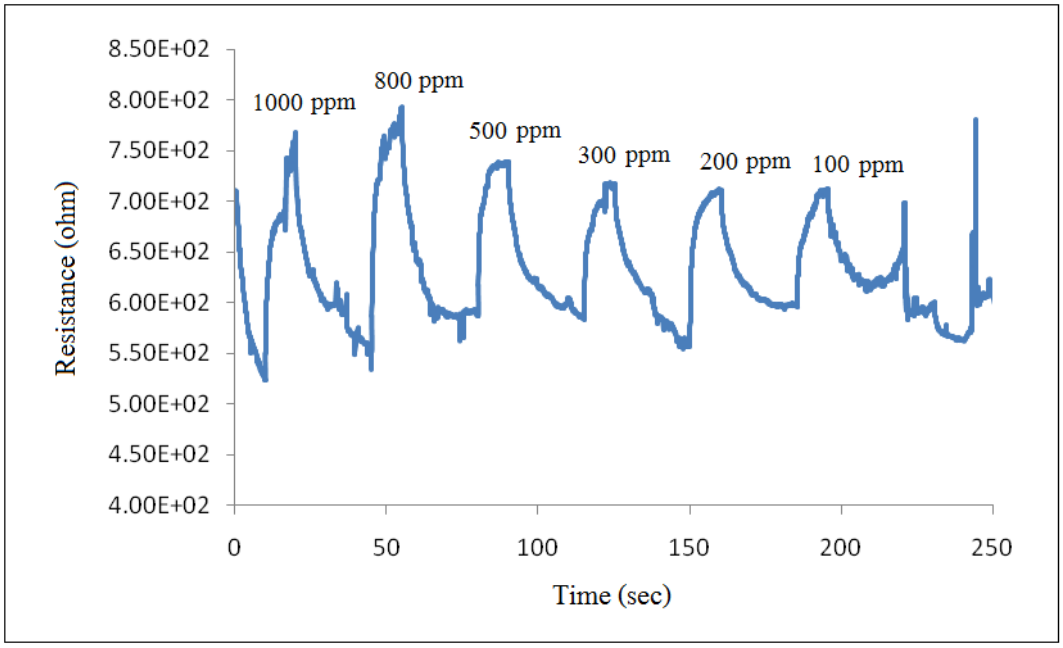

Fig. 29. Response curve of $LaCoO_3$ calcined 900 °C to 50 – 1000 ppm ethanol gas.

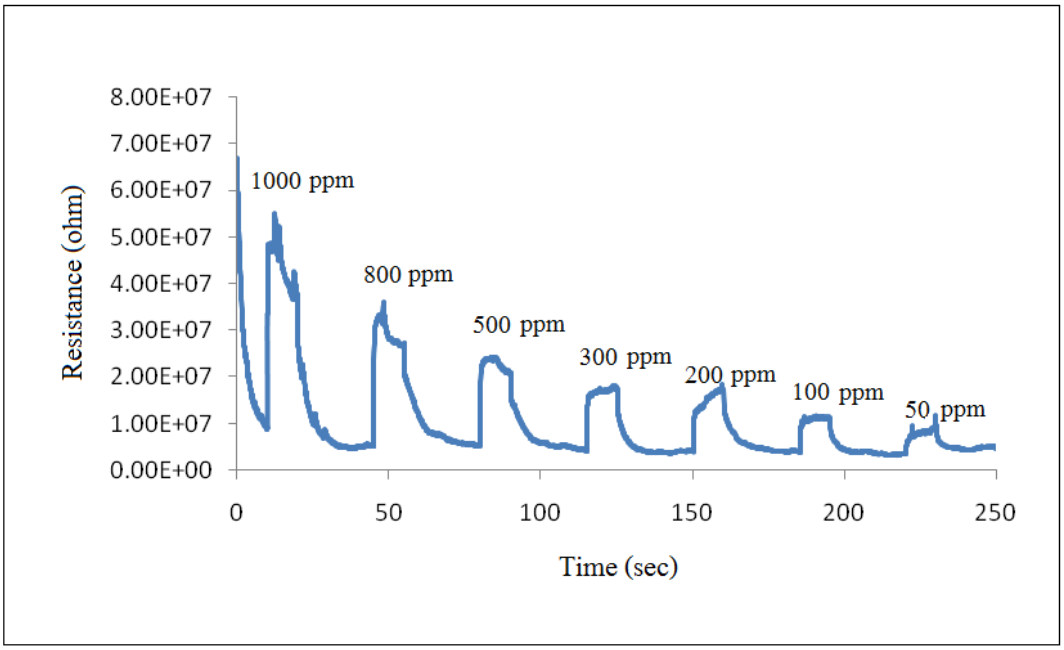

Fig. 30. Response curve of $LaFeO_3$ calcined 900 °C to 50 – 1000 ppm ethanol gas.

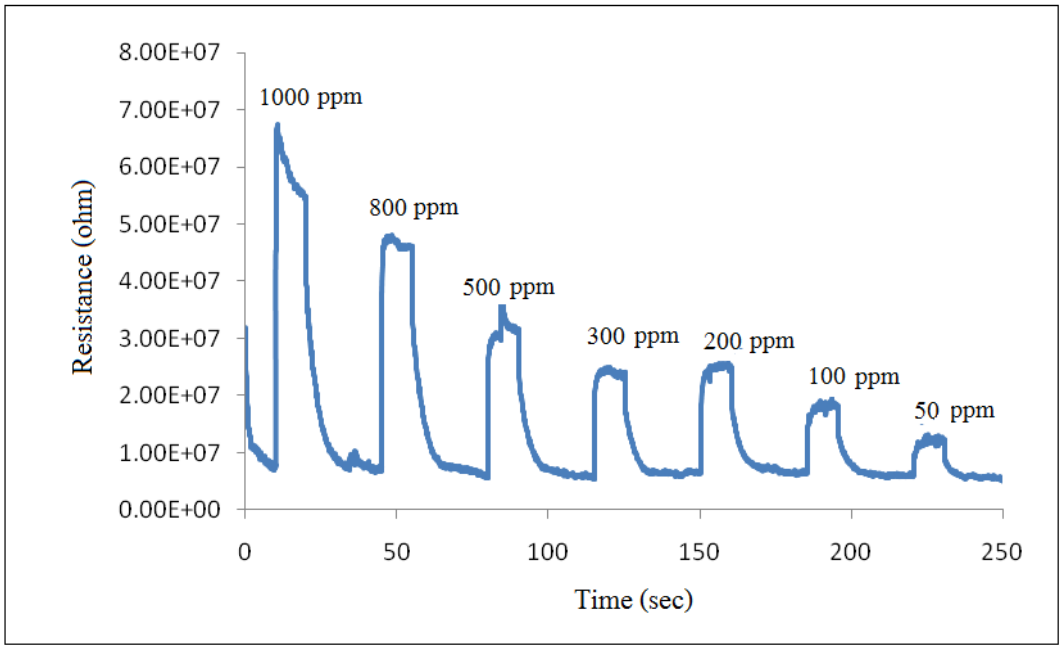

Fig.31. Response curve of $LaCoO_3$ calcined 600 °C to 50 – 1000 ppm ethanol gas.

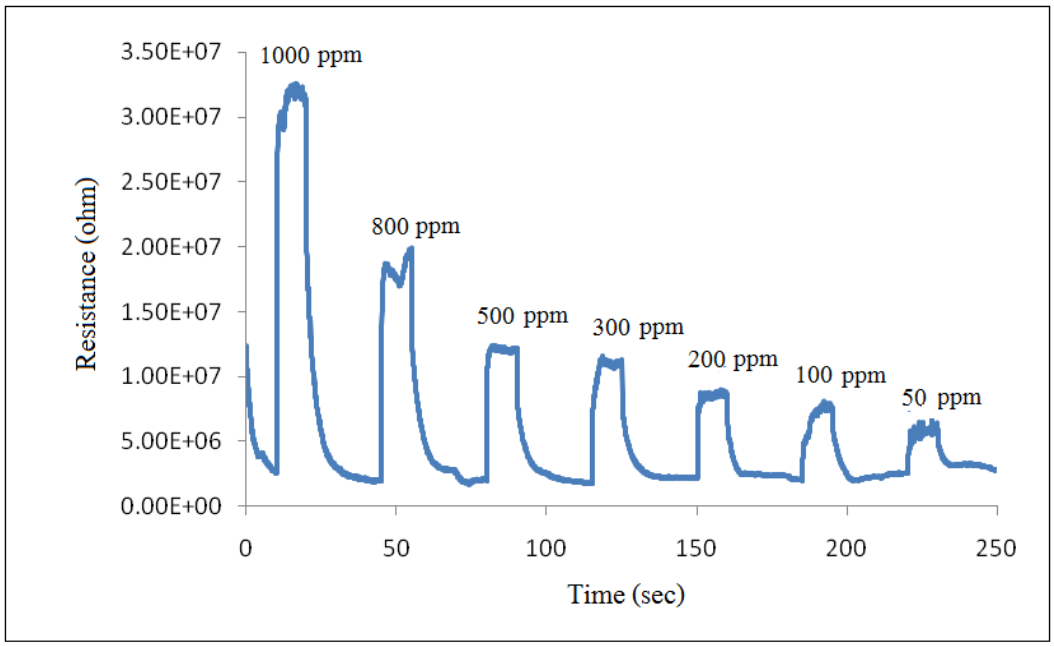

Fig.32. Response curve of $LaFeO_3$ calcined 800 °C to 50 – 1000 ppm ethanol gas.

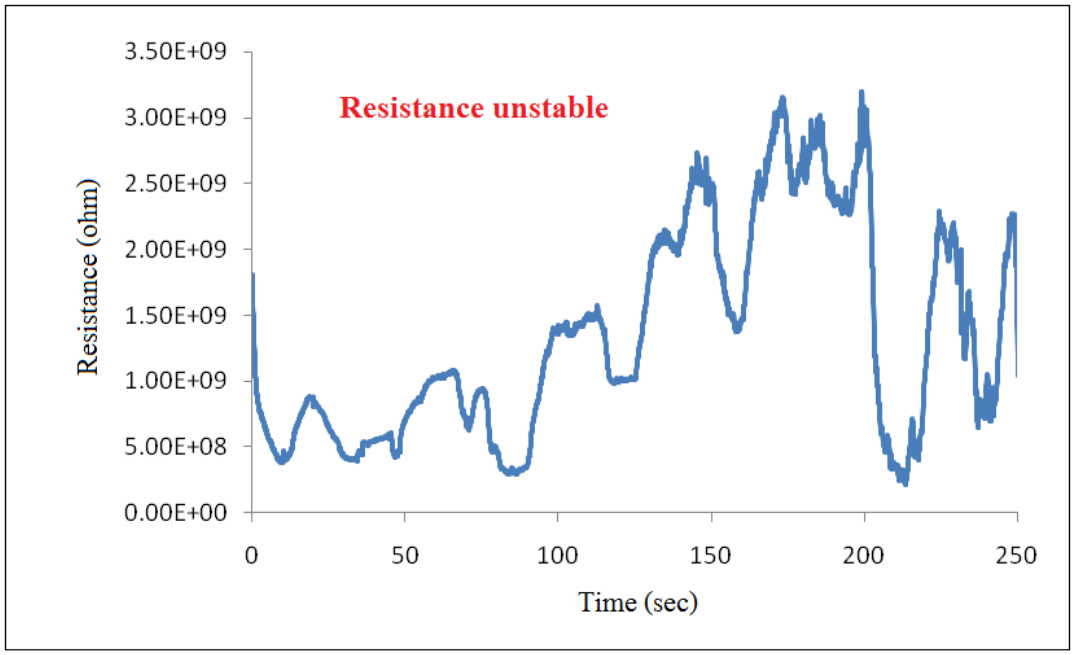

Fig.33. Response curve of $LaGdO_3$ calcined 1200 °C to 50 – 1000 ppm ethanol gas.

Table 4. Response to ethanol gas of $LaMO_3$ (M = Al, Co, Fe, Gd) calcined at 900 °C.

Response to ethanol	Concentration of ethanol (ppm)					
	50	100	200	300	500	1000
$LaAlO_3$	3.18	4.28	5.68	6.81	9.22	16.60
$LaCoO_3$	-	-	-	-	-	-
$LaFeO_3$	2.60	2.81	4.26	4.13	3.83	5.08
$LaGdO_3$	-	-	-	-	-	-

Table 5. Response to ethanol gas of $LaCoO_3$ and $LaFeO_3$ calcined at 600 °C and 800 °C.

Response to ethanol	Concentration of ethanol (ppm)					
	50	100	200	300	500	1000
$LaCoO_3$	2.05	2.81	3.85	4.27	5.27	7.19
$LaFeO_3$	2.33	3.73	3.83	6.17	5.99	9.99

3.2.2 Adsorption of heavy metal ions in water.

3.2.2.1 Effect of contact time and metal ion initial concentration

In this study, the contact time and the removal percentage of $LaMO_3$ adsorbent (M = Al, Co, Fe, and Gd) were studied using standard solutions of heavy metal ions **:** cadmium and lead, the concentration of cadmium 103.9 – 2629.4 mg/L and 186.6 – 4745.5 mg/L for lead. All the data are shown in Appendix A, Tables 1 – 14.

The data of other sets of experiments, such as, the effect of pH and recyclability at various concentrations of metals ions are also given in the Appendix B, Tables 1 – 2 and Appendix C, Tables 1 – 8.

3.2.2.2 Adsorption isotherms

Adsorption isotherms are the basic requirements for the analysis and design of the adsorption separation process. In order to optimize the design of a specific adsorbate/adsorbent system to remove heavy metal ion from effluents, it is important to establish the most appropriate correlation for the experimental equilibrium curves . The widely used isotherms by several researchers for different adsorbate/adsorbent systems are Langmuir and Freundlich. Linear regression is the most commonly used technique to estimate the adsorption isotherm parameters. So it will be an inappropriate technique to use the linearization method for estimating the equilibrium isotherm parameters. The non-linear Langmuir equation, the Langmuir isotherm equation, the non- linear form of Freundlich model and the

Linear form of Freundlich model are shown in equations 10 – 13 (B. Armagan et al, 2013).

3.2.2.2.1 Langmuir isotherm

The non-linear Langmuir equation is

$$q = \frac{q_{max} K_L C}{1 + K_L C} \qquad \text{..... (10)}$$

where K_L is the equilibrium constant (L/mg), q_{max} is the maximum adsorption capacity (mg/g) of adsorbent, C is the equilibrium concentrations (mg/L), and q is the amount of metals adsorbed at equilibrium (mg/g).

The linear form of Langmuir isotherm (Eq. 11) is :

$$\frac{C}{q} = \frac{1}{K_I q_{max}} + \frac{C}{q_{max}} \qquad \text{..... (11)}$$

The Langmuir equation is applicable to homogeneous sorption, where the sorption of each sorbate molecule onto the surface has equal sorption activation energy.

3.2.2.2.2 Freundlich isotherm

The Freundlich equation is an empirical model allowing for multilayer adsorption on sorbent. The non linear form of Freundlich model is Eq. (12).

$$q_e = K_F C_e^{1/n} \qquad \text{..... (12)}$$

The Linear form of Freundlich model can be expressed as Eq. (13):

$$\log q_e = \log K_F + \frac{\log C_e}{n} \qquad \text{..... (13)}$$

where q_e is a loading of adsorbate on adsorbent at equilibrium (mg/g), K_F is indicator of sorption capacity ($mg^{1-1/n} L^{1/n} g^{-1}$), n is adsorption energetic and C_e is aqueous concentration of adsorbate at equilibrium (mg/L).

The Freundlich equation is employed to describe heterogeneous systems and reversible adsorption and is not restricted to the formation of monolayer.

Figs. 34 – 37 show the Langmuir and Freundlich isotherms of Cd^{2+} and Pb^{2+} adsorption. The Langmuir isotherm was plotted using the recipvocal of the concentration of adsorbate at equilibrium (C_e, mg/L) versus the loading of adsorbate on adsorbent at equilibrium (q_e, mg/g). The value of log q_e versus log C_e for Cd^{2+} and Pb^{2+} adsorption were used to plot the Freundlich isotherm. The linear equations and R^2_s resulted from these plots are compiled and given in Tables 6–7.

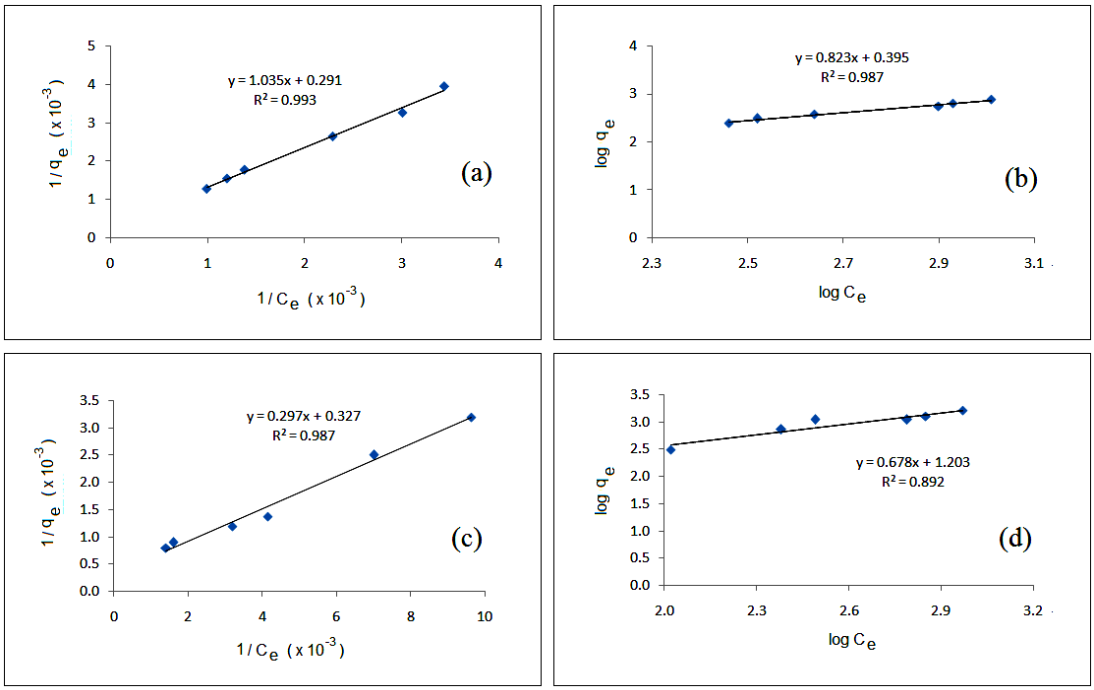

Fig. 34. For $LaAlO_3$: (a) and (b) Langmuir isotherm and Freundlich isotherm of Cd^{2+} adsorption, (c) and (d) Langmuir isotherm and Freundlich isotherm of Pb^{2+} adsorption.

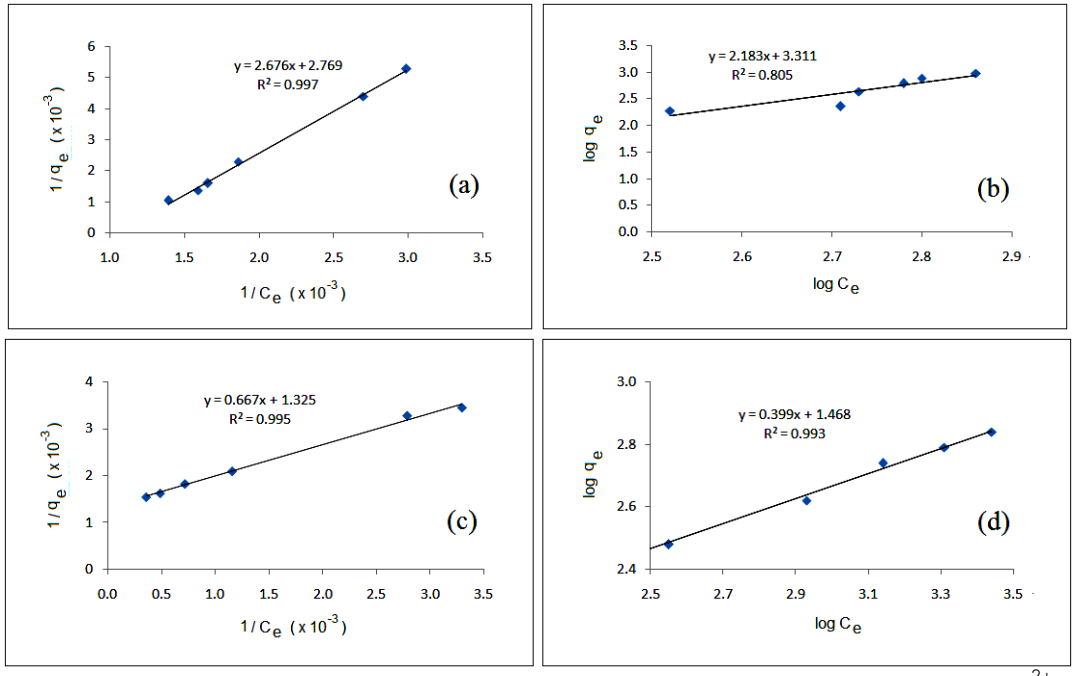

Fig. 35. For $LaCoO_3$: (a) and (b) Langmuir isotherm and Freundlich isotherm of Cd^{2+} adsorption,(b) and (d) Langmuir isotherm and Freundlich isotherm of Pb^{2+} adsorption.

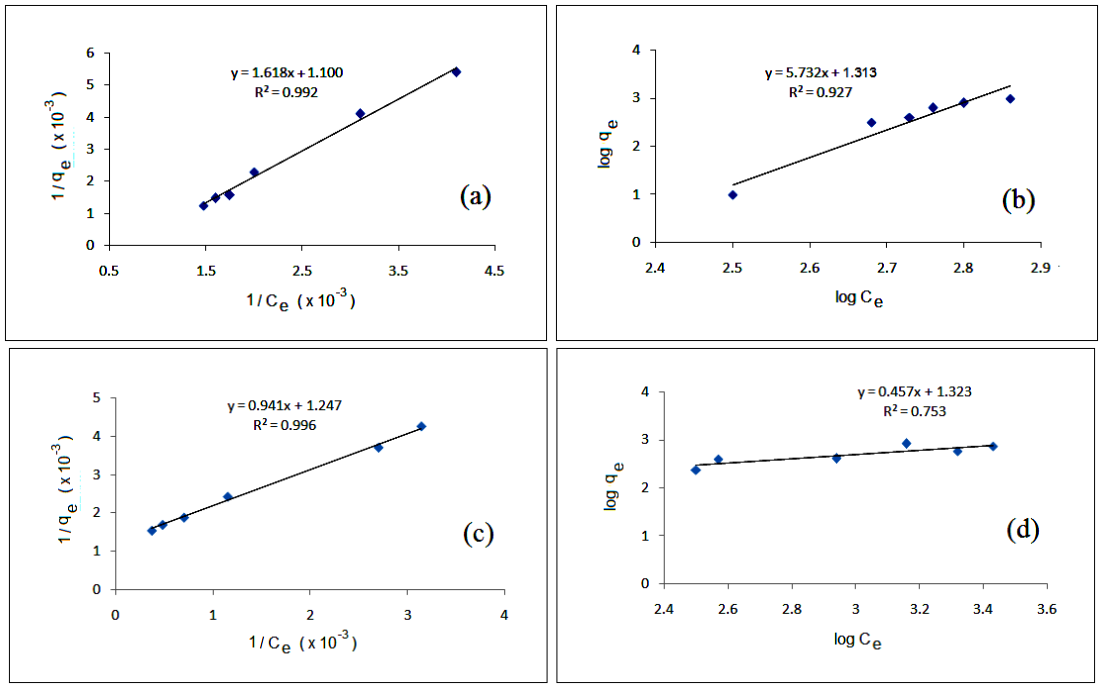

Fig. 36. For $LaFeO_3$: (a) and (b) Langmuir isotherm and Freundlich isotherm of Cd^{2+} adsorption, (c) and (d) Langmuir isotherm and Freundlich isotherm of Pb^{2+} adsorption.

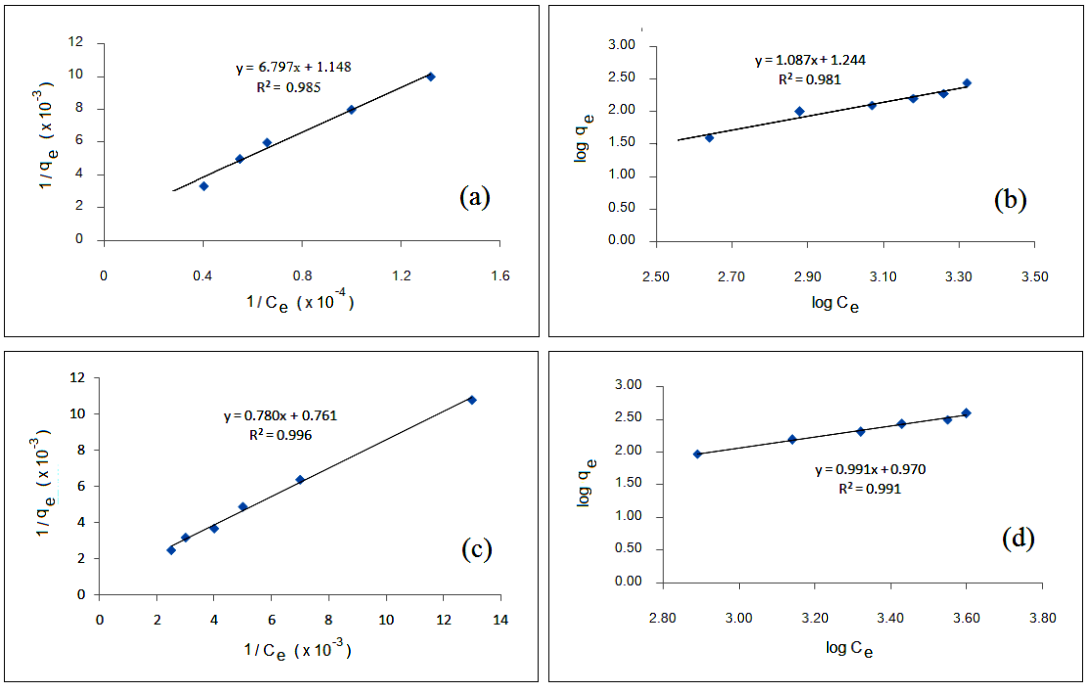

Fig. 37. For $LaGdO_3$: (a) and (b) Langmuir isotherm and Freundlich isotherm of Cd^{2+} adsorption, (c) and (d) Langmuir isotherm and Freundlich isotherm of Pb^{2+} adsorption.

Table 6. Equations and values of R^2 of Langmuir and Freundlich models for Cd^{2+} adsorption.

$LaMO_3$	Langmuir model		Freundlich model	
	Equation	R^2	Equation	R^2
$LaAlO_3$	y = 1.035x + 0.291	0.993	y = 0.823x +0.395	0.987
$LaCoO_3$	y = 2.676x + 2.769	0.997	y = 2.183x + 3.311	0.805
$LaFeO_3$	y = 1.618x + 1.100	0.992	y = 5.732x + 1.313	0.927
$LaGdO_3$	y = 6.797x + 1.148	0.985	y = 1.087x + 1.244	0.981

Table 7. Equations and values of R^2 of Langmuir and Freundlich models for Pb^{2+} adsorption.

$LaMO_3$	Langmuir model		Freundlich model	
	Equation	R^2	Equation	R^2
$LaAlO_3$	y = 0.297x + 0.327	0.987	y = 0.678x + 1.203	0.892
$LaCoO_3$	y = 0.667x + 1.325	0.995	y = 0.399x + 1.468	0.993
$LaFeO_3$	y = 0.941x + 1.247	0.996	y = 0.457x + 1.323	0.753
$LaGdO_3$	y = 0.780x + 0.761	0.996	y = 0.991x + 0.970	0.991

CHAPTER 4

DISCUSSIONS

4.1 Preparations of $LaMO_3$ (M = Al, Co, Fe, Gd) powders

In the present study, $LaMO_3$ (M = Al, Co, Fe, Gd) powders were prepared by the co-precipitation method. The process may be described by the following chemical reactions.

$$2\,La(NO_3)_3 + 2M(NO_3)_3 + 6\,K_2CO_3 \longrightarrow La_2(CO_3)_3 + M_2(CO_3)_3 + 12\,KNO_3$$

$$La_2(CO_3)_3 + M_2(CO_3)_3 \xrightarrow{\text{high temp 1}} La_2O_3 + M_2O_3 + 6\,CO_2$$

$$La_2O_3 + M_2O_3 \xrightarrow{\text{high temp 2}} 2\,LaMO_3$$

where M = Al, Fe, Co, Gd ; high temp 2 > high temp 1

The precursor first obtained was a mixture of $La_2(CO_3)_3$ and $M_2(CO_3)_3$ which later was subjected to calcination. As the temperature rose, the carbonates decomposed to the corresponding oxides and subsequently merged to form the corresponding perovskite at high temperature. The formation of oxides prior to formation of perovskite phase was evidenced from the XRD patterns displayed in Fig. 2 when the heating temperatures were still lower than the threshold perovskite formation temperature. When M = Co, the initial +2 charge was oxidized by oxygen during the heating stage to +3. Phase analyses of all samples were studied by powder X-ray diffraction. The XRD pattern of $LaAlO_3$ matched with the JCPDS file number 85-0848 of $LaAlO_3$ perovskite phase having hexagonal structure, $LaCoO_3$ with JCPDS file number 48-0123 of rhombohedral $LaCoO_3$ perovskite, $LaFeO_3$ with the JCPDS file number 37-1493 of $LaFeO_3$ perovskite having orthorhombic structure, and $LaGdO_3$ with the JCPDS file number 42-1465 of monoclinic structures. Using the Debye-Scherrer equation and the XRD peak informations yielded the average crystallite sizes of 75, 79, 73 and 71 nm for $LaAlO_3$, $LaCoO_3$, $LaFeO_3$, and $LaGdO_3$, respectively. The appearances of all four XRD patterns are sufficiently clean from other unwanted peaks such that they can be considered as high purity perovskites.

The different properties of $LaMO_3$ (M= Al, Co, Fe, Gd) are due to the different of M type in $LaMO_3$. The surface area of $LaMO_3$ (M= Al, Co, Fe) calcined at 900 ℃ for 2 h cannot be calculated with BET method because of their small pore size. The size of Al^{3+} in $LaMO_3$ (53 ppm) is smaller than Co^{3+} and Fe^{3+} so the structure of LaAlO3 is more compact than the others. Due to the small pore size, the surface area of $LaAlO_3$ in this study was presented as the Langmuir surface area. $LaCoO_3$ and $LaFeO_3$ calcined at 900 ℃ exhibited high temperature effect as the grain growth became larger and increasingly more dense, the grain shape changes, and the decrease of porosity due to very small pore and surface area. In Table 3, the surface area of $LaCoO_3$ and $LaFeO_3$ are about the same because of the ionic radii of Co^{3+} is equal to that of Fe^{3+} (= 60 ppm). The radii of Gd^{3+} in $LaGdO_3$ is 93.5 ppm which is it larger than all the other three metal ions, enabling its surface area can calculated with BET method (http://www.wiredchemist.com /chemistry/data/metallic-radii).

4.2 Gas sensing property

The sensitivities of $LaMO_3$ (M = Al, Co, Fe, Gd) film-based sensor were tested against four common gases (CO_2, SO_2, H_2, and EtOH) at 350 ℃ with the gas concentration range 50 - 1000 ppm. The sensor showed no response to CO_2, SO_2, and H_2 gases but exhibited small positive response with ethanol gas as shown in Fig. 38. In general, the response increased with an increase of ethanol gas concentration with $LaAlO_3$ showed the best response. The results exhibited by $LaAlO_3$ film prepared from 900 ℃ calcination were 3.18, 4.28, 5.68, 6.81, 9.22, 16.60 (units of R_e/R_a) when exposed to 50, 100, 200, 300, 500, and 1000 ppm of ethanol gas, respectively. The performance was obtained from the $LaFeO_3$ calcined at 900 ℃ with the response to EtOH at 50, 100, 200, 300, 500, and 1000 ppm concentrations were 2.60, 2.81, 4.26, 4.13, 3.83, 5.08 (units of R_e/R_a) under the same conditions (Fig. 38). $LaFeO_3$ calcined at 800 ℃ (Fig. 40) showed better response to EtOH than that calcined at 900 ℃ (the responses to EtOH at 50, 100, 200, 300, 500, 800, and 1000 ppm concentrations were 2.33, 3.73, 3.83, 6.17, 5.99, and 9.99 units of R_e/R_a) the value very nearly to $LaCoO_3$ calcined at 600 ℃ exhibited similar sensitivity to $LaFeO_3$ at 800 ℃ (Fig. 39) (the responses to EtOH at 50, 100, 200, 300, 500, 800, and 1000 ppm concentrations were 2.33, 3.73, 3.83, 6.17, 5.99, and 9.99 units of R_e/R_a). This could be because of the surface area of $LaCoO_3$ ~ $LaFeO_3$. However, $LaCoO_3$ (900 ℃) and $LaGdO_3$ (1200 ℃) showed no sensitivity to EtOH as the resistance became unstable. One can see that the efficiencies as gas sensor of $LaCoO_3$ and $LaFeO_3$

dramatically increased several folds and increased significantly with increasing ethanol concentrations.

The superior gas response of $LaAlO_3$ should be partly attributed to its higher surface area and porosity compared with those of $LaFeO_3$ and $LaCoO_3$ sensors. The morphology of $LaAlO_3$ along with its relatively small crystallite size could provide extra ethanol adsorption sites and enhanced sensor response.

The change in resistance of the $LaMO_3$ sensors was studied using to 50–1000 ppm ethanol at 350 °C. It can be seen that the $LaAlO_3$ sensor exhibited much higher baseline resistance than $LaFeO_3$ and $LaCoO_3$ sensors. Upon exposure to ethanol vapor, the resistance of the $LaAlO_3$ sensor decreased rapidly and then gradually recovered to its baseline value after ethanol vapor was released, indicating an n-type semiconducting behavior towards a reducing gas (T. Samerjai, et al., 2012). On the other hand, the resistances of the $LaFeO_3$ and $LaCoO_3$ sensors increased abruptly after exposure to ethanol pulses confirming their p-type semiconducting characteristics in agreement with most other reports (P. Song, et al., 2014).

The corresponding n-type and p-type ethanol responses of $LaAlO_3$ and $LaFeO_3$ or $LaCoO_3$ sensors calculated according to the modified power law: $y = a \cdot x^b + 1$, where y is a response, x is a gas concentration, a is a proportional constant and b is an exponent. The proportional constant was correlated to the gas sensitivity while the exponent was related to the active preadsorbed oxygen species responsible for observed gas-sensing mechanisms. It can be seen that $LaAlO_3$ had the highest proportional constant of 0.1847, which was 1.6 and 5.7 times as high as those of $LaFeO_3$ and $LaCoO_3$, respectively. The results confirmed that $LaAlO_3$ had the highest ethanol sensitivity among these $LaMO_3$ sensors. The exponent values of $LaMO_3$ sensors slightly fluctuatd between 0.4 and 0.6 (~0.5) implying that the active adsorbed surface oxygen species interacting with ethanol molecules were mainly O^{2-} for all of these $LaMO_3$ sensors (S.C. Naisbitt, et al., 2006). The attained ethanol-sensing performances of $LaMO_3$ sensors particularly $LaAlO_3$ are well sufficient for the drunken driving application, which requires the legal detection threshold of 200 ppm (equivalent to 50 mg% in blood) (S. Zhan, et al., 2013). For the respective response and recovery times of $LaMO_3$ sensors as a function of gas concentration, at high ethanol concentration of 1000 ppm, the $LaAlO_3$ sensor exhibited a fair response time, which was slightly longer than those of $LaFeO_3$ and $LaCoO_3$. In contrast, the recovery time of $LaAlO_3$ sensor was relatively short compared with those of $LaFeO_3$ and $LaCoO_3$ sensors. As the gas concentration decreased, the response time quickly

increased because of slower gas adsorption dynamic while the recovery time slowly decreased due to less amount of gas desorption. Thus, $LaFeO_3$ and $LaCoO_3$ sensors displays relatively rapid adsorption rate and quick approach to steady-state response compared with $LaAlO_3$. The distinct natures may be associated with their p-type and n-type sensing behaviors to be further discussed in the next section. On the other hand, the $LaAlO_3$ sensor exhibits higher gas desorption rate than $LaFeO_3$ and $LaCoO_3$ sensors. This behaviors might be related to their differences in structural morphologies. The morphology of $LaAlO_3$ could allow better gas release after desorption than agglomerated particle structures of $LaFeO_3$ and $LaCoO_3$. Overall, the $LaAlO_3$ sensor exhibited superior ethanol-sensing performances with high response, satisfactory response time, and relatively short recovery time.

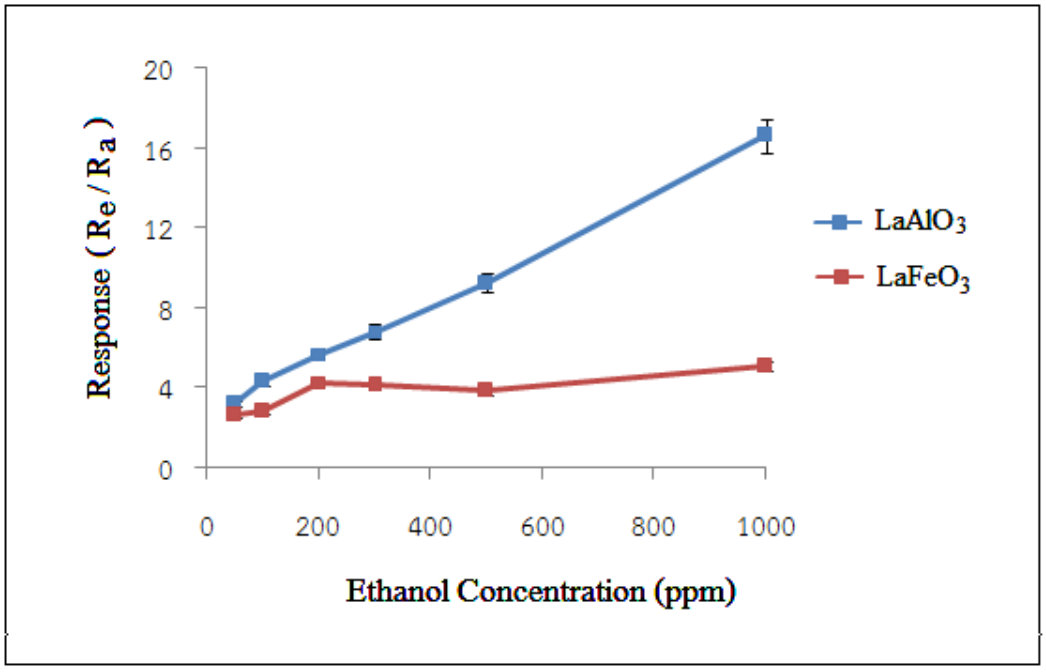

Fig. 38. Ethanol sensor measurement of $LaMO_3$ (M = Al, Co, Fe, Gd) films (calcined at 900 °C)

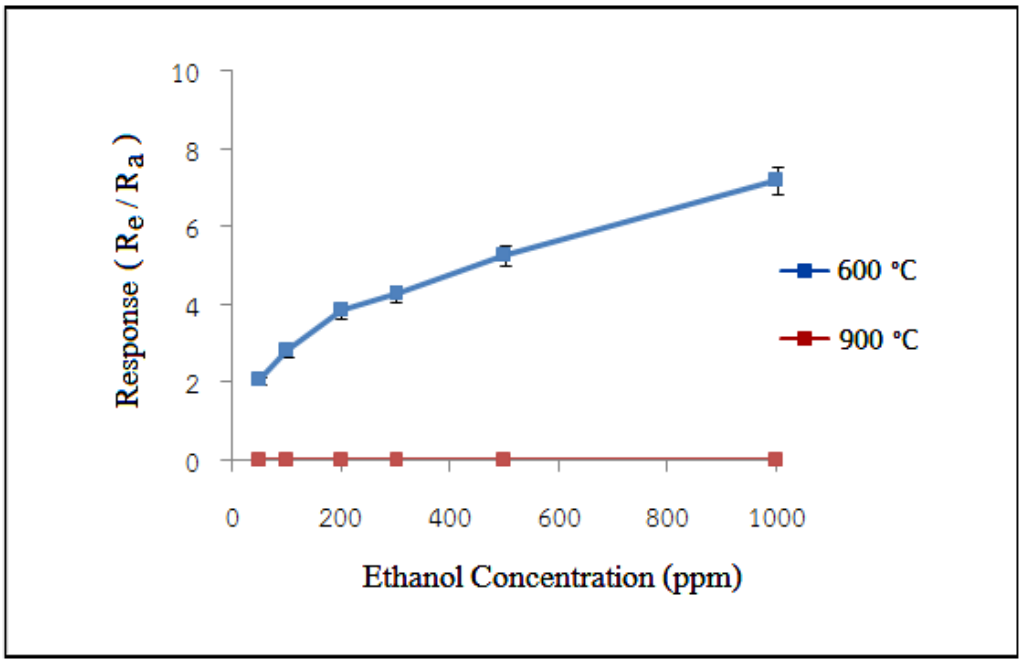

Fig. 39. Ethanol sensor measurement of $LaCoO_3$ films.

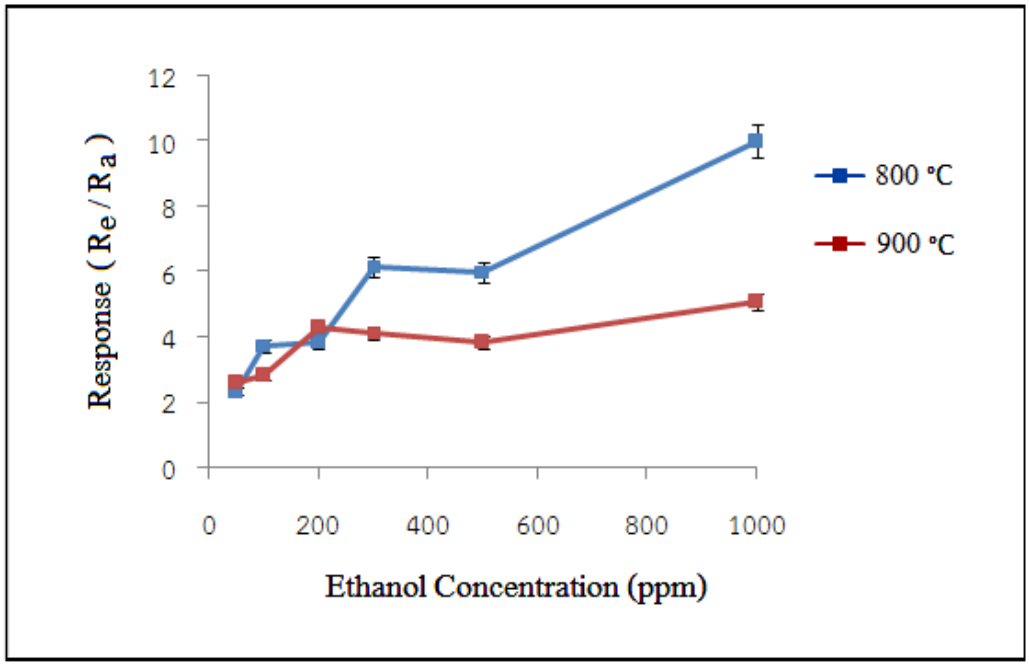

Fig. 40. Ethanol sensor measurement of $LaFeO_3$ films.

4.3 Ethanol gas sensing mechanism

From the results, $LaAlO_3$ nanostructures prepared by co-precipitation exhibited n-type conductivity with relatively high ethanol response while $LaFeO_3$ and $LaCoO_3$ sensors displayed p-type sensing behavior with low responses. The distinct semiconducting nature between $LaAlO_3$ and the other two perovskite oxides may be explained based on different natures of these B-site cations. In the former case, $LaAlO_3$ has nearly ideal crystal consisting of La^{3+}, Al^{3+} and O^{2-} occupying all sites in the perovskite structure. At elevated temperatures, oxygen atoms can be released from lattice site due to thermal excitation, inducing oxygen vacancies, oxygen gas molecules, and electrons according to the defect reactions (M.E. Mazhar, et al., 2016, C. Balamurugan, et al., 2015).

$$O_o^x \rightarrow \tfrac{1}{2}O_2 + V_o^{\bullet} + e^- \quad (14)$$

$$V_o^{\bullet} \rightarrow V_o^{\bullet\bullet} + e^- \quad (15)$$

where O_o^x, O_2, $V_o^{\bullet}$, $V_o^{\bullet\bullet}$ and e^- are a neutral oxygen site, an oxygen gas molecule, an oxygen vacancy with single positive charge, an oxygen vacancy with double positive charge, and an electron, respectively. The oxygen vacancies in the metal oxide are the centers of the positive charges and the electrons around oxygen vacancies can be excited to the conduction band at elevated temperatures, inducing an n-type conductivity. For $LaAlO_3$, oxygen atoms are quite strongly bound to the cations and high thermal energy is needed to induce the reactions. Thus, the electron concentration in $LaAlO_3$ structure is quite low, leading to a high baseline electrical resistance as observed previously. In the case of $LaFeO_3$ and $LaCoO_3$, B-site cations will be formed in mixed valency states, comprising Fe^{3+} and Fe^{2+} or Co^{3+} and Co^{2+} (C.H. Chen, et al., 2015). The low valency states will act as virtual substitutional dopants at the B-site according to the quasi defect reaction:

$$RO\,(-R_2O_3) \rightarrow R_R^{'} + h^{\bullet} + O_o^x \quad (16)$$

where R, RO, R_2O_3, $R_R^{'}$, $h^{\bullet}$, and e^- are a B-site transition atom (Fe or Co), a quasi-molecule with R^{2+} oxidation state, a quasi-molecule with R^{3+} oxidation state, a R^{2+}—R^{3+} substitutional site with a single negative charge, and a hole with a single positive charge, respectively. The reaction generated hole charge carriers whose density was far greater than electrons induced by oxygen vacancies. As a result, $LaFeO_3$ and $LaCoO_3$ displayed p-type conductivity. From the experimental data, the

$LaCoO_3$ sensor exhibited higher p-type conductivity than the $LaFeO_3$ device. This is in agreement with other reports that $LaCoO_3$ had high conductivity due to relative high density of reduced Co states (Co^{2+}) (C.H. Chen, et al., 2015).

On surface, oxygen molecules were adsorbed and formed chemisorbed oxygen species including O_2^-, O^-, and O_2^- by capturing electrons from metal oxides. The type and density of oxygen species mainly depended on metal oxide materials and temperature. Generally, O_2^-, O^-, and O^{2-} species were dominant below 100 ℃, between 100 and 300 ℃ and above 300 ℃, respectively (T. Samerjai, et al., 2012). Correspondingly, they desorbed from the surface at temperatures of 80, 130, and 250 ℃, respectively. From the power-law analysis, the dominant oxygen species on $LaMO_3$ surfaces was O^{2-} at 350 ℃, conforming to the characteristic of typical semiconducting metal oxides. For n-type metal oxides, electrons were captured from conduction band, leading to a decrease of electron density and an increase of surface resistance. In the case of p-type semiconducting oxides including $LaFeO_3$ and $LaCoO_3$, oxygen adsorption extracted electrons from valence band leading to an increase in the number of holes and a lower surface resistance.

Upon exposure to ethanol vapor at an elevated temperature, ethanol molecules were adsorbed and then reacted with preadsorbed oxygen ions on the metal oxide surface according to the reactions (T. Addabbo, et al., 2015, X. Wan, et al., 2014, Y. Zhang, et al., 2014).

$$C_2H_5OH + 6O^- \rightarrow 2CO_2 + 3H_2O + 6e^- \quad (17)$$

$$C_2H_5OH + 6O^{2-} \rightarrow 2CO_2 + 3H_2O + 12e^- \quad (18)$$

In the reactions, ethanol molecules were decomposed into CO_2 and H_2O while electrons were released from oxygen species into the conduction band of metal oxide. For n-type metal oxides, the concentration of electrons was increased, leading to a decrease of sensor resistance. In the case of p-type semiconducting oxides, injected electrons recombined with holes in the valence band resulting in a decrease of hole concentration and a higher sensor resistance. The magnitude of change in resistance or response primarily depended on the type and amount of preadsorbed oxygen species on perovskite oxide surface. At the high working temperature of 350 ℃, the oxygen species on all $LaMO_3$ surfaces were confirmed to be mainly O^{2-}, which gave the highest number of electrons per reaction. Thus, the distinct responses among $LaMO_3$ sensors should be mainly attributed to the

difference in the amount of oxygen adsorption sites, which was generally increased with increasing surface area and porosity of sensor material. From the results, the sensor response of $LaMO_3$ sensors was roughly proportional to the Langmuir surface area confirming the morphological effect of different $LaMO_3$ nanostructures produced by the same co-precipitation method.

4.4 Heavy metal ions adsorption

It is a commonly known fact that the anions are favorably adsorbed by the adsorbent at lower pH values, and at high pH values cations are favorably adsorbed. The surfaces of metal oxides were found to be completely covered by positively charged (H^+) ions at lower pH range, which inhibited the adsorption of heavy metal ions over them. At higher pH, metal oxides were converted into a deprotonated oxides which favored the adsorption of heavy metal ions on their surfaces.

The effect of contact time and metal ion concentration for the removal of cadmium and lead on $LaMO_3$ (M = Al, Fe, Co) perovskites nanoparticles were studied as being explained in Section 2.3.5.2; 2.3.5.2.1, and 2.3.5.2.2. The experimental data are shown in the Appendix A, Tables 1 – 14. The graphs plotted from these data are displayed as Figs. 41 – 48.

The adsorption capacities for Cd^{2+} and Pb^{2+} were determined with different stirring times. The results indicated that the amount adsorbed increased with an increase in stirring time and reached equilibrium at 1 min for both Cd^{2+} and Pb^{2+} ions.

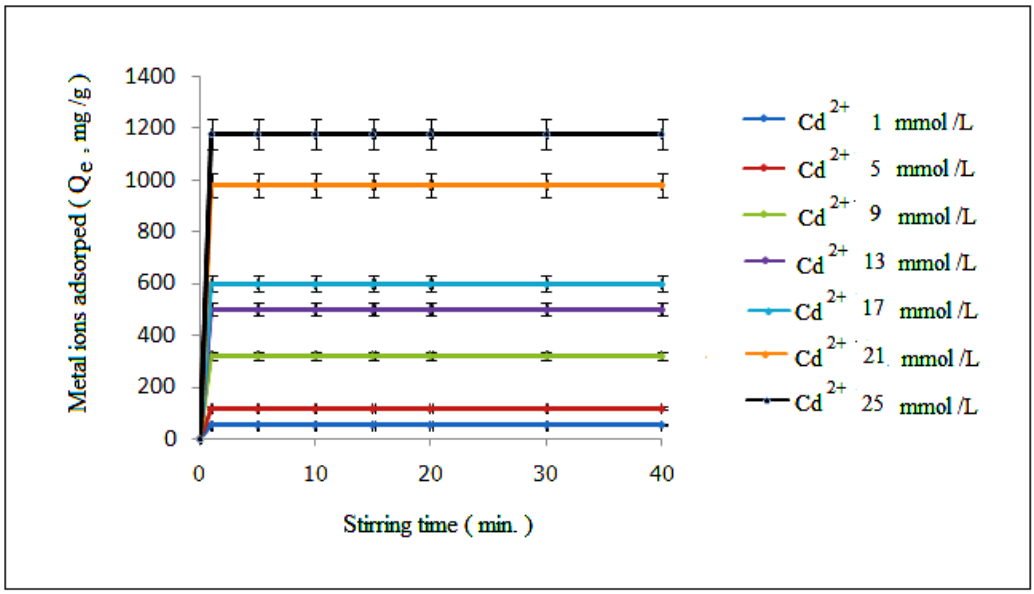

Fig. 41. The effect of contact time and concentration of Cd^{2+} to the adsorptivity of $LaAlO_3$.

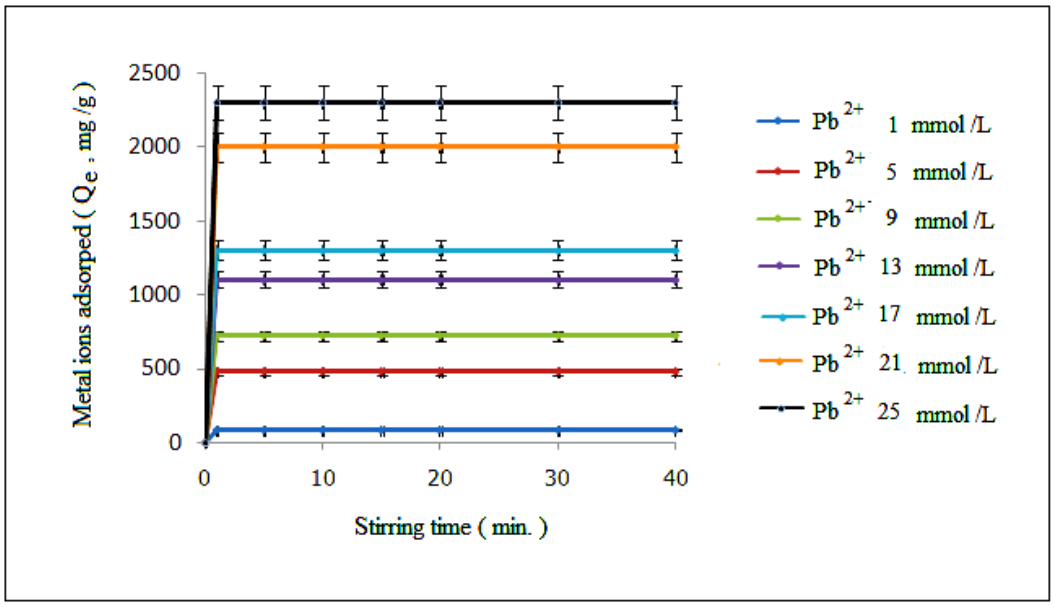

Fig. 42. The effect of contact time and concentration of Pb^{2+} to the adsorptivity of $LaAlO_3$.

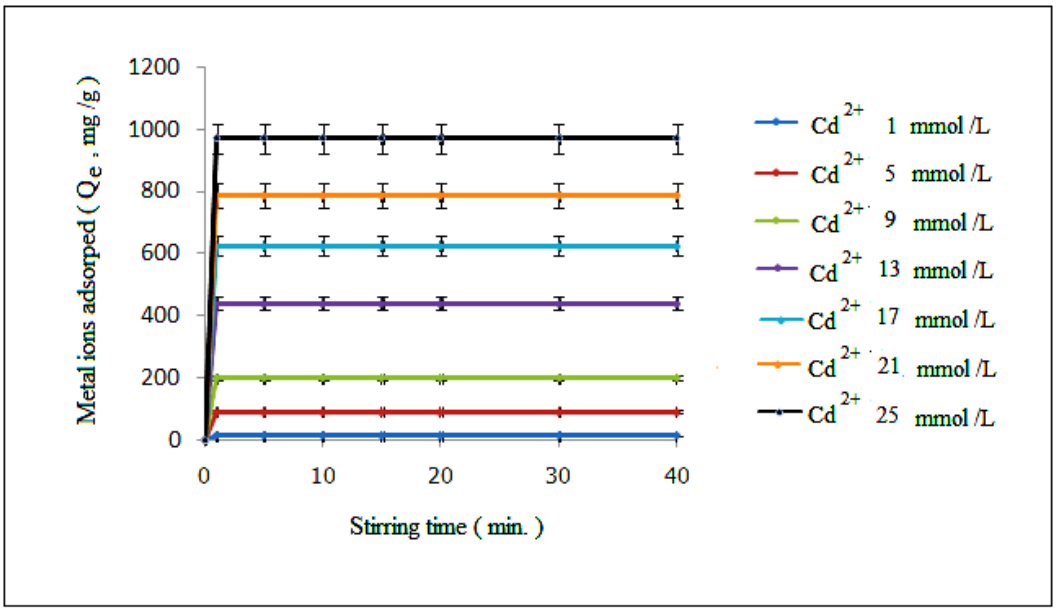

Fig. 43. The effect of contact time and concentration of Cd^{2+} to the adsorptivity of $LaCoO_3$.

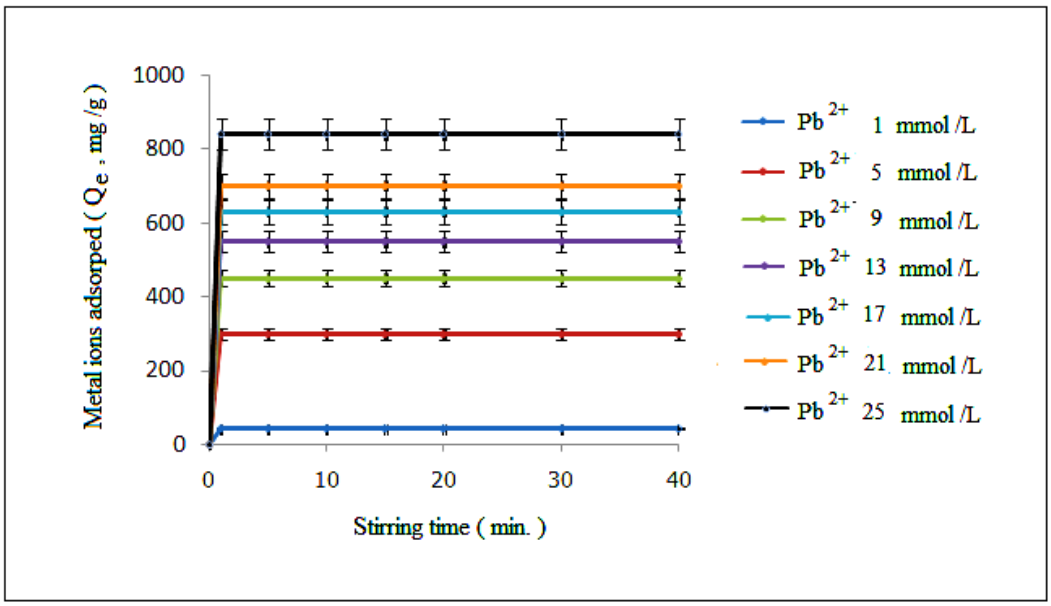

Fig. 44. The effect of contact time and concentration of Pb^{2+} to the adsorptivity of $LaCoO_3$.

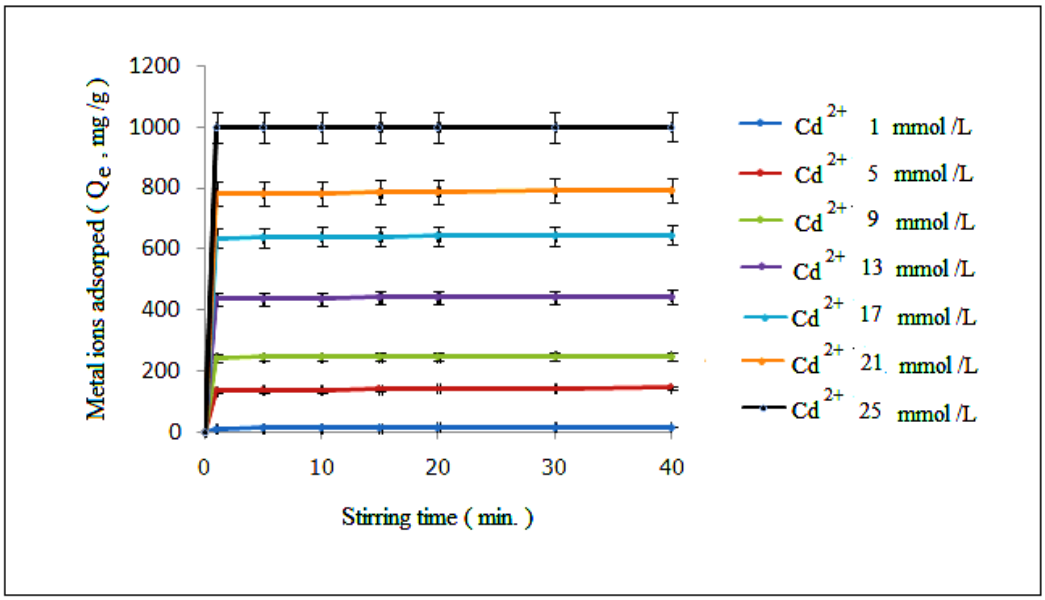

Fig. 45. The effect of contact time and concentration of Cd^{2+} to the adsorptivity of $LaFeO_3$.

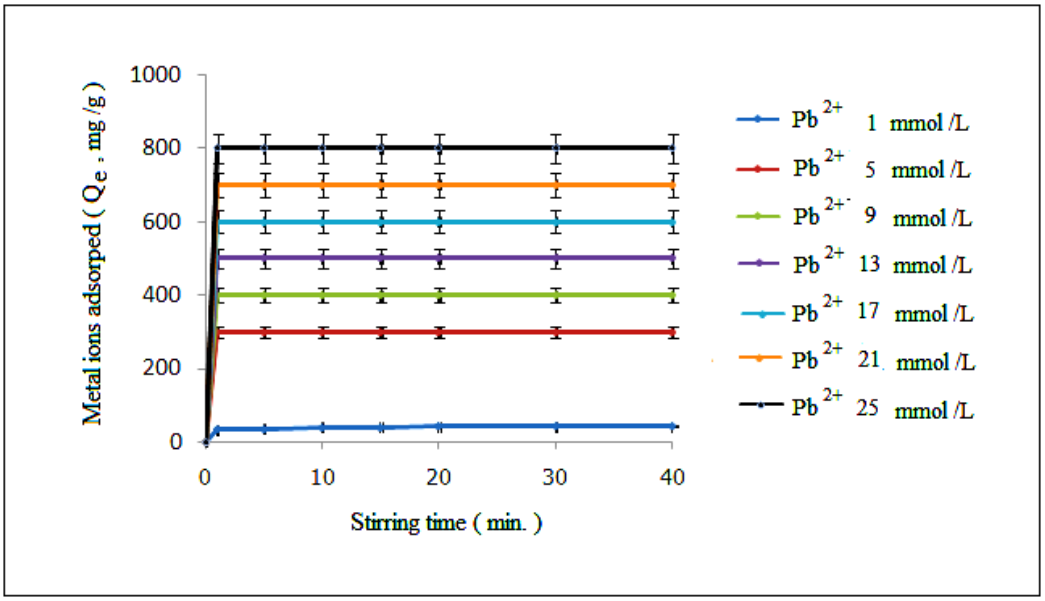

Fig. 46. The effect of contact time and concentration of Pb^{2+} to the adsorptivity of $LaFeO_3$.

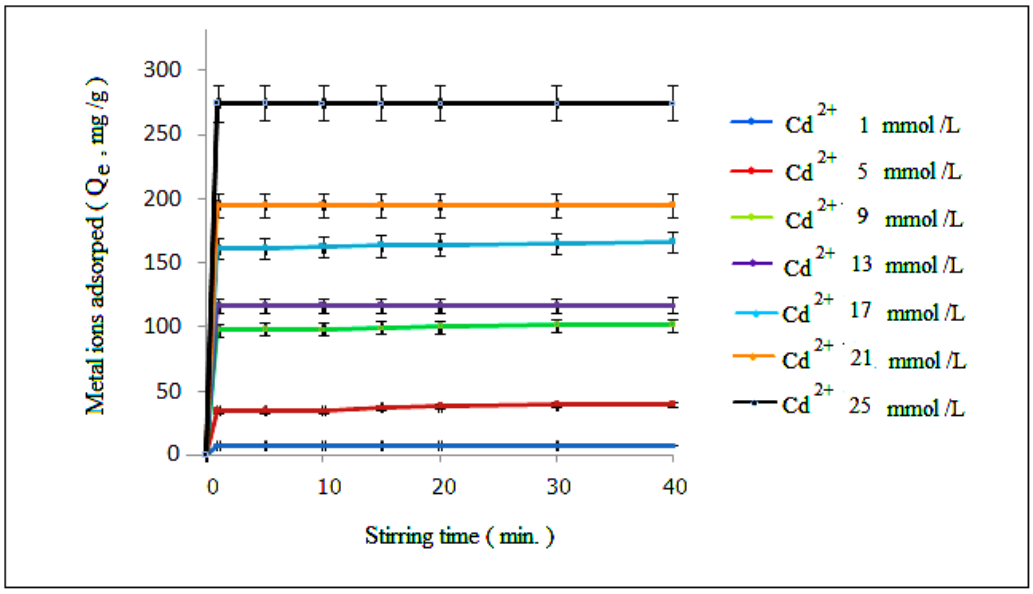

Fig. 47. The effect of contact time and concentration of Cd^{2+} to the adsorptivity of $LaGdO_3$.

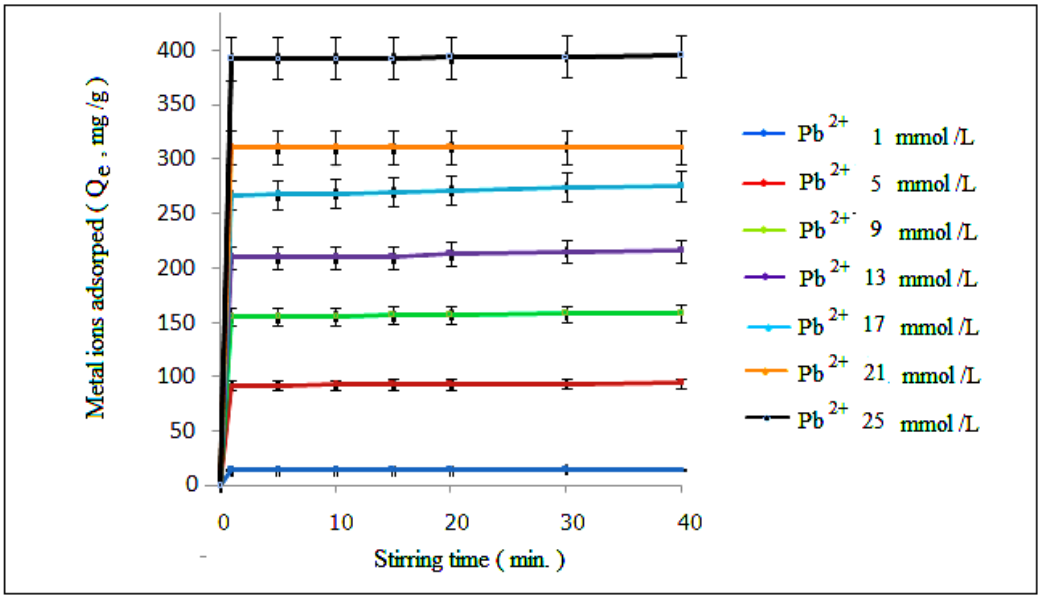

Fig. 48. The effect of contact time and concentration of Pb^{2+} to the adsorptivity of $LaGdO_3$.

The adsorption capacities for 1 min equilibrium of Cd^{2+} and Pb^{2+} were determined at different concentrations and are shown in Figs. 49 – 50. The results indicated that the amount adsorbed increased with an increase in concentration of Cd^{2+} and Pb^{2+} ions.

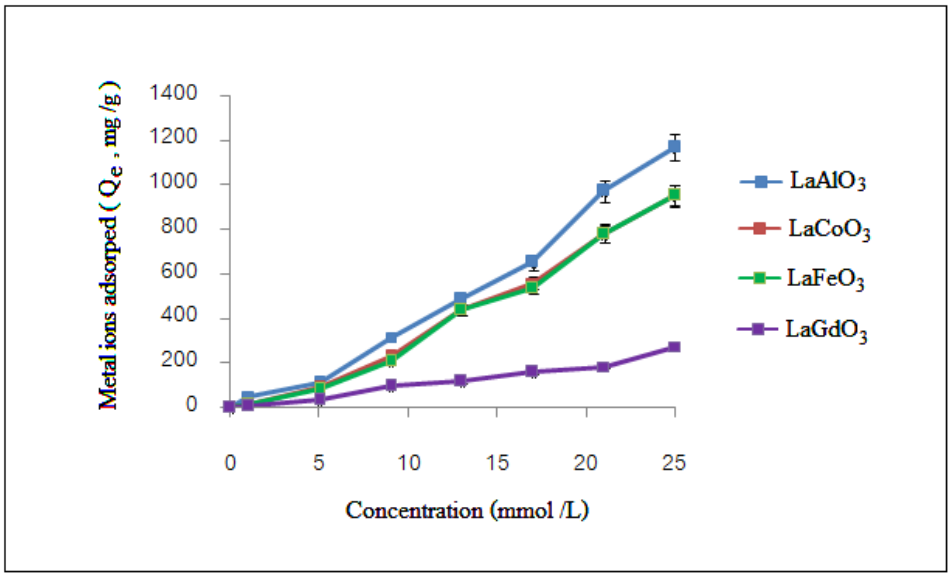

Fig. 49. The effect of metal concentration on Cd^{2+} adsorption of $LaMO_3$ (M = Al, Co, Fe and Gd) (stirring time= 1 min).

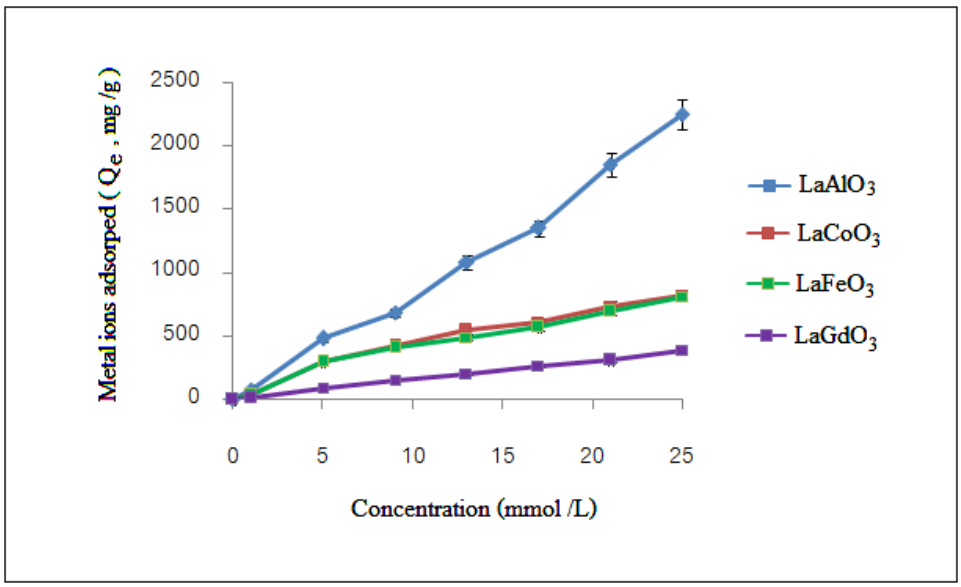

Fig. 50. The effect of metal concentration on Pb^{2+} adsorption of $LaMO_3$ (M = Al, Co, Fe and Gd) (stirring time= 1 min).

The adsorption of Cd^{2+} and Pb^{2+} ions onto $LaMO_3$ (M = Al, Co, Fe, Gd) resulted from the electrostatic attraction between positively charged sorbate and negatively charged sorbent. On varying the pH of the solution, one can see that the adsorption efficiency increased with pH as shown in Figs. 51 – 52. The pH_{pzc} of $LaAlO_3$, $LaCoO_3$, $LaFeO_3$, and $LaGdO_3$ were 11.0, 9.2, 9.0, and 8.1, respectively (Figs. 8 – 11). However, the pH variation shown in Figs. 55 – 56 ranged only from 1 to 6 due to precipitation beyond the critical pH of each metal ion, *ca.* 6 for Cd^{2+} and *ca.* 4 for Pb^{2+} (S.B. Chem et al, 2010). Normally, the $LaMO_3$ (M = Al, Co, Fe, Gd) surface are negatively charged due to the coverage of oxide anions. At low pH, the concentration of H^+ was high, the oxides were almost fully protonated rendering the surface charge to be positive which repelled with the positive charge of the in-coming metal ions. So at low pH, the adsorption was low as shown in Figs. 51 – 52. As the pH increased, the surface protonation became less and hence the surface charge was less positive and more adsorption became more possible causing the adsorption to increase with pH.

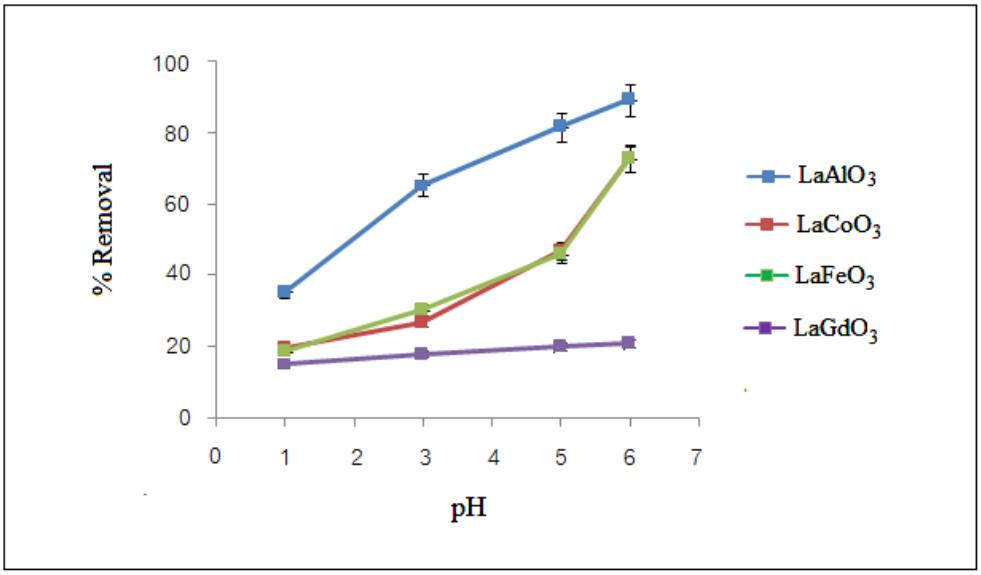

Fig. 51. The effect of pH on adsorption of Cd^{2+} by $LaMO_3$ (M = Al, Co, Fe, Gd).

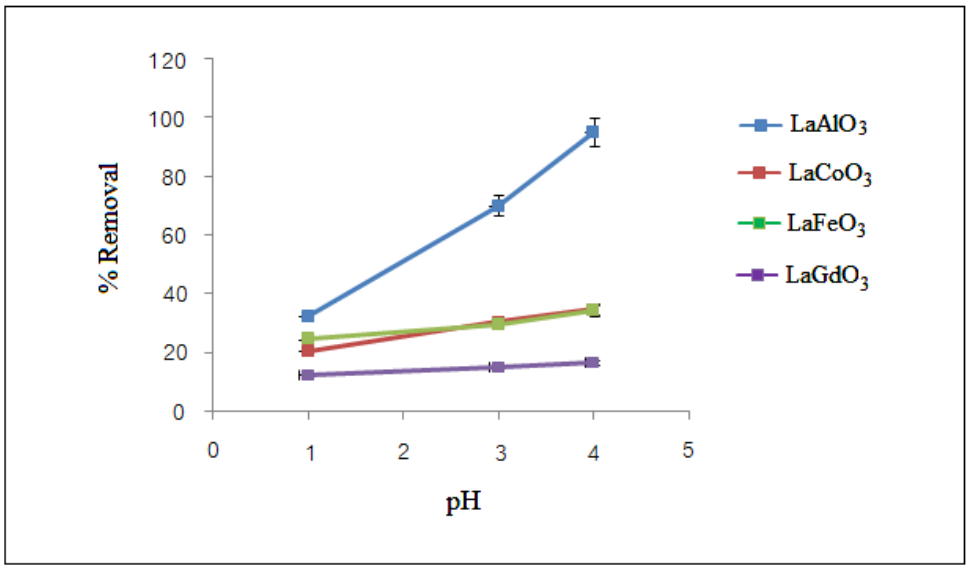

Fig. 52. The effect of pH on adsorption of Pb^{2+} of $LaMO_3$ (M = Al, Co, Fe, Gd).

4.4.1 Analyses of adsorbent surface

After adsorption experiments, the adsorbent was recovered and investigated with the EDX spectrometer. The resulting EDX spectra showed the presence of either Cd^{2+} or Pb^{2+} indicating the $LaMO_3$ (M = Al, Co, Fe, Gd) perovskite could really "catch" these two heavy metal ions by adsorption (Figs. 53 – 56). The elemental mapping associated with each spectrum revealed that the adsorbed metal ions (Cd^{2+} or Pb^{2+}) were distributed evenly on the adsorbent surface.

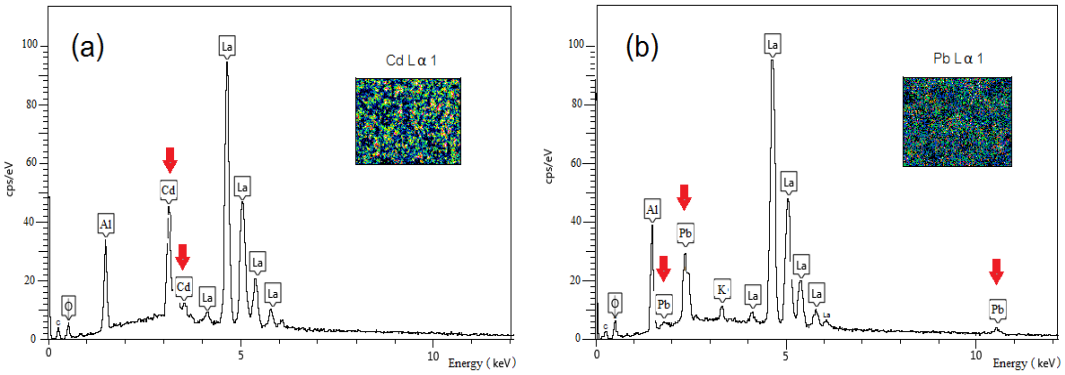

Fig. 53. EDX spectra of $LaAlO_3$ after adsorption of (a) Cd^{2+} and (b) Pb^{2+} ions.

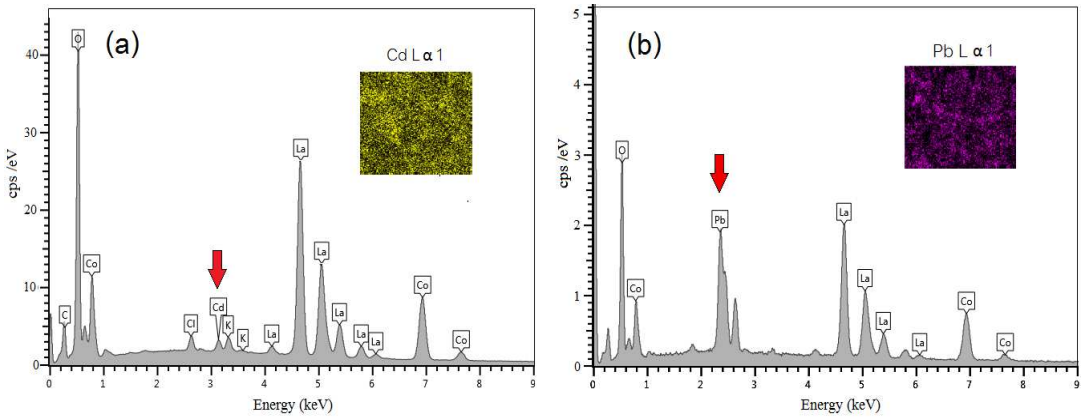

Fig. 54. EDX spectra of $LaCoO_3$ after adsorption of (a) Cd^{2+} and (b) Pb^{2+} ions.

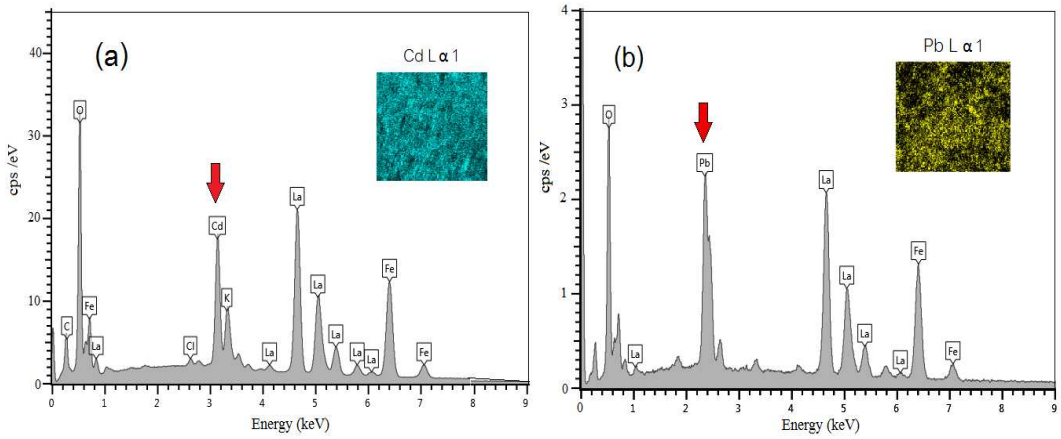

Fig. 55. EDX spectra of $LaFeO_3$ after adsorption of (a) Cd^{2+} and (b) Pb^{2+} ions.

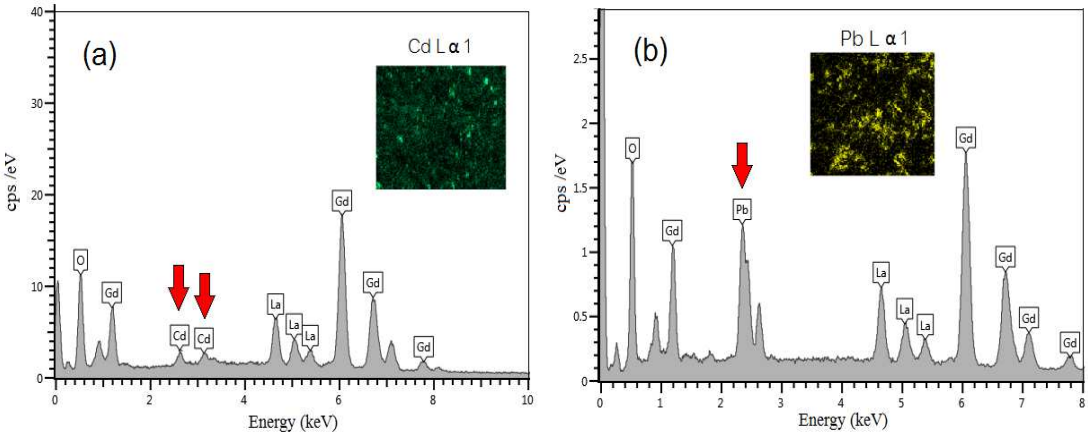

Fig. 56. EDX spectra of $LaGdO_3$ after adsorption of (a) Cd^{2+} and (b) Pb^{2+} ions.

4.4.2 Recyclability of $LaMO_3$ (M = Al, Co, Fe, Gd) adsorbent

The used $LaMO_3$ adsorbents could be recycled with efficiency slightly lower than the first use if generated with 0.1 M EDTA solution. On the other hand, reuse without regeneration showed poor performance as shown in Figs. 57 – 60. The role of EDTA in this "cleaning" operation is to remove the metal ions adsorbed on the surface of $LaCoO_3$ through its well recognized chelating capability. However, the cleansing was not 100 % effective as evidenced by the EDX spectra in Figs. 61 – 64 where small amount of metal ions (Cd^{2+} or Pb^{2+}) still remained on the $LaMO_3$ surface. The remaining amount occupied some active sites thus leaving less than full capacity of active sites available for the next round of use. So the efficiency of the recycle run was slightly less than that observed in the first use. The reuse after regeneration of each use was repeated three times with similar results the average of which is shown as the red bar graph in Figs. 57 – 60. The reuse without regeneration (the green bar graph) was the result from only one reuse since the amount of metal ions was accumulated so much that the next adsorption was very low and useless.

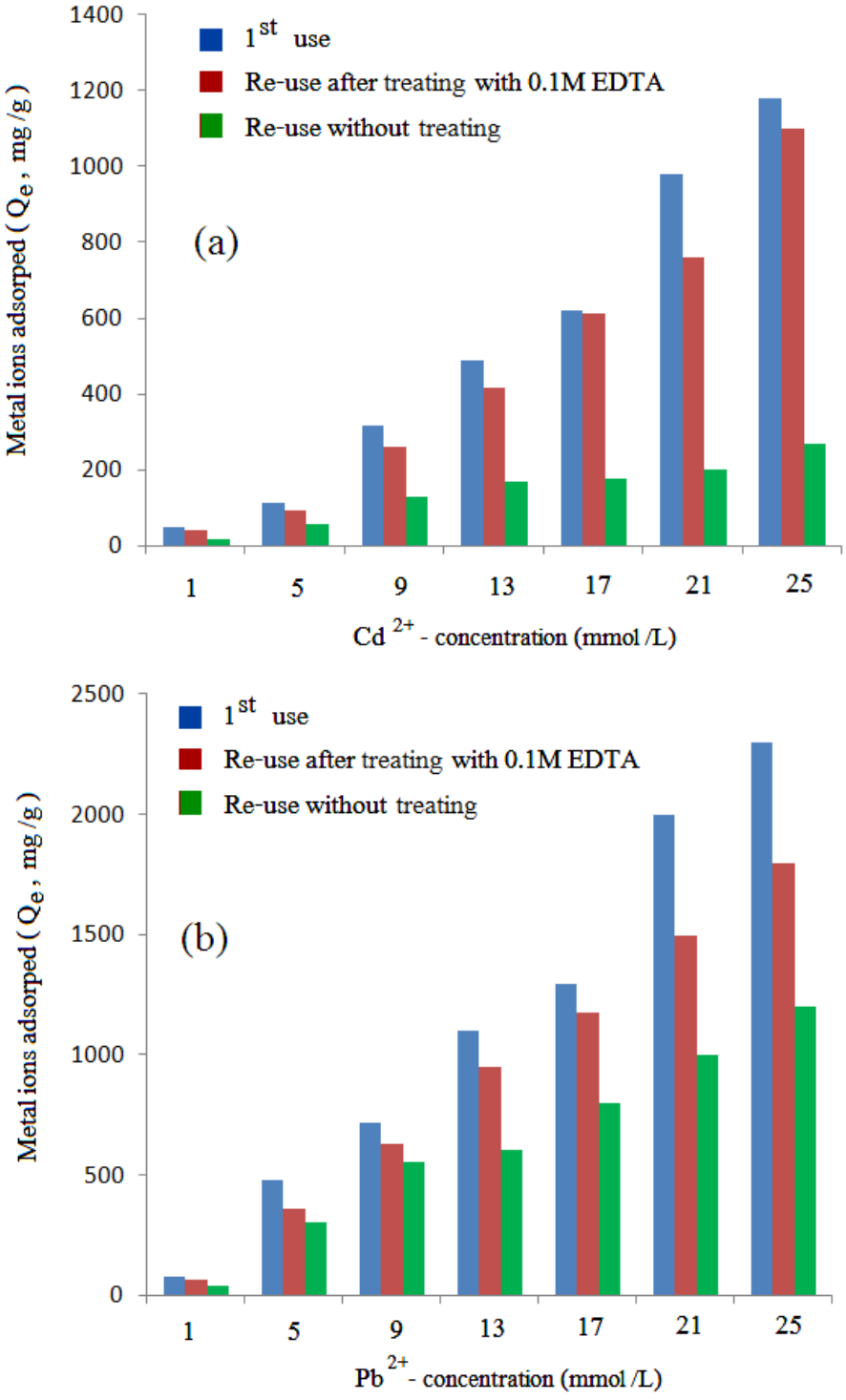

Fig. 57. The recycling uses of $LaAlO_3$ with: (a) Cd^{2+} ion and (b) Pb^{2+} ion (concentration 1 – 25 mmol /L).

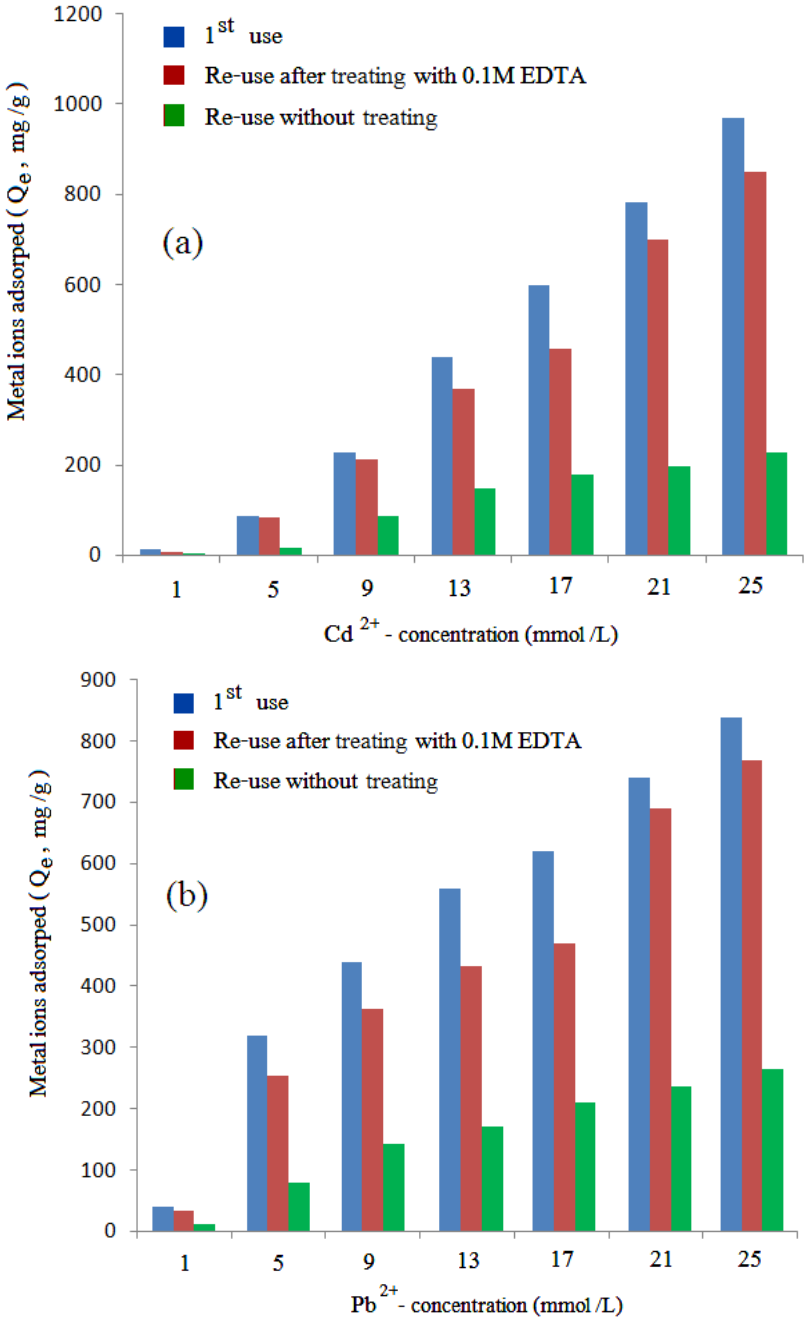

Fig. 58. The recycling uses of $LaCoO_3$ with: (a) Cd^{2+} ion and (b) Pb^{2+} ion (concentration 1 – 25 mmol /L).

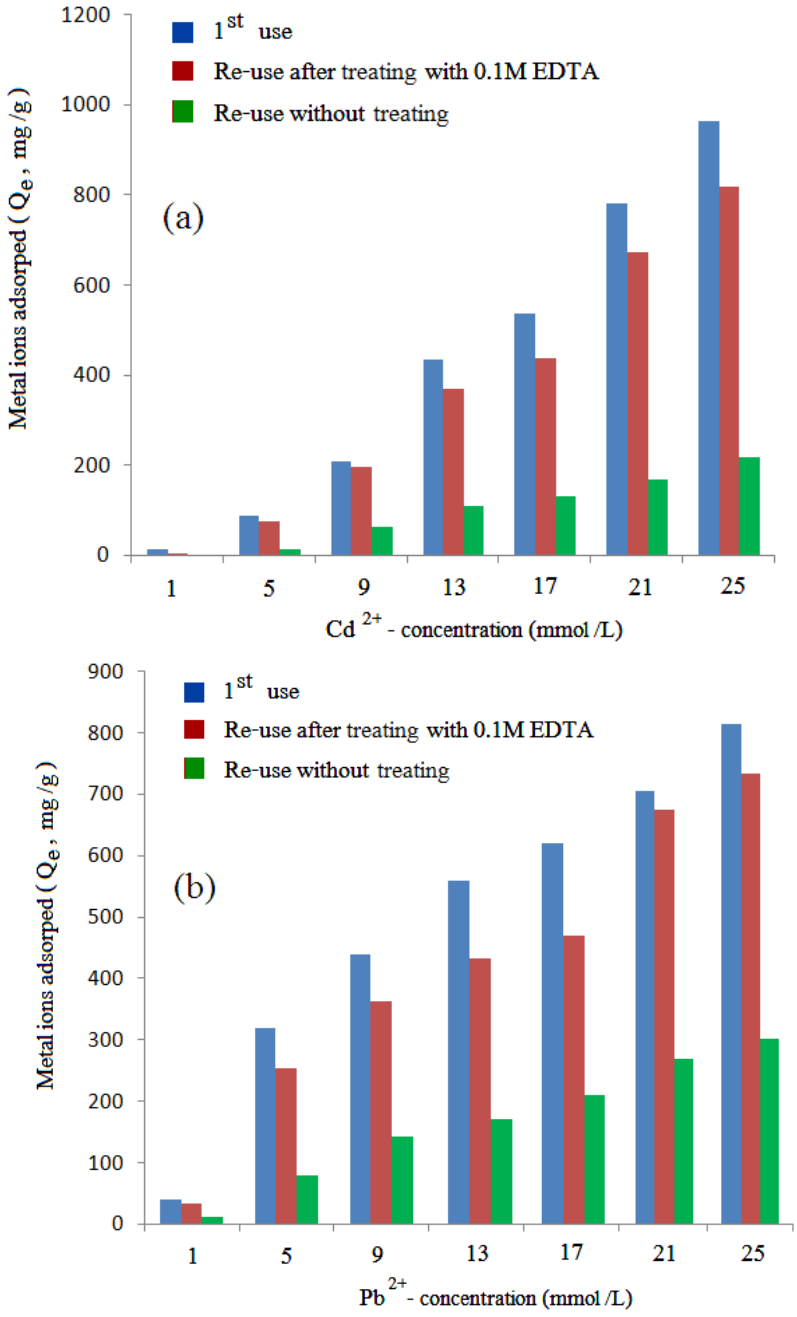

Fig. 59. The recycling uses of $LaFeO_3$ with: (a) Cd^{2+} ion and (b) Pb^{2+} ion (concentration 1 – 25 mmol /L).

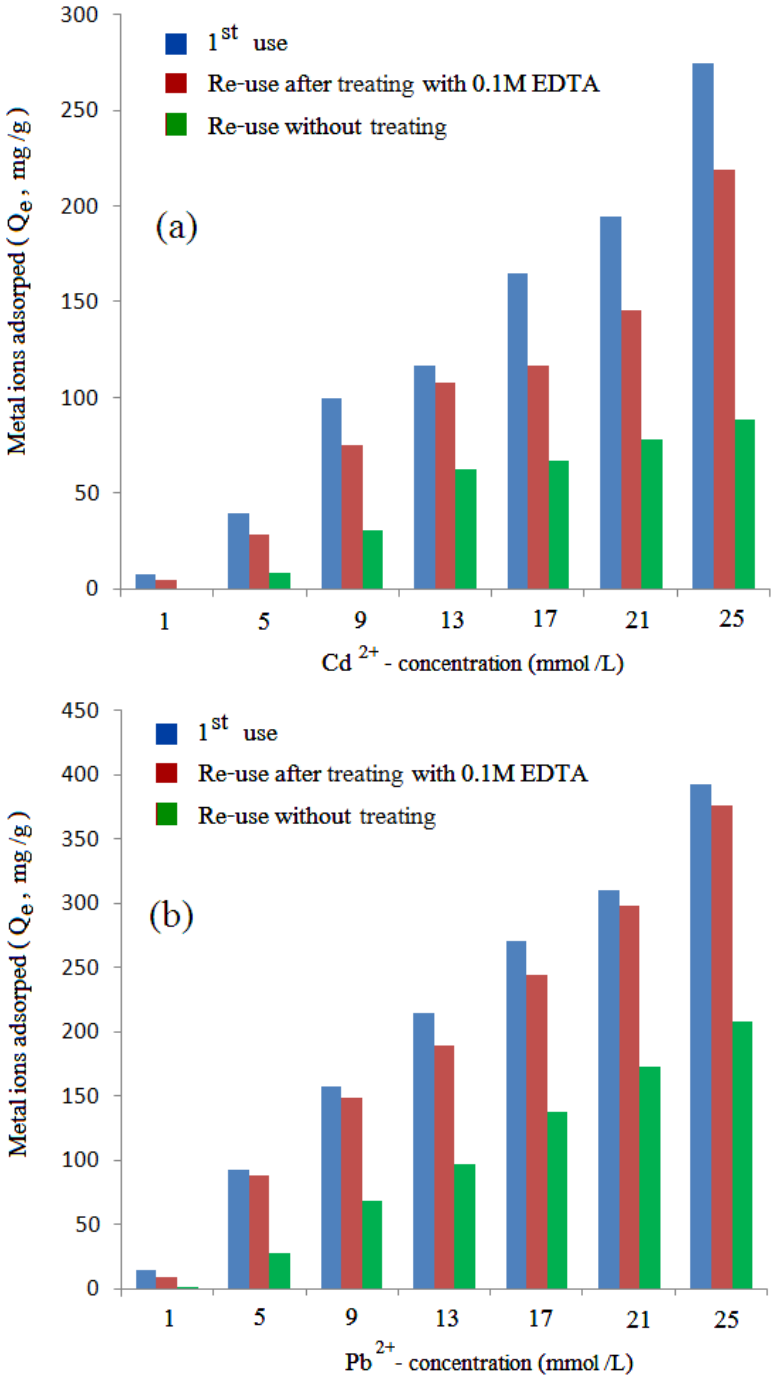

Fig. 60. The recycling uses of $LaGdO_3$ with: (a) Cd^{2+} ion and (b) Pb^{2+} ion (concentration 1 – 25 mmol /L).

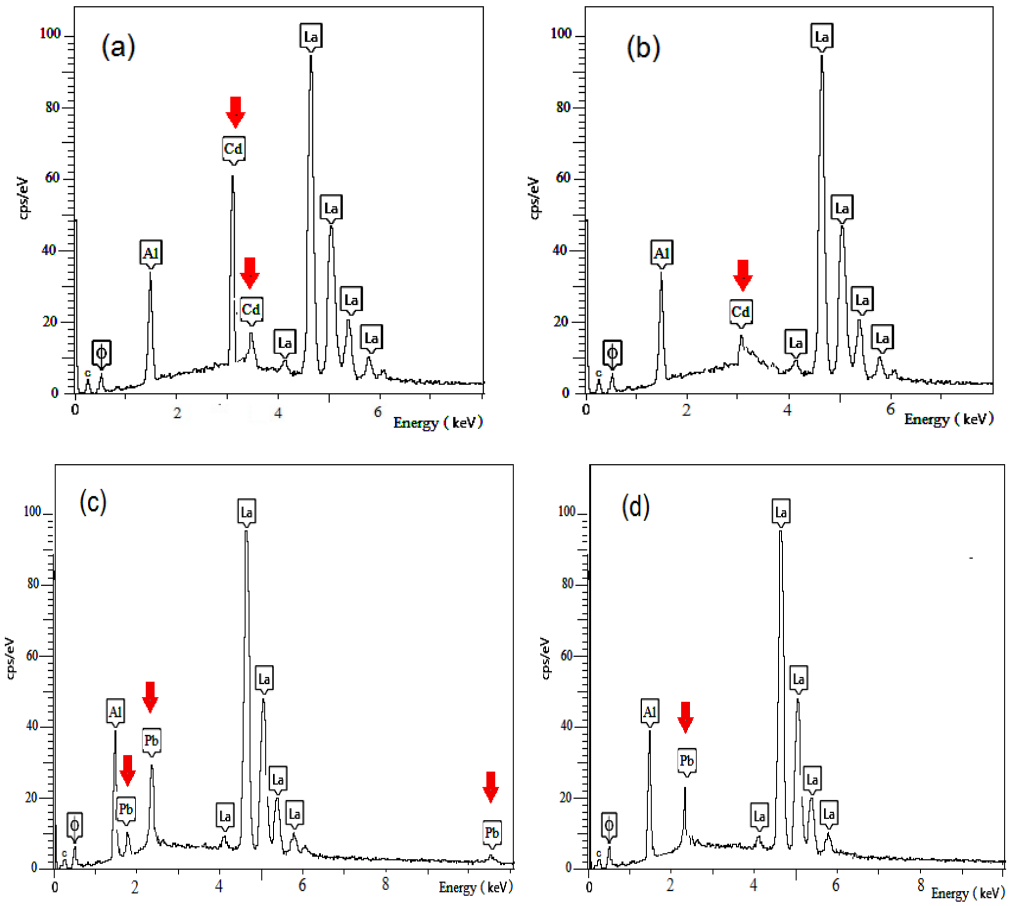

Fig. 61. EDX spectra of the reused $LaAlO_3$: (a) after Cd adsorption, (b) after being treated with EDTA, (c) after Pb adsorption, and (d) after being treated with EDTA.

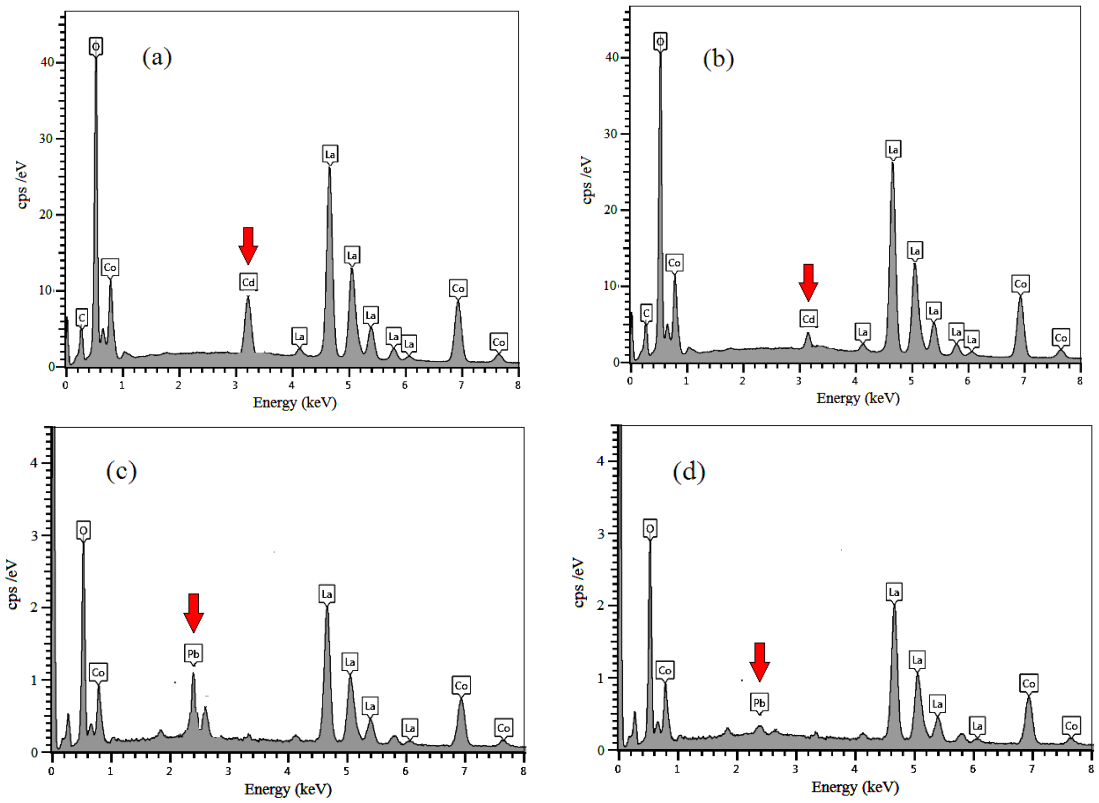

Fig. 62. EDX spectra of the reused $LaCoO_3$: (a) after Cd adsorption, (b) after being treated with EDTA, (c) after Pb adsorption, and (d) after being treated with EDTA.

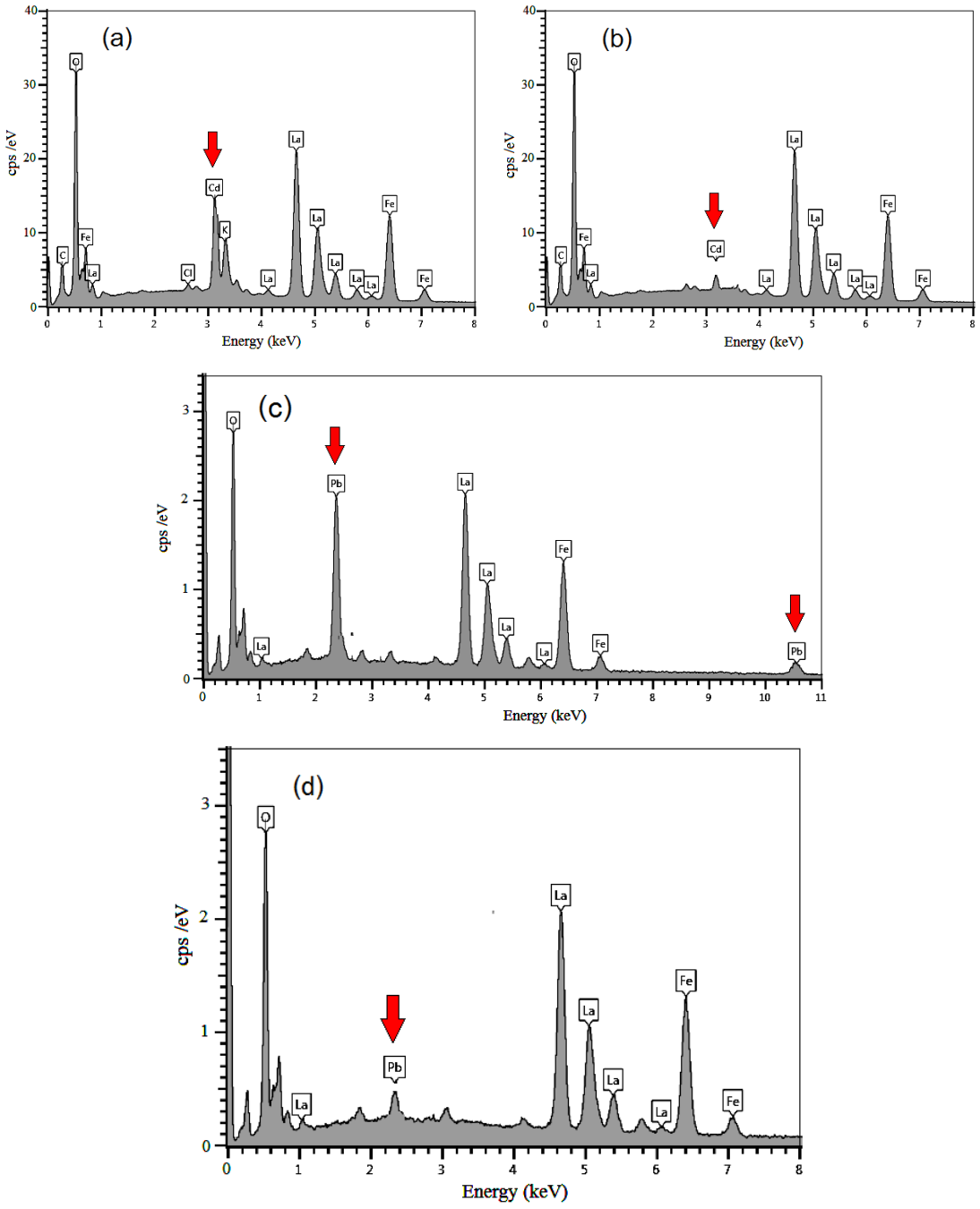

Fig. 63. EDX spectra of the reused $LaFeO_3$: (a) after Cd adsorption, (b) after being treated with EDTA, (c) after Pb adsorption, and (d) after being treated with EDTA.

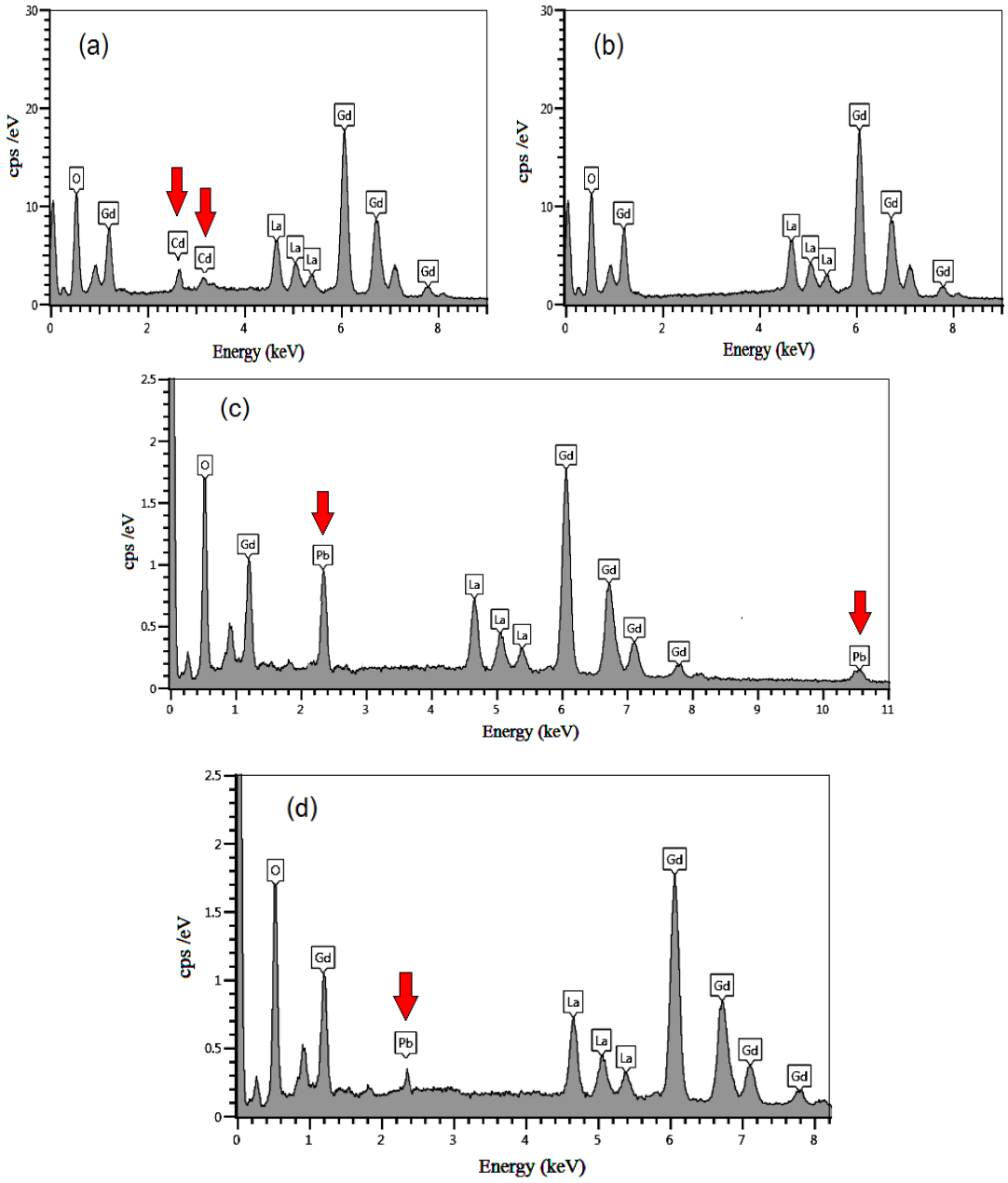

Fig. 64. EDX spectra of the reused $LaGdO_3$: (a) after Cd adsorption, (b) after being treated with EDTA, (c) after Pb adsorption, and (d) after being treated with EDTA.

4.4.3 Adsorption isotherms

Heavy metal ions (Cd^{2+} and Pb^{2+}) adsorption isotherm data starting at different initial concentrations were investigated and compared to the models of Langmuir and Freundlich. The Langmuir model assumes that adsorption occurs at specific homogeneous sites on the adsorbent and is used successfully in many monolayer adsorption processes.

A linear relationship between the amount of $LaMO_3$ (g) against the concentration of cadmium (and lead) ions in the remaining solution (mmol/L) was observed (Figs. 54 – 55). The values of linear correlation coefficients R^2 and Langmuir parameters are given in Tables 6 – 7 and Table 8. The results fitted well with the Langmuir model. The maximum adsorption capacities (q_m) of $LaMO_3$ are: $LaAlO_3$ 3.44 mg/g for Cd^{2+} and 3.06 mg/g for Pb^{2+}, $LaCoO_3$ 0.36 mg/g for Cd^{2+} and 0.76 mg/g for Pb^{2+}, $LaFeO_3$ 0.91 mg/g for $Cd^{2+}$and 0.80 mg/g for Pb^{2+}, $LaGdO_3$ 0.87 mg/g for Cd^{2+} and 1.31 mg/g for Pb^{2+}. The K_L values of $LaAlO_3$, $LaCoO_3$, $LaFeO_3$ and $LaGdO_3$ were found to be 0.28, 1.04, 0.68 and 0.17 $mg^{-1}L$, respectively, for cadmium ion and 1.10, 1.98, 1.33 and 0.99 $mg^{-1}L$, respectively, for lead ion.

The value of q_m obtained above may be on the low side of q_m values of the same metal ions adsorbed on many types of adsorbent reported by several researchers. Examples are: 0.373 mg/g for Cd^{2+} and 0.3103 mg/g for Pb^{2+} on biosorbent (Sulaymon et al 2010), 2.88 mg/g for Cd^{2+} and 2.90 mg/g for Pb^{2+} on activated carbon prepared from plant leaves (Singanan 2011) , 12.05 mg/g for Cd^{2+} and 9.407 mg/g for Pb^{2+} on oil shale ash (Zhu et al 2012).

Table 8. Adsorption isotherms parameters for cadmium and lead ions on $LaMO_3$ (M = Al, Co, Fe, Gd).

M^{2+}	$LaMO_3$	Langmuir model			Freundlich model		
		q_m	K_L	R^2	n	K_F	R^2
Cd^{2+}	$LaAlO_3$	3.44	0.28	0.993	1.22	1.48	0.987
	$LaCoO_3$	0.361	1.04	0.997	0.46	27.41	0.805
	$LaFeO_3$	0.91	0.68	0.992	0.17	3.72	0.927
	$LaGdO_3$	0.87	0.17	0.985	0.92	3.50	0.981
Pb^{2+}	$LaAlO_3$	3.06	1.10	0.987	1.47	3.33	0.892
	$LaCoO_3$	0.76	1.98	0.995	2.51	4.34	0.993
	$LaFeO_3$	0.80	1.33	0.996	2.19	3.75	0.753
	$LaGdO_3$	1.31	0.99	0.996	1.01	2.64	0.991

Although the value of q_m was not particularly high, $LaMO_3$ (M = Al, Co, Fe, Gd) perovskites have an advantage in recyclability. The efficiency in the reuse was slightly lower than that of the freshly prepared sample but it remained almost constant afterwards. The ease of preparation at lower calcination temperature is another advantage to be considered. The results from our study showed that $LaMO_3$ (M = Al, Co, Fe, Gd) perovskites should attract more interest from researchers due to its potential to be used as in gas sensoring as well as in wastewater treatment.

Table 9 is the compilation of q_m values for Cd(II) and Pb(II) ions measured with the use of several adsorbents reported in the literatures. These adsorbents can be divided broadly into two types according to their origins: one originated from biological materials; the other from inorganic minerals. The values of q_m in Table 8 for Cd(II) and Pb(II) ions are higher than many, but not all, of adsorbents produced from biological materials. It is worth noting the high value of q_m's exhibited by the adsorbents produced or originated from natural inorganic materials. The high adsorptivity of inorganic adsorbents might be ascribed to the distinct charges on their surfaces. Porosity could be another factor to increase adsorptivity.

Table 9. Comparison of q_m values from various adsorbents for Cd(II) and Pb(II) ions.

	M^{2+} ions	q_m (mg/g)	Adsorbents	References
Biological origins				
	Cd	0.42	Powder of dried carrot residues	(S. Ata, et al., 2012)
	Pb	0.52		
	Cd	0.37	Baker's yeast biomass	(A.H. Sulaymon, et al., 2010)
	Pb	0.31		
	Cd	36.60	Powder of dried olive tree pruning wastes	(O.Uzunosmanoglu, et al., 2011)
	Pb	46.20		
	Cd	7.19	Almond shells	(M. Mehrasbi et al., 2009)
	Pb	8.13		
	Cd	7.54	Powder of dried radish peels	(J. Anwar et al., 2009)
	Pb	1.23		
	Cd	2.88	Activated biocarbon	(M. Singanan., 2011)
	Pb	2.90		
Inorganic mineral origins				
	Cd	10.37	Polyphosphate-modified kaolinite clay	(M.W. Amer et al., 2010)
	Pb	25.13		
	Cd	18.52	Calcite	(O. Yavuz et al., 2007)
	Pb	19.92		
	Cd	14.61	Chemically treated sodic bentonite clay	(L.S.G. Galindo et al., 2013)
	Pb	22.79		
	Cd	12.05	Modified oil shale ash	(B.L. Zhu et al., 2012)
	Pb	9.41		

Table 9 (cont). Comparison of q_m values from various adsorbents for Cd(II) and Pb(II) ions.

	M2+ ions	qm (mg/g)	Adsorbents	References
Inorganic mineral origins				
	Cd	27.44	Calcium alginate beads	(A.C. Villanueva et al., 2014)
	Pb	150.40		
	Cd	9.27	RSA clinoptilolite treated with Na^+	(B. Taenzana et al., 2011)
	Pb	19.84		
	Cd	10.82	USA clinoptilolite treated with Na^+	
	Pb	4.01		

CHAPTER 5

CONCLUSIONS

Nanocrystalline $LaMO_3$ (M = Al, Co, Fe, Gd) perovskites in powder form were prepared using the conventional co-precipitation method followed by calcination at normally high temperature of 900 °C for use in comparison with samples prepared at lower calcination temperatures. The products were characterized with XRD, EDX, SEM, TEM, and BET which revealed significant differences in physical properties of the samples. The test for using it as ethanol gas sensor was carried out at 350 °C. Though the samples from high calcination temperature showed good response toward ethanol, the samples from lower calcination temperature showed even greater sensitivity giving results that were much better than many sensors ever reported. Besides gas sensoring property, $LaMO_3$ (M = Al, Co, Fe, Gd) perovskite also acted as metal ions adsorbers in the toxic heavy metal ions (cadmium and lead) adsorption experiment. Heavy metal ion adsorption isotherm data were studied. The adsorption isotherms of Cd^{2+} and Pb^{2+} ion were better described by the Langmuir isotherm models.

REFFERENCES

Alfaro-Cuevas-Villanueva, R., Hidalgo-Vazquez, AR., Penagos, CJC., Cortes-Martinez, R. 2014. Thermodynamic, kinetic, and equilibrium parameters for the removal of lead and cadmium from aqueous solutions with calcium alginate beads. http://dx.doi.org/10.1155/2014/647512 (accessed 1/1/ 2016).

Abazari, R. and Sanati, S. 2013. "Perovskite $LaFeO_3$ nanoparticles synthesized by the reverse microemulsion nanoreactors in the presence of aerosol-OT: morphology, crystal structure, and their optical properties", SuperlatticeMicrost. 64 (2013) 148-157.

Addabbo, T.; Bertocci, F.; Fort, A.; Gregorkiewitz, M.; Mugnaini, M.; Spinicci, R. and Vignoli, V. 2015. "Gas sensing properties and modeling of $YCoO_3$ based perovskite materials", Sensors and Actuators B: Chemical 221 (2015) 1137-1155.

Ajami, S.; Mortazavi, Y.; Khodadadi, A.; Pourfayaz, F. and Mohajerzadeh, S. 2006. "Highly selective sensor to CH_4 in presence of CO and ethanol using $LaCoO_3$ perovskite filter with Pt/SnO_2", Sensors and Actuators B: Chemical. 117 (2006) 420-425.

Anwar, J.; Shafique, U.; Salman, M.; Zaman, W.; Anwar, S. and Anzano, J.M. 2009. "Removal of chromium (III) by using coal as adsorbent", Journal of Hazardous Materials. 1-3 (2009) 797-801.

Anwar, J., Shafique, U., Waheed-uz-Zaman, MS., Memoona, M. 2009. "Adsorption study of cadmium(II) and lead(II) on radish peels". Journal of Scientific Research. 39 (2009) 29-34.

Amer, MW., Khalili, FI., Awwad, AM. 2010. "Adsorption of lead, zinc and cadmium ions on polyphosphate-modified kaolinite clay. Journal of Environmental" Chemistry and Ecotoxicology. 2 (2010) 1-8.

Armagan, B. and Toprak, F. 2013. “Optimum isotherm parameters for reactive azo dye onto pistachio nut shells : comparison of linear and non-linear methods”, Pol. J. Environ.Stud. 22 (2013),1007-1011.

Atta, N.F.; Galal, A. and Ekram, H.E.A. 2016. “Perovskite Nanomaterials – Synthesis, Characterization, and Applications”, Energy Engineering. 3 (2016) 1-2.

Banat, IM., Nigam, P., Singh, D., Marchant, R. 1996. Remediation of dyes in textile effluent : a critical review on current treatment technogies with a proposed alternative. Bioresource Technology. 58 (1996) 217-227.

Balamurugan, C. and Lee, D. W. 2015. “Perovskite hexagonal $YMnO_3$ nanopowder as p-type semiconductor gas sensor for H_2S detection”, Sensors and Actuators B: Chemical 221 (2015) 857-866.

Berchmans, L. J.; Angappan, S.; Visuvasam, A. and Kumar, K.B.R. 2008. “Preparation and characterization of $LaAlO_3$”, Materials Chemistry and Physics. 109 (2008) 113-118.

Bhakta, J.N., Munekage, Y. 2011. “Role of ecosystem components in Cd removal process of aquatic ecosystem”, Ecological Engineering. 32 (2011) 274 – 280.

Bhargav, K.K.; Maity, A.; Ram, S. and Majumder, S.B. 2014. “Low temperature butane sensing using catalytic nano-crystalline lanthanum ferrite sensing element”, Sensors and Actuators B: Chemical. 195 (2014) 303-312.

Biswas, AK., Tortajada, C. 2011. Water quality management : an introductory frame work. Water Resources Management . 27 (2014) 5-11.

Brosha, E.L.; Mukundan, R.; Brown, D.R.; Garzon, F.H.; Visser, J.H.; Zanini, M.; Zhou, Z. and Logothetis, E.M. 2000. “CO/HC sensors based on thin films of $LaCoO_3$ and $La_{0.8}Sr_{0.2}CoO_3$ metal oxides”, Sensors and Actuators B: Chemical. 69 (2000) 171-182.

Carotta, M.C.; Butturi, M.A.; Martinelli, G.; Sadaoka, Y.; Nunziante, P. and Traversa, E. 1997. "Microstructural evolution of nanosized $LaFeO_3$ powders from the thermal decomposition of a cyano-complex for thick film gas sensors", Sensor Actuat.B-Chem. 44 (1997) 590-594.

Chen, H.; Ma, S.Y.; Jiao, H.Y.; Yang, G.J.; Xu, X.L.; Wang, T.T.; Jiang, X.H. and Zhang, Z.Y. 2016. "The effect microstructure on the gas properties of Ag doped zinc oxide sensors: Spheres and sea-urchin-like nanostructures" Journal of Alloys and Compounds. 687 (2016) 342-351.

Chen, X.; Li, D.M.; Liang, S.F.; Zhan, S.and Liu, M. 2013. "Gas sensing properties of surface acoustic wave NH_3 gas sensor based on Pt doped polypyrrole sensitive film", Sensors and Actuators B: Chemical. 177 (2013) 364-369.

Chen, Q., Yin, D., Zhu, S. and Hu, X. 2012. "Adsorption of cadmium(II) on humic acid coated titanium dioxide", Journal of Colloid and Interface Science. 367 (2012) 241 – 248.

Consuelo, P.; Octavio, S.; Ignacio M. and Julio, L.B. 2009. "Binary diffusion coefficients for 2,3-dimethylaniline, 2,6-dimethylaniline, 2-methylanisole, 4-methylanisole and 3-nitrotoluene in supercritical carbon dioxide" The Journal of Supercritical Fluids. 48 (2009) 1-8.

Chu, X.; Zhou, S.; Zhang, W. and Shui, H. 2009. "Trimethylamine sensing properties of nano-$LaFeO_3$ prepared using solid-state reaction in the presence of PEG400", Mater. Sci. Eng. B. 164 (2009) 65-69.

Chu, X.; Zhou, S.; Zhang, W. and Shui, H. 2009. "Trimethylamine sensing properties of nano-$LaFeO_3$ prepared using solid-state reaction in the presence of PEG400", Materials Science and Engineering: B. 164 (2009) 65-69.

Eren, E., Gumas, H. 2011. Characterization of the structural properties and Pb(II) adsorption behavior of iron oxide coated sepiolite. Desalination. 273 (2011) 276-284.

Eren, E.; Cubuk, O.; Ciftci, H.; Eren, B. and Caglar, B. 2010. "Adsorption of basic dye from aqueous solutions by modified sepiolite: Equilibrium, kinetics and thermodynamics study", Desalination. 252 (2010) 88-96.

Fan, K.; Qin, H.; Zhang, Z.; Sun, L. and Hu, J. 2012. "Gas sensing properties of nanocrystalline $La_{0.75}Ba_{0.25}FeO_3$ thick –film sensors", Sensor Actuat. B-Chem. 171-172 (2012) 302-308.

Fan, H.; Zhang, T.; Xu, X. and Lv, N. 2011. "Fabrication of N-type Fe_2O_3 and P-type $LaFeO_3$ nanobelts by electrospinning and determination of gas-sensing properties", Sensors and Actuators B: Chemical. 153 (2011) 83-88.

Farhadi, S. and Sepahvand, S. 2010. "Microwave-assisted solid-state decomposition of $La[Co(CN)_6]\cdot 5H_2O$ precursor: A simple and fast route for the synthesis of single phase perovskite-type $LaCoO_3$ nanoparticles", J. Alloys Compd. 489 (2010) 586-591.

Fergus, J. W. 2007. "Perovskite oxides for semiconductor-based gas sensors", Sensors and Actuators B: Chemical. 123 (2007) 1169-1179.

Feng, C.; Ruan, S.; Li, J.; Zou, B.; Luo, J.; Chen, W.; Dong, W. and Wu, F. 2011. "Ethanol sensing properties of $LaCo_xFe_{1-x}O_3$ nanoparticles: Effects of calcination temperature, Co- doping, and carbon nanotube- treatment", Sensors and Actuators B: Chemical. 155 (2011) 232-238.

Fu, S.; Niu, H.; Tao, Z.; Song, J.; Mao, C.; Zhang, S.; Chen, C. and Wang, D. 2013. "Low temperature synthesis and photocatalytic property of perovskite type $LaCoO_3$ hollow spheres", Journal of Alloys and Compounds, 576 (2013) 5-12.

Galvan, M.C.A.; Constantinou, D. A.; Navarro, R.M.; Villoria, J.A.; Fierro, J.L.G. and Efstathiou, A.M. 2011. "Surface reactivity of $LaCoO_3$ and $Ru/LaCoO_3$ towards CO, CO_2 and C_3H_8: Effect of H_2 and O_2 pretreatments", Applied Catalysis B: Environmental. 102 (2011) 291-301.

Galindo, LSG., Neto, AFA., Silva, MGC., Vieira, MGA. 2013. Removal of cadmium(II) and lead(II) ions from aqueous phase on sodic bentonite. Materials Research. 16 (2013) 515-527.

Galindo, H.; Carvajal, Y. and Suib, S.L. 2010. "Sulfonation of the surface of cordierite monoliths through a novel multi-step wet chemical process" Microporous and Mesoporous Materials. 135 (2010) 37-44.

Gargori, C.; Cerro, S.; Galindo, R.; García, A.; Llusar, M. and Monrós, G. 2012. "Iron and chromium doped perovskite ($CaMO_3$ M=Ti, Zr) ceramic pigments, effect of mineralizer", Ceramics International. 38 (2012) 4453-4460.

Gharaibeh, S.H., Abu-el-shar, W.Y. and Al-Kofahi, M.M. 1998. "Removal of selected heavy metals from aqueous solutions using processed solid residue of olive mill products", Water Research. 32 (1998) 498 – 502.

Ghasdi, M.; Alamdari, H.; Royer, S. and Adnot, A. 2011. "Electrical and CO gas sensing properties of nanostructured $La_{1-x}Ce_xCoO_3$ perovskite prepared by activated reactive synthesis ", Sensors and Actuators B: Chemical. 156 (2011) 147-155.

Ghasdi, M. and Alamdari, H. 2010. "CO sensitive nanocrystalline $LaCoO_3$ perovskite sensor Prepared by high energy ball milling", Sensors and Actuators B. 148 (2010) 478–485.

Ghiloufi, I.; Ghoul, J.E.; Modwi, A. and Mir, L.E. 2016. "Ga-doped ZnO for adsorption of heavy metals from aqueous solution", Materials Science in Semiconductor Processing 42 (2016) 102 – 106.

Giang, H.T.; Duy, H.T.; Ngan, P.Q.; Thai, G.H.; Thu, D.T.; Thu, D.T. and Toan, N.N. 2011. "Hydrocarbon gas sensing of nano-crystalline perovskite oxides $LnFeO_3$ (*Ln* = La, Nd and Sm) ", Sensors and Actuators B: Chemical. 158 (2011) 246-251.

Haas, O., Struis, R.P.W.J. and McBreen, J. M. 2004. "Synchrotron X-ray absorption of $LaCoO_3$ perovskite", Journal of Solid State Chemistry. 117 (2004) 1000-1010.

Hadjiivanov, K., Vasileva, E., Kantcheva, M. and Klissurski, D. 1991. "Ir spectroscopy study of silver ions adsorbed on titania (anatase)", Materials Chemistry and Physics. 28 (1991) 367-377.

Haiyun S. and Qiuhua Y. 2008. "Study on reaction mechanism of low temperature preparation of nanocrystalline $LaCoO_{3-\lambda}$" Journal of Rare Earths. 26 (2008) 681-683.

Hua, M.; Zhang, S.; Pan, B.; Zhang, W.; Lv, L. and Zhang, Q. 2012. "Heavy metal removal from water/wastewater by nanosized metal oxides: A review", Journal of Hazardous Materials, 211-212 (2012) 317-331.

Huelin, SR., Longerich, HP., Wilton, DHC., Fryer, BJ., Li, Y., Wang, X. 2006. The determination of trace elements in Fe-Mn oxide coatings on pebbles using I.A.- ICP- MS. Journal of Geochemical Exploration. 91 (2006) 110-124.

Huang, J.; Cao, Y.; Liu, Z.; Deng, Z. and Wang, W. 2012. "Application of titanate nanoflowers for dye removal: A comparative study with titanate nanotubes and nanowires", Chemical Engineering Journal. 191 (2012) 38-44.

Ianos, R.; Lazau, R.; Borcanescu, S. and Babuta, R. 2014. "Single-step combustion Synthesis of $LaAlO_3$ powders and their sintering behavior", Ceram. Int. 40 (2014) 7561-7565.

Junwu, Z.; Xiaojie, S.; Yanping, W.; Xin, W.; Xujie, Y. and Lude, L. 2007. "Solution-phase synthesis and characterization of perovskite $LaCoO_3$ nanocrystals via a co precipitation route", J. Rare Earths. 25 (2007) 601-604.

Jazi, M.B.; Arshadi, M.; Amiri, M.J. and Gil, A. 2014. "Kinetic and thermodynamic investigations of Pb(II) and Cd(II) adsorption on nanoscale organo-functionalized SiO_2-Al_2O_3", Journal of Colloid and Interface Science. 422 (2014) 16-24.

Junjiang, Z.; Hailong, L.; Linyun, Z.; Ping, X.; Xuelian, X.; Xiangguang, Y.; Zhen, Z. and Jinlin, L. 2014. "Perovskite Oxides: Preparation, Characterizations, and Applications in Heterogeneous Catalysis", ACS Catal. 4 (2014) 2917–2940.

Kaituo, W.; Xuehang, W.; Wenxei, W.; Yongni, L. and Sen, L. 2014. "Synthesis of perovskite $LaCoO_3$ by thermal decomposition of oxalates : Phase evolution and kinetics of the thermal transformation of the precursor", Ceram. Int. 40 (2014) 5997-6004.

Kaiwen, Z.; Xuehang, W.; Wenwei, W.; Jun, X.; Siqi, T. and Sen, L. 2013. "Nanocrystalline $LaFeO_3$ preparation and thermal process of precursor", Adv. Powder Technol. 24 (2013) 359-363.

Kharton, V.V.; Figueiredo, F.M.; Kovalevsky, A.V.; Viskup, A.P.; Naumovich, E.N.; Yaremchenko, A.A.; Bashmakov, I.A. and Marques, F.M.B. 2001. "Processing, microstructure and properties of $LaCoO_3$ ceramics", Journal of the European Ceramic Society. 21 (2001) 2301-2309.

Kharton, V.V.; Naumovich, E.N. and Nikolaev, A.V. 1996. "Materials of high-temperature electrochemical oxygen membranes" Journal of Membrane Science. 111 (1996) 149-157.

Kleveland, K.; Einarsrud, M.A. and Grande, T. 2000. "Sintering of $LaCoO_3$ based ceramics", J.Eur.Ceram. Soc. 20 (2000) 185-193.

Kim, M.S. and Chung, J.G. 2001. "A study on the adsorption characteristics of orthophosphates on rutile-type titanium dioxide in aqueous solutions", J. Colliod Interf.Sci. 233 (2001) 31-37.

Kumar, K.Y.; Muralidhara, H.B.; Nayaka, Y.A.; Balasubramanyam, J. and Hanumanthappa, H. 2013. "Low-cost synthesis of metal oxide nanoparticles and their application in adsorption of commercial dye and heavy metal ion in aqueous solution" Powder Technology. 246 (2013) 125-136.

Li, Z.; Zhang, S. and Lee, W.E. 2007. "Molten salt synthesis of $LaAlO_3$ powder at low temperatures", Journal of the European Ceramic Society. 27 (2007) 3201–3205.

Li, W.; Zhuo, M.W. and Shi, J.L. 2004. "Synthesizing nano $LaAlO_3$ powders via co-precipitation method", Materials Letters. 58 (2004) 365-368.

Li, K.; Wang, D.; Wu, F.; Xie, T. and Li, T. 2000. "Surface electronic states and photovoltage gas-sensitive characters of nanocrystalline $LaFeO_3$", Mater. Chem. Phys. 64 (2000) 269-272.

Liu, X.; Cheng, B.; Hu, J.; Qin, H. and Jiang, M. 2008. "Semiconducting gas sensor for ethanol based on $LaMg_xFe_{1-x}O_3$ nanocrystals", Sensor Actuat. B-Chem. 129 (2008) 53-58.

Liu, X.; Cheng, B.; Hu, J.; Qin, H. and Jiang, M. 2008. "Semiconducting gas sensor for ethanol based on $LaMgxFe_{1-x}O_3$ nanocrystals", Sensors and Actuators B: Chemical. 129 (2008) 53-58.

Lee, CI., Yang, WF., Hsieh, CI. 2004. Removal of copper (II) by manganese-coated sand in a liquid fluidized-bed reactor. Journal of Hazardous Materials. 114 (2004) 45-51.

Lee, W.Y.; Yun, H.J. and Yoon, J.W. 2014."Characterization and magnetic properties of $LaFeO_3$ nanofibers synthesized by electrospining", J. Alloys Compd. 583 (2014) 320-324.

Lee, S.M.; Kim, S.K.; Yoo, J.W. and Kim, H.T. 2005. "Crystallization behavior and mechanical properties of porcelain bodies containing zinc oxide additions", Journal of the European Ceramic Society. 25 (2005) 1829-1834.

Lo, W.C.; Au, K.; Chan, N.Y.; Huang, H.; Lam, C.H. and Dai, J.Y. 2013. "First principles study of transport properties of $LaAlO_3/SrTiO_3$heterostructure with water adsorbates", Solid State Communications. 169 (2013) 46–49.

Mazhar, M.E.; Faglia, G.; Comini, E.; Zappa, D.; Baratto, C. and Sberveglieri, G. 2016. "Kelvin probe as an effective tool to develop sensitive p-type CuO gas sensors", Sensors and Actuators B: Chemical. 222 (2016) 1257 – 1263.

Mehrasbi, MR., Farahmandkia, Z., Taghibeibloo, B., Taromi, A. 2009. Adsorption of lead and cadmium from aqueous solution by using almond shells. Water Air and Soil Pollution. 199 (2009) 343-351.

Meziani, D.; Reziga, A.; Rekhila, G.; Bellal, B. and Trari, M. 2014. "Hydrogen evolution under visible light over $LaCoO_3$ prepared by chemical route", Energy Conversion and Management. 82 (2014) 244–249.

Mohapatra, M., Anand, S. 2007. Study on sorption of Cd(II) on Tata chromite mine overburden. Journal of Hazardous Materials. 148 (2007) 553-559.

Moon, S.E.; Lee, H.K.; Choi, N.J.; Lee, J.; Choi, C.A.; Yang, W.S.; Kim, J.; Jong, J.J. and Yoo, D. J. 2013. "Low power consumption micro C2H5OH gas sensor based on microheater and screen printing technique", Sensors and Actuators B: Chemical, 187 (2013) 598–603.

Moon, S. E.; Lee, J.W.; Choi, N.J.; Lee, H.K.; Yang, W. S.; Kim, J. and Park, Y. 2012. "High-response and low-power-consumption CO micro gas sensor based on nano-powders and a microheater", J. Korean Phys. Soc. 60 (2012) 235-239.

Nada, F.A.; Shimaa, M.; Ekram, H.E. and Galal, A. 2014. "Nano-perovskite carbon paste composite electrode for the simultaneous determination of dopamine, ascorbic acid and uric acid", Electrochimica Acta. 128 (2014) 16-24.

Negahdari, Z. and Willert-Porada, M. 2009. "Microstructure Tailored Functionally Graded Alumina/Lanthanum Hexaaluminate Ceramics for Application as Thermal Barrier Coatings", Advanced Engineering Materials 11 (2009) 1034 – 1038.

Ouyang, S.; Song, X.; Wang, Y.; Ru, H.; Shaw, N.; Jiang, Y.; Niu, F.; Zhu, Y. and Qiu, W. 2011. "Structural analysis of the STING adaptor protein reveals a hydrophobic dimer interface and mode of cyclic di-GMP binding", Immunity 36 (2011) 1073-1086.

Pavunny, S. P.; Scott, J. F. and Katiyar, R. S. 2014. "Lanthanum Gadolinium Oxide: A New Electronic Device Material for CMOS Logic and Memory Devices", Materials 7 (2014) 2669-2696.

Pavunny, S. P.; Thomas, R.; . Kumar, A.; Murari, N. M. and Katiyar, R. S. 2011. "Dielectric properties and electrical conduction of high-k $LaGdO_3$ ceramics", Journal of Applied Physics. 111 (2012) 102811-102816.

Pena, M.A. and Fierro, J.L.G. 2001. "Chemical Structure and Performance of Perovskite Oxides", American Chemical Society. 101 (2001) 1981-2017.

Predoana, L.; Malic, B.; Crisan, D.;Dragan, N.; Anastasescu, M.; Moreno, J.C.; Scurtu, R. and Zaharescu, M. 2012. "$LaCoO_3$ ceramics obtained from reactive powders", Ceramics International. 38 (2012) 5433–5443.

Predoana, L.; Malic, B.; Kosec, M. and Zaharescu, M. 2007. "Characterization of $LaCoO_3$ powders obtained by water-based sol–gel method with citric acid", Journal of the European Ceramic Society. 27(2007) 4407-4411.

Popa, M. and Kakihana, M. 2002. "Synthesis of Lanthanum Cobaltite ($LaCoO_3$) by the Polymerizable Complex Route", Solid State Ionics. 151 (2002) 251-257.

Popa, M.; Frantti, J. and Kakihana, M. 2002. "Characterization of $LaMeO_3$ (Me: Mn, Co, Fe) perovskite powders obtained by polymerizable complex method", Solid State Ionics. 154-155 (2002) 135-141.

Rahmani, A.; Mousavi, H.Z. and Fazli, M. 2010. "Effect of nanostructure alumina on adsorption of heavy metals", Desalination. 253 (2010) 94-100.

Rao, M.M., Ramesh, A., Rao, G.P.C. and Seshaiah, K. 2006. "Removal of copper and cadmium from the aqueous solutions by activated carbon derived from ceiba pentandra hills", J. Hazard. Mater. B. 129 (2006) 123 – 129.

Rauf, MA., Qadri, SM., Ashraf, S., Al-Mansoori, KM. 2009. Sorption and desorption of Pb^{2+} ions by dead Sargassum sp. Biomass. Chemical Engineering Journal. 150 (2009) 90- 95.

Robinson, T., McMullan, G., Marchant, R., Nigam, P. 2004. Adsorption studies of toluidine blue from aqueous solution onto gypsum. Bioresource Technology. 77 (2004) 247-255.

Rusevova, K.; Koferstein, R.; Rosell, M.; Richnow, H.H.; Kopinke, F.D. and Georgi, A. 2014. "$LaFeO_3$ and $BiFeO_3$ perovskites as nanocatalysts for contaminant degradation in heterogeneous Fenton –like reactions", Chem. Eng. J. 239 (2014) 322-331.

Sathitwitayakul, T.; Kuznetsov, M.V.; Parkin, I.P. and Binions, R. 2012. "The gas sensing properties of some complex metal oxides prepared by self propagating high-temperature synthesis", Materials Letters. 75 (2012) 36-38.

Sharma, DC., Forster, CF. 1994. A preliminary examination into the adsorption of hexavalent chromium using low cost adsorbents. Bioresource Technology. 47, 257-264.

Singanan, M. and Peters, E. 2011. "Removal of toxic heavy metals from synthetic wastewater using a novel biocarbon technology", Journal of Environmental Chemical Engineering.1 (2013) 884 – 890.

Singanan, M. 2011. Removal of lead(II) and cadmium(II) ions from wastewater using activated biocarbon. ScienceAsia. 37 (2011) 115-119.

Shen, H.; Yang, Q. and LI, N. 2008. "Study on reaction mechanism of temperature preparation of nanocrystalline $LaCoO_{3-\lambda}$", Journal of Rare Earths. 26 (2008) 681-683.

Shi, J.; Yan, R.; Zhu, Y. and Zhang, X. 2003. "Determination of NH_3 gas by combination of nanosized $LaCoO_3$ converter with chemiluminescence detector", Talanta. 61 (2003) 157-164.

Song, P.; Zhang, H.; Han, D.; Li, J.; Yang, Z. and Wang, Q. 2014. "Preparation of biomorphic porous $LaFeO_3$ by sorghum strawbiotemplate method and its acetone sensing properties", Sensors and Actuators B 196 (2014) 140-146.

Song, P.; Zhang, H.; Han, D.; Li, J.; Yang, Z. and Wang, Q. 2014. "Hydrothermal synthesis of porous In_2O_3 nanospheres with superior ethanol sensing properties", Sensor Actuat. B-Chem. 196 (2014) 434-439.

Song, P.; Wang, Q. and Yang, Z. 2012. "Preparation, characterization and acetone sensing properties of Ce-doped SnO_2 hollow spheres", Sensor Actuat. B-Chem. 173 (2012) 839-846.

Song, P.; Wang, Q.; Zhang, Z. and Yang, Z. 2010. "Synthesis and gas sensing properties of biomorphic $LaFeO_3$ hollow fibers templated from cotton", Sensors and Actuators B: Chemical. 147 (2010) 248-254.

Song, P.; Wang, Q.; Zhang, Z. and Yang, Z. 2010. "Synthesis and gas sensing properties of biomorphic $LaFeO_3$ hollow fibers templated from cotton", Sensors and Actuators B: Chemical. 147 (2010) 248-254.

Sonsteby, H.H.; Ostreng, E.; Fjellvåg, H. and Nilsen, O. 2014. "Deposition and x-ray characterization of epitaxial thin films of $LaAlO_3$", Thin Solid Films. 550 (2014) 90-94.

Sulaymon, A.H., Abid, B.A. and Al-Najar, J. 2010. "Removal of lead copper chromium and cobalt ions onto granular activated carbon in batch and fixed-bed adsorbers", Chemical Engineering Journal. 155 (2010) 647 – 653.

Sulaymon, AH., Ebrahim, SE., Al-Musawi, TJ., Abdullah, SM. 2010. Removal of lead, cadmium, and mercury ions using biosorption. Iraqi Journal of Chemical and Petroleum Engineering. 11 (2010) 1-13.

Tao, S.; Gao, F.; Liu, X. and Surensen, O. T. 2000. "Ethanol-sensing characteristics of barium stannate prepared by chemical precipitation", Sensor Actuat. B-Chem. 71 (2000) 223-227.

Tao, S.; Gao, F.; Liu, X. and Surensen, O. T. 2000. "Ethanol-sensing characteristics of barium stannate prepared by chemical precipitation", Sensor Actuat. B-Chem. 71 (2000) 223-227.

Tao, S.; Gao, F.; Liu, X. and Surensen, O. T. 2000. "Ethanol-sensing characteristics of barium stannate prepared by chemical precipitation", Sensor Actuat. B-Chem. 71 (2000) 223-227.

Tian, Z.; Huang, W. and Liang, Y. 2009. "Preparation of spherical nanoparticles of $LaAlO_3$ via the reverse microemulsion process", Ceram. Int. 35 (2009) 661-664.

Tian, Z.Q.; Yu, H.T. and Wang, Z.L. 2007. "Combustion synthesis and characterization of nanocrystalline $LaAlO_3$ powders, Mater". Chem. Phys. 106 (2007) 126-129.

Tompsett, G.A.; Phillips, R.J.; Sammes, N.M. and Cartner, A.M. 1998. "Characterisation of $LaGdO_3$ by X-ray powder diffraction and Raman spectroscopy", Solid State Communications. 108 (1998) 655-660.

Uzunosmanoglu, O., Uzanik, A., Engin, MS. 2011. The removal of cadmium(II), copper(II) and lead(II) from aqueous solutions by olive tree pruning waste. Fresenius Environmental Bulletin. 20 (2011) 3135-3140.

Venkateshama, V.; Madhua, G.M.; Satyanarayanab, S.V. and Preethama, H.S. 2013. "Adsorption of lead on gel combustion derived nano ZnO", Procedia Engineering 51 (2013) 308 – 313.

Villoria, JA., Alvarez-Galvana, MC., Al-Zahranib, SM., Palmisanoc, P., Specchiac, S., Specchiac, V, 2011. Oxidative reforming of diesel fuel over.$LaCoO_3$ perovskite derived catalysts: Influence of perovskite synthesis method on catalyst properties and performance. Applied Catalysis B: Environmental. 105 (2011) 276-288.

Wan, X.; Wang, J.; Zhu, L. and Tang, J. 2014. "Gas sensing properties of Cu_2O and its particle size and morphology-dependent gas-detection sensitivity", J. Mater. Chem. A (2014) 13641-13647.

Wang, X.; Qin, H.; Sun, L. and Hu, J. 2013. "CO_2 sensing properties and mechanism of nanocrystalline $LaFeO_3$ sensor", J. Sensor Actuat. B-Chem. 188 (2013) 965-971.

Wang, X.; Qin, H.; Sun, L. and Hu, 2013. "CO_2 sensing properties and mechanism of nanocrystalline $LaFeO_3$ sensor", J. Sensors and Actuators B: Chemical. 188 (2013) 965–971.

Wang, Y.; Zhu, J.; Zhang, L.; Yang, X.; Lu, L. and Wang, X. 2006. "Preparation and characterization of perovskite $LaFeO_3$nanocrystals", Materials Letters. 60 (2006) 1767-1770.

Wang, Y., Wong, K.H., Shin, F.G. and Choy, C.L. 2002. "Fatigue in asymmetric-field-driven ferroelectric thin films", Physics Letters A. 304 (2002) 54-59.

Worayingyong, A.; Kangvansura, P.; Ausadasuk, S. and Praserthdam, P. 2008. "The effect of preparation: Pechini and Schiff base methods, on adsorbed oxygen of $LaCoO_3$ perovskite oxidation catalysts", Colloids and Surfaces A: Physicochemical and Engineering Aspects, 315 (2008) 217-22

Wu, X.H.; Wang, Y.D.; Liu, H.L.; Li, Y.F. and Zhou, Z.L. 2002. "Preparation and gas-sensing properties of perovskite-type $MSnO_3$ (M=Zn, Cd, Ni)", Materials Letters. 56 (2002) 732-736.

Yang, J.; Li, R.; Zhou, J.; Li, X.; Zhang, Y.; Long, Y. and Li, Y. 2010. "Synthesis of $LaMO_3$ (M =Fe, Co, Ni) using nitrate or nitrite molten salts", Journal of Alloys and Compounds. 508 (2010) 301–308.

Yu, H.F., Wang, J., Wang, S.S. and ManKuo, Y. 2009. "Thermochemical behavior of Metallic citrate precursors for the production of pure $LaAlO_3$", Journal of Physics and Chemistry of Solids. 70 (2009) 218-223.

Yude, W.; Xiaodan, S.; Yanfeng, L.; Zhenlai, Z. and Xinghui, W. 2000. "Perovskite-type $NiSnO_3$ used as the ethanol sensitive material", Solid-State Electronics. 44 (2000) 2009-2014.

Zhang, Y.M.; Zhang, J.; Chen, Z.L. ; Zhu, Z.Q. and Liu, Q.J. 2014. "Improvement of response to formaldehyde at Ag–$LaFeO_3$ based gas sensors through incorporation of SWCNTs", Sensor Actuat. B-Chem. 195 (2014) 509-514.

Zhang, D.; Zhang, C.L. and Zhou, P. 2011. "Preparation of porous nano-calcium titanate microspheres and its adsorption behavior for heavy metal ion in water", Journal of Hazardous Materials. 186 (2011) 971-977.

Zhang, Y.; Liu, Q.; Zhang, J.; Zhu, Q. and Zhu, Z. 2014. "A highly sensitive and selective formaldehyde gas sensor using a molecular imprinting technique based on Ag–$LaFeO_3$", J. Mater. Chem 2 (2014) 10067 – 10072.

Zhao, S.; Sin, J.K.O.; Xu, B.; Zhao, M.; Peng, Z. and Cai, H. 2000. "A high performance ethanol sensor based on field-effect transistor using a $LaFeO_3$ nano-crystalline thin-film as a gate electrode", Sensor Actuat. B-Chem. 64 (2000) 83-87.

Zhao, J.; Liu, Y.; Li, X.; Lu, G.; You, L.; Liang, X.; Liu, F.; Zhang, T. and Du, Y. 2013. "Highly sensitive humidity sensor based on high surface area mesoporous $LaFeO_3$ prepared by a nanocasting route", Sensor Actuat. B-Chem. 181 (2013) 802-809.

Zhao, J.; Liu, Y.; Li, X.; Lu, G.; You, L.; Liang, X.; Liu, F.; Zhang, T. and Du, Y. 2013. "Highly sensitive humidity sensor based on high surface area mesoporous $LaFeO_3$ prepared by a nanocasting route", Sensors and Actuators B: Chemical. 181 (2013) 802–809.

Zhou, D.; Huang, G.; Chen, X.; Xu, J. and Gong, S. 2004. "Synthesis of $LaAlO_3$ via ethylenediaminetetraacetic acid precursor", Materials Chemistry and Physics. 84 (2004) 33-36.

Zhao, S.; Sin, J.K.O.; Xu, B.; Zhao, M.; Peng, Z. and Cai, H. 2000. "A high performance ethanol sensor based on field-effect transistor using a $LaFeO_3$ nano-crystalline thin-film as a gate electrode", Sensors and Actuators B: Chemical. 64 (2000) 83-87.

APPENDIX

Appendix A

Table 1. Effect of contact time and metal ion initial concentration of $LaMO_3$ (M = Al, Co, Fe, Gd) in standard Cd 1 = 1 mmol/L = 103.9 mg/L.

Strr. min.	No	$LaAlO_3$			$LaCoO_3$			$LaFeO_3$			$LaGdO_3$		
		C_e	Q_e	% Ads.	C_e	Q_e	% Ads.	C_e	Q_e	% Ads.	C_e	Q_e	% Ads.
1	1	1.307	51.30	98.74	76.90	13.50	25.99	81.60	11.15	22.33	87.78	8.06	15.51
	2	1.212	51.34	98.83	77.24	13.33	25.70	81.60	11.15	22.33	87.78	8.06	15.51
	3	1.991	50.95	98.08	77.03	13.44	25.89	79.00	12.45	23.97	87.78	8.06	15.51
	$\bar{x}$	1.503	51.20	98.55	77.06	13.42	25.86	80.70	11.58	22.88	87.78	8.06	15.51
	S.D	0.35	0.17	0.33	0.14	0.07	0.12	1.23	0.62	0.77	0.00	0.00	0.00
5	1	1.028	51.44	99.01	76.90	13.50	25.99	81.20	11.35	21.85	87.77	8.07	15.52
	2	1.320	51.29	98.73	76.72	13.59	26.18	78.80	12.55	24.16	87.77	8.07	15.52
	3	1.016	51.44	99.02	76.70	13.60	26.18	77.50	13.20	25.41	87.77	8.07	15.52
	$\bar{x}$	1.121	51.39	98.92	76.77	13.56	26.12	79.20	12.37	23.81	87.77	8.07	15.52
	S.D	0.14	0.07	0.13	0.09	0.05	0.09	1.53	0.77	1.47	0.00	0.00	0.00
10	1	1.085	51.41	98.96	76.80	13.55	26.08	78.50	12.70	24.45	87.75	8.08	15.54
	2	1.120	51.39	98.92	76.21	13.85	26.67	78.40	12.75	24.45	87.76	8.07	15.53
	3	1.070	51.42	98.97	76.39	13.76	26.47	76.30	13.80	26.56	87.76	8.07	15.53
	$\bar{x}$	1.092	51.41	98.95	76.47	13.72	26.41	77.70	13.08	25.15	87.76	8.07	15.53
	S.D	0.02	0.01	0.02	0.25	0.07	0.25	1.23	0.62	0.99	87.76	0.00	0.00

Appendix A

Table 1. Effect of contact time and metal ion initial concentration of $LaMO_3$ (M = Al, Co, Fe, Gd) in standard Cd 1 = 1 mmol/L = 103.9 mg/L.

Strr. min.	No	$LaAlO_3$			$LaCoO_3$			$LaFeO_3$			$LaGdO_3$		
		C_e	Q_e	% Ads.	C_e	Q_e	% Ads.	C_e	Q_e	% Ads.	C_e	Q_e	% Ads.
15	1	0.419	51.74	99.60	76.60	13.65	26.28	76.60	13.65	26.28	87.75	8.08	15.54
	2	0.442	51.73	99.57	76.00	13.80	26.56	74.90	14.50	27.91	87.76	8.07	15.53
	3	0.394	51.75	99.62	76.30	13.80	26.56	75.30	14.30	27.53	87.76	8.07	15.53
	$\bar{X}$	0.418	51.74	99.60	76.40	13.75	26.47	75.60	14.15	27.24	87.76	8.07	15.53
	S.D	0.02	0.00	0.02	0.14	0.07	0.13	0.73	0.36	0.70	87.76	0.00	0.00
20	1	0.397	51.75	99.62	76.40	13.75	26.47	74.60	14.65	28.20	87.74	8.08	15.55
	2	0.382	51.76	99.63	76.00	13.95	26.85	73.80	15.05	28.97	87.74	8.08	15.55
	3	0.380	51.76	99.63	76.30	13.80	26.56	72.70	15.60	30.03	87.74	8.08	15.55
	$\bar{X}$	0.386	51.76	99.63	76.23	13.83	26.63	73.70	15.10	29.07	87.74	8.08	15.55
	S.D	0.00	0.00	0.00	0.17	0.09	0.16	0.78	0.39	0.75	0.00	0.00	0.00
30	1	0.355	51.77	99.66	76.36	13.77	26.51	74.40	14.75	28.39	87.70	8.10	15.59
	2	0.376	51.76	99.64	76.00	13.95	26.85	71.00	16.45	31.67	87.63	8.14	15.66
	3	0.374	51.76	99.64	76.20	13.85	26.66	72.20	15.85	30.51	87.67	8.12	15.62
	$\bar{X}$	0.368	51.76	99.64	76.19	13.86	26.67	72.50	15.68	30.19	87.67	8.12	15.62
	S.D	0.00	0.00	0.00	0.15	0.07	0.14	1.41	0.70	1.36	0.03	0.01	0.03

Appendix A

Table 1. Effect of contact time and metal ion initial concentration of $LaMO_3$ (M = Al, Co, Fe, Gd) in standard Cd 1 = 1 mmol/L = 103.9 mg/L.

Strr. min.	No	$LaAlO_3$			$LaCoO_3$			$LaFeO_3$			$LaGdO_3$		
		C_e	Q_e	% Ads.	C_e	Q_e	% Ads.	C_e	Q_e	% Ads.	C_e	Q_e	% Ads.
40	1	0.291	51.80	99.72	76.30	13.80	26.56	73.00	15.45	29.74	87.41	8.25	15.87
	2	0.304	51.80	99.72	74.60	14.65	28.20	69.30	17.30	33.30	87.43	8.24	15.87
	3	0.293	51.80	99.72	75.90	14.00	26.95	70.00	16.95	32.63	87.40	8.25	15.87
	$\overline{X}$	0.296	51.80	99.72	75.60	14.15	27.24	70.80	16.57	31.89	87.41	8.25	15.87
	S.D	0.00	0.00	0.00	0.73	0.36	0.70	1.61	0.81	1.54	0.01	0.00	0.00

Appendix A

Table 2. Effect of contact time and metal ion initial concentration of $LaMO_3$ (M = Al, Co, Fe, Gd) in standard Cd 2 = 5 mmol/L = 513.6 mg/L.

Strr. min.	No	$LaAlO_3$			$LaCoO_3$			$LaFeO_3$			$LaGdO_3$		
		C_e	Q_e	% Ads.	C_e	Q_e	% Ads.	C_e	Q_e	% Ads.	C_e	Q_e	% Ads.
1	1	290.60	111.50	43.42	334.90	89.35	34.79	342.80	85.40	33.26	448.66	32.47	12.64
	2	290.80	111.40	43.38	334.60	89.50	34.85	344.40	84.60	32.94	449.76	31.92	12.43
	3	290.10	111.75	43.52	334.80	89.40	34.81	345.20	84.20	32.79	449.75	31.92	12.43
	$\bar{X}$	290.50	111.55	43.44	334.77	89.42	34.82	344.13	84.73	33.00	449.39	32.11	12.50
	S.D	0.29	0.41	0.06	0.12	0.06	0.03	1.00	0.50	0.20	0.52	0.26	0.10
5	1	288.30	112.65	43.87	334.40	89.60	34.89	340.10	86.75	33.78	443.32	35.14	13.68
	2	287.10	113.25	44.10	334.00	89.80	34.97	339.60	87.00	33.88	443.20	35.20	13.61
	3	288.70	112.45	43.79	334.60	89.50	34.85	341.70	85.95	33.47	443.68	34.96	13.61
	$\bar{X}$	288.03	112.78	43.92	334.33	89.63	34.90	340.47	86.57	33.71	443.40	35.10	13.63
	S.D	0.68	0.34	0.13	0.25	0.12	0.10	0.90	0.45	0.17	0.20	0.10	0.03
10	1	286.00	113.80	44.31	333.80	89.90	35.00	339.20	87.20	33.96	442.91	35.35	13.76
	2	284.20	114.70	44.67	334.00	89.80	34.97	338.20	87.70	34.15	442.65	35.48	13.81
	3	285.90	113.85	44.33	333.80	89.90	35.01	337.80	87.90	34.23	442.90	35.35	13.77
	$\bar{X}$	285.37	114.12	44.44	333.87	89.87	34.99	338.40	87.60	34.11	442.82	35.39	13.78
	S.D	0.83	0.41	0.17	0.09	0.05	0.02	0.60	0.29	0.11	0.12	0.06	0.02

Appendix A

Table 2. Effect of contact time and metal ion initial concentration of $LaMO_3$ (M = Al, Co, Fe, Gd) in standard Cd 2 = 5 mmol/L = 513.6 mg/L.

Strr. min.	No	$LaAlO_3$			$LaCoO_3$			$LaFeO_3$			$LaGdO_3$		
		C_e	Q_e	% Ads.	C_e	Q_e	% Ads.	C_e	Q_e	% Ads.	C_e	Q_e	% Ads.
15	1	285.30	114.15	44.45	332.60	90.50	35.24	336.70	88.45	34.44	439.94	36.83	14.34
	2	285.00	114.30	44.51	333.40	90.10	35.09	336.50	88.55	34.48	438.88	37.36	14.55
	3	284.70	114.45	44.57	333.00	90.30	35.16	336.10	88.75	34.56	437.94	37.83	14.73
	$\bar{X}$	285.00	114.30	44.51	333.00	90.30	35.16	336.43	88.58	34.49	438.12	37.67	14.54
	S.D	0.24	0.12	0.05	0.33	0.16	0.06	0.25	0.13	0.20	0.82	0.41	0.16
20	1	283.90	114.85	44.72	332.00	90.80	35.36	335.80	88.90	34.62	437.08	38.26	14.90
	2	282.40	115.60	45.02	332.40	90.60	35.28	336.20	88.70	34.54	435.80	38.90	15.15
	3	283.00	115.30	44.90	332.80	90.40	35.20	336.20	88.70	34.54	436.06	38.77	15.10
	$\bar{X}$	283.10	115.25	44.88	332.40	90.60	35.28	336.07	88.77	34.57	436.31	38.64	15.05
	S.D	0.62	0.31	0.12	0.33	0.16	0.07	0.19	0.09	0.04	0.55	0.28	0.11
30	1	280.80	116.40	45.33	331.50	91.05	35.46	335.00	89.30	34.77	435.06	39.27	15.29
	2	279.10	117.25	45.66	331.80	90.90	35.40	335.40	89.10	34.70	435.30	39.15	15.25
	3	279.60	117.00	45.56	332.00	90.80	35.36	335.80	88.90	34.62	432.42	40.59	15.81
	$\bar{X}$	279.83	116.88	45.52	331.77	90.92	35.41	335.40	89.10	34.70	432.26	39.67	15.45
	S.D	0.71	0.36	0.14	0.20	0.10	0.04	0.33	0.16	0.08	0.15	0.07	0.26

Appendix A

Table 2. Effect of contact time and metal ion initial concentration of $LaMO_3$ (M = Al, Co, Fe, Gd) in standard Cd 2 = 5 mmol/L = 513.6 mg/L.

Strr. min.	No	$LaAlO_3$			$LaCoO_3$			$LaFeO_3$			$LaGdO_3$		
		C_e	Q_e	% Ads.	C_e	Q_e	% Ads.	C_e	Q_e	% Ads.	C_e	Q_e	% Ads.
40	1	278.20	117.70	45.83	331.40	91.10	35.48	331.40	91.10	35.48	432.24	40.68	15.84
	2	278.90	117.35	45.70	331.00	91.30	35.55	331.00	91.30	35.55	432.12	40.74	15.86
	3	278.00	117.80	45.87	331.20	91.20	35.51	331.20	91.20	35.51	431.66	40.97	15.95
	$\overline{X}$	278.37	117.62	45.80	331.20	91.20	35.51	331.20	91.20	35.51	432.01	40.80	15.88
	S.D	0.39	0.19	0.07	0.16	0.08	0.03	0.16	0.08	0.03	0.25	0.13	0.05

Appendix A

Table 3. Effect of contact time and metal ion initial concentration of $LaMO_3$ (M = Al, Co, Fe, Gd) in standard Cd 3 = 9 mmol/L = 962.20 mg/L.

Strr. min.	No	$LaAlO_3$			$LaCoO_3$			$LaFeO_3$			$LaGdO_3$		
		C_e	Q_e	% Ads.	C_e	Q_e	% Ads.	C_e	Q_e	% Ads.	C_e	Q_e	% Ads.
1	1	332.40	314.90	65.45	509.20	226.50	47.80	545.20	208.50	43.34	771.40	95.40	19.83
	2	332.00	315.10	65.50	506.60	227.80	47.35	545.20	208.50	43.34	772.80	94.70	19.68
	3	332.10	315.05	65.49	506.80	227.70	47.33	545.20	208.50	43.34	773.80	94.20	19.58
	$\overline{X}$	332.27	315.02	65.48	507.53	227.33	47.49	545.20	208.50	43.34	772.80	94.77	19.70
	S.D	0.20	0.09	0.02	1.18	0.59	0.22	0.00	0.00	0.00	0.99	0.50	0.10
5	1	332.20	315.00	65.47	506.20	228.00	47.39	544.40	208.90	43.42	764.80	98.70	20.52
	2	331.50	315.35	65.55	506.20	228.00	47.39	543.60	209.30	43.50	765.20	98.50	20.47
	3	331.90	315.15	65.51	506.00	228.10	47.41	543.20	209.50	43.55	767.00	97.60	20.29
	$\overline{X}$	331.87	315.17	65.51	506.13	228.03	47.40	543.73	209.23	43.49	765.80	98.27	20.43
	S.D	0.29	0.14	0.03	0.09	0.05	0.01	0.50	0.25	0.05	0.97	0.48	0.10
10	1	331.70	315.25	65.53	506.00	228.10	47.41	543.20	209.50	43.55	764.00	99.10	20.60
	2	330.40	315.90	65.66	505.80	228.20	47.43	543.20	209.50	43.55	764.20	99.00	20.58
	3	331.10	315.55	65.59	504.80	228.70	47.54	542.80	210.20	43.69	766.00	98.10	20.39
	$\overline{X}$	331.07	315.57	65.59	505.53	228.33	47.46	543.07	209.73	43.60	764.80	98.73	20.52
	S.D	0.53	0.27	0.05	0.52	0.26	0.06	0.19	0.09	0.07	0.90	0.45	0.09

Appendix A

Table 3. Effect of contact time and metal ion initial concentration of $LaMO_3$ (M = Al, Co, Fe, Gd) in standard Cd 3 = 9 mmol/L = 962.20 mg/L.

Strr. min.	No	$LaAlO_3$			$LaCoO_3$			$LaFeO_3$			$LaGdO_3$		
		C_e	Q_e	% Ads.	C_e	Q_e	% Ads.	C_e	Q_e	% Ads.	C_e	Q_e	% Ads.
15	1	330.70	315.75	65.63	504.40	228.90	47.58	542.80	209.70	43.59	762.60	99.80	20.74
	2	330.00	316.10	65.70	503.00	229.60	47.72	541.80	210.20	43.38	761.60	100.30	20.85
	3	331.00	315.60	65.60	503.60	229.30	47.66	541.60	210.30	43.41	762.20	100.00	20.79
	$\overline{X}$	330.57	315.82	65.64	503.66	229.27	47.65	542.07	210.07	43.46	762.20	100.03	20.79
	S.D	0.42	0.21	0.04	0.57	0.29	0.06	0.52	0.26	0.09	0.42	0.21	0.05
20	1	326.40	317.90	66.08	500.80	230.70	47.95	540.60	210.80	43.82	762.40	99.90	20.76
	2	326.00	318.10	66.12	500.80	230.70	47.95	540.80	210.70	43.80	761.80	100.20	20.83
	3	325.90	318.15	66.13	503.00	229.60	47.72	540.20	211.00	43.86	762.00	100.10	20.81
	$\overline{X}$	326.10	318.05	66.11	501.53	230.33	47.87	540.53	210.83	43.83	762.00	100.10	20.80
	S.D	0.22	0.11	0.02	1.04	0.52	0.11	0.25	0.12	0.03	0.26	0.13	0.03
30	1	325.60	318.30	66.16	498.60	231.80	48.18	539.40	211.40	43.94	759.00	101.60	21.12
	2	324.90	318.65	66.23	486.00	238.10	49.49	539.60	211.30	43.92	759.20	101.50	21.10
	3	326.20	318.00	66.10	499.60	231.30	48.08	539.60	211.30	43.92	760.40	100.90	20.97
	$\overline{X}$	325.57	318.32	66.16	494.73	233.73	48.58	539.53	211.33	43.93	759.60	101.33	21.06
	S.D	0.53	0.27	0.05	6.19	3.09	0.64	0.09	0.05	0.01	0.62	0.31	0.07

Appendix A

Table 3. Effect of contact time and metal ion initial concentration of $LaMO_3$ (M = Al, Co, Fe, Gd) in standard Cd 3 = 9 mmol/L = 962.20 mg/L.

Strr. min.	No	$LaAlO_3$			$LaCoO_3$			$LaFeO_3$			$LaGdO_3$		
		C_e	Q_e	% Ads.	C_e	Q_e	% Ads.	C_e	Q_e	% Ads.	C_e	Q_e	% Ads.
40	1	320.30	320.95	66.71	485.60	238.30	49.53	537.20	212.50	44.17	758.20	102.00	21.20
	2	318.80	321.70	66.87	481.20	240.50	50.00	537.60	212.30	44.13	759.05	101.58	21.11
	3	320.10	321.05	66.73	485.60	238.30	49.53	537.90	212.15	44.10	760.10	101.05	21.00
	$\overline{X}$	319.73	321.23	66.77	484.13	239.03	49.69	537.57	212.32	44.13	759.12	101.54	21.10
	S.D	0.67	0.33	0.07	2.07	1.04	0.22	0.29	0.14	0.02	0.78	0.39	0.06

Appendix A

Table 4. Effect of contact time and metal ion initial concentration of $LaMO_3$ (M = Al, Co, Fe, Gd) in standard Cd 4 = 13 mmol/L = 1412.60 mg/L.

Strr. min.	No	$LaAlO_3$			$LaCoO_3$			$LaFeO_3$			$LaGdO_3$		
		C_e	Q_e	% Ads.	C_e	Q_e	% Ads.	C_e	Q_e	% Ads.	C_e	Q_e	% Ads.
1	1	436.90	487.85	69.07	538.40	437.10	61.84	539.80	436.40	61.79	1179.83	116.39	16.48
	2	436.00	488.30	69.13	537.20	437.70	61.97	540.40	436.10	61.74	1179.75	116.43	16.48
	3	436.20	488.20	69.12	539.20	436.70	61.89	540.40	436.10	61.74	1179.75	116.43	16.48
	$\overline{X}$	436.37	488.12	69.11	538.27	437.17	61.90	540.20	436.20	61.76	1179.78	116.42	16.48
	S.D	0.39	0.19	0.03	0.75	0.38	0.04	0.28	0.14	0.02	0.04	0.02	0.00
5	1	433.70	489.45	69.30	538.00	437.30	61.91	538.40	437.10	61.89	1179.81	116.40	16.48
	2	433.10	489.75	69.34	531.40	440.60	62.38	539.00	436.80	61.84	1179.74	116.43	16.48
	3	434.00	489.30	69.28	535.60	438.50	62.08	539.00	436.80	61.84	1179.74	116.43	16.48
	$\overline{X}$	433.60	489.50	69.31	535.00	438.80	62.12	538.80	436.90	61.86	1179.76	116.42	16.48
	S.D	0.29	0.19	0.03	0.90	0.45	0.06	0.28	0.14	0.02	0.03	0.02	0.00
10	1	431.70	490.45	69.44	532.80	439.90	62.28	538.20	437.20	61.90	1179.73	116.44	16.49
	2	431.20	490.70	69.47	530.20	441.20	62.47	539.00	436.80	61.84	1179.82	116.39	16.48
	3	431.90	490.35	69.43	534.00	439.30	62.20	538.00	436.95	61.86	1179.71	116.45	16.49
	$\overline{X}$	431.60	490.50	69.45	532.33	440.13	62.32	538.40	436.98	61.87	1179.75	116.43	16.49
	S.D	0.29	0.15	0.02	2.97	1.48	0.11	0.43	0.22	0.03	0.05	0.02	0.00

Appendix A

Table 4. Effect of contact time and metal ion initial concentration of $LaMO_3$ (M = Al, Co, Fe, Gd) in standard Cd 4 = 13 mmol/L = 1412.60 mg/L.

Strr. min.	No	$LaAlO_3$			$LaCoO_3$			$LaFeO_3$			$LaGdO_3$		
		C_e	Q_e	% Ads.	C_e	Q_e	% Ads.	C_e	Q_e	% Ads.	C_e	Q_e	% Ads.
15	1	431.30	490.65	69.47	531.30	440.65	62.39	529.00	441.80	62.55	1179.57	116.52	16.50
	2	430.80	490.90	69.50	530.80	440.90	62.42	529.60	441.50	62.51	1179.64	116.48	16.49
	3	431.00	490.80	69.49	531.00	440.80	62.41	530.60	441.00	62.44	1179.57	116.52	16.50
	$\bar{X}$	431.03	490.78	69.49	51.03	440.78	62.41	529.73	441.43	62.50	1179.59	116.51	16.50
	S.D	0.21	0.10	0.01	0.21	0.10	0.01	0.66	0.33	0.05	0.03	0.02	0.00
20	1	430.10	491.25	69.55	530.10	441.25	62.47	528.80	442.05	62.59	1179.47	116.57	16.50
	2	428.70	491.95	69.65	528.70	441.95	62.57	529.00	441.80	62.55	1179.39	116.61	16.51
	3	429.90	491.35	69.57	529.90	441.35	62.49	530.60	441.00	62.44	1179.47	116.57	16.50
	$\bar{X}$	429.57	491.52	69.59	529.57	441.52	62.51	529.47	441.62	62.53	1179.44	116.58	16.50
	S.D	0.62	0.31	0.04	0.62	0.31	0.04	0.81	0.40	0.06	0.04	0.02	0.00
30	1	430.10	491.25	69.55	530.10	441.25	62.47	528.60	442.25	62.62	1179.40	116.60	16.51
	2	428.00	492.30	69.70	528.00	442.30	62.62	528.60	442.25	62.62	1179.37	116.62	16.51
	3	429.80	491.40	69.57	529.80	441.40	62.49	529.00	441.80	62.55	1179.39	116.61	16.51
	$\bar{X}$	429.30	491.65	69.61	529.30	441.65	62.53	528.73	442.10	62.60	1179.39	116.61	16.51
	S.D	0.93	0.46	0.07	0.93	0.46	0.07	0.19	0.09	0.03	0.01	0.00	0.00

Appendix A

Table 4. Effect of contact time and metal ion initial concentration of $LaMO_3$ (M = Al, Co, Fe, Gd) in standard Cd 4 = 13 mmol/L = 1412.60 mg/L.

Strr. min.	No	$LaAlO_3$			$LaCoO_3$			$LaFeO_3$			$LaGdO_3$		
		C_e	Q_e	% Ads.	C_e	Q_e	% Ads.	C_e	Q_e	% Ads.	C_e	Q_e	% Ads.
40	1	428.40	492.10	69.67	523.40	444.90	63.00	524.40	444.10	62.87	1178.27	117.17	16.59
	2	428.20	492.20	69.69	521.40	445.60	63.09	526.60	443.15	62.74	1178.22	117.19	16.59
	3	429.00	491.80	69.63	523.60	444.50	62.93	525.80	443.75	62.83	1178.28	117.17	16.59
	$\overline{X}$	428.53	492.03	69.66	522.80	445.00	63.01	525.60	443.67	62.81	1178.26	117.18	16.59
	S.D	0.34	0.17	0.03	0.99	0.45	0.07	0.91	0.45	0.05	0.03	0.01	0.00

Appendix A

Table 5. Effect of contact time and metal ion initial concentration of $LaMO_3$ (M = Al, Co, Fe, Gd) in standard Cd 5 = 17 mmol/L = 1845.00 mg/L.

Strr. min.	No	$LaAlO_3$			$LaCoO_3$			$LaFeO_3$			$LaGdO_3$		
		C_e	Q_e	% Ads.	C_e	Q_e	% Ads.	C_e	Q_e	% Ads.	C_e	Q_e	% Ads.
1	1	599.60	622.70	67.50	724.80	560.10	60.72	773.20	535.90	58.09	1526.40	159.30	17.27
	2	602.80	621.10	67.33	724.10	560.45	60.75	771.20	536.90	58.20	1526.80	159.10	17.25
	3	600.60	622.20	67.45	723.90	560.55	60.76	774.60	535.20	58.05	1525.80	159.60	17.30
	$\overline{X}$	601.00	622.00	67.43	724.27	560.37	60.74	773.00	536.00	58.10	1526.33	159.23	17.27
	S.D	0.69	0.35	0.07	0.39	0.19	0.02	1.40	0.70	0.06	0.41	0.21	0.02
5	1	599.00	623.00	67.53	721.90	561.55	60.87	769.40	537.80	58.29	1526.20	159.40	17.28
	2	600.60	622.20	67.45	720.70	562.15	60.94	767.40	538.80	58.41	1526.20	159.40	17.28
	3	599.60	622.70	67.50	721.00	562.00	60.92	769.40	537.80	58.29	1525.30	159.85	17.33
	$\overline{X}$	599.73	622.63	67.49	721.20	561.90	60.91	768.73	538.13	58.33	1525.90	159.55	17.30
	S.D	0.66	0.33	0.03	0.51	0.25	0.03	0.94	0.47	0.06	0.42	0.21	0.02
10	1	598.20	623.40	67.58	716.30	564.35	61.18	768.60	538.20	58.34	1522.40	161.30	17.49
	2	599.80	622.60	67.49	715.80	564.60	61.20	761.80	541.60	58.71	1520.60	162.20	17.58
	3	598.40	623.30	67.57	716.20	564.40	61.18	768.80	538.10	58.33	1517.00	164.00	17.78
	$\overline{X}$	598.80	623.10	67.55	716.10	564.45	61.19	766.40	539.30	58.46	1520.00	162.50	17.62
	S.D	0.71	0.36	0.04	0.22	0.11	0.01	3.25	1.63	0.18	2.24	1.12	0.12

Appendix A

Table 5. Effect of contact time and metal ion initial concentration of $LaMO_3$ (M = Al, Co, Fe, Gd) in standard Cd 5 = 17 mmol/L = 1845.00 mg/L.

Strr. min.	No	$LaAlO_3$			$LaCoO_3$			$LaFeO_3$			$LaGdO_3$		
		C_e	Q_e	% Ads.	C_e	Q_e	% Ads.	C_e	Q_e	% Ads.	C_e	Q_e	% Ads.
15	1	597.40	623.80	67.62	701.90	571.55	61.96	760.80	542.10	58.76	1519.00	163.00	17.67
	2	598.60	623.20	67.52	701.40	571.80	61.98	761.40	541.80	58.73	1518.00	163.50	17.72
	3	598.00	623.50	67.59	701.60	571.70	61.97	768.40	538.30	58.35	1518.40	163.30	17.70
	$\overline{X}$	598.00	623.50	67.58	701.63	571.68	61.97	763.53	540.73	58.61	1518.40	163.30	17.70
	S.D	0.49	0.24	0.04	0.21	0.10	0.00	3.45	1.72	0.19	0.42	0.21	0.02
20	1	594.00	625.50	67.80	676.90	584.05	63.31	760.60	542.20	69.92	1515.60	164.70	17.85
	2	598.60	623.20	67.52	677.00	584.00	63.31	760.20	542.40	69.64	1516.00	164.50	17.83
	3	595.00	625.00	67.75	676.30	584.35	63.34	761.00	542.00	69.59	1516.20	164.40	17.82
	$\overline{X}$	595.87	624.57	67.69	676.73	584.13	63.32	760.60	542.20	69.62	1516.00	164.53	17.83
	S.D	1.98	0.99	0.37	0.31	0.15	0.01	0.33	0.16	0.17	0.26	0.13	0.01
30	1	592.80	626.10	67.87	665.20	589.90	63.95	760.60	542.20	69.62	1514.80	165.10	17.90
	2	598.00	623.50	67.59	664.70	590.15	63.97	760.20	542.40	69.64	1514.20	165.40	17.93
	3	590.60	627.20	67.99	665.00	590.00	63.96	760.40	542.30	69.63	1514.60	165.20	17.91
	$\overline{X}$	593.80	625.60	67.82	664.97	590.02	63.96	760.40	542.30	69.63	1514.53	165.23	17.91
	S.D	3.10	2.23	0.17	0.21	0.10	0.01	0.16	0.08	0.00	0.22	0.11	0.01

Appendix A

Table 5. Effect of contact time and metal ion initial concentration of $LaMO_3$ (M = Al, Co, Fe, Gd) in standard Cd 5 = 17 mmol/L = 1845.00 mg/L.

Strr. min.	No	$LaAlO_3$			$LaCoO_3$			$LaFeO_3$			$LaGdO_3$		
		C_e	Q_e	% Ads.	C_e	Q_e	% Ads.	C_e	Q_e	% Ads.	C_e	Q_e	% Ads.
40	1	590.80	627.10	67.98	615.80	614.60	66.62	753.40	545.80	70.00	1512.40	166.30	18.03
	2	591.00	627.00	67.97	616.10	614.45	66.61	753.40	545.80	70.00	1511.80	166.60	18.06
	3	590.60	627.20	67.99	616.30	614.35	66.60	752.80	546.10	70.04	1512.60	166.20	18.02
	$\overline{X}$	590.80	627.10	67.98	616.07	614.47	66.61	753.20	545.90	70.01	1512.27	166.37	18.04
	S.D	0.16	0.08	0.01	0.21	0.10	0.00	0.28	0.14	0.02	0.34	0.17	0.02

Appendix A

Table 6. Effect of contact time and metal ion initial concentration of $LaMO_3$ (M = Al, Co, Fe, Gd) in standard Cd 6 = 21 mmol/L = 2189.00 mg/L.

Strr. min.	No	$LaAlO_3$			$LaCoO_3$			$LaFeO_3$			$LaGdO_3$		
		C_e	Q_e	% Ads.	C_e	Q_e	% Ads.	C_e	Q_e	% Ads.	C_e	Q_e	% Ads.
1	1	242.00	973.50	88.94	622.80	783.10	71.55	628.60	780.20	71.28	1820.40	184.30	16.84
	2	240.89	974.06	89.00	623.20	782.90	71.53	631.00	779.00	71.17	1819.20	184.90	16.89
	3	241.10	973.95	88.99	623.20	782.90	71.53	631.00	779.00	71.17	1819.40	184.80	16.88
	$\bar{X}$	241.33	973.84	88.98	623.07	782.97	71.54	630.20	779.40	71.21	1819.60	184.67	16.87
	S.D	0.48	0.24	0.03	0.19	0.09	0.01	1.13	0.57	0.05	0.53	0.26	0.02
5	1	235.30	976.85	89.25	623.40	782.80	71.52	625.20	781.90	71.44	1815.00	187.00	17.09
	2	233.17	977.92	89.35	622.40	783.30	71.57	624.00	782.50	71.49	1814.20	187.40	17.12
	3	232.48	978.26	89.38	622.40	783.30	71.57	624.80	782.10	71.46	1816.20	186.40	17.03
	$\bar{X}$	233.65	977.68	89.33	622.20	783.13	71.55	624.67	782.17	71.46	1815.20	186.93	17.08
	S.D	1.20	0.60	0.06	0.28	0.14	0.02	0.50	0.25	0.02	0.82	0.41	0.04
10	1	233.80	977.60	89.32	621.50	783.75	71.61	625.20	781.90	71.44	1813.80	187.60	17.14
	2	233.00	978.00	89.36	621.80	783.60	71.59	624.00	782.50	71.49	1813.00	188.00	17.18
	3	232.10	978.45	89.40	621.00	784.00	71.63	623.80	782.60	71.50	1813.60	187.70	17.15
	$\bar{X}$	232.97	978.02	89.36	622.07	783.78	71.61	624.33	782.33	71.48	1813.40	187.77	17.16
	S.D	0.69	0.35	0.03	1.00	0.17	0.02	0.62	0.31	0.03	0.35	0.17	0.02

Appendix A

Table 6. Effect of contact time and metal ion initial concentration of $LaMO_3$ (M = Al, Co, Fe, Gd) in standard Cd 6 = 21 mmol/L = 2189.00 mg/L.

Strr. min.	No	$LaAlO_3$			$LaCoO_3$			$LaFeO_3$			$LaGdO_3$		
		C_e	Q_e	% Ads.	C_e	Q_e	% Ads.	C_e	Q_e	% Ads.	C_e	Q_e	% Ads.
15	1	230.50	979.29	89.47	621.40	783.80	71.61	624.80	782.10	71.46	1801.80	193.60	17.69
	2	230.43	979.29	89.47	619.00	785.00	71.72	623.20	782.90	71.53	1801.80	193.60	17.69
	3	231.64	979.68	89.42	615.20	786.90	71.90	623.60	782.70	71.51	1804.00	192.50	17.59
	$\bar{X}$	230.86	979.09	89.45	618.53	785.23	71.74	623.87	782.57	71.50	1802.40	193.23	17.66
	S.D	0.55	0.29	0.02	2.55	1.28	0.12	0.68	0.34	0.03	1.05	0.52	0.05
20	1	227.60	980.70	89.60	611.20	788.90	72.08	622.60	783.40	71.56	1800.40	194.30	17.75
	2	226.02	981.49	89.67	612.80	788.10	72.01	623.00	783.00	71.54	1799.20	194.90	17.81
	3	224.94	982.03	89.72	612.40	788.30	72.02	623.40	782.80	71.52	1800.60	194.20	17.74
	$\bar{X}$	226.19	981.41	89.66	612.13	788.43	72.04	623.00	783.07	71.54	1800.00	194.47	17.77
	S.D	1.09	0.55	0.05	0.68	0.34	0.03	0.33	0.25	0.02	0.62	0.31	0.03
30	1	221.40	983.80	89.89	611.20	788.90	72.08	621.60	783.70	71.60	1800.20	194.40	17.76
	2	218.60	985.20	90.01	610.60	789.20	72.11	622.60	783.20	71.56	1800.00	194.50	17.77
	3	220.10	984.45	89.95	600.00	794.50	72.59	621.20	783.90	71.62	1799.40	194.80	17.80
	$\bar{X}$	220.03	984.48	89.95	607.27	790.87	72.26	621.80	783.60	71.59	1799.80	194.57	17.78
	S.D	1.14	0.57	0.05	5.14	2.57	0.23	0.59	0.29	0.03	0.35	0.17	0.02

Appendix A

Table 6. Effect of contact time and metal ion initial concentration of $LaMO_3$ (M = Al, Co, Fe, Gd) in standard Cd 6 = 21 mmol/L = 2189.00 mg/L.

Strr. min.	No	$LaAlO_3$			$LaCoO_3$			$LaFeO_3$			$LaGdO_3$		
		C_e	Q_e	% Ads.	C_e	Q_e	% Ads.	C_e	Q_e	% Ads.	C_e	Q_e	% Ads.
40	1	219.33	984.84	89.98	603.80	792.60	72.42	614.00	787.50	71.95	1800.05	194.48	17.77
	2	218.20	985.40	90.03	604.80	792.10	72.37	616.60	786.20	71.83	1796.80	196.10	17.92
	3	219.96	984.52	89.95	604.00	792.50	72.41	614.00	787.50	71.95	1798.02	195.49	17.86
	$\overline{x}$	219.16	984.92	89.99	604.20	792.40	72.40	614.87	787.07	71.91	1798.29	195.36	17.85
	S.D	0.73	0.36	0.03	0.43	0.22	0.02	1.23	0.61	0.06	1.34	0.67	0.06

Appendix A

Table 7. Effect of contact time and metal ion initial concentration of $LaMO_3$ (M = Al, Co, Fe, Gd) in standard Cd 7 = 25 mmol/L = 2629.40 mg/L.

Strr. min.	No	$LaAlO_3$			$LaCoO_3$			$LaFeO_3$			$LaGdO_3$		
		C_e	Q_e	% Ads.	C_e	Q_e	% Ads.	C_e	Q_e	% Ads.	C_e	Q_e	% Ads.
1	1	291.90	1168.75	88.90	724.80	952.30	72.43	720.20	954.60	72.61	2080.71	274.35	20.87
	2	290.00	1169.70	88.97	726.40	951.50	72.37	718.60	955.40	72.67	2080.70	274.35	20.87
	3	291.20	1169.10	88.93	725.40	952.00	72.41	719.00	955.20	72.66	2080.71	274.35	20.87
	$\overline{X}$	291.03	1169.18	88.93	725.53	951.93	72.40	719.20	955.07	72.65	2080.71	274.35	20.87
	S.D	0.78	0.39	0.03	0.66	0.33	0.03	0.68	0.34	0.03	0.00	0.00	0.00
5	1	289.40	1170.00	88.99	675.60	976.90	74.31	709.80	959.80	73.00	2080.57	274.42	20.87
	2	289.12	1170.14	89.00	667.20	981.10	74.63	702.20	963.60	73.29	2080.51	274.45	20.88
	3	290.67	1169.37	88.95	677.60	975.90	74.23	705.20	962.10	73.18	2080.62	274.39	20.87
	$\overline{X}$	289.73	1169.84	88.98	673.47	977.97	74.39	705.73	961.83	73.16	2080.57	274.42	20.87
	S.D	0.67	0.33	0.02	4.51	2.25	0.17	3.13	1.56	0.12	0.05	0.02	0.00
10	1	288.90	1170.25	89.01	666.40	981.50	74.66	702.20	963.60	73.29	2080.43	274.49	20.88
	2	288.04	1170.68	89.05	665.80	981.80	74.68	702.40	963.50	73.29	2080.22	274.59	20.89
	3	287.49	1170.96	89.07	666.00	981.70	74.67	703.60	962.90	73.24	2080.33	274.54	20.88
	$\overline{X}$	288.14	1170.63	89.04	666.07	981.67	74.67	702.73	963.33	73.27	2080.33	274.54	20.88
	S.D	0.58	0.29	0.03	0.25	0.12	0.00	0.62	0.31	0.02	0.09	0.04	0.00

Appendix A

Table 7. Effect of contact time and metal ion initial concentration of $LaMO_3$ (M = Al, Co, Fe, Gd) in standard Cd 7 = 25 mmol/L = 2629.40 mg/L.

Strr. min.	No	$LaAlO_3$			$LaCoO_3$			$LaFeO_3$			$LaGdO_3$		
		C_e	Q_e	% Ads.	C_e	Q_e	% Ads.	C_e	Q_e	% Ads.	C_e	Q_e	% Ads.
15	1	286.70	1171.35	89.10	666.00	981.70	74.67	698.80	965.30	73.42	2080.35	274.53	20.88
	2	285.50	1171.95	89.14	664.00	982.70	74.75	700.00	964.70	73.38	2080.19	274.61	20.89
	3	285.38	1172.01	89.15	665.80	981.80	74.68	703.60	962.90	73.24	2080.29	274.56	20.88
	$\bar{X}$	285.38	1171.77	89.13	665.27	982.07	74.70	700.80	964.30	73.35	2080.28	274.57	20.88
	S.D	0.60	0.30	0.02	0.90	0.45	0.04	700.00	1.02	0.08	0.07	0.03	0.00
20	1	281.80	1173.80	89.28	663.00	983.20	74.79	696.00	966.70	73.53	2079.33	274.74	20.90
	2	281.00	1174.20	89.31	647.00	991.20	75.39	700.80	964.30	73.35	2079.97	274.72	20.90
	3	280.33	1174.54	89.34	664.80	982.30	74.72	703.20	963.10	73.26	2080.01	274.70	20.89
	$\bar{X}$	281.04	1174.18	89.31	658.27	985.57	74.97	700.00	964.70	73.38	2079.97	274.72	20.90
	S.D	0.60	0.30	0.02	8.00	4.00	0.30	2.99	1.50	0.10	0.03	0.02	0.00
30	1	279.60	1174.90	89.37	644.00	992.70	75.51	695.20	967.10	73.56	2079.92	274.74	20.90
	2	277.40	1176.00	89.45	647.00	991.20	75.39	693.80	967.80	73.61	2079.85	274.78	20.90
	3	278.01	1175.70	89.43	645.20	992.10	75.46	695.20	967.10	73.56	2079.95	274.73	20.90
	$\bar{X}$	278.34	1175.53	89.42	645.40	992.00	75.45	694.73	967.33	73.58	2079.91	274.75	20.90
	S.D	0.93	0.46	0.03	1.23	0.62	0.05	0.66	0.33	0.02	0.04	0.02	0.00

Appendix A

Table 7. Effect of contact time and metal ion initial concentration of $LaMO_3$ (M = Al, Co, Fe, Gd) in standard Cd 7 = 25 mmol/L = 2629.40 mg/L.

Strr. min.	No	$LaAlO_3$			$LaCoO_3$			$LaFeO_3$			$LaGdO_3$		
		C_e	Q_e	% Ads.	C_e	Q_e	% Ads.	C_e	Q_e	% Ads.	C_e	Q_e	% Ads.
40	1	275.40	1177.00	89.53	643.91	992.75	75.51	691.50	969.00	73.70	2079.88	274.76	20.90
	2	272.94	1178.23	89.62	643.04	993.18	75.54	690.10	969.65	73.75	2079.81	274.80	20.90
	3	274.70	1177.35	89.55	643.58	992.91	75.52	690.00	969.70	73.76	2079.79	274.81	20.90
	$\overline{X}$	274.35	1177.53	89.57	643.84	992.95	75.52	690.53	969.45	73.74	2079.83	274.79	20.90
	S.D	1.03	0.52	0.04	0.19	0.10	0.01	0.68	0.32	0.03	0.04	0.02	0.00

Appendix A

Table 8. Effect of contact time and metal ion initial concentration of $LaMO_3$ (M = Al, Co, Fe, Gd) in standard Pb 1 = 1 mmol/L = 186.6 mg/L.

Strr. min.	No	$LaAlO_3$			$LaCoO_3$			$LaFeO_3$			$LaGdO_3$		
		C_e	Q_e	% Ads.	C_e	Q_e	% Ads.	C_e	Q_e	% Ads.	C_e	Q_e	% Ads.
1	1	25.93	80.34	86.10	103.10	41.75	44.74	117.32	34.64	37.13	157.50	14.55	15.59
	2	25.80	80.40	86.17	102.90	41.85	44.85	119.06	33.77	36.20	157.68	14.46	15.50
	3	25.90	80.35	86.12	103.00	41.80	44.80	118.82	33.78	36.32	157.58	14.51	15.55
	$\bar{X}$	25.88	80.36	86.13	103.00	41.80	44.80	118.40	34.00	36.55	157.59	14.51	15.55
	S.D	0.06	0.03	0.03	0.08	0.04	0.05	0.77	0.39	0.41	0.07	0.04	0.04
5	1	25.81	80.40	86.17	102.60	42.00	45.01	113.62	36.49	39.11	157.41	14.60	15.64
	2	25.62	80.49	86.27	102.20	42.20	45.23	115.12	36.41	38.31	157.63	14.49	15.53
	3	25.61	80.50	86.28	102.40	42.10	45.11	114.40	36.45	38.69	157.48	14.56	15.61
	$\bar{X}$	25.68	80.46	86.24	102.40	42.10	45.11	114.40	36.45	38.69	157.51	14.55	15.59
	S.D	0.09	0.05	0.05	0.16	0.08	0.09	0.61	0.31	0.33	0.09	0.05	0.05
10	1	22.03	82.91	88.19	102.40	42.10	45.11	106.80	39.90	42.77	157.21	14.70	15.75
	2	22.08	82.26	88.17	102.10	42.25	45.28	107.14	39.88	42.58	157.28	14.66	15.71
	3	21.96	82.61	88.23	102.10	42.25	45.28	106.66	39.91	42.84	156.91	14.85	15.91
	$\bar{X}$	21.06	82.29	88.20	102.20	42.20	45.23	106.90	39.90	42.71	157.13	14.74	15.79
	S.D	0.24	0.02	0.03	0.14	0.07	0.08	0.20	0.10	0.11	0.16	0.08	0.09

Appendix A

Table 8. Effect of contact time and metal ion initial concentration of $LaMO_3$ (M = Al, Co, Fe, Gd) in standard Pb 1 = 1 mmol/L = 186.6 mg/L.

Strr. min.	No	$LaAlO_3$			$LaCoO_3$			$LaFeO_3$			$LaGdO_3$		
		C_e	Q_e	% Ads.	C_e	Q_e	% Ads.	C_e	Q_e	% Ads.	C_e	Q_e	% Ads.
15	1	20.79	82.91	88.86	102.10	42.25	45.28	105.80	40.40	43.30	157.00	14.80	15.86
	2	21.02	82.79	88.74	102.00	42.30	45.33	106.01	40.39	43.19	156.93	14.84	15.90
	3	21.38	82.61	88.54	102.05	42.28	45.31	105.93	40.39	43.23	156.80	14.90	15.97
	$\bar{X}$	21.06	82.77	88.71	102.05	42.28	45.31	105.90	40.39	43.25	156.91	14.85	15.91
	S.D	0.24	0.12	0.13	0.04	0.02	0.02	0.09	0.05	0.05	0.08	0.04	0.05
20	1	20.28	83.16	89.13	102.00	42.30	45.33	102.98	41.81	44.81	156.60	15.00	16.08
	2	20.72	82.94	88.90	102.00	42.30	45.33	102.74	41.82	44.94	156.69	14.96	16.03
	3	21.08	82.76	88.70	101.90	42.35	45.39	103.10	41.81	44.75	156.62	14.99	16.07
	$\bar{X}$	20.69	82.95	88.91	101.97	42.32	45.35	102.90	41.81	44.86	156.64	14.98	16.06
	S.D	0.33	0.16	0.18	0.05	0.02	0.03	0.15	0.08	0.08	0.04	0.02	0.02
30	1	19.64	83.48	89.47	101.80	42.40	45.44	102.00	42.30	45.34	156.03	15.29	16.38
	2	19.82	83.39	89.38	101.70	42.45	45.49	102.52	42.27	45.06	155.87	15.37	16.47
	3	19.83	83.39	89.38	101.95	42.33	45.36	102.22	42.29	45.22	156.05	15.28	16.37
	$\bar{X}$	19.76	83.42	89.41	101.82	42.39	45.43	102.20	42.29	45.23	155.98	15.31	16.41
	S.D	0.09	0.04	0.04	0.10	0.05	0.05	0.22	0.11	0.12	0.08	0.04	0.05

Appendix A

Table 8. Effect of contact time and metal ion initial concentration of $LaMO_3$ (M = Al, Co, Fe, Gd) in standard Pb 1 = 1 mmol/L = 186.6 mg/L.

Strr. min.	No	$LaAlO_3$			$LaCoO_3$			$LaFeO_3$			$LaGdO_3$		
		C_e	Q_e	% Ads.	C_e	Q_e	% Ads.	C_e	Q_e	% Ads.	C_e	Q_e	% Ads.
40	1	19.14	83.73	89.74	101.60	42.50	45.55	101.06	42.77	45.84	155.49	15.56	16.67
	2	19.19	83.71	89.72	101.90	42.35	45.39	101.42	42.75	45.82	155.60	15.50	16.61
	3	19.33	83.64	89.64	101.50	42.55	45.60	100.40	42.80	45.87	155.43	15.59	16.70
	$\overline{X}$	19.22	83.69	89.70	101.67	42.47	45.51	101.00	42.77	45.84	155.51	15.55	16.66
	S.D	0.08	0.04	0.04	0.17	0.09	0.09	0.42	0.21	0.02	0.07	0.04	0.04

Appendix A

Table 9. Effect of contact time and metal ion initial concentration of $LaMO_3$ (M = Al, Co, Fe, Gd) in standard Pb 2 = 5 mmol/L = 967.7 mg/L.

Strr. min.	No	$LaAlO_3$			$LaCoO_3$			$LaFeO_3$			$LaGdO_3$		
		C_e	Q_e	% Ads.	C_e	Q_e	% Ads.	C_e	Q_e	% Ads.	C_e	Q_e	% Ads.
1	1	8.733	479.48	99.10	359.60	304.05	62.84	370.62	298.54	61.77	782.45	92.63	19.14
	2	8.217	479.74	99.15	357.60	305.05	63.05	368.80	299.45	61.79	782.58	92.56	19.13
	3	8.160	479.77	99.15	358.20	304.75	62.98	370.92	298.39	61.77	782.53	92.59	19.14
	$\bar{X}$	8.370	479.66	99.13	358.50	304.60	62.95	370.10	298.79	61.78	782.52	92.59	19.14
	S.D	0.26	0.13	0.02	0.83	0.42	0.09	0.94	0.47	0.01	0.05	0.03	0.00
5	1	8.423	479.64	99.13	356.60	305.55	63.15	367.22	300.24	62.05	782.19	92.76	19.17
	2	7.920	479.89	99.18	353.20	307.25	63.50	367.00	300.35	62.05	782.44	92.63	19.14
	3	8.104	479.80	99.16	354.40	306.65	63.38	368.78	299.46	62.04	782.45	92.63	19.14
	$\bar{X}$	8.149	479.78	99.16	354.73	306.49	63.34	367.70	300.02	62.05	782.36	92.67	19.15
	S.D	0.21	0.10	0.02	1.41	0.71	0.15	0.79	0.40	0.00	0.12	0.06	0.01
10	1	4.650	481.53	99.52	355.40	306.15	63.27	312.76	327.47	67.68	782.01	92.85	19.19
	2	4.412	481.64	99.54	352.20	307.75	63.60	314.34	326.68	67.67	782.20	92.75	19.17
	3	4.600	481.55	99.52	352.60	307.55	63.56	314.70	326.50	67.66	782.23	92.74	19.17
	$\bar{X}$	4.554	481.57	99.53	353.40	307.15	63.48	313.90	326.90	67.67	782.15	92.78	19.18
	S.D	0.10	0.05	0.01	1.42	0.71	0.15	0.84	0.42	0.01	0.10	0.05	0.01

Appendix A

Table 9. Effect of contact time and metal ion initial concentration of $LaMO_3$ (M = Al, Co, Fe, Gd) in standard Pb 2 = 5 mmol/L = 967.7 mg/L.

Strr. min.	No	$LaAlO_3$			$LaCoO_3$			$LaFeO_3$			$LaGdO_3$		
		C_e	Q_e	% Ads.	C_e	Q_e	% Ads.	C_e	Q_e	% Ads.	C_e	Q_e	% Ads.
15	1	2.938	482.38	99.70	328.22	319.74	66.08	298.60	334.55	69.14	781.49	93.11	19.24
	2	2.961	482.37	99.69	328.20	319.75	66.08	291.60	338.05	69.15	781.35	93.18	19.26
	3	3.001	482.35	99.69	328.34	319.68	66.07	295.60	336.05	69.14	781.68	93.01	19.22
	$\overline{X}$	2.967	482.37	99.69	328.25	319.73	66.08	295.27	336.22	69.14	781.51	93.32	19.24
	S.D	0.03	0.01	0.00	0.06	0.03	0.00	2.87	1.43	0.00	0.14	0.07	0.02
20	1	2.310	482.70	99.76	311.50	328.10	67.81	293.14	337.28	69.71	780.38	93.66	19.36
	2	2.037	482.83	99.79	311.69	328.01	67.79	294.56	336.57	69.69	780.40	93.65	19.36
	3	2.094	482.80	99.79	311.57	328.07	67.80	294.42	336.64	69.69	780.27	93.72	19.37
	$\overline{X}$	2.147	482.78	99.79	311.59	328.06	67.80	294.02	336.84	69.69	780.35	93.68	19.36
	S.D	0.12	0.06	0.10	0.08	0.04	0.00	0.64	0.32	0.00	0.06	0.03	0.00
30	1	1.425	483.14	99.85	301.21	333.25	68.87	292.52	337.59	69.77	779.64	94.03	19.43
	2	1.440	483.13	99.85	301.44	333.13	68.85	294.40	336.65	69.75	779.83	93.94	19.41
	3	1.447	483.13	99.85	301.47	333.12	68.85	292.74	337.48	69.77	779.95	93.88	19.40
	$\overline{X}$	1.437	483.13	99.85	301.37	333.17	68.86	293.22	337.24	69.77	779.81	93.95	19.41
	S.D	0.00	0.00	0.00	0.12	0.06	0.01	0.84	0.42	0.00	0.13	0.06	0.01

Appendix A

Table 9. Effect of contact time and metal ion initial concentration of $LaMO_3$ (M = Al, Co, Fe, Gd) in standard Pb 2 = 5 mmol/L = 967.7 mg/L.

Strr. min.	No	$LaAlO_3$			$LaCoO_3$			$LaFeO_3$			$LaGdO_3$		
		C_e	Q_e	% Ads.	C_e	Q_e	% Ads.	C_e	Q_e	% Ads.	C_e	Q_e	% Ads.
40	1	1.325	483.19	99.86	295.64	336.03	69.45	292.11	337.80	69.81	778.90	94.40	19.51
	2	1.221	483.24	99.87	295.49	336.11	69.46	291.52	338.09	69.80	778.75	94.48	19.53
	3	1.380	483.16	99.86	295.53	336.09	69.46	292.28	337.71	69.80	779.04	94.33	19.50
	$\overline{X}$	1.309	483.20	99.86	295.55	336.08	69.46	291.97	337.87	69.80	778.90	94.40	19.51
	S.D	0.07	0.03	0.00	0.06	0.03	0.00	0.27	0.14	0.00	0.12	0.06	0.01

Appendix A

Table 10. Effect of contact time and metal ion initial concentration of $LaMO_3$ (M = Al, Co, Fe, Gd) in standard Pb 3 = 9 mmol/L = 1695.3 mg/L.

Strr. min.	No	$LaAlO_3$			$LaCoO_3$			$LaFeO_3$			$LaGdO_3$		
		C_e	Q_e	% Ads.	C_e	Q_e	% Ads.	C_e	Q_e	% Ads.	C_e	Q_e	% Ads.
1	1	328.40	683.45	80.63	860.40	417.45	49.25	872.10	411.60	48.56	1384.72	155.29	18.32
	2	328.00	683.65	80.66	860.80	417.25	49.23	871.78	411.76	48.58	1384.65	155.23	18.32
	3	327.90	683.70	80.66	859.90	417.70	49.28	871.76	411.77	48.58	1384.96	155.17	18.31
	$\bar{X}$	328.10	683.60	80.65	860.37	417.70	49.25	871.88	411.71	48.57	1384.78	155.26	18.32
	S.D	0.22	0.11	0.01	0.37	0.18	0.02	1.56	0.78	0.01	0.13	0.07	0.00
5	1	291.00	702.15	82.84	843.60	425.85	50.24	870.32	412.49	48.66	1384.66	155.32	18.32
	2	290.60	702.35	82.86	838.00	428.65	50.57	870.44	412.43	48.66	1384.52	155.39	18.33
	3	290.90	702.20	82.85	845.20	425.05	50.14	870.76	412.27	48.64	1384.95	155.18	18.31
	$\bar{X}$	290.83	702.23	82.85	842.27	426.52	50.32	870.51	412.40	48.65	1384.71	155.54	18.32
	S.D	0.17	0.09	0.00	3.09	1.54	0.18	1.86	0.93	0.01	0.18	0.09	0.00
10	1	288.10	703.60	83.01	819.00	438.15	51.69	869.16	413.07	48.73	1383.85	155.73	18.37
	2	288.30	703.50	83.00	813.20	441.05	52.03	869.50	412.90	48.71	1384.07	155.62	18.36
	3	288.00	703.65	83.02	819.40	437.95	51.67	869.12	413.09	48.73	1383.96	155.67	18.36
	$\bar{X}$	288.13	703.58	83.01	817.20	439.05	51.80	869.27	413.02	48.72	1383.96	155.67	18.36
	S.D	0.12	0.06	0.01	2.83	1.42	0.17	1.70	0.85	0.01	0.09	0.04	0.00

Appendix A

Table 10. Effect of contact time and metal ion initial concentration of $LaMO_3$ (M = Al, Co, Fe, Gd) in standard Pb 3 = 9 mmol/L = 1695.3 mg/L.

Strr. min.	No	$LaAlO_3$			$LaCoO_3$			$LaFeO_3$			$LaGdO_3$		
		C_e	Q_e	% Ads.	C_e	Q_e	% Ads.	C_e	Q_e	% Ads.	C_e	Q_e	% Ads.
15	1	279.00	708.15	83.55	811.60	441.85	52.13	868.68	413.31	48.76	1381.75	156.78	18.50
	2	278.80	708.25	83.56	810.40	442.45	52.20	868.60	413.35	48.76	1381.74	156.78	18.50
	3	279.10	708.10	83.54	808.60	443.35	52.30	868.68	413.31	48.76	1381.67	156.82	18.50
	$\bar{X}$	278.97	708.17	83.55	810.20	442.55	52.21	868.65	413.32	48.76	1381.72	156.79	18.50
	S.D	0.12	0.06	0.00	1.23	0.62	0.07	0.04	0.02	0.00	0.04	0.02	0.00
20	1	258.00	718.65	84.79	787.20	454.04	53.57	867.02	414.14	48.86	1380.89	157.21	18.55
	2	257.60	718.85	84.81	785.40	454.95	53.67	867.42	413.94	48.83	1380.61	157.35	18.56
	3	257.80	718.75	84.80	783.60	455.85	53.78	867.96	413.67	48.80	1380.92	157.19	18.54
	$\bar{X}$	257.80	718.75	84.80	785.40	454.95	53.67	867.47	413.92	48.83	1380.81	157.25	18.55
	S.D	0.16	0.08	0.00	1.47	0.73	0.09	3.85	1.93	0.02	0.14	0.07	0.00
30	1	250.10	722.60	85.25	739.60	477.85	56.37	866.94	414.18	48.86	1379.69	157.81	18.62
	2	250.00	722.65	85.26	738.60	478.35	56.43	866.46	414.42	48.89	1379.56	157.87	18.62
	3	250.70	722.30	85.22	740.20	477.55	56.34	867.74	413.78	48.81	1379.69	157.81	18.62
	$\bar{X}$	250.93	722.52	85.24	739.47	477.92	56.38	867.05	414.13	48.85	1379.65	157.83	18.62
	S.D	0.73	0.15	0.02	0.66	0.33	0.04	5.28	2.64	0.03	0.06	0.03	0.00

Appendix A

Table 10. Effect of contact time and metal ion initial concentration of $LaMO_3$ (M = Al, Co, Fe, Gd) in standard Pb 3 = 9 mmol/L = 1695.3 mg/L.

Strr. min.	No	$LaAlO_3$			$LaCoO_3$			$LaFeO_3$			$LaGdO_3$		
		C_e	Q_e	% Ads.	C_e	Q_e	% Ads.	C_e	Q_e	% Ads.	C_e	Q_e	% Ads.
40	1	242.30	726.50	85.71	735.10	480.10	56.64	865.20	415.05	48.96	1378.74	158.28	18.67
	2	240.80	727.25	85.80	738.00	478.65	56.47	865.86	414.72	48.93	1378.62	158.34	18.68
	3	241.50	726.90	85.76	739.20	478.05	56.40	865.38	414.96	48.95	1378.64	158.33	18.68
	$\overline{X}$	241.53	726.88	85.76	737.43	478.93	56.50	865.48	414.91	48.95	1378.67	158.32	18.68
	S.D	0.61	0.31	0.04	1.72	0.86	0.10	0.28	0.14	0.01	0.05	0.03	0.00

Appendix A

Table 11. Effect of contact time and metal ion initial concentration of $LaMO_3$ (M = Al, Co, Fe, Gd) in standard Pb 4 = 13 mmol/L = 2484.6 mg/L.

Strr. min.	No	$LaAlO_3$			$LaCoO_3$			$LaFeO_3$			$LaGdO_3$		
		C_e	Q_e	% Ads.	C_e	Q_e	% Ads.	C_e	Q_e	% Ads.	C_e	Q_e	% Ads.
1	1	312.00	1086.30	87.44	1392.40	546.10	43.95	1502.00	491.30	39.55	2080.00	202.30	16.28
	2	311.90	1086.35	87.45	1396.20	544.20	43.80	1491.60	496.50	39.97	2080.60	202.00	16.26
	3	312.40	1086.10	87.43	1392.00	546.30	43.97	1508.80	487.90	39.27	2080.40	202.10	16.27
	$\bar{X}$	312.10	1086.25	87.44	1393.53	545.53	43.91	1500.80	491.90	39.60	2080.33	202.13	16.27
	S.D	0.22	0.11	0.00	1.89	0.95	0.08	7.07	3.54	0.29	0.25	0.12	0.00
5	1	311.20	1086.70	87.47	1383.00	551.30	44.34	1487.60	498.50	40.13	2079.20	202.70	16.32
	2	310.70	1086.95	87.49	1394.00	545.30	43.89	1490.60	497.00	40.01	2079.80	202.40	16.29
	3	311.00	1086.80	87.48	1384.00	549.90	44.26	1484.60	500.00	40.25	2079.80	202.40	16.29
	$\bar{X}$	310.97	1086.82	87.48	1386.93	548.83	44.16	1487.60	498.50	40.13	2079.60	202.50	16.30
	S.D	0.21	0.10	0.00	5.13	2.57	0.19	2.45	1.22	0.10	0.28	0.14	0.01
10	1	309.00	1087.80	87.56	1376.99	553.81	44.58	1462.20	511.20	41.15	2077.20	203.70	16.40
	2	309.10	1087.75	87.56	1374.23	555.19	44.69	1464.80	509.90	41.04	2078.20	203.20	16.36
	3	307.80	1088.40	87.61	1377.28	553.66	44.57	1474.80	504.90	40.64	2077.73	203.40	16.37
	$\bar{X}$	308.63	1087.98	87.58	1376.17	554.22	44.61	1467.27	508.67	40.94	2077.73	203.43	16.38
	S.D	0.59	0.30	0.02	1.37	0.69	0.05	5.43	2.72	0.22	0.41	0.21	0.02

Appendix A

Table 11. Effect of contact time and metal ion initial concentration of $LaMO_3$ (M = Al, Co, Fe, Gd) in standard Pb 4 = 13 mmol/L = 2484.6 mg/L.

Strr. min.	No	$LaAlO_3$			$LaCoO_3$			$LaFeO_3$			$LaGdO_3$		
		C_e	Q_e	% Ads.	C_e	Q_e	% Ads.	C_e	Q_e	% Ads.	C_e	Q_e	% Ads.
15	1	303.20	1090.70	87.80	1371.00	556.80	44.82	1450.20	517.20	41.63	2067.60	208.50	16.78
	2	302.60	1091.00	87.82	1372.42	556.09	44.76	1461.60	511.50	41.17	2064.80	209.90	16.90
	3	303.00	1090.80	87.80	1376.99	553.81	44.58	1455.60	514.50	41.42	2062.00	211.30	17.01
	$\bar{X}$	302.93	1090.83	87.81	1373.47	555.57	44.72	1455.80	514.40	41.41	2064.80	209.90	16.90
	S.D	0.25	0.12	0.01	2.56	1.28	0.10	4.66	2.33	0.19	2.29	1.14	0.09
20	1	293.30	1095.65	88.20	1369.90	557.35	44.86	1449.80	517.40	41.65	2058.00	213.30	17.17
	2	292.90	1095.85	88.21	1370.30	557.15	44.85	1450.20	517.20	41.63	2059.00	212.80	17.13
	3	293.10	1095.75	88.20	1372.80	555.90	44.75	1449.10	517.75	41.68	2058.20	213.20	17.16
	$\bar{X}$	293.10	1095.75	88.20	1371.00	556.80	44.82	1449.70	517.45	41.65	2058.40	213.10	17.15
	S.D	0.16	0.08	0.00	1.28	0.64	0.05	0.45	0.23	0.02	0.84	0.42	0.02
30	1	270.20	1107.20	89.13	1368.10	558.25	44.94	1447.40	518.60	41.75	2054.50	215.05	17.31
	2	269.70	1107.45	89.15	1369.90	557.35	44.86	1446.60	519.00	41.78	2052.80	215.90	17.38
	3	269.90	1107.35	89.14	1371.00	556.80	44.82	1446.40	519.10	41.79	2053.70	215.45	17.34
	$\bar{X}$	269.93	1107.33	89.14	1369.67	557.47	44.87	1446.80	518.90	41.77	2053.67	215.47	17.34
	S.D	0.21	0.10	0.00	1.20	0.60	0.05	0.43	0.22	0.02	0.69	0.35	0.03

Appendix A

Table 11. Effect of contact time and metal ion initial concentration of $LaMO_3$ (M = Al, Co, Fe, Gd) in standard Pb 4 = 13 mmol/L = 2484.6 mg/L.

Strr. min.	No	$LaAlO_3$			$LaCoO_3$			$LaFeO_3$			$LaGdO_3$		
		C_e	Q_e	% Ads.	C_e	Q_e	% Ads.	C_e	Q_e	% Ads.	C_e	Q_e	% Ads.
40	1	251.80	1116.40	89.87	1352.00	566.30	45.58	1430.80	526.90	42.41	2044.60	220.00	17.71
	2	252.00	1116.30	89.86	1358.70	562.95	45.32	1426.20	529.20	42.60	2046.80	218.90	17.62
	3	252.30	1116.15	89.85	1350.50	567.05	45.65	1430.00	527.30	42.45	2044.40	220.10	17.72
	$\overline{X}$	252.03	1116.28	89.86	1350.40	565.43	45.52	1429.00	527.80	42.49	2045.27	219.67	17.68
	S.D	0.21	0.10	0.00	1.35	0.68	0.13	2.01	1.00	0.08	1.08	0.54	0.05

Appendix A

Table 12. Effect of contact time and metal ion initial concentration of $LaMO_3$ (M = Al, Co, Fe, Gd) in standard Pb 5 = 17 mmol/L = 3251.6 mg/L.

Strr. min.	No	$LaAlO_3$			$LaCoO_3$			$LaFeO_3$			$LaGdO_3$		
		C_e	Q_e	% Ads.	C_e	Q_e	% Ads.	C_e	Q_e	% Ads.	C_e	Q_e	% Ads.
1	1	712.00	1269.80	78.10	2024.60	613.50	37.74	2108.40	571.60	35.16	2717.80	266.90	16.42
	2	711.70	1269.95	78.11	2016.60	617.50	37.98	2104.20	573.70	35.29	2717.00	267.30	16.44
	3	712.10	1269.75	78.10	2023.80	613.90	37.76	2109.00	571.30	35.14	2719.77	265.92	16.36
	$\bar{X}$	711.93	1269.83	78.10	2010.67	614.97	37.83	2107.20	572.20	35.20	2718.19	266.71	16.41
	S.D	0.17	0.09	0.00	3.60	1.80	0.11	2.14	1.07	0.07	1.16	0.58	0.03
5	1	710.70	1270.45	78.14	2015.80	617.90	38.01	2103.40	574.10	35.31	2716.60	267.50	16.45
	2	709.90	1270.85	78.17	2007.00	622.30	38.28	2103.80	573.90	35.30	2716.40	267.60	16.46
	3	710.20	1270.70	78.16	2023.60	614.00	37.77	2104.00	573.80	35.29	2716.80	267.40	16.45
	$\bar{X}$	710.27	1270.67	78.16	2015.47	618.07	38.02	2103.73	573.93	35.30	2716.60	267.50	16.45
	S.D	0.33	0.17	0.01	6.78	3.39	0.21	0.25	0.12	0.00	0.16	0.08	0.00
10	1	709.00	1271.30	78.20	2016.00	617.80	38.00	2101.80	574.90	35.36	2714.00	268.80	16.53
	2	709.20	1271.20	78.19	2000.00	625.80	38.49	2100.60	575.50	35.40	2714.60	268.50	16.51
	3	708.90	1271.35	78.20	2017.00	617.30	37.97	2102.70	574.45	35.33	2714.40	268.60	16.52
	$\bar{X}$	709.03	1271.28	78.20	2011.00	620.30	38.15	2101.70	574.95	35.36	2714.33	268.63	16.52
	S.D	0.12	0.06	0.00	7.79	3.89	0.27	0.86	0.43	0.03	0.25	0.12	0.00

Appendix A

Table 12. Effect of contact time and metal ion initial concentration of $LaMO_3$ (M = Al, Co, Fe, Gd) in standard Pb 5 = 17 mmol/L = 3251.6 mg/L.

Strr. min.	No	$LaAlO_3$			$LaCoO_3$			$LaFeO_3$			$LaGdO_3$		
		C_e	Q_e	% Ads.	C_e	Q_e	% Ads.	C_e	Q_e	% Ads.	C_e	Q_e	% Ads.
15	1	693.40	1279.10	78.68	2009.60	621.00	38.20	2096.60	577.50	35.52	2712.20	269.70	16.59
	2	693.00	1279.30	78.69	1999.20	626.20	38.52	2099.40	576.10	35.43	2711.40	270.10	16.61
	3	692.50	1279.55	78.70	2001.80	624.90	38.44	2097.22	577.19	35.50	2711.00	270.30	16.63
	$\overline{X}$	692.97	1279.32	78.69	2003.53	624.03	38.39	2097.74	576.93	35.48	2711.50	270.03	16.61
	S.D	0.37	0.18	0.00	4.42	2.21	0.14	1.20	0.60	0.04	0.50	0.25	0.02
20	1	675.50	1288.05	79.23	1988.20	631.70	38.85	2085.20	583.20	35.87	2709.40	271.10	16.67
	2	675.00	1288.30	79.24	1989.00	631.30	38.83	2085.80	582.90	35.85	2708.20	271.70	16.71
	3	675.10	1288.25	79.24	1992.00	629.80	38.74	2083.00	584.30	35.94	2708.00	271.80	16.72
	$\overline{X}$	675.20	1288.20	79.24	1989.73	630.93	38.81	2084.67	583.47	35.89	2708.53	271.53	16.70
	S.D	0.22	0.11	0.00	1.64	0.82	0.05	1.20	0.60	0.04	0.62	0.31	0.02
30	1	660.20	1295.70	79.23	1990.60	630.50	38.78	2081.30	585.15	35.99	2703.14	274.23	16.87
	2	659.80	1295.90	79.24	1986.40	632.60	38.91	2084.60	583.50	35.89	2702.60	274.50	16.88
	3	660.00	1295.80	79.24	1987.00	362.30	38.89	2083.40	584.10	35.93	2702.20	274.70	16.90
	$\overline{X}$	660.00	1295.80	79.24	1988.00	631.80	38.86	2083.10	584.25	35.94	2702.65	274.48	16.88
	S.D	0.16	0.08	0.00	0.49	0.25	0.06	1.36	0.68	0.04	0.39	0.19	0.01

Appendix A

Table 12. Effect of contact time and metal ion initial concentration of $LaMO_3$ (M = Al, Co, Fe, Gd) in standard Pb 5 = 17 mmol/L = 3251.6 mg/L.

Strr. min.	No	$LaAlO_3$			$LaCoO_3$			$LaFeO_3$			$LaGdO_3$		
		C_e	Q_e	% Ads.	C_e	Q_e	% Ads.	C_e	Q_e	% Ads.	C_e	Q_e	% Ads.
40	1	630.30	1310.65	80.62	1980.02	635.79	39.11	2078.20	586.70	36.09	2700.93	275.34	16.94
	2	629.70	1310.95	80.63	1980.70	635.45	39.09	2078.00	586.80	36.09	2700.46	275.57	16.95
	3	629.90	1310.85	80.63	1988.40	631.60	38.85	2074.60	588.50	36.20	2700.73	275.44	16.94
	$\overline{X}$	629.97	1310.82	80.63	1983.04	634.28	39.02	2076.93	587.33	36.13	2700.71	275.45	16.94
	S.D	0.25	0.12	0.00	3.80	1.90	0.12	1.65	0.83	0.05	0.19	0.10	0.00

Appendix A

Table 13. Effect of contact time and metal ion initial concentration of $LaMO_3$ (M = Al, Co, Fe, Gd) in standard Pb 6 = 21 mmol/L = 4136.2 mg/L.

Strr. min.	No	$LaAlO_3$			$LaCoO_3$			$LaFeO_3$			$LaGdO_3$		
		C_e	Q_e	% Ads.	C_e	Q_e	% Ads.	C_e	Q_e	% Ads.	C_e	Q_e	% Ads.
1	1	427.60	1854.30	89.66	2659.65	738.28	35.70	2740.80	697.70	33.74	3515.83	310.19	15.00
	2	429.20	1853.50	89.62	2659.88	738.16	35.69	2737.00	699.60	33.83	3515.70	310.25	15.00
	3	427.14	1854.53	89.67	2659.80	738.20	35.69	2737.40	699.40	33.84	3515.87	310.17	15.00
	$\bar{X}$	427.98	1854.11	89.65	2659.78	738.21	35.69	2738.40	698.90	33.80	3515.80	310.20	15.00
	S.D	0.88	0.44	0.02	0.10	0.05	0.00	1.70	0.85	0.05	0.07	0.04	0.00
5	1	264.20	1936.00	93.61	2658.66	738.77	35.72	2730.20	703.00	34.00	3515.33	310.44	15.01
	2	263.37	1936.42	93.63	2658.50	738.85	35.73	2726.60	704.80	34.08	3515.66	310.27	15.00
	3	264.00	1936.10	93.62	2658.05	739.08	35.74	2725.80	705.20	34.10	3515.56	310.32	15.01
	$\bar{X}$	263.86	1936.17	93.62	2658.40	738.90	35.73	2727.53	704.34	34.06	3515.52	310.24	15.01
	S.D	0.35	0.18	0.00	0.26	0.13	0.00	1.91	0.96	0.04	0.14	0.07	0.00
10	1	200.50	1967.85	95.15	2656.50	739.85	35.77	2726.20	705.00	34.09	3514.72	310.74	15.03
	2	198.85	1968.68	95.19	2656.85	739.68	35.77	2721.60	707.30	34.21	3515.02	310.59	15.02
	3	201.16	1967.52	95.14	2656.95	739.63	35.76	2724.20	706.00	34.14	3514.90	310.65	15.02
	$\bar{X}$	200.17	1968.02	95.16	2656.77	739.72	35.77	2724.00	706.10	34.15	3514.88	310.66	15.02
	S.D	0.97	0.49	0.02	0.19	0.10	0.00	1.88	0.94	0.05	0.12	0.06	0.00

Appendix A

Table 13. Effect of contact time and metal ion initial concentration of $LaMO_3$ (M = Al, Co, Fe, Gd) in standard Pb 6 = 21 mmol/L = 4136.2 mg/L.

Strr. min.	No	$LaAlO_3$			$LaCoO_3$			$LaFeO_3$			$LaGdO_3$		
		C_e	Q_e	% Ads.	C_e	Q_e	% Ads.	C_e	Q_e	% Ads.	C_e	Q_e	% Ads.
15	1	138.00	1999.10	96.66	2653.94	741.13	35.84	2704.20	716.00	34.63	3514.45	310.88	15.03
	2	138.50	1998.85	96.65	2653.87	741.17	35.84	2707.40	714.40	34.55	3514.51	310.85	15.03
	3	139.41	1998.40	96.63	2653.70	741.25	35.84	2706.30	715.00	34.58	3514.57	310.82	15.03
	$\bar{X}$	138.64	1998.78	96.65	2653.84	741.18	35.84	2705.97	715.13	34.59	3514.51	310.85	15.03
	S.D	0.58	0.29	0.01	0.10	0.05	0.00	1.33	0.66	0.03	0.05	0.02	0.00
20	1	112.00	2012.10	97.29	2651.23	742.49	35.90	2689.20	723.50	34.99	3514.31	310.95	15.04
	2	112.60	2011.80	97.28	2651.33	742.44	35.90	2688.80	723.70	35.00	3514.67	310.77	15.03
	3	112.00	2012.10	97.29	2651.39	742.41	35.90	2685.60	725.30	35.08	3514.33	310.94	15.03
	$\bar{X}$	112.20	2012.00	97.29	2651.32	742.45	35.90	2687.87	724.17	35.02	3514.44	310.89	15.03
	S.D	0.28	0.14	0.00	0.07	0.04	0.00	1.61	0.81	0.04	0.17	0.08	0.00
30	1	111.40	2012.40	97.31	2649.25	743.48	35.95	2681.00	727.60	35.18	3513.87	311.17	15.05
	2	111.90	2012.15	97.29	2649.30	743.45	35.95	2682.80	726.70	35.13	3514.10	311.05	15.04
	3	110.61	2012.80	97.33	2649.28	743.46	35.95	2681.40	727.40	35.17	3513.79	311.21	15.05
	$\bar{X}$	111.30	2012.45	97.31	2649.28	743.46	35.95	2681.13	727.23	35.16	3513.92	311.14	15.05
	S.D	0.53	0.27	0.02	0.02	0.01	0.00	0.77	0.39	0.02	0.13	0.07	0.00

Appendix A

Table 13. Effect of contact time and metal ion initial concentration of $LaMO_3$ (M = Al, Co, Fe, Gd) in standard Pb 6 = 21 mmol/L = 4136.2 mg/L.

Strr. min.	No	$LaAlO_3$			$LaCoO_3$			$LaFeO_3$			$LaGdO_3$		
		C_e	Q_e	% Ads.	C_e	Q_e	% Ads.	C_e	Q_e	% Ads.	C_e	Q_e	% Ads.
40	1	110.20	2013.00	97.34	2646.74	744.73	36.01	2668.80	733.70	35.48	3513.42	311.39	15.06
	2	111.16	2012.52	97.31	2646.85	744.68	36.01	2664.60	735.80	35.58	3513.38	311.41	15.06
	3	109.95	2013.13	97.34	2646.80	744.70	36.01	2669.00	733.60	35.48	3513.52	311.34	15.05
	$\overline{X}$	110.44	2012.88	97.33	2646.80	744.70	36.01	2667.47	734.37	35.51	3513.44	311.38	15.06
	S.D	0.52	0.26	0.01	0.05	0.02	0.00	2.03	1.01	0.05	0.06	0.03	0.00

Appendix A

Table 14. Effect of contact time and metal ion initial concentration of $LaMO_3$ (M = Al, Co, Fe, Gd) in standard Pb 7 = 25 mmol/L = 4745.5 mg/L.

Strr. min.	No	$LaAlO_3$			$LaCoO_3$			$LaFeO_3$			$LaGdO_3$		
		C_e	Q_e	% Ads.	C_e	Q_e	% Ads.	C_e	Q_e	% Ads.	C_e	Q_e	% Ads.
1	1	243.30	2251.00	94.87	3091.80	826.85	34.85	3119.40	813.05	34.27	3960.71	392.40	16.54
	2	245.50	2250.00	94.83	3089.40	828.05	34.90	3122.00	811.75	34.22	3960.68	392.41	16.54
	3	242.81	2251.35	94.88	3104.20	820.65	34.91	3116.40	814.55	34.33	3960.73	392.39	16.54
	$\overline{X}$	243.87	2250.82	94.86	3095.13	825.18	34.78	3119.27	813.12	34.27	3960.71	392.40	16.54
	S.D	1.17	0.59	0.02	6.49	3.25	0.11	2.29	1.14	0.05	0.02	0.01	0.00
5	1	215.24	2265.13	95.46	3083.00	831.25	35.04	3117.80	813.85	34.31	3960.20	392.65	16.55
	2	215.42	2265.04	95.46	3077.00	834.25	35.17	3111.00	817.25	34.45	3960.08	392.71	16.55
	3	215.36	2265.07	95.46	3094.00	825.75	34.81	3112.80	816.35	34.41	3960.08	392.71	16.55
	$\overline{X}$	215.34	2265.08	95.46	3084.67	830.42	35.01	3113.87	815.82	34.39	3960.12	392.69	16.55
	S.D	0.07	0.04	0.00	7.04	3.52	0.11	2.88	1.44	0.06	0.06	0.03	0.00
10	1	201.90	2271.80	95.75	3079.20	833.15	35.12	3111.00	817.25	34.45	3959.91	392.80	16.55
	2	201.10	2270.20	95.76	3070.40	837.55	35.30	3107.00	819.25	34.53	3959.77	392.87	16.56
	3	200.77	2272.37	95.77	3082.00	831.75	35.06	3108.00	818.75	34.53	3959.85	392.83	16.56
	$\overline{X}$	201.26	2271.46	95.76	3077.20	834.15	35.16	3108.67	818.42	34.50	3959.84	392.83	16.56
	S.D	0.47	0.92	0.00	4.94	2.47	0.10	1.70	0.85	0.04	0.06	0.03	0.00

Appendix A

Table 14. Effect of contact time and metal ion initial concentration of $LaMO_3$ (M = Al, Co, Fe, Gd) in standard Pb 7 = 25 mmol/L = 4745.5 mg/L.

Strr. min.	No	$LaAlO_3$			$LaCoO_3$			$LaFeO_3$			$LaGdO_3$		
		C_e	Q_e	% Ads.	C_e	Q_e	% Ads.	C_e	Q_e	% Ads.	C_e	Q_e	% Ads.
15	1	184.19	2280.66	96.12	3062.60	841.45	35.47	3090.20	827.65	34.89	3959.66	392.92	16.56
	2	182.90	2281.30	96.15	3061.80	841.85	35.49	3094.40	825.55	34.80	3959.62	392.94	16.56
	3	183.83	2280.84	96.13	3074.00	835.75	35.23	3092.20	826.65	34.84	3959.65	392.93	16.56
	$\overline{X}$	183.64	2280.93	96.13	3066.13	839.68	35.40	3092.27	826.62	34.84	3959.64	392.93	16.56
	S.D	0.54	0.27	0.01	5.57	2.79	0.12	2.94	1.47	0.04	0.02	0.01	0.00
20	1	156.70	2294.40	96.70	3051.80	846.85	35.70	3084.00	830.75	35.02	3959.47	393.02	16.56
	2	156.00	2294.75	96.71	3059.00	843.25	35.54	3082.20	831.65	35.06	3959.54	392.98	16.56
	3	155.20	2295.15	96.73	3060.20	845.65	35.52	3086.00	829.75	34.98	3959.60	392.95	16.56
	$\overline{X}$	155.97	2294.77	96.71	3057.00	844.25	35.59	3084.07	830.72	35.02	3959.54	392.98	16.56
	S.D	0.61	0.31	0.01	3.71	1.86	0.08	1.55	0.78	0.03	0.05	0.03	0.00
30	1	151.60	2296.95	96.81	3049.30	848.10	35.74	3081.40	832.05	35.07	3956.74	394.38	16.62
	2	150.90	2297.30	96.82	3048.60	848.45	35.76	3080.60	832.45	35.09	3956.64	394.43	16.62
	3	153.10	2296.20	96.77	3052.70	846.40	35.67	3083.20	831.15	35.03	3956.70	394.40	16.62
	$\overline{X}$	151.87	2296.82	96.80	3050.20	847.65	35.72	3081.73	831.88	35.06	3956.69	394.40	16.62
	S.D	0.92	0.46	0.02	1.79	0.90	0.04	1.09	0.54	0.03	0.04	0.02	0.00

Appendix A

Table 14. Effect of contact time and metal ion initial concentration of $LaMO_3$ (M = Al, Co, Fe, Gd) in standard Pb 7 = 25 mmol/L = 4745.5 mg/L.

Strr. min.	No	$LaAlO_3$			$LaCoO_3$			$LaFeO_3$			$LaGdO_3$		
		C_e	Q_e	% Ads.	C_e	Q_e	% Ads.	C_e	Q_e	% Ads.	C_e	Q_e	% Ads.
40	1	148.30	2298.60	96.87	3043.00	851.25	35.88	3080.00	832.75	35.10	3956.47	394.52	16.63
	2	149.45	2298.03	96.85	3041.50	852.00	35.91	3080.50	832.50	35.09	3956.54	394.48	16.63
	3	149.00	2298.25	96.86	3048.30	848.60	35.77	3080.30	832.60	35.09	3956.60	394.45	16.63
	$\overline{X}$	148.92	2298.29	96.86	3044.27	850.62	35.85	3080.27	832.62	35.09	3956.54	394.48	16.63
	S.D	0.47	0.23	0.00	2.92	1.46	0.08	2.92	1.46	0.00	0.05	0.03	0.00

Appendix B

Table 1. Effect of pH to the adsorption of $LaMO_3$ (M = Al, Co, Fe, Gd) in standard Cd 7 = 25 mmol/L = 2629.40 mg/L

pH	No	$LaAlO_3$			$LaCoO_3$			$LaFeO_3$			$LaGdO_3$		
		C_e (mg/L)	Q_e (mg/g)	% Ads.	C_e (mg/L)	Q_e (mg/g)	% Ads.	C_e (mg/L)	Q_e (mg/g)	% Ads.	C_e (mg/L)	Q_e (mg/g)	% Ads.
1	1	1703.40	463.00	35.22	2116.00	256.70	19.53	2139.80	244.80	18.62	2229.00	200.20	15.23
	2	1704.20	462.60	35.19	2114.80	257.30	19.57	2139.40	245.00	18.64	2227.20	201.10	15.30
	3	1706.00	461.70	35.13	2113.00	258.20	19.64	2137.20	246.10	18.72	2230.80	199.30	15.16
	$\overline{X}$	1704.53	462.43	35.18	2114.60	257.40	19.58	2138.80	245.30	18.66	2229.00	200.20	15.23
	S.D	1.09	0.54	0.04	1.14	0.57	0.05	1.14	0.57	0.04	1.47	0.73	0.06
3	1	912.80	858.30	65.28	1927.20	351.10	26.71	1833.64	397.88	30.26	2161.10	234.15	17.81
	2	913.20	858.10	65.27	1928.40	350.50	26.66	1834.16	397.62	30.24	2161.00	234.20	17.81
	3	916.20	856.60	65.16	1927.60	350.90	26.69	1834.00	397.70	30.23	2161.00	234.15	17.81
	$\overline{X}$	914.07	857.67	65.23	1927.80	350.83	26.69	1833.93	397.73	30.23	2161.10	234.15	17.81
	S.D	1.52	0.76	0.05	0.50	0.25	0.02	0.22	0.11	0.02	0.06	0.03	0.00

Appendix B

Table 1(cont.) Effect of pH to the adsorption of $LaMO_3$ (M = Al, Co, Fe, Gd) in standard Cd 7 = 25 mmol/L = 2629.40 mg/L

pH	No	$LaAlO_3$			$LaCoO_3$			$LaFeO_3$			$LaGdO_3$		
		C_e (mg/L)	Q_e (mg/g)	% Ads.	C_e (mg/L)	Q_e (mg/g)	% Ads.	C_e (mg/L)	Q_e (mg/g)	% Ads.	C_e (mg/L)	Q_e (mg/g)	% Ads.
5	1	491.20	1069.10	81.32	1399.60	614.90	46.77	1510.20	559.60	45.56	2104.67	262.37	19.96
	2	487.80	1070.80	81.45	1400.40	614.50	46.74	1508.20	560.60	45.63	2104.72	262.34	19.95
	3	488.40	1070.50	81.43	1402.00	613.70	46.68	1505.60	561.90	45.73	2104.60	262.40	19.96
	$\overline{X}$	489.13	1070.13	81.40	1400.67	614.37	46.73	1508.00	560.70	45.64	2104.66	262.37	19.96
	S.D	1.52	0.76	0.06	1.00	0.50	0.04	1.88	0.94	0.07	0.05	0.02	0.00
6	1	291.90	1168.75	88.90	720.20	954.60	72.61	724.80	952.30	72.43	2080.71	274.35	20.87
	2	290.00	1169.70	88.97	718.60	955.40	72.67	726.40	951.50	72.37	2080.70	274.35	20.87
	3	291.20	1169.10	88.93	719.00	955.20	72.66	725.40	952.00	72.41	2080.71	274.35	20.87
	$\overline{X}$	291.03	1169.18	88.93	719.20	955.07	72.65	725.53	951.93	72.40	2080.71	274.35	20.87
	S.D	0.78	0.39	0.03	0.68	0.34	0.03	0.66	0.33	0.03	0.00	0.00	0.00

Appendix B

Table 2. Effect of pH to the adsorption of $LaMO_3$ (M = Al, Co, Fe, Gd) in standard Pb 7 = 25 mmol/L = 4745.5 mg/L

pH	No	$LaAlO_3$			$LaCoO_3$			$LaFeO_3$			$LaGdO_3$		
		C_e (mg/L)	Q_e (mg/g)	% Ads.	C_e (mg/L)	Q_e (mg/g)	% Ads.	C_e (mg/L)	Q_e (mg/g)	% Ads.	C_e (mg/L)	Q_e (mg/g)	% Ads.
1	1	3234.00	755.75	31.85	3794.00	475.75	20.50	3566.00	589.75	24.86	4157.98	293.76	12.38
	2	3234.00	755.75	31.85	3784.00	480.75	20.26	3604.00	570.75	24.05	4158.40	293.55	12.37
	3	3202.00	771.75	32.53	3782.20	481.65	20.30	3576.00	584.75	24.64	4158.10	293.70	12.38
	$\overline{X}$	3223.33	761.08	32.08	3786.73	479.38	20.35	3582.00	581.75	24.52	4158.16	293.67	12.38
	S.D	15.08	7.54	0.32	5.19	2.60	0.11	16.08	8.04	0.34	0.18	0.09	0.00
3	1	1448.00	1648.75	69.49	3291.80	726.85	30.63	3360.00	692.75	29.20	4037.67	353.92	14.92
	2	1434.00	1655.75	69.78	3289.40	728.05	30.68	3344.00	700.75	29.54	4037.00	354.25	14.93
	3	1422.73	1661.39	70.02	3304.20	720.65	30.37	3334.00	705.75	29.75	4038.34	353.58	14.90
	$\overline{X}$	1434.91	1655.30	69.76	3295.13	725.18	30.56	3346.00	699.75	29.50	4037.67	353.92	14.92
	S.D	10.34	5.17	0.22	6.49	3.25	3.10	10.71	5.35	0.23	0.55	0.27	0.01

Appendix B

Table 2 (cont.) Effect of pH to the adsorption of $LaMO_3$ (M = Al, Co, Fe, Gd) in standard Pb 7 = 25 mmol/L = 4745.5 mg/L

pH	No	$LaAlO_3$			$LaCoO_3$			$LaFeO_3$			$LaGdO_3$		
		C_e (mg/L)	Q_e (mg/g)	% Ads.	C_e (mg/L)	Q_e (mg/g)	% Ads.	C_e (mg/L)	Q_e (mg/g)	% Ads.	C_e (mg/L)	Q_e (mg/g)	% Ads.
4	1	243.30	243.30	94.87	3091.80	826.85	34.85	3119.40	813.05	34.27	3960.71	392.40	16.54
	2	245.50	245.50	94.83	3089.40	828.05	34.90	3122.00	811.75	34.22	3960.68	392.41	16.54
	3	242.81	242.81	94.88	3104.20	820.65	34.91	3116.40	814.55	34.33	3960.73	392.39	16.54
	$\overline{X}$	243.87	243.87	94.86	3095.13	825.18	34.78	3119.27	813.12	34.27	3960.71	392.40	16.54
	S.D	1.17	0.59	0.02	6.49	3.25	0.10	2.29	1.14	0.23	0.02	0.01	0.00

Appendix C

Table 1. Recyclability of $LaAlO_3$ in standard cadmium concentration of 1 – 25 mmol /L

Cd^{2+} mmol/L	No	Untreated with EDTA			Treated with 0.1 M EDTA								
		C_e (mg/L)	Q_e (mg/g)	% Ads.	1st of treated			2nd of treated			3rd of treated		
					C_e (mg/L)	Q_e (mg/g)	% Ads.	C_e (mg/L)	Q_e (mg/g)	% Ads.	C_e (mg/L)	Q_e (mg/g)	% Ads.
1	1	70.15	16.88	32.48	17.54	43.18	83.12	16.86	43.52	83.77	17.89	43.01	82.78
	2	69.55	17.18	33.06	17.39	43.26	83.26	16.53	43.69	84.09	18.04	42.93	82.64
	3	69.21	17.35	33.39	17.30	43.30	83.35	16.70	43.60	83.93	17.91	43.00	82.76
	$\overline{X}$	69.64	17.14	32.98	17.41	43.25	83.24	16.70	43.60	83.93	17.95	42.98	82.73
	S.D	0.39	0.19	0.39	0.10	0.05	0.09	0.13	0.07	0.13	0.07	0.03	0.06
5	1	407.50	53.28	20.66	326.77	93.42	36.38	328.19	92.71	36.10	327.76	92.92	36.18
	2	409.10	52.25	20.35	327.28	93.16	36.28	327.98	92.81	36.14	327.82	92.89	36.17
	3	409.40	52.10	20.29	327.35	93.13	36.26	328.04	92.78	36.13	327.87	92.87	36.16
	$\overline{X}$	408.52	52.54	20.43	327.13	93.24	36.31	328.07	92.77	36.12	327.82	92.89	36.17
	S.D	0.85	0.42	0.16	0.26	0.13	0.05	0.09	0.05	0.02	0.05	0.02	0.00

Appendix C

Table 1 (Cont.) Recyclability of $LaAlO_3$ in standard cadmium concentration of 1 – 25 mmol /L

Cd^{2+} mmol/L	No	Untreated with EDTA			Treated with 0.1 M EDTA								
					1st of treated			2nd of treated			3rd of treated		
		C_e (mg/L)	Q_e (mg/g)	% Ads.	C_e (mg/L)	Q_e (mg/g)	% Ads.	C_e (mg/L)	Q_e (mg/g)	% Ads.	C_e (mg/L)	Q_e (mg/g)	% Ads.
9	1	754.00	104.10	21.63	438.50	261.85	54.43	436.76	262.72	54.61	437.51	262.35	54.53
	2	756.40	102.90	21.39	439.10	261.55	54.36	436.64	262.78	54.62	437.48	262.36	54.53
	3	756.80	102.70	21.35	439.20	261.50	54.35	436.57	262.82	54.63	437.65	262.28	54.52
	$\overline{x}$	755.60	103.23	21.46	438.90	261.63	54.38	436.66	262.77	54.62	437.55	262.33	54.53
	S.D	1.24	0.62	0.12	0.31	0.16	0.04	0.08	0.04	0.00	0.07	0.04	0.00
13	1	1114.98	148.81	21.07	572.05	420.28	52.42	570.20	421.20	52.56	573.82	419.39	52.30
	2	1115.83	148.39	21.01	572.70	419.95	52.38	570.28	421.16	52.55	573.80	419.40	52.30
	3	1116.50	148.05	20.96	572.85	419.88	52.37	570.22	421.19	52.55	573.79	419.41	52.30
	$\overline{x}$	1115.77	148.42	21.01	572.53	420.04	52.39	570.23	421.18	52.55	573.80	419.40	52.30
	S.D	0.62	0.31	0.05	0.35	0.17	0.02	0.03	0.02	0.00	0.01	0.00	0.00

Appendix C

Table 1 (Cont.) Recyclability of $LaAlO_3$ in standard cadmium concentration of 1 – 25 mmol /L

Cd^{2+} mmol/L	No	Untreated with EDTA			Treated with 0.1 M EDTA								
		C_e (mg/L)	Q_e (mg/g)	% Ads.	1st of treated			2nd of treated			3rd of treated		
					C_e (mg/L)	Q_e (mg/g)	% Ads.	C_e (mg/L)	Q_e (mg/g)	% Ads.	C_e (mg/L)	Q_e (mg/g)	% Ads.
17	1	1489.35	177.83	19.28	628.00	608.50	65.96	624.11	610.45	66.17	627.10	608.95	66.01
	2	1489.89	177.56	19.25	628.00	608.50	65.96	624.20	610.40	66.17	627.40	608.80	65.99
	3	1489.35	177.83	19.28	628.40	608.30	65.94	624.60	610.20	66.15	627.80	608.60	65.97
	$\overline{x}$	1489.53	177.74	19.27	628.13	608.43	65.95	624.30	610.35	66.16	627.43	608.78	65.99
	S.D	0.25	0.13	0.01	0.19	0.09	0.01	0.22	0.11	0.01	0.29	0.14	0.02
21	1	1786.50	201.25	18.39	670.00	724.10	69.39	669.98	759.51	69.39	671.51	758.75	69.32
	2	1786.90	201.05	18.37	670.50	723.85	69.37	670.18	759.41	69.38	671.48	758.76	69.32
	3	1787.20	200.90	18.36	670.80	723.70	69.36	669.85	759.58	69.40	671.36	758.82	69.33
	$\overline{x}$	1786.87	201.07	18.37	670.43	723.88	69.37	670.00	759.50	69.39	671.45	758.78	69.32
	S.D	0.29	0.14	0.01	0.33	0.17	0.01	0.14	0.07	0.00	0.06	0.03	0.00

Appendix C

Table 1 (Cont.) Recyclability of $LaAlO_3$ in standard cadmium concentration of 1 – 25 mmol /L

Cd^{2+} mmol/L	No	Untreated with EDTA			Treated with 0.1 M EDTA								
		C_e (mg/L)	Q_e (mg/g)	% Ads.	1st of treated			2nd of treated			3rd of treated		
					C_e (mg/L)	Q_e (mg/g)	% Ads.	C_e (mg/L)	Q_e (mg/g)	% Ads.	C_e (mg/L)	Q_e (mg/g)	% Ads.
25	1	2097.15	266.13	20.24	418.37	1105.52	84.09	420.91	1104.25	83.99	422.01	1103.70	83.95
	2	2098.55	265.43	20.19	418.88	1105.26	84.07	420.66	1104.37	84.00	422.04	1103.68	83.95
	3	2098.21	265.60	20.20	419.12	1105.14	84.06	420.74	1104.33	84.00	421.89	1103.76	83.95
	$\overline{x}$	2097.97	265.72	20.21	418.79	1105.31	84.07	420.77	1104.32	84.00	421.98	1103.71	83.95
	S.D	0.60	0.30	0.02	0.31	0.16	0.01	0.10	0.05	0.00	0.06	0.03	0.00

Appendix C

Table 2. Recyclability of $LaAlO_3$ in standard lead concentration of 1 – 25 mmol /L

Pb^{2+} mmol/L	No	Untreated with EDTA			Treated with 0.1 M EDTA								
					1st of treated			2nd of treated			3rd of treated		
		C_e (mg/L)	Q_e (mg/g)	% Ads.	C_e (mg/L)	Q_e (mg/g)	% Ads.	C_e (mg/L)	Q_e (mg/g)	% Ads.	C_e (mg/L)	Q_e (mg/g)	% Ads.
1	1	108.80	38.90	41.69	47.28	69.66	74.66	46.40	70.10	75.13	48.20	69.20	74.17
	2	112.20	37.20	39.87	46.80	69.90	74.92	46.44	70.08	75.11	47.90	69.35	74.33
	3	111.20	37.70	40.41	45.84	70.38	75.43	46.47	70.07	75.10	48.44	69.08	74.04
	$\overline{x}$	110.70	37.93	40.66	46.64	69.98	75.00	46.44	70.08	75.11	48.18	69.21	74.18
	S.D	1.42	0.71	0.48	0.60	0.30	0.32	0.03	0.01	0.01	0.22	0.11	0.12
5	1	358.05	304.83	63.00	243.49	362.11	74.84	245.90	360.90	74.59	245.20	361.25	74.66
	2	359.50	304.10	62.85	244.70	361.50	74.71	246.10	360.80	74.57	245.90	360.90	74.59
	3	360.00	303.85	63.00	243.20	362.25	71.84	245.70	361.00	74.61	246.10	360.80	74.57
	$\overline{x}$	359.18	304.26	62.95	243.80	361.95	74.81	245.90	360.90	74.59	245.70	360.98	74.61
	S.D	0.83	0.41	0.07	0.65	0.32	0.07	0.16	0.08	0.02	0.39	0.19	0.04

Appendix C

Table 2 (cont.) Recyclability of $LaAlO_3$ in standard lead concentration of 1 – 25 mmol /L

Pb^{2+} mmol/L	No	Untreated with EDTA			Treated with 0.1 M EDTA								
		C_e (mg/L)	Q_e (mg/g)	% Ads.	1st of treated			2nd of treated			3rd of treated		
					C_e (mg/L)	Q_e (mg/g)	% Ads.	C_e (mg/L)	Q_e (mg/g)	% Ads.	C_e (mg/L)	Q_e (mg/g)	% Ads.
9	1	607.30	544.00	64.18	439.70	627.80	74.06	440.55	627.38	74.01	436.34	629.48	74.26
	2	606.80	544.25	64.21	442.70	636.30	73.89	440.28	627.51	74.03	436.54	629.38	74.25
	3	610.00	542.65	64.02	440.60	627.35	74.01	440.49	627.41	74.02	436.56	629.37	74.25
	$\bar{x}$	608.00	543.63	64.14	441.00	630.48	73.99	440.44	627.43	74.02	436.48	629.41	74.25
	S.D	1.41	0.70	0.08	1.26	0.63	0.07	0.12	0.06	0.00	0.10	0.05	0.00
13	1	1289.80	597.40	48.09	582.03	951.29	76.57	580.80	951.90	76.62	576.66	953.97	76.79
	2	1282.00	601.30	48.40	583.22	950.69	76.53	580.80	951.90	76.62	576.61	954.00	76.79
	3	1284.50	598.55	48.30	583.34	950.63	76.52	580.77	951.92	76.63	576.58	954.01	76.79
	$\bar{x}$	1285.43	599.08	48.26	582.87	950.87	76.54	580.79	951.91	76.62	576.62	954.99	76.79
	S.D	3.25	1.63	0.13	1.10	0.55	0.02	0.01	0.01	0.00	0.03	0.02	0.00

Appendix C

Table 2 (Cont.) Recyclability of $LaAlO_3$ in standard lead concentration of 1 – 25 mmol /L

Pb^{2+} mmol/L	No	Untreated with EDTA			Treated with 0.1 M EDTA								
		C_e (mg/L)	Q_e (mg/g)	% Ads.	1st of treated			2nd of treated			3rd of treated		
					C_e (mg/L)	Q_e (mg/g)	% Ads.	C_e (mg/L)	Q_e (mg/g)	% Ads.	C_e (mg/L)	Q_e (mg/g)	% Ads.
17	1	1806.90	722.35	44.43	902.30	1174.65	72.25	900.88	1175.36	72.29	899.67	1175.97	72.33
	2	1807.20	722.20	44.42	902.40	1174.60	72.25	901.12	1175.24	72.29	899.63	1175.99	72.33
	3	1832.70	709.45	43.64	902.81	1174.90	72.23	900.71	1175.45	72.30	899.71	1175.95	72.33
	$\overline{x}$	1815.60	718.00	44.16	902.17	1174.72	72.24	900.90	1175.35	72.29	899.67	1175.97	72.33
	S.D	12.09	6.05	0.37	0.26	0.13	0.01	0.17	0.08	0.00	0.03	0.02	0.00
21	1	2361.10	887.55	42.92	1146.70	1494.75	72.28	1148.80	1493.70	72.23	1146.60	1494.80	72.28
	2	2355.90	890.15	43.04	1147.32	1494.44	72.26	1148.20	1494.00	72.24	1146.48	1494.86	72.28
	3	2361.62	887.29	42.90	1148.81	1493.70	72.23	1148.78	1493.71	72.23	1146.63	1494.79	72.28
	$\overline{x}$	2359.54	888.33	42.95	1157.61	1494.30	72.26	1148.59	1493.80	72.23	1146.57	1494.82	72.28
	S.D	2.58	1.29	0.06	10.08	5.04	0.02	0.28	0.14	0.00	0.06	0.03	0.00

Appendix C

Table 2 (Cont.) Recyclability of $LaAlO_3$ in standard lead concentration of 1 – 25 mmol /L

Pb^{2+} mmol/L	No	Untreated with EDTA			Treated with 0.1 M EDTA								
					1st of treated			2nd of treated			3rd of treated		
		C_e (mg/L)	Q_e (mg/g)	% Ads.	C_e (mg/L)	Q_e (mg/g)	% Ads.	C_e (mg/L)	Q_e (mg/g)	% Ads.	C_e (mg/L)	Q_e (mg/g)	% Ads.
25	1	2815.43	965.04	40.67	1186.39	1779.56	75.00	1182.80	1781.35	75.08	1180.18	1782.66	75.13
	2	2814.96	965.27	40.68	1186.02	1779.74	75.01	1182.20	1781.65	75.09	1180.20	1782.65	75.13
	3	2815.39	965.06	40.67	1185.95	1779.78	75.01	1182.43	1781.54	75.08	1180.20	1782.65	75.13
	$\overline{x}$	2815.26	965.12	40.67	1186.12	1779.69	75.01	1182.48	1781.51	75.08	1180.19	1782.65	75.13
	S.D	0.21	0.11	0.00	0.19	0.10	0.00	0.25	0.12	0.00	0.01	0.00	0.00

Appendix C

Table 3. Recyclability of $LaCoO_3$ in standard cadmium concentration of 1 – 25 mmol /L

Cd^{2+} mmol/L	No	Untreated with EDTA			Treated with 0.1 M EDTA								
					1st of treated			2nd of treated			3rd of treated		
		C_e (mg/L)	Q_e (mg/g)	% Ads.	C_e (mg/L)	Q_e (mg/g)	% Ads.	C_e (mg/L)	Q_e (mg/g)	% Ads.	C_e (mg/L)	Q_e (mg/g)	% Ads.
1	1	101.50	1.20	2.31	92.30	5.80	11.16	91.07	6.42	12.35	90.98	6.46	12.44
	2	101.78	1.06	2.04	91.90	6.00	11.55	91.18	6.36	12.24	90.90	6.50	12.51
	3	101.87	1.02	1.95	92.50	5.70	10.97	91.11	6.40	12.31	90.92	6.49	12.49
	$\overline{x}$	101.72	1.09	2.10	92.23	5.83	11.23	91.12	6.39	12.30	90.93	6.48	12.48
	S.D	0.33	0.16	0.15	0.25	0.12	0.24	0.05	0.02	0.05	0.03	0.02	0.03
5	1	479.40	17.10	6.66	344.90	84.35	32.85	340.60	86.50	33.68	339.01	87.30	33.99
	2	479.25	17.18	6.69	344.60	84.50	32.91	340.85	86.38	33.64	338.94	87.33	34.01
	3	479.80	16.90	6.58	344.80	84.40	32.87	340.74	86.43	33.66	338.97	87.32	34.00
	$\overline{x}$	479.48	17.06	6.64	344.77	84.42	32.88	340.73	86.44	33.66	338.97	87.32	34.00
	S.D	0.18	0.09	0.05	0.12	0.06	0.03	0.10	0.05	0.02	0.03	0.01	0.00

Appendix C

Table 3 (Cont.) Recyclability of $LaCoO_3$ in standard cadmium concentration of 1 – 25 mmol /L

Cd^{2+} mmol/L	No	Untreated with EDTA			Treated with 0.1 M EDTA								
					1st of treated			2nd of treated			3rd of treated		
		C_e (mg/L)	Q_e (mg/g)	% Ads.	C_e (mg/L)	Q_e (mg/g)	% Ads.	C_e (mg/L)	Q_e (mg/g)	% Ads.	C_e (mg/L)	Q_e (mg/g)	% Ads.
9	1	786.70	87.75	18.24	538.50	211.85	44.43	537.45	212.38	44.54	537.51	212.35	44.53
	2	786.90	87.65	18.22	539.10	211.55	44.36	536.45	212.88	44.64	537.48	212.36	44.53
	3	787.30	87.45	18.18	539.20	211.50	44.35	536.53	212.84	44.63	537.65	212.28	44.52
	$\overline{x}$	786.97	87.62	18.21	538.90	211.63	44.38	536.45	212.70	44.60	537.55	212.33	44.53
	S.D	0.25	0.12	0.03	0.33	0.16	0.04	0.58	0.29	0.05	0.07	0.04	0.00
13	1	1123.10	144.75	20.49	670.02	371.29	52.57	669.86	371.37	52.58	664.45	374.08	52.96
	2	1123.60	144.50	20.46	670.72	370.94	52.52	669.64	371.48	52.60	664.58	374.01	52.95
	3	1122.90	144.85	20.51	670.80	370.90	52.51	669.90	371.35	52.58	664.53	374.04	52.96
	$\overline{x}$	1123.20	144.70	20.49	670.51	371.04	52.53	669.80	371.40	52.59	664.52	374.04	52.96
	S.D	0.47	0.23	0.02	0.39	0.20	0.02	0.11	0.06	0.01	0.05	0.03	0.00

Appendix C

Table 3 (Cont.) Recyclability of $LaCoO_3$ in standard cadmium concentration of 1 – 25 mmol /L

Cd^{2+} mmol/L	No	Untreated with EDTA			Treated with 0.1 M EDTA								
		C_e (mg/L)	Q_e (mg/g)	% Ads.	1st of treated			2nd of treated			3rd of treated		
					C_e (mg/L)	Q_e (mg/g)	% Ads.	C_e (mg/L)	Q_e (mg/g)	% Ads.	C_e (mg/L)	Q_e (mg/g)	% Ads.
17	1	1493.90	175.55	19.03	926.80	459.10	49.77	924.91	460.05	49.87	927.10	458.95	49.75
	2	1493.30	175.85	19.06	928.00	458.50	49.70	924.69	460.16	49.88	927.40	458.80	49.73
	3	1493.10	175.95	19.07	928.40	458.30	49.68	924.66	460.17	49.88	927.80	458.60	49.71
	$\overline{x}$	1493.43	175.78	19.05	927.60	458.63	49.72	924.75	460.13	49.88	927.43	458.78	49.73
	S.D	0.34	0.17	0.02	0.69	0.35	0.04	0.11	0.06	0.00	0.29	0.14	0.02
21	1	1786.60	201.20	18.38	797.81	695.60	63.55	793.55	697.73	63.75	794.03	697.49	63.73
	2	1785.30	201.85	18.44	797.01	696.00	63.59	796.90	696.05	63.60	794.23	697.39	63.72
	3	1789.00	200.00	18.27	797.17	695.92	63.58	797.30	695.85	63.58	794.26	697.37	63.72
	$\overline{x}$	1786.97	201.02	18.36	797.33	695.84	63.57	795.92	696.54	63.64	794.17	697.42	63.72
	S.D	1.53	0.77	0.07	0.35	0.17	0.02	1.68	0.84	0.08	0.10	0.05	0.00

Appendix C

Table 3 (Cont.) Recyclability of $LaCoO_3$ in standard cadmium concentration of 1 – 25 mmol /L

Cd^{2+} mmol/L	No	Untreated with EDTA			Treated with 0.1 M EDTA								
		C_e (mg/L)	Q_e (mg/g)	% Ads.	1st of treated			2nd of treated			3rd of treated		
					C_e (mg/L)	Q_e (mg/g)	% Ads.	C_e (mg/L)	Q_e (mg/g)	% Ads.	C_e (mg/L)	Q_e (mg/g)	% Ads.
25	1	2174.10	227.65	17.32	956.28	836.56	63.63	947.67	840.87	63.96	951.77	838.82	63.80
	2	2175.46	226.97	17.26	956.94	836.23	63.61	947.00	841.20	63.98	951.00	839.20	63.83
	3	2174.69	227.36	17.29	957.33	836.04	63.59	948.34	840.53	63.93	951.34	839.03	63.82
	$\overline{x}$	2174.75	227.33	17.29	956.85	836.28	63.61	947.67	840.87	63.96	951.37	839.35	63.82
	S.D	0.41	0.21	0.02	0.58	0.29	0.02	0.55	0.27	0.02	0.32	0.16	0.00

Appendix C

Table 4. Recyclability of $LaCoO_3$ in standard lead concentration of 1 – 25 mmol /L

Pb^{2+} mmol/L	No	Untreated with EDTA			Treated with 0.1 M EDTA								
		C_e (mg/L)	Q_e (mg/g)	% Ads.	1st of treated			2nd of treated			3rd of treated		
					C_e (mg/L)	Q_e (mg/g)	% Ads.	C_e (mg/L)	Q_e (mg/g)	% Ads.	C_e (mg/L)	Q_e (mg/g)	% Ads.
1	1	165.90	10.35	11.09	122.90	31.85	34.14	121.19	32.71	35.05	123.55	31.53	33.79
	2	165.10	10.75	11.52	122.90	31.85	34.14	121.25	32.68	35.02	123.49	31.56	33.82
	3	167.30	9.65	10.34	122.70	31.95	34.24	120.99	32.81	35.16	123.27	31.67	33.94
	$\overline{x}$	166.10	10.25	10.98	122.83	31.88	34.17	121.14	32.73	35.08	123.44	31.59	33.85
	S.D	0.91	0.45	0.49	0.09	0.05	0.05	0.11	0.06	0.06	0.12	0.06	0.06
5	1	819.15	74.28	15.35	462.90	252.40	52.16	461.17	253.27	52.34	460.89	253.41	52.37
	2	820.00	73.85	15.26	462.90	252.40	52.16	461.20	253.25	52.34	460.90	253.40	52.37
	3	821.03	73.34	15.16	462.70	252.50	52.19	461.26	253.22	52.33	460.90	253.40	52.37
	$\overline{x}$	820.06	73.82	15.26	462.83	252.43	52.17	461.21	253.25	52.34	460.90	253.40	52.37
	S.D	0.77	0.38	0.08	0.09	0.05	0.01	0.04	0.02	0.02	0.00	0.00	0.00

Appendix C

Table 4 (Cont.) Recyclability of $LaCoO_3$ in standard lead concentration of 1 – 25 mmol /L

Pb^{2+} mmol/L	No	Untreated with EDTA			Treated with 0.1 M EDTA								
		C_e (mg/L)	Q_e (mg/g)	% Ads.	1st of treated			2nd of treated			3rd of treated		
					C_e (mg/L)	Q_e (mg/g)	% Ads.	C_e (mg/L)	Q_e (mg/g)	% Ads.	C_e (mg/L)	Q_e (mg/g)	% Ads.
9	1	1412.40	141.45	16.69	974.52	360.39	42.52	970.00	362.65	42.78	976.43	359.44	42.40
	2	1413.20	141.05	16.64	974.10	360.60	42.54	970.00	362.65	42.78	976.40	359.45	42.41
	3	1412.80	141.25	16.66	973.98	360.66	42.55	969.77	362.77	42.80	976.42	359.44	42.40
	$\overline{X}$	1412.80	141.25	16.66	974.20	360.55	42.54	969.92	362.69	42.79	976.42	359.44	42.40
	S.D	0.42	0.21	0.02	0.49	0.25	0.01	0.11	0.05	0.01	0.01	0.00	0.00
13	1	2141.75	171.43	13.80	1623.91	430.35	34.64	1620.80	431.90	34.77	1624.88	429.86	34.60
	2	2141.04	171.78	13.83	1623.08	430.76	34.67	1620.77	431.90	34.77	1624.90	429.85	34.60
	3	2141.60	171.50	13.81	1623.49	430.56	34.66	1620.57	432.02	34.78	1624.91	429.85	34.60
	$\overline{X}$	2141.46	171.57	13.81	1623.49	430.56	34.66	1620.71	431.95	34.77	1624.90	429.85	34.60
	S.D	0.31	0.15	0.01	0.34	0.17	0.01	0.10	0.05	0.00	0.01	0.00	0.00

Appendix C

Table 4 (Cont.) Recyclability of $LaCoO_3$ in standard lead concentration of 1 – 25 mmol /L

Pb^{2+} mmol/L	No	Untreated with EDTA			Treated with 0.1 M EDTA								
		C_e (mg/L)	Q_e (mg/g)	% Ads.	1st of treated			2nd of treated			3rd of treated		
					C_e (mg/L)	Q_e (mg/g)	% Ads.	C_e (mg/L)	Q_e (mg/g)	% Ads.	C_e (mg/L)	Q_e (mg/g)	% Ads.
17	1	2830.70	210.45	12.94	2313.30	469.15	28.86	2310.22	470.69	28.95	2312.18	469.71	28.89
	2	2832.60	209.50	12.89	2310.40	470.60	28.95	2310.28	470.66	28.95	2312.50	469.55	28.88
	3	2829.70	210.95	12.97	2310.70	470.45	28.94	2310.25	470.68	28.95	2312.39	469.61	28.88
	$\overline{x}$	2831.00	210.30	12.93	2311.47	470.07	28.92	2310.25	470.68	28.95	2312.36	469.62	28.88
	S.D	1.20	0.60	0.03	1.30	0.65	0.04	0.02	0.01	0.00	0.13	0.07	0.00
21	1	3660.85	237.68	11.49	2698.00	719.10	34.77	2754.19	691.01	33.41	2709.18	713.51	34.50
	2	3661.04	237.58	11.49	2694.40	720.90	34.86	2754.07	691.07	33.42	2709.19	713.51	34.50
	3	3660.96	237.62	11.49	2696.80	719.70	34.80	2754.11	691.05	33.41	2709.19	713.51	34.50
	$\overline{x}$	3660.95	237.63	11.49	2696.40	719.90	34.81	2754.12	691.04	33.41	2709.19	713.51	34.50
	S.D	0.08	0.04	0.00	1.50	0.75	0.04	0.05	0.03	0.00	0.00	0.00	0.00

Appendix C

Table 4 (Cont.) Recyclability of $LaCoO_3$ in standard lead concentration of 1 – 25 mmol /L

Pb^{2+} mmol/L	No	Untreated with EDTA			Treated with 0.1 M EDTA								
					1st of treated			2nd of treated			3rd of treated		
		C_e (mg/L)	Q_e (mg/g)	% Ads.	C_e (mg/L)	Q_e (mg/g)	% Ads.	C_e (mg/L)	Q_e (mg/g)	% Ads.	C_e (mg/L)	Q_e (mg/g)	% Ads.
25	1	4211.00	267.25	11.26	3206.00	769.75	32.44	3204.11	770.70	32.48	3206.20	769.65	32.43
	2	4213.00	266.25	11.22	3207.89	768.81	32.40	3204.10	770.70	32.48	3206.15	769.68	32.43
	3	4216.00	264.75	11.16	3206.62	769.44	32.43	3204.30	770.60	32.48	3206.13	769.69	32.43
	$\overline{x}$	4213.33	266.08	11.21	3206.84	769.33	32.43	3204.17	770.67	32.48	3206.16	769.67	32.43
	S.D	2.05	1.03	0.04	0.79	0.39	0.00	0.09	0.05	0.00	0.03	0.01	0.00

Appendix C

Table 5. Recyclability of $LaFeO_3$ in standard cadmium concentration of 1 – 25 mmol /L

Cd^{2+} mmol/L	No	Untreated with EDTA			Treated with 0.1 M EDTA								
		C_e (mg/L)	Q_e (mg/g)	% Ads.	1st of treated			2nd of treated			3rd of treated		
					C_e (mg/L)	Q_e (mg/g)	% Ads.	C_e (mg/L)	Q_e (mg/g)	% Ads.	C_e (mg/L)	Q_e (mg/g)	% Ads.
1	1	102.70	0.60	1.15	97.90	3.00	5.77	94.80	4.55	8.89	93.56	5.17	9.95
	2	102.60	0.65	1.25	97.70	3.10	5.97	94.65	4.63	8.90	93.53	5.19	9.98
	3	102.70	0.60	1.15	97.90	3.00	5.77	94.88	4.51	8.89	93.50	5.20	10.01
	$\overline{x}$	102.67	0.62	1.18	97.80	3.03	5.84	94.78	4.56	8.89	93.53	5.19	9.98
	S.D	0.05	0.02	0.05	0.01	0.00	0.09	0.10	0.05	0.00	0.02	0.01	0.02
5	1	490.30	11.65	4.54	357.30	78.15	30.43	359.90	76.85	29.93	358.57	77.52	30.18
	2	490.40	11.60	4.52	357.80	77.90	30.34	359.74	76.93	29.96	358.62	77.49	30.17
	3	489.74	11.93	4.65	357.40	78.10	30.42	359.62	76.99	29.98	358.55	77.53	30.18
	$\overline{x}$	490.15	11.73	4.57	357.50	78.05	30.40	359.75	76.92	29.96	358.58	77.51	30.18
	S.D	0.29	0.15	0.06	0.22	0.11	0.04	0.11	0.06	0.02	0.03	0.01	0.00

Appendix C

Table 5 (Cont.) Recyclability of $LaFeO_3$ in standard cadmium concentration of 1 – 25 mmol /L

Cd^{2+} mmol/L	No	Untreated with EDTA			Treated with 0.1 M EDTA								
					1st of treated			2nd of treated			3rd of treated		
		C_e (mg/L)	Q_e (mg/g)	% Ads.	C_e (mg/L)	Q_e (mg/g)	% Ads.	C_e (mg/L)	Q_e (mg/g)	% Ads.	C_e (mg/L)	Q_e (mg/g)	% Ads.
9	1	856.80	52.70	10.95	564.72	198.74	41.31	565.69	198.26	41.21	566.82	197.69	41.09
	2	854.00	54.10	11.24	565.03	198.59	41.28	565.48	198.36	41.23	566.74	197.73	41.10
	3	856.40	52.90	10.99	564.52	198.84	41.33	565.61	198.30	41.22	566.77	197.72	41.10
	$\overline{X}$	855.60	52.23	11.06	564.52	198.72	41.31	565.59	198.31	41.22	566.78	197.71	41.10
	S.D	0.69	0.35	0.13	0.21	0.10	0.02	0.09	0.04	0.00	0.03	0.02	0.00
13	1	1216.50	98.05	13.88	686.52	363.04	51.40	674.60	369.00	52.24	672.92	369.84	52.36
	2	1214.98	98.81	13.99	686.14	363.23	51.43	676.80	367.90	52.09	672.83	369.89	52.37
	3	1215.83	98.39	13.96	686.29	263.16	51.42	675.60	368.50	52.17	672.79	369.91	52.37
	$\overline{X}$	1215.77	98.42	13.94	686.32	363.14	51.42	675.67	368.47	52.17	672.85	369.88	52.37
	S.D	0.34	0.17	0.05	0.16	0.08	0.01	0.90	0.45	0.06	0.05	0.03	0.00

Appendix C

Table 5 (Cont.) Recyclability of $LaFeO_3$ in standard cadmium concentration of 1 – 25 mmol /L

Cd^{2+} mmol/L	No	Untreated with EDTA			Treated with 0.1 M EDTA								
		C_e (mg/L)	Q_e (mg/g)	% Ads.	1st of treated			2nd of treated			3rd of treated		
					C_e (mg/L)	Q_e (mg/g)	% Ads.	C_e (mg/L)	Q_e (mg/g)	% Ads.	C_e (mg/L)	Q_e (mg/g)	% Ads.
17	1	1589.35	127.83	13.86	969.20	437.90	47.47	968.61	438.20	47.50	964.72	440.14	47.71
	2	1589.35	127.83	13.86	969.81	437.60	47.44	969.23	437.99	47.47	964.65	440.18	47.72
	3	1589.89	127.56	13.83	967.75	438.63	47.55	969.02	437.99	47.48	964.96	440.02	47.70
	$\overline{x}$	1589.53	127.74	13.85	968.92	438.04	47.49	968.95	438.03	47.48	964.78	440.11	47.71
	S.D	0.76	0.38	0.01	0.86	0.43	0.05	0.26	0.13	0.01	0.13	0.07	0.00
21	1	1895.14	146.93	13.42	841.89	673.56	61.54	840.80	674.10	61.59	842.20	673.40	61.53
	2	1892.37	148.32	13.55	841.75	673.63	61.55	840.00	674.50	61.63	843.80	672.60	61.45
	3	1890.20	149.40	13.65	841.00	674.00	61.58	840.00	674.50	61.63	843.47	672.77	61.47
	$\overline{x}$	1892.57	148.22	13.54	841.55	673.73	61.56	840.27	674.37	61.62	843.16	672.92	61.48
	S.D	2.02	1.01	0.09	0.39	0.20	0.02	0.38	0.19	0.02	0.69	0.34	0.03

Appendix C

Table 5 (Cont.) Recyclability of $LaFeO_3$ in standard cadmium concentration of 1 – 25 mmol /L

Cd^{2+} mmol/L	No	Untreated with EDTA			Treated with 0.1 M EDTA								
		C_e (mg/L)	Q_e (mg/g)	% Ads.	1st of treated			2nd of treated			3rd of treated		
					C_e (mg/L)	Q_e (mg/g)	% Ads.	C_e (mg/L)	Q_e (mg/g)	% Ads.	C_e (mg/L)	Q_e (mg/g)	% Ads.
25	1	2200.96	214.22	16.29	997.40	816.00	62.07	996.86	816.27	62.09	990.20	819.60	62.34
	2	2201.03	214.19	16.29	996.42	816.49	62.10	996.91	816.25	62.09	990.47	819.47	62.33
	3	2201.46	213.97	16.27	996.90	816.25	62.09	997.21	816.10	62.07	990.38	819.51	62.33
	$\overline{x}$	2201.15	214.13	16.28	996.91	816.25	62.09	996.99	816.21	62.08	990.35	819.53	62.33
	S.D	0.22	0.11	0.01	0.40	0.20	0.01	0.15	0.08	0.00	0.11	0.06	0.00

Appendix C

Table 6. Recyclability of $LaFeO_3$ in standard lead concentration of 1 – 25 mmol /L

Pb^{2+} mmol/L	No	Untreated with EDTA			Treated with 0.1 M EDTA								
					1st of treated			2nd of treated			3rd of treated		
		C_e (mg/L)	Q_e (mg/g)	% Ads.	C_e (mg/L)	Q_e (mg/g)	% Ads.	C_e (mg/L)	Q_e (mg/g)	% Ads.	C_e (mg/L)	Q_e (mg/g)	% Ads.
1	1	171.20	7.70	8.25	131.20	27.70	29.69	128.88	28.86	30.93	130.13	28.24	30.26
	2	169.30	8.65	9.27	129.30	28.65	30.71	128.05	29.28	31.38	130.37	28.12	30.13
	3	169.10	8.75	9.38	129.10	28.75	28.75	128.67	28.97	31.05	130.32	28.14	30.16
	$\overline{x}$	169.87	8.37	8.97	129.87	28.37	29.72	128.53	29.04	31.12	130.27	28.17	30.18
	S.D	0.95	0.41	0.51	0.95	0.47	0.80	0.35	0.18	0.19	0.10	0.05	0.06
5	1	830.80	68.45	14.15	468.60	249.55	51.58	470.50	248.60	51.38	468.77	249.47	51.56
	2	830.60	68.55	14.17	468.80	249.45	51.56	470.39	248.66	51.39	468.79	249.46	51.56
	3	830.47	68.62	14.18	470.10	248.80	51.42	470.40	248.65	51.39	468.80	249.45	51.56
	$\overline{x}$	830.62	68.54	14.17	469.17	249.27	51.52	470.43	248.64	51.39	468.79	249.46	51.56
	S.D	0.14	0.07	0.01	0.67	0.33	0.07	0.05	0.02	0.00	0.01	0.00	0.00

Appendix C

Table 6 (Cont.) Recyclability of $LaFeO_3$ in standard lead concentration of 1 – 25 mmol /L

Pb^{2+} mmol/L	No	Untreated with EDTA			Treated with 0.1 M EDTA								
		C_e (mg/L)	Q_e (mg/g)	% Ads.	1st of treated			2nd of treated			3rd of treated		
					C_e (mg/L)	Q_e (mg/g)	% Ads.	C_e (mg/L)	Q_e (mg/g)	% Ads.	C_e (mg/L)	Q_e (mg/g)	% Ads.
9	1	1419.71	137.80	16.26	978.30	358.50	42.29	980.55	357.18	42.14	981.30	357.00	42.12
	2	1419.77	137.77	16.25	978.65	358.33	42.27	980.90	357.20	42.14	981.91	356.70	42.08
	3	1419.60	137.85	16.26	978.49	358.41	42.28	980.80	357.25	42.15	981.62	356.84	42.10
	$\overline{x}$	1419.69	137.81	16.26	978.48	358.41	42.28	980.88	357.21	42.14	981.61	356.85	42.10
	S.D	0.07	0.04	0.00	0.14	0.07	0.00	0.06	0.03	0.00	0.25	0.13	0.02
13	1	2049.20	217.70	17.52	1649.77	417.42	33.60	1651.48	416.56	33.53	1648.46	418.07	33.65
	2	2048.80	217.90	17.54	1649.60	417.50	33.61	1651.48	416.56	33.53	1648.47	418.07	33.65
	3	2048.40	218.10	17.55	1649.69	417.46	33.60	1651.47	416.56	33.53	1648.47	418.07	33.65
	$\overline{x}$	2048.80	217.90	17.54	1649.69	417.46	33.60	1651.48	416.56	33.53	1648.47	418.07	33.65
	S.D	0.33	0.16	0.02	0.07	0.03	0.00	0.00	0.00	0.00	0.00	0.00	0.00

Appendix C

Table 6 (Cont.) Recyclability of $LaFeO_3$ in standard lead concentration of 1 – 25 mmol /L

Pb^{2+} mmol/L	No	Untreated with EDTA			Treated with 0.1 M EDTA								
		C_e (mg/L)	Q_e (mg/g)	% Ads.	1st of treated			2nd of treated			3rd of treated		
					C_e (mg/L)	Q_e (mg/g)	% Ads.	C_e (mg/L)	Q_e (mg/g)	% Ads.	C_e (mg/L)	Q_e (mg/g)	% Ads.
17	1	2738.96	256.32	15.76	2326.46	462.57	28.45	2324.61	463.50	28.50	2327.94	461.83	28.40
	2	2738.95	256.33	15.71	2326.28	462.66	28.46	2324.60	463.50	28.50	2327.94	461.83	28.40
	3	2738.90	256.35	15.79	2326.37	462.62	28.45	2324.63	463.49	28.50	2327.93	461.83	28.40
	$\overline{x}$	2738.94	256.33	15.75	2326.37	462.62	28.45	2324.61	463.50	28.50	2327.94	461.83	28.40
	S.D	0.03	0.01	0.03	0.07	0.04	0.00	0.01	0.00	0.00	0.00	0.00	0.00
21	1	3583.20	276.50	13.37	2758.80	688.70	33.30	2756.39	689.91	33.36	2760.39	687.91	33.26
	2	3583.41	276.40	13.37	2757.60	689.30	33.33	2756.25	689.98	33.36	2760.27	687.97	33.27
	3	3583.44	276.38	13.37	2743.80	696.20	33.66	2756.33	689.94	33.36	2760.25	687.98	33.27
	$\overline{x}$	3283.35	276.43	13.37	2753.40	691.40	33.43	2756.32	689.94	33.36	2760.30	687.95	33.27
	S.D	0.11	0.05	0.00	6.81	3.41	0.16	0.06	0.03	0.00	0.06	0.03	0.00

Appendix C

Table 6. Recyclability of $LaFeO_3$ in standard lead concentration of 1 – 25 mmol /L

Cd^{2+} mmol/L	No	Untreated with EDTA			Treated with 0.1 M EDTA								
		C_e (mg/L)	Q_e (mg/g)	% Ads.	1st of treated			2nd of treated			3rd of treated		
					C_e (mg/L)	Q_e (mg/g)	% Ads.	C_e (mg/L)	Q_e (mg/g)	% Ads.	C_e (mg/L)	Q_e (mg/g)	% Ads.
25	1	4128.60	308.45	13.00	3262.22	741.64	31.26	3260.90	742.30	31.28	3261.98	741.76	31.26
	2	4128.70	308.40	13.00	3262.20	741.65	31.26	3260.60	742.45	31.29	3261.88	741.81	31.26
	3	4128.00	308.75	13.02	3262.18	741.66	31.26	3260.73	742.39	31.29	3261.91	741.80	31.26
	$\overline{x}$	4128.43	308.53	13.01	3262.20	741.65	31.26	3260.74	742.38	31.29	3261.92	741.79	31.26
	S.D	0.31	0.16	0.01	0.02	0.01	0.00	0.12	0.06	0.00	0.04	0.02	0.00

Appendix C

Table 7. Recyclability of $LaGdO_3$ in standard cadmium concentration of 1 – 25 mmol /L

Cd^{2+} mmol/L	No	Untreated with EDTA			Treated with 0.1 M EDTA								
					1st of treated			2nd of treated			3rd of treated		
		C_e (mg/L)	Q_e (mg/g)	% Ads.	C_e (mg/L)	Q_e (mg/g)	% Ads.	C_e (mg/L)	Q_e (mg/g)	% Ads.	C_e (mg/L)	Q_e (mg/g)	% Ads.
1	1	102.80	0.55	1.06	92.50	5.70	10.97	93.67	5.12	9.85	93.84	5.03	9.68
	2	102.50	0.70	1.35	92.80	5.55	10.68	93.68	5.11	9.84	93.82	5.04	9.70
	3	102.80	0.55	1.06	92.80	5.55	10.68	93.67	5.12	9.85	93.88	5.01	9.64
	$\overline{x}$	102.70	0.60	1.16	92.70	5.60	10.78	93.67	5.12	9.85	93.85	5.03	9.67
	S.D	0.14	0.07	0.14	0.14	0.07	0.14	0.00	0.00	0.00	0.03	0.01	0.03
5	1	497.03	8.29	3.22	456.90	28.35	11.04	462.22	25.69	10.00	464.27	24.67	9.60
	2	496.90	8.35	3.25	457.24	28.18	10.97	462.43	25.59	9.96	464.15	24.73	9.63
	3	497.24	8.18	3.18	457.03	28.29	11.01	462.61	25.50	9.93	464.59	24.51	9.54
	$\overline{x}$	497.06	8.27	3.22	457.06	28.27	11.01	462.42	25.59	9.96	464.34	24.64	9.59
	S.D	0.14	0.07	0.03	0.14	0.07	0.03	0.16	0.08	0.03	0.19	0.09	0.04

Appendix C

Table 7 (Cont.) Recyclability of $LaGdO_3$ in standard cadmium concentration of 1 – 25 mmol /L

Cd^{2+} mmol/L	No	Untreated with EDTA			Treated with 0.1 M EDTA								
					1st of treated			2nd of treated			3rd of treated		
		C_e (mg/L)	Q_e (mg/g)	% Ads.	C_e (mg/L)	Q_e (mg/g)	% Ads.	C_e (mg/L)	Q_e (mg/g)	% Ads.	C_e (mg/L)	Q_e (mg/g)	% Ads.
9	1	902.80	29.70	6.18	802.20	80.00	16.63	813.17	74.52	15.49	819.00	71.60	14.88
	2	902.20	30.00	6.24	802.60	79.80	16.59	813.08	74.56	15.50	818.58	71.81	14.93
	3	902.60	29.80	6.20	802.80	79.70	16.57	812.97	74.62	15.51	818.05	72.08	14.98
	$\overline{X}$	902.80	29.70	6.18	802.80	79.70	16.57	813.07	74.57	15.50	818.54	71.83	14.93
	S.D	0.37	0.18	0.04	0.37	0.18	0.04	0.08	0.04	0.00	0.39	0.19	0.04
13	1	1297.60	57.50	8.14	1217.00	97.80	13.84	1213.40	99.60	14.10	1212.40	100.10	14.17
	2	1297.00	57.80	8.18	1217.60	97.50	13.80	1213.30	99.65	14.11	1210.60	101.00	14.30
	3	1296.80	57.90	8.20	1216.80	97.90	13.86	1213.25	99.68	14.11	1210.00	101.30	14.34
	$\overline{X}$	1297.00	57.73	8.17	1217.00	97.73	13.83	1213.32	99.64	14.11	1211.00	100.80	14.27
	S.D	0.37	0.18	0.03	0.37	0.18	0.03	0.06	0.03	0.00	1.02	0.51	0.10

Appendix C

Table 7 (Cont.) Recyclability of $LaGdO_3$ in standard cadmium concentration of 1 – 25 mmol /L

Cd^{2+} mmol/L	No	Untreated with EDTA			Treated with 0.1 M EDTA								
		C_e (mg/L)	Q_e (mg/g)	% Ads.	1st of treated			2nd of treated			3rd of treated		
					C_e (mg/L)	Q_e (mg/g)	% Ads.	C_e (mg/L)	Q_e (mg/g)	% Ads.	C_e (mg/L)	Q_e (mg/g)	% Ads.
17	1	1712.42	66.29	7.18	1612.31	116.35	12.61	1611.72	116.64	12.64	1614.30	115.35	12.50
	2	1712.31	66.35	7.19	1612.29	116.36	12.61	1611.87	116.57	12.65	1614.10	115.45	12.51
	3	1712.29	66.36	7.19	1612.42	116.29	12.60	1611.82	116.59	12.65	1614.30	115.35	12.50
	$\overline{x}$	1712.34	66.33	7.19	1612.34	116.33	12.61	1611.80	116.60	12.65	1614.23	115.38	12.50
	S.D	0.06	0.03	0.00	0.06	0.03	0.00	0.06	0.03	0.00	0.09	0.05	0.00
21	1	2035.49	76.76	7.02	1894.48	147.26	13.45	1904.86	142.07	12.98	1900.85	144.08	13.16
	2	2034.48	77.26	7.07	1896.10	146.45	13.38	1904.91	142.05	12.98	1900.30	144.35	13.19
	3	2036.10	76.45	6.99	1895.49	146.76	13.41	1904.84	142.08	12.98	1900.25	144.38	13.19
	$\overline{x}$	2035.36	76.82	7.02	1895.36	146.82	13.41	1904.87	142.07	12.98	1900.47	144.27	13.18
	S.D	0.67	0.33	0.00	0.67	0.33	0.00	0.53	0.26	0.00	0.27	0.14	0.01

Appendix C

Table 7 (Cont.) Recyclability of $LaGdO_3$ in standard cadmium concentration of 1 – 25 mmol /L

Cd^{2+} mmol/ L	No	Untreated with EDTA			Treated with 0.1 M EDTA								
					1st of treated			2nd of treated			3rd of treated		
		C_e (mg/L)	Q_e (mg/g)	% Ads.	C_e (mg/L)	Q_e (mg/g)	% Ads.	C_e (mg/L)	Q_e (mg/g)	% Ads.	C_e (mg/L)	Q_e (mg/g)	% Ads.
25	1	2454.04	87.68	6.67	2194.04	217.68	16.56	2204.06	212.67	16.18	2206.68	211.63	16.08
	2	2453.98	87.71	6.67	2193.98	217.71	16.56	2204.01	212.70	16.18	2206.76	211.32	16.08
	3	2454.06	87.67	6.67	2194.06	217.67	16.56	2204.03	212.69	16.18	2206.71	211.35	16.08
	$\overline{x}$	2454.03	87.69	6.67	2194.03	217.69	16.56	2204.03	212.69	16.18	2206.72	211.43	16.08
	S.D	0.03	0.02	0.00	0.03	0.02	0.00	0.02	0.01	0.00	0.03	0.02	0.00

Appendix C

Table 8. Recyclability of $LaGdO_3$ in standard lead concentration of 1 – 25 mmol /L

Pb^{2+} mmol/L	No	Untreated with EDTA			Treated with 0.1 M EDTA								
		C_e (mg/L)	Q_e (mg/g)	% Ads.	1st of treated			2nd of treated			3rd of treated		
					C_e (mg/L)	Q_e (mg/g)	% Ads.	C_e (mg/L)	Q_e (mg/g)	% Ads.	C_e (mg/L)	Q_e (mg/g)	% Ads.
1	1	182.13	2.24	2.40	161.96	12.32	13.20	168.83	8.89	9.52	167.83	9.39	10.06
	2	181.96	2.32	2.49	162.13	12.24	13.11	168.18	9.21	9.87	167.70	9.45	10.13
	3	182.05	2.28	2.45	162.05	12.28	13.16	168.69	8.96	9.60	167.87	9.37	10.04
	$\overline{x}$	182.05	2.28	2.45	162.05	12.28	13.16	168.57	9.02	9.66	167.80	9.40	10.08
	S.D	0.07	0.03	0.04	0.07	0.03	0.04	0.28	0.14	0.15	0.07	0.04	0.04
5	1	911.64	28.03	5.79	791.86	87.92	18.17	808.61	79.55	16.44	804.81	81.45	16.83
	2	911.86	27.92	5.77	791.64	88.03	18.19	809.23	79.24	16.38	804.89	81.41	16.82
	3	911.90	27.90	5.77	791.90	87.90	18.17	809.02	79.34	16.40	804.84	81.43	16.83
	$\overline{x}$	911.80	27.95	5.76	791.80	87.95	18.18	808.95	79.38	16.41	804.85	81.43	16.83
	S.D	0.11	0.06	0.01	0.11	0.06	0.01	0.26	0.13	0.03	0.03	0.02	0.00

Appendix C

Table 8 (Cont.) Recyclability of $LaGdO_3$ in standard lead concentration of 1 – 25 mmol /L

Pb^{2+} mmol/L	No	Untreated with EDTA			Treated with 0.1 M EDTA								
		C_e (mg/L)	Q_e (mg/g)	% Ads.	1st of treated			2nd of treated			3rd of treated		
					C_e (mg/L)	Q_e (mg/g)	% Ads.	C_e (mg/L)	Q_e (mg/g)	% Ads.	C_e (mg/L)	Q_e (mg/g)	% Ads.
9	1	1558.47	68.42	8.07	1398.44	148.43	17.51	1398.10	148.60	17.53	1403.80	145.75	17.19
	2	1558.44	68.43	8.07	1398.47	148.42	17.51	1397.55	148.88	17.56	1404.00	145.65	17.18
	3	1558.43	68.44	8.07	1398.43	148.44	17.51	1398.14	148.58	17.53	1404.00	146.65	17.18
	$\overline{x}$	1558.45	68.44	8.07	1398.45	148.44	17.51	1397.93	148.69	17.54	1403.93	145.68	17.18
	S.D	0.02	0.01	0.00	0.02	0.01	0.00	0.27	0.13	0.01	0.09	0.05	0.00
13	1	2289.79	97.41	4.69	2109.92	187.34	15.08	2099.92	192.34	15.48	2097.05	192.78	15.60
	2	2289.92	97.34	4.68	2109.83	187.39	15.08	2099.93	192.34	15.48	2095.90	194.35	15.64
	3	2289.83	97.39	4.68	2109.79	187.41	15.09	2099.90	192.35	15.48	2095.45	194.58	15.66
	$\overline{x}$	2289.85	97.38	4.68	2109.85	187.38	15.08	2099.92	192.34	15.48	2096.13	194.24	15.63
	S.D	0.05	0.03	0.00	0.05	0.03	0.00	0.01	0.00	0.00	0.67	0.34	0.03

Appendix C

Table 8 (Cont.) Recyclability of $LaGdO_3$ in standard lead concentration of 1 – 25 mmol /L

Pb^{2+} mmol/L	No	Untreated with EDTA			Treated with 0.1 M EDTA								
		C_e (mg/L)	Q_e (mg/g)	% Ads.	1st of treated			2nd of treated			3rd of treated		
					C_e (mg/L)	Q_e (mg/g)	% Ads.	C_e (mg/L)	Q_e (mg/g)	% Ads.	C_e (mg/L)	Q_e (mg/g)	% Ads.
17	1	2974.26	138.67	6.15	2754.03	248.79	15.30	2768.55	241.53	14.86	2761.89	244.86	15.06
	2	2974.03	138.79	6.15	2754.23	248.69	15.30	2768.90	241.35	14.84	2761.81	244.90	15.06
	3	2974.23	138.69	6.15	2754.26	248.67	15.30	2768.30	241.65	14.86	2761.84	244.88	15.06
	$\overline{x}$	2974.17	138.72	6.15	2754.17	248.72	15.30	2768.58	241.51	14.85	2761.85	244.88	15.06
	S.D	0.10	0.05	0.00	0.10	0.05	0.00	0.25	0.12	0.01	0.03	0.02	0.00
21	1	3788.82	173.69	7.25	3567.32	284.44	13.75	3542.77	296.72	14.35	3545.84	295.18	14.27
	2	3787.32	174.44	7.28	3569.06	283.57	13.71	3542.75	296.73	14.35	3545.82	295.19	14.27
	3	3789.06	173.57	7.28	3568.82	283.69	13.72	3542.80	296.70	14.35	3545.87	295.17	14.27
	$\overline{x}$	3788.40	173.90	7.26	3568.40	283.90	13.73	3542.77	296.72	14.35	3545.84	295.18	14.27
	S.D	0.77	0.38	0.02	0.77	0.38	0.02	0.02	0.01	0.00	0.02	0.01	0.00

Appendix C

Table 8 (Cont.) Recyclability of $LaGdO_3$ in standard lead concentration of 1 – 25 mmol /L

Pb^{2+} mmol/ L	No	Untreated with EDTA			Treated with 0.1 M EDTA								
		C_e (mg/L)	Q_e (mg/g)	% Ads.	1st of treated			2nd of treated			3rd of treated		
					C_e (mg/L)	Q_e (mg/g)	% Ads.	C_e (mg/L)	Q_e (mg/g)	% Ads.	C_e (mg/L)	Q_e (mg/g)	% Ads.
25	1	4328.80	208.35	8.78	3989.62	377.94	15.93	3997.80	373.85	15.76	4001.81	371.85	15.67
	2	4329.62	207.94	8.76	3988.80	378.35	15.95	3998.09	373.71	15.75	4001.80	371.85	15.67
	3	4329.92	207.79	8.75	3989.92	377.79	15.92	3997.71	373.90	15.76	4001.80	371.85	15.67
	$\overline{x}$	4329.45	208.03	8.76	3989.45	378.03	15.93	3997.87	373.82	15.76	4001.80	371.85	15.57
	S.D	0.35	0.18	0.01	0.35	0.18	0.01	0.16	0.08	0.00	0.00	0.00	0.00

VITAE

Name Mrs. Wankassama Haron
Student ID 5410230025
Educational Attainment

Degree	Name of Institution	Year of Graduation
B. Sc. (Chemistry)	Thaksin University	2004
B.Pol.Sc. (Political Science)	Sukhothai Thammathirat University	2006
M. Sc. (Chemistry)	Kasetsart University	2008

Scholarship Awards during Enrolment

1. Office of the Higher Education Commission, Scholarship for Lecturer Development in 2011
2. The Thesis Research Fund through the Graduate School, Prince of Songkla University

List of Publication and Proceeding

Publications

1. **Wankassama Haron**, Anurat Wisitsoraat, and Sumpun Wongnawa, "Comparison of Nanocrystalline $LaMO_3$ (M = Co, Al) Perovskite Oxide Prepared by Co-Precipitation Method" *International Journal of Chemical Engineering and Applications*, 5 (2014) **123-126.**
2. **Wankassama Haron**, Anurat Wisitsoraat, Uraiwan Sirimahachai , and Sumpun Wongnawa, "Synthesis, characterization and application of nano-LaMO3 (M= Al, Co, Fe) perovskites as adsorbents for removal of cadmium ions from water" *International Journal of Applied Chemistry,* xxx (2016) **xxx – xxx.**

Proceedings

1. **Wankassama Haron**, Anurat Wisitsoraat, and Sumpun Wongnawa, *"Comparison of Nanocrystalline $LaMO_3$ (M = Co, Al) Perovskite Oxide Prepared by Co-Precipitation Method"* International Conference on Chemical Science and Engineering (ICCSE 2013), Kuala Lumpur, Malaysia. 29 – 30 December 2013.
2. **Wankassama Haron**, Anurat Wisitsoraat, and Sumpun Wongnawa, *"Nanocrystalline $LaFeO_3$ Perovskite Oxide Prepared at Lower Temperature with Improved Ethanol Gas Sensoring"* International Conference on Biotechnology, Nanotechnology & Environmental Engineering (ICBNE'15), Bangkok, Thailand. 22 – 23 April, 2015.